University of Leicester

Molecular characterization of the Parkinson's associated protein DJ-1

A thesis submitted for the degree of
Doctor of Philosophy

by

Mahdieh Hassanjani M.Sc.

Department of Genetics
University of Leicester

December 2014

Dedicated to my family in acknowledgement of their lifetime love, support and encouragement ….

Molecular characterization of the Parkinson's associated protein DJ-1

Mahdieh Hassanjani

Department of Genetics, University of Leicester

ABSTRACT

Mutations in DJ-1 (*PARK7*), a conserved protein of 189 amino acids, cause autosomal recessive cases of Parkinson's disease (PD). DJ-1 appears to play a central role in protecting cells from oxidative stress, which likely has relevance for its role in PD pathogenesis. Biochemical and crystallographic approaches indicate that DJ-1 dimerizes, which is likely fundamental for its stability and normal function. A main focus of this thesis was identifying and characterizing DJ-1 dimerization modifiers through an unbiased screen of a kinase and phosphatase inhibitor library, taking advantage of bimolecular fluorescence complementation (BiFC) as a readout for DJ-1 dimerisation in living cells. To address this aim, we generated HEK 293T cell clones stably over-expressing DJ-1 BiFC constructs and optimised high throughput Cell^R-Scan^R screening. This approach identified two kinase inhibitors (Bosutinib and KW2449) which decrease DJ-1 dimerisation in an oxidative stress-dependent manner. Furthermore, to indicate whether or not the observed effects of the kinase inhibitors on DJ-1 dimerization were due to a direct alteration of DJ-1 phosphorylation status or were indirect effects, we studied DJ-1 phosphorylation at all potential sites on its dimerization and stability by generating phosphomimic and phosphoblocking mutants. This work indicates that phosphorylation of key residues of DJ-1 likely dramatically reduces its stablilty. Additionally, by using the BiFC approach we found a direct interaction in living cells of DJ-1 with microtubule-associated protein tau, which is known to be hyper phosphorylated and aggregated in neurodegenerative disorders like Alzheimer's disease and Parkinson's disease. These analyses suggest that alterations in DJ-1 dimerization, stability and phosphorylation status in normal conditions and in response to oxidative stress may shed more light on DJ-1 function and its role associated with PD pathogenesis.

ACKNOWLEDGEMENTS

Throughout my PhD course there have been many great people who have provided support, patience and guidance, without whom none of this work would have been possible. It is to them that I owe my deepest gratitude.

I would like to thank Dr. Flaviano Giorgini for providing me with the opportunity to work within his research group during this PhD project. His kind support, guidance and boundless encouragement has been wonderful over the past four years. I especially grateful for all his support while writing this thesis, I would not have reached this stage without his feedback and advice.

I would like to extend my sincere gratitude to Dr. Mariaelena Repici for her kind mentorship and advice as well as her unwavering support and understanding throughout the course of the PhD. I would also like to thank Dr. Kornelis R.Straatman for all of his help with the microscopy work and Dr. Robert Mason for his suggestion and ideas.

I wish to express my gratitude to the amazing people whose wonderful moral support, help and efforts has seen me through the last four years be it when life showed me it's unkind face or during times of difficulty within the lab. These great people were always on hand to offer reassurance, and as such I would like to thank Sue, Gurdeep, Raheleh, Mahsa, Houra, Narges, Ehsan, Hanieh, Somayeh, Shadab, Carlo, Mathura, Shanow, Susy, Aisha, Usha, Razan, Amin and other past members of the lab 106 and 102.

Last but by no means least, this journey would not have been possible without the support of my family, whose love, good wishes and encouragement has always inspired me and enable me to reach to this stage without losing perspective of what is truly important in life! I would especially like to express my heart-felt thanks to the super hero of my life, my beloved father, who provided me the opportunity to live my childhood dream of becoming scientist.

ABBREVIATION:

ABL1	c-able oncogene product 1
Aβ	Amyloid β
AD	Alzheimer's disease
ASK1	Apoptosis signal-regulating kinase 1
ATP	Adenosine Triphosphate
BiFC	Bimolecular fluorescence complementation
c-Abl	Abelson tyrosine kinase
CaMK-II	Calcium/calmodulin-dependent kinase II
CCS	Copper chaperone for SOD1
Cdk5	Cyclin-dependent kinase 5
CFP	Cyan fluorescent protein
CLSM	Confocal laser scanning microscope
CNS	Central nervous system
CSF	Cerebrospinal fluid
DA	Neurotransmitter dopamine
DDC	L-DOPA carboxylase
DCFDA	Dye dichloro-dihydrofluorescein dictate
DLBs	Dementia with Lewy bodies
DMSO	Dimethyl sulfoxide
DNA	Deoxyribonucleic acid
EGF	Epidermal growth factor
ER	Endoplasmic reticulum
FGF	Fibroblast growth factor
GFP	Green fluorescent protein
GSK-3β	Glycogen synthase kinase 3 β
GVD	Granulovacuolar degeneration
HD	Huntington’s disease
hESC	Human embryonic stem cell
HNE	4- hydroxy-2-nonenal
HPII	Hydroperoxidase II
IFN-γ	Interferon-gamma
Jaks	Janus kinase
JNK	c-Jun NH2-terminal kinase
KIF1B	Kinesin family member 1B
LB	Luria broth
LBs	Lewy bodies
LC3-I	Microtubule-associated protein light chain 3
LDH	Lactate dehydrogenease
LDLR	Low-density lipoprotein receptor
LRRK2	Leucine-rich repeat kinase 2
mM	Millimolar
MAP	Microtubule-associated protein
MPP+	1-methyl-4-phenylpyridinium
MS	Mass spectrometry

MST1	Mammalian Ste-20 like kinase 1
MTBR	Microtubules binding repeats
µg	Microgram
µl	Microlitre
µM	Micromolar
NGF	Nerve growth factor
NFL	Neurofilament light subunit
NMDA	N-methyl-D-aspartic acid
nm	Nanometre
NPCs	Cortical neuronal progenitor cells
Nrf2	Nuclear factor erythroid-2 related factor 2
ODS	Octadecyl sulfate
OMM	Outer mitochondria membrane
PBS	Phosphate buffered Saline
PCR	Polymerase chain reaction
PD	Parkinson's disease
PDK	PIP3-dependent kinase
PI3K	Phosphatidylinositol-3 kinase
Pin1	Peptidyl-prolyl cis/trans isomerase
PIP2	Phosphatidylinositol (4,5)- bisphosphate
PIP3	Phosphatidylinositol (3,4,5)-trisphosphate
PKA	cAMP-dependent protein kinase
PKCδ	Protein-Kinase C-delta
PrxI	Antioxidant protein peroxiredoxin I
PSF	Protein associated splicing factor
PTKs	Protein tyrosine kinases
PTMs	Protein post-translational modifications
PVD	Polyvinylidene Fluoride
REM	Rapid eye movement
RFP	Red fluorescent protein
ROS	Reactive oxygen species
SDS	Sodium dodecyl sulfate
SDS-PAGE	Sodium dodecyl sulfate polyacrylamide gel electrophoresis
SEM	Standard error of the mean
SH	Src homology
SHP-1	Src-homology 2 [SH2] domain-containing protein tyrosine phosphatase-1
SN	Substantia nigra
SOD	Superoxide desmutase
STAT1	Signal-transducer and activator of transcription
STS	Starusporin
TBE	Tris Borate EDTA
TBST	Tris-buffered saline Tween 20
TEMED	Tetramethylethylenediamine
TH	Tyrosine hydroxylase
VMAT2	Vesicular monoamine transporter 2

YFP	Yellow fluorescent protein
4E-BP1	4E-binding protein 1

CONTENTS:

Chapter 1: Introduction

Chapter 2: Materials and Methods

Chapter 3: Screening for chemical modifiers of DJ-1 dimerization in living cells

Chapter 4: Exploring the functional implications of DJ-1 phosphorylation

Chapter 5: Exploring the relationship between DJ-1 and tau

Chapter 6: Discussion and future directions

Appendices

List of figures

List of tables

Chapter 1
Introduction
1-1 Parkinson's disease (PD)

Parkinson's disease (PD) is the second most common neurodegenerative disorder and affects 1-2 % of the population above 65 years of age (Dorsey et al., 2007). This devastating disorder is characterized by loss of dopaminergic neurons in the substantia nigra (SN) and appearance of intraneuronal inclusions known as Lewy bodies (LBs) (Figure 1.1.1) (Hirsch et al., 1989). Typical clinical manifestations of PD patients include motor symptoms such as bradykinesia, rigidity, tremor, and postural instability and non-motor symptoms including loss of olfaction, constipation, rapid eye movement (REM) and sleep disorder (Schapira and Jenner, 2011, Venderova and Park, 2012, Trempe and Fon, 2013). The etiology of PD is extremely complex, encompassing both genetic and environmental factors (Nuytemans et al., 2010). While most cases of PD (more than 90 %) are idiopathic, a small number are caused by mutations in single genes that follow Mendelian patterns of inheritance (Martin et al., 2011). Environmental factors can also contribute to disease: indeed, the accumulation of environmental toxins such as pesticides and metals is one of the major risk factors for developing late onset PD (Bjorkblom et al., 2013). Although PD was first described over two centuries ago the cellular and molecular mechanisms underlying this disease are poorly understood and there is no effective treatment to stop its progression. Studies on genes associated with familial forms of PD may help the understanding of cellular mechanisms underlying the pathogenesis of both sporadic and familial forms of PD.

Over 500 distinct DNA alterations have been identified in the five major genes associated with familial forms of PD: α-synuclein (*PARK1*), Parkin (*PARK2*), PTEN-induced putative kinase I (*PINK1*), DJ-1 (*PARK7*), and leucine-rich repeat kinase 2 (LRRK2) (de Lau and Breteler, 2006, Nuytemans et al., 2010). UCH-L1 and HTRA2 are two other genes that have been discovered to be related to PD pathogenesis (Nuytemans et al., 2010). Although the pathophysiological mechanisms underlying how mutations in these genes lead to the selective loss of dopaminergic neurons are still unclear, oxidative stress, mitochondria dysfunction and impaired autophagy are speculated to play critical roles in PD (Table 1.1.1) (Inden et al., 2011).

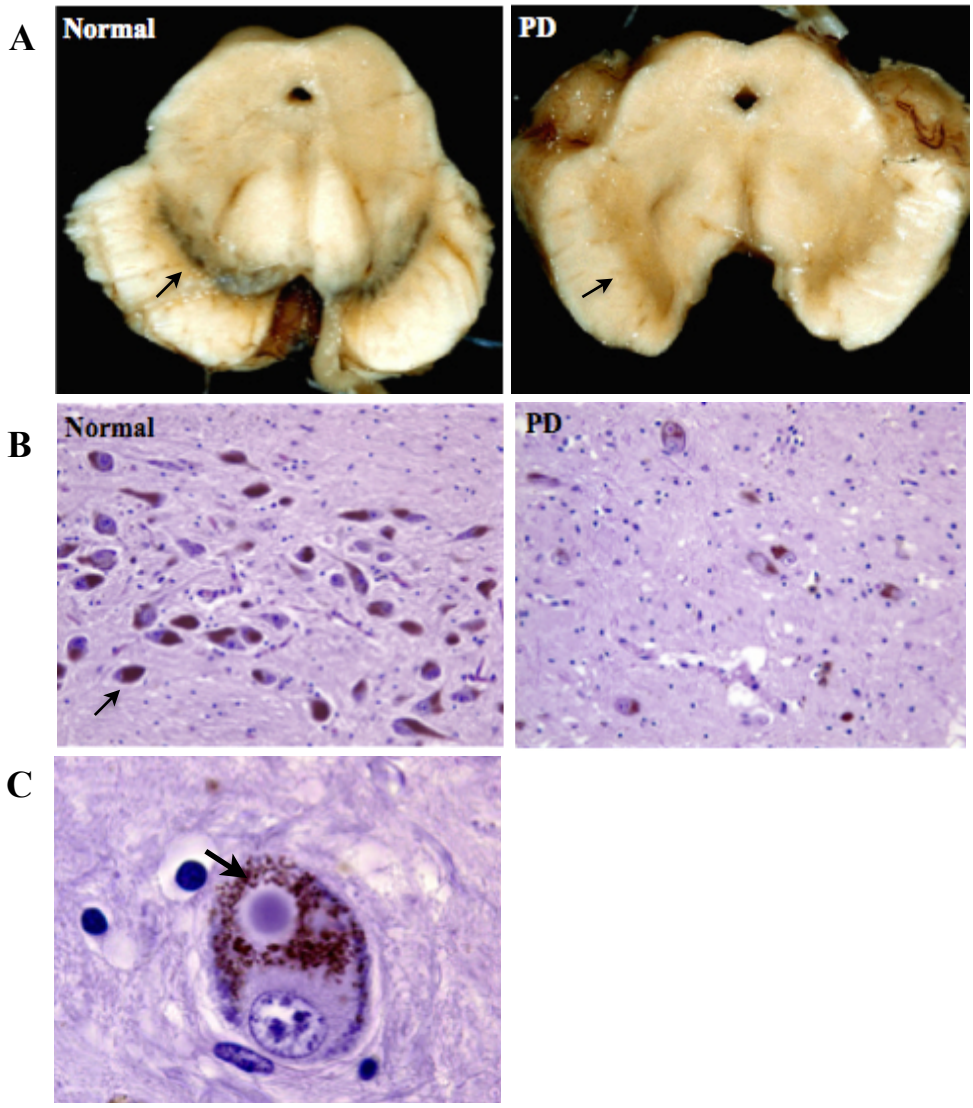

Figure 1.1.1 The substantia nigra in the midbrain is the most susceptible region in the brain of PD patients. **A)** Dopaminergic neurons (pigmented neurons) that control motor function are lost in PD substantia nigra. **B)** Normal and PD substantia nigra at the same magnification, clearly showing pigmented neurons are lost in PD cases **C)** Lewy bodies (the red-brown melanin granules) are eosinophilic cytoplasmic inclusions that mainly consist of α-synuclein ((Agamanolis) 2011, Ch.9, Neurophatology. Available at: http://neuropathology-web.org/chapter9/chapter9dPD.html (Accessed: 7 Dec 2014)).

Gene	Chromosome	Inheritance	Protein	Protein function	Clinical features
α-synuclein (*PARK1*)	4q21	AD	α-synuclein	LB component	Early onset, rapid progression, Similar to IPD
Parkin (*PARK2*)	6q25.2-27	AR	Ubiquitin ligase	UPS component	Early onset, Slow progression Early dystonia, and dyskiesia
PARK3	2p13	AD	_	_	Similar to IPD, Levodopa-responsive
PARK4	4p16	AD	_	_	Early onset, Similar to IPD, Dementia and dysautonomia
UCHL-1 (*PARK5*)	4p14	AD	UCHL-1	UPS component	Similar to IPD
PINK1 (*PARK6*)	1p35-36	AR	PTEN-induce kinase	Protection against mitochondrial dysfunction	Early onset, Benign course, Levodopa-reponsive
DJ-1 (*PARK7*)	1p36	AR	DJ-1	Protection against oxidative stress	Early onset, Levodopa-response
LRRK2 (*PARK8*)	12p11.2-q13.1	AD	Dardarin	unknown	Similar to IPD
PARK9	1p36	AR	_	_	Parkinsonism with spasticity, Dementia, Supranuclear palsy
PARK10	1p32	unknown	_		Similar to IPD
PARK11	2q36-37	unknown	_	_	NO definite phenotype reported
NR4A2	2q22-q23	AD*	Nuclear receptor	Differentiation or survival of dopaminergic neurons	Late onset

AD=autosomal dominant; AR=autosomal recessive; IPD=idiopathic PD; UPS=ubiquitin protease system. * As yet unclear whether or not causal or susceptibility gene.

Table 1.1.1 Genes associated with familial forms of PD. Although only ~10 % of PD cases are monogenetic with clear Mendelian inheritance, studying the structure, localization and function of these disease-causing proteins may pave the way for investigating novel therapeutic strategies (de Lau and Breteler, 2006).

1-2 Oxidative stress, mitochondrial dysfunction and autophagy play roles in PD pathogenesis

There is ample evidence that oxidative stress is a common mechanism underlying cellular death and dysfunction in both idiopathic and familial forms of PD (Hwang, 2013). Neurotransmitter dopamine (DA) metabolism, mitochondrial dysfunction, iron, neuroinflammation, calcium, and aging are the major sources and mechanisms of reactive oxygen species (ROS) production (Dias et al., 2013, Hwang, 2013). Furthermore, cellular homeostatic processes such as the ubiquitin-proteasome system and mitophagy are affected by oxidative stress (Dias et al., 2013). Despite that DA is normally located in vesicles, excess cytosolic DA can be oxidized and generate DA quinone which plays a role in PD pathogenesis by modifying intercellular macromolecules that function in cell survival processes, as well as PD-related proteins including, α-synuclein (α-Syn), Parkin, DJ-1 and UCH-L1 (Conway et al., 2001, LaVoie et al., 2005, Martinez-Vicente et al., 2008, Van Laar and Berman, 2009, Hwang, 2013). Indeed, reactive DA (DA quinone) forms 5-cysteinyl-DA through covalent binding to the thiol group of target proteins (Graham et al., 1978, Ito et al., 1988, Hastings et al., 1996). Since many critical cellular and mitochondrial proteins contain cysteine residues which are vital for their normal structure and function, DA quinone modification could have detrimental effects on cells by altering the structures and functions of these proteins (Berman and Hastings, 1999, LaVoie and Hastings, 1999, Premkumar and Simantov, 2002). Covalently modified monomers of α-Syn by DA quinone form cytotoxic protofibrils that not only are hardly degraded but also inhibit normal degradation of other proteins by blocking chaperone-mediated autophagy (Conway et al., 2001, Martinez-Vicente et al., 2008). DA quinone also covalently modifies Parkin leading to its insolubility and inactivation of its E3 ubiquitin ligase function (LaVoie et al., 2005). DA quinone modifications of DJ-1 and UCH-L1 have been identified in mitochondria of rat's brain and differentiated SH-SY5Y cells that seem to disrupt their antioxidant and ubiquitin-proteasome system functions respectively (Van Laar et al., 2009). DA quinone also triggers mitochondrial respiratory chains by covalently modifying complex I (75 kDa and 30 kDa subunits), and complex III (ubiquinol-cytochrome c reductase core protein 1 and Rieske Fe-S protein), and subsequently increasing ROS production (Van Laar et al., 2009). Additionally, DA

oxidation also leads to mitochondrial dysfunction and swelling in the brain by altering mitochondrial respiration and inducing their permeability transition (Berman and Hastings, 1999, Lee et al., 2002).

Mitochondria are dynamic organelles involved in energy production, calcium homeostasis, stress response and cell death and their dysfunction is strongly implicated in neurodegeneration (Zhu and Chu, 2010). Indeed, mitochondrial dysfunction plays an important role in PD pathogenesis as its disruption increases ROS levels (Schapira, 2004, Bueler, 2009, Van Laar and Berman, 2009, Winklhofer and Haass, 2010, Zhu and Chu, 2010, Larsen et al., 2011, Hwang, 2013). Evidence for the role of mitochondrial dysfunction in PD emerged in 1990 when a study discovered that complex I activity is reduced in the SN of PD patients (Schapira et al., 1990). Analysis of brain tissue from PD patients has shown deficiencies in mitochondrial respiratory complex I in the substantia nigra pars compacta and cerebral cortex (Schapira et al., 1990, Cooper et al., 1992, Blin et al., 1994, Haas et al., 1995, Parker et al., 2008). The hypothesis that complex I dysfunction may play a key role in pathogenesis is supported by studies showing that pharmacological inhibition of complex I by compounds including rotenone leads to experimental parkinsonisms (Larsen et al., 2011). Furthermore, direct molecular links between PD and mitochondrial dysfunction have been established by identifying three PD autosomal recessive causative mutations in Parkin, in PINK1 and DJ-1 that contribute to mitochondria function (Kitada et al., 1998, Bonifati et al., 2003, Paisan-Ruiz et al., 2004, Knott and Bossy-Wetzel, 2008, Van Laar and Berman, 2009, Burbulla et al., 2010). Furthermore, dopaminergic neurons are prone to oxidative stress since they possess iron which contributes to oxidative stress through catalysing the Fenton reaction, but they also express tyrosine hydroxylase and monoamine oxidase, both of which are ROS-generating enzymes (Halliwell, 1992, Hwang, 2013).

Neuronal loss in PD is related as well to chronic neuroinflammation that is controlled by microglia, the main immune responsive cells in the central nervous system (CNS) (Hwang, 2013). Microglia can become activated in response to an injury or a toxic insult, releasing free radicals such as nitric oxidase and superoxidase that contribute to oxidative stress (Hwang, 2013).

Much research in the neurodegenerative disease field has focused on protein degradation, turnover and related protein aggregation. Autophagy is one the major proteolytic systems involved in protein degradation and is vital for the maintenance of protein homeostasis in cells (Lynch-Day et al., 2012). Extensive studies have shown that autophagy plays a critical role in PD pathogenesis since dysregulation of this pathway has been observed in PD patient brains and in animal PD models (Lynch-Day et al., 2012). Mitophagy which is a selective autophagy for mitochondrial degradation is implicated in PD pathogenesis through the PINK1-Parkin mediated pathway (Klionsky et al., 2007, Lynch-Day et al., 2012). Of note, a number of genes implicated in PD (α-synuclein, LRRK2, PINK1 and Parkin) contribute to autophagy (Bandyopadhyay and Cuervo, 2007, Alegre-Abarrategui and Wade-Martins, 2009, Lynch-Day et al., 2012). Recent studies on DJ-1 function have also discovered a link between DJ-1 and autophagy, since depletion of DJ-1 in both *Drosophila* and human neuroblastoma cells leads to mitochondrial dysfunction and subsequently autophagy impairment (Hao et al., 2010, Thomas et al., 2011).

1-3 PD associated genes

1-3-1 α-Synuclein (SNCA)

The first PD causative mutation was discovered in the gene encoding α-Synuclein (SNCA) in 1997, which was previously mapped to the chromosome 4 position q21-q22 (4q21-q22) (Chen et al., 1995, Shibasaki et al., 1995, Polymeropoulos et al., 1997). Together with the observation of Spillantini et al. that α-Synuclein (α-Syn) is one of the major fibrillar components of LBs in familial and sporadic form of PD (Spillantini et al., 1997), this indicated α-Syn as a major player in the disease onset. Missense mutations associated with rare familial autosomal dominant forms of PD (A53T, A30P, E46K) promote α-Syn aggregation (Polymeropoulos et al., 1997, Conway et al., 1998, Greenbaum et al., 2005) and mutations associated with familial PD in which SNCA is duplicated or triplicated (Singleton et al., 2003, Chartier-Harlin et al., 2004) also increase the propensity of the protein to aggregate (Minton, 2005). In idiopathic PD, polymorphisms in SNCA have been identified as risk factors for development of the disease (Satake et al., 2009, Simon-Sanchez et al., 2009).

Wild type α-Syn has been identified as an intrinsically unfolded protein associated with lipid membranes (Davidson et al., 1998). It is a small protein (14.5 kDa) of 144 amino acids encoded by three alternative SNCA transcripts (Davidson et al., 1998), highly expressed in the brain and enriched in presynaptic nerve terminals. An amphipathic domain at the N-terminus of the protein is able to specifically associate with membrane microdomains (Fortin et al., 2004). Studies on α-Syn function have shown its role in the regulation of dopamine (DA) transmission and synaptic vesicle dynamics. Indeed, α-Syn regulates the production of dopamine in cultured cells through its interaction with tyrosine hydroxylase (TH), the enzyme which converts tyrosine to L-DOPA in the dopamine synthesis pathway (Venda et al., 2010). Over-expression of α-Syn in cells reduces the activity of the TH promoter, leading to reduced levels of TH, and thus to reduced L-DOPA (Venda et al., 2010). Consistent with a role for α-Syn in down-regulating dopamine biosynthesis in cell culture models, reduced TH activity has been observed in several mouse models over-expressing wild type α-Syn (Venda et al., 2010).

Larsen et al. in 2006 suggested α-Syn might modulate synaptic vesicle priming (Larsen et al., 2006). Since the level of α-Syn presumably influences synaptic function it could be speculated that levels of this protein might lead to early and pre-symptomatic changes in vulnerable neurons (Biskup et al., 2008). α-Syn, natively unfolded, is characterized by a high conformational plasticity induced by the environment. Indeed, monomeric and oligomeric alpha-helix and beta-sheet conformations can be found as well as different protein aggregates, from amorphous ones to amyloid-like fibrils (Uversky, 2003). Under certain conditions in fact, aggregation of 2 or more monomers leads to the formation of soluble oligomeric species, which have also been termed protofibrils because they are fibrillization intermediates (Walsh et al., 1997), and eventually fibrils and inclusion bodies. Studies using protein-fragment complementation demonstrated that α-Syn oligomers are associated with enhanced toxicity in cell culture models (Outeiro et al., 2008, Putcha et al., 2010, Danzer et al., 2011) and recently, α-Syn oligomers have been identified in plasma (El-Agnaf et al., 2006) and cerebrospinal fluid (CSF) (Tokuda et al., 2010) of PD patients.

1-3-2 Leucine-rich repeat kinase 2 (LRRK2)

Mutations in the Leucine-rich repeat kinase 2 (LRRK2) gene are the most common genetic cause of PD (Biskup et al., 2008), with a frequency of 5-7 % in patients with a family history. These patients show typical L-DOPA responsive parkinsonism with middle or late onset. LRRK2 gene spans a genomic region of 144 kb, with 51 exons encoding a rather large (2,527 amino acids) peptide, also called dardarin, containing multiple, independent domains. Sequence analysis suggests that these domains include an armadillo and ankyrin repeat region, leucine-rich repeats (LRR), a Roc GTPase domain (followed by an associated C-terminal of Roc [COR] domain), a tyrosine kinase-like (TKL) family kinase domain, and a WD40 repeat (Cookson, 2010). Studies of LRRK2 using various model organisms indicate this protein modulates survival of dopaminergic neurons, authophagy, and neuronal outgrowth (Smith et al., 2005, Liu et al., 2008b, Saha et al., 2009, Yao et al., 2010, Chan et al., 2011, Skibinski et al., 2014). Additionally, work has revealed LRRK2 also regulates MAP kinase signalling pathways (Carballo-Carbajal et al., 2010, Hsu et al., 2010). Meanwhile, LRRK2 interacts with various proteins, suggesting that important functions of this protein might be directly linked to its kinase function (Boon et al., 2014). Recent work by Skibinski et al. indicated that pharmacological inhibition of LRRK2 kinase activity modulates its stability and localization although its protein level is more important in predicting toxicity in neurons (Skibinski et al., 2014). LRRK2 is located in presynaptic terminals where it localizes to vesicles and endosomes (Biskup et al., 2008). It has also been shown that LRRK2 regulates synaptic vesicle endocytosis by direct interaction with the early endosome marker protein Rab5 and EndoA (Shin et al., 2008, Matta et al., 2012).

1-3-3 Parkin

Mutations in the Parkin gene have been reported as the most common autosomal recessive cause of PD (Kitada et al., 1998, Corti et al., 2011, Martin et al., 2011). This gene encodes a 465 amino acid E3 ubiquitin ligase protein which can mediate mono or polyubiqutination of proteins through different ubiquitin linkages (lysine 27, 29, 48, and 63 of ubiquitin) (Scarffe et al., 2014). There is evidence that Parkin not only mediates ubiquitinylation through Lysine 48 (K48), which targets ubiquitinylated pro-

teins to the proteosomal degradation system, but also via Lysine 63 (K63) that might function in intracellular signalling processes (Lim et al., 2005). Accumulation of potentially toxic proteins might be detrimental for vulnerable neurons such as dopaminergic neurons. Parkin may be involved in the formation of LB inclusions associated with PD (Lim et al., 2005). Postmortem studies on PD brain and mouse models of PD indicated that Parkin is inactivated by post-translational modifications including oxidation, nitrosylation, addition of dopamine, and phosphorylation by c-Abl which is a fundamental stress-activated tyrosine kinase shown to be activated in the brains of sporadic forms of PD and animal models of PD (this kinase will be described in more detail in Chapter 3) (Walden and Martinez-Torres, 2012, Dawson and Dawson, 2014, Scarffe et al., 2014). Parkin exerts it effect in multiple cellular compartments such as cytosol, synaptic terminals, mitochondria, and nucleus (Scarffe et al., 2014). It is recruited to mitochondria upon depolarization of the outer mitochondria membrane by PINK1 where it ubiquitinates mitochondrial proteins targeting them for degradation (Narendra et al., 2008, Narendra et al., 2009). Furthermore, Parkin has been shown to play a role in mitochondrial morphogenesis and biogenesis in proliferating cells, possibly via transcription and replication of mitochondrial DNA (Kuroda et al., 2006).

1-3-4 PINK1

Loss of function of PINK1 is the second most common cause of early onset autosomal recessive PD (Valente et al., 2004, Corti et al., 2011, Scarffe et al., 2014). As PINK1 encodes a mitochondrial serine/threonine kinase involved in mitochondrial response to cellular and oxidative stress, mutations in this gene link PD to mitochondrial dysfunction (Biskup et al., 2008). This response seems to be mediated by regulation of calcium efflux from the mitochondria, influencing processes such as mitochondrial trafficking (Gandhi et al., 2009, Wang and Schwarz, 2009, Weihofen et al., 2009), ROS formation, mitochondrial respiration efficiency (Liu et al., 2009), and opening of the mitochondrial permeability transition pore (Gandhi et al., 2009). It has revealed that PINK1 response to oxidative stress involves interaction with cell death inhibitors and chaperones (Plun-Favreau et al., 2007, Pridgeon et al., 2007, Wang et al., 2007). Recent studies showed that PINK1 mainly localizes in the outer mitochondria membrane

(OMM) with its C-terminal end and its kinase domain located in the cytosol, suggesting that its PD related substrates might be in the cytosol and/or on the OMM (Zhou et al., 2008). In addition it also has been demonstrated that PINK1 function is linked to fission and fusion machinery in fly and mammalian cell mitochondria (Poole et al., 2008, Yang et al., 2008). Interestingly, PINK1 and Parkin participate in the same pathway with PINK1 functions upstream of Parkin (Clark et al., 2006). Indeed, in *Drosophila* PINK1 is required to recruit Parkin to dysfunctional mitochondria and promote their degradation and (known as mitophagy) PINK1 and Parkin mediate the ubiquitination of the pro-fusion factor Mfn on the outer surface of mitochondria, indicating a role for PINK1/ Parkin in mitochondrial fission/fusion (Ziviani et al., 2010). The PINK1-Parkin role in regulating mitochondrial function suggests that mitochondrial dysfunction is one of the central mechanisms in PD pathogenesis.

1-3-5 DJ-1

DJ-1 is a PD and cancer-associated protein that plays a major role in the oxidative stress response through different signaling pathways. Mutations in the DJ-1 gene (*PARK7*) are the third most common autosomal recessive genetic cause of PD. The DJ-1 gene is located on the short arm of human chromosome 1 (P36.2-p36.3), a region which has been declared as a hot spot of chromosome abnormalities in various tumors (Nagakubo et al., 1997, Taira et al., 2001). It spans a 24kb genomic region and was identified by homozygosity mapping in an extended Dutch family (Taira et al., 2001, van Duijn et al., 2001, Abou-Sleiman et al., 2003, Bonifati et al., 2003). The DJ-1 gene contains eight exons, the first two of which are noncoding and a number of splice variants have been identified (Taira et al., 2001, Abou-Sleiman et al., 2003). The gene encodes a small protein of 189 amino acids that is ubiquitously expressed in the brain and extra cerebral tissues, and is appears to be more abundant in the SN or ventral midbrain area, as compared to the hippocampus and cerebral cortex (Bonifati et al., 2003, Olzmann et al., 2004). DJ-1 is highly evolutionary conserved with orthologues being present in the majority of organisms from human to bacteria (Bonifati et al., 2003). Extensive studies have shown DJ-1 is localized in the cytoplasm, nucleus and the inner membrane space

and matrix of mitochondria (Bonifati et al., 2003, Canet-Aviles et al., 2004, Zhang et al., 2005, Shinbo et al., 2006).

1-3-5-1 DJ-1 structure

DJ-1 is a small protein containing 189 amino acids with a molecular mass of 19.8 kDa (Hod et al., 1999). Structural studies of DJ-1 have shown that this protein forms homodimers and its monomer contains an α/β sandwich fold, comprised of 11 β-strands and 8 α-helices in each monomer allowing for extensive interactions between the two DJ-1 monomers (Moore et al., 2003, Wilson et al., 2003). A seven stranded sheet (β1, β2, β5-β7 and β10,β11) forms a central β-sheet core in which six parallel strands are arranged in a manner similar to the Rossmann fold, a protein structural motif often found in proteins that bind to nucleotides with a differences occurring on the third strand (β5, with only two residues) which is extremely short (Tao and Tong, 2003). However, outside of this β-sheet core β3 and β4 strands assemble as a β hairpin conformation involved in DJ-1 dimerization (Tao and Tong, 2003). Helices H1, H7 and H8 flank one side of the central β-sheet core while helices 2 to 6 (H2-H6) are located on the other side of this core (Huai et al., 2003). In addition, the highly conserved residue His-126 has been indicated as a putative active site for the DJ-1 protein that is formed by β-α-β conformation through αF helix interactions with β8 and β9 strands (Figure 1.3.1) (Tao and Tong, 2003). The dimer interface encompasses β3, α1, α8 and α9 and notably an intermolecular β-sheet is established across the Val-51, Ile-52, and Cys-53 positioned in β3-strand (Honbou et al., 2003). Interaction between α-helices is mainly through hydrophobic bonds while there are distinct hydrogen and ionic interactions (Honbou et al., 2003). A number of these hydrophobic interactions including Met-17, Ile-21, His-126, Pro-127, Pro-158 and Phe-162 are highly conserved across evolution, and Met-17 and Phe-162 are suggested to be fundamental for DJ-1 dimerization as these two residues are the core for hydrophobic interactions (Honbou et al., 2003).

DJ-1 backbone conformational analysis demonstrated that most residues except Cys106 in this protein have energy-favored conformation (in which the total potential energy is globally minimized) (Huai et al., 2003). This unusual structure might be compensated through two hydrogen bounds, one between the Cys106 backbone nitrogen

and the carboxyl oxygen of Ser155 and another across the carboxyl oxygen of Cys106 and the His126 backbone nitrogen (Huai et al., 2003). Structural studies of DJ-1 suggest that the putative active site is located near the interface of the dimer (Tao and Tong, 2003). Indeed, two DJ-1 monomers are arranged in a head to tail fashion, with both active sites located on the opposite side of the dimer structure (Tao and Tong, 2003). Interestingly, the familial PD linked L166P DJ-1 mutation prevents dimer formation, since Leu 166 is located in the middle of α8 strand and mutation in this position breaks α-helical structure and consequently disrupts the DJ-1 dimer interface (Honbou et al., 2003, Olzmann et al., 2004). This disease-causing effect of the L166P mutation indicates functional importance of the DJ-1 C-terminal segment and more significantly highlights that DJ-1 may function only as dimer (Tao and Tong, 2003). In contrast, DJ-1 containing the E64D mutation is still able to form dimers and is structurally similar to the wild type protein (Hering et al., 2004).

Structural analysis and comparison of DJ-1 with other proteins has shown that DJ-1 is most analogous to the monomeric unit of protease I, an intercellular cysteine protease from *Pyrococcus horikoshii* (Honbou et al., 2003). Structural studies of monomeric DJ-1 and its comparison with protease I (a member of the PfpI family), have shown that the connecting loop between β5 and α5 in monomer DJ-1 creates a nucleophile elbow similar to protease I, and that the critical residue C106 in the oxidized form of DJ-1 is located into this loop (Honbou et al., 2003, Tao and Tong, 2003). Furthermore, DJ-1 shows fundamental structural similarity with the C-terminal domain of the catalase hydroperoxidase II (HPII) (Bravo et al., 1999, Horvath and Grishin, 2001). Despite the structural homology between DJ-1/ThiJ/PfpI superfamily and type I glutamine amidotransferase (GAT) domains, which possess a Cys-His-Glu/Asp catalytic triad, it has been reported there are considerable differences between these two proteins (Horvath and Grishin, 2001, Tao and Tong, 2003). Accordingly, the structural diversion of DJ-1 with GAT domains suggests it is unlikely that DJ-1 has a GAT function (Tao and Tong, 2003). Simultaneous mutation of S57R, E96G and H126Y in DJ-1 showed interruption in its interaction with PIASxα (protein inhibitor of activated STAT), which is a negative regulator of the androgen receptor (Takahashi et al., 2001). This study by Takahashi et al. has supported the hypothesis of the functional importance of His126

(Takahashi et al., 2001). Since all these three residues in DJ-1 are highly conserved, it could be speculated these residues bear significant structural roles, although their spatial position in the DJ-1 protein (~ 25Å from each other), suggested it is unlikely these residues are directly associated with PIASxα interaction (Tao and Tong, 2003). Although aspects of DJ-1 function are still unclear, structural studies may shed more light on its functional properties.

Crystal structure of human DJ-1

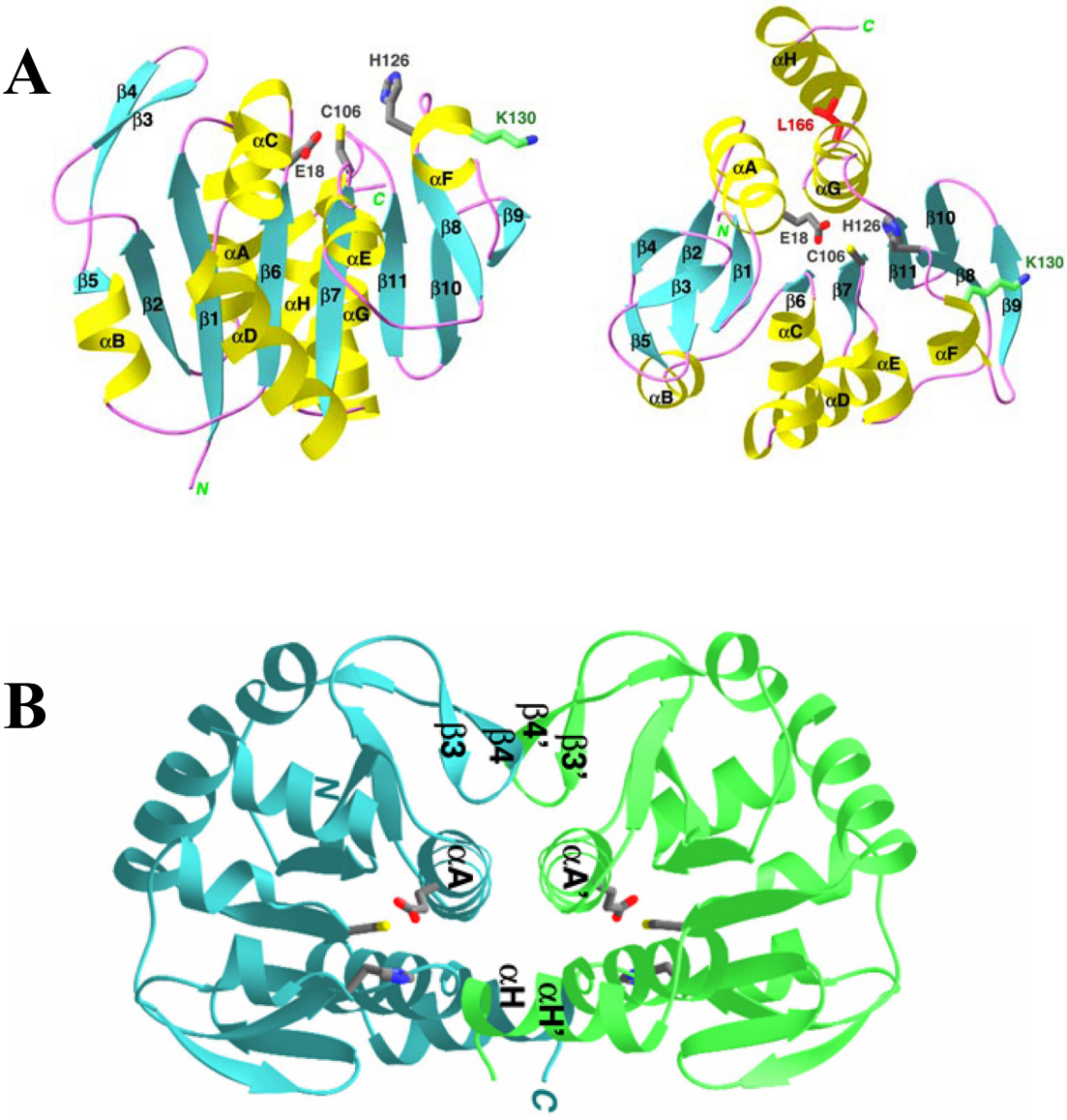

Figure 1.3.1 Crystal structure of the human DJ-1 monomer (A) and homodimer (B). **A)** schematic drawing of the DJ-1 structure in two different views that represents β-strands, α-helices and some the important functional residues. **B)** 3D structural study of human DJ-1 demonstrated that DJ-1 forms homodimer and these data were confirmed by biological approaches (adapted from (Tao and Tong, 2003, Canet-Aviles et al., 2004)).

1-3-5-2 DJ-1 function

DJ-1 was first identified as a novel oncogene in association with activated ras (Nagakubo et al., 1997). High expression of DJ-1 is a causative risk factor for several cancers including prostate cancer, breast cancer, ovarian carcinoma and lung carcinoma (MacKeigan et al., 2003, Hod, 2004, Lev et al., 2006, Davidson et al., 2008). While excess DJ-1 leads to cancer, DJ-1 loss of function triggers early onset Parkinson's disease (Ariga et al., 2013).

DJ-1 plays a role in several cellular pathways and processes including cell survival, cellular transformation, response to oxidative stress, RNA binding, androgen receptor signalling, protection from glyoxals and spermatogenesis and fertilization (Hod et al., 1999, Mitsumoto and Nakagawa, 2001, Takahashi et al., 2001, Okada et al., 2002, Lev et al., 2006, Lee et al., 2012). Below I discuss some of the cellular functions that have associated with DJ-1.

1-3-5-2-1 Mitochondrial function of DJ-1

DJ-1 functions as a promoter for mitochondrial stabilizing anti-oxidant and anti-apoptosis mechanisms in non-astrocytic primary cells and cell lines (Canet-Aviles et al., 2004, Taira et al., 2004, Junn et al., 2005, Xu et al., 2005, Zhou and Freed, 2005, Clements et al., 2006, Aleyasin et al., 2007, Liu et al., 2008a, Blackinton et al., 2009). Larsen et al. showed that DJ-1 knocked-down in astrocytes caused a significant reduction in mitochondrial motility and a trend towards decreased mitochondria fission (Larsen et al., 2011). It has also been found that DJ-1 is over-expressed in reactive astrocytes in PD and in other neurodegenerative diseases but not in neurons (Rizzu et al., 2004, Mullett et al., 2009). Although the role of DJ-1 in maintaining mitochondrial function has been established it is not clear how DJ-1 regulates this process, and how mitochondrial dysfunction is induced by DJ-1 deficiency. Mutations in DJ-1 result in mitochondrial fragmentation through impairment of the complex I assembly pathway, the same process that is heavily implicated in PD pathogenesis (Heo et al., 2012). Work by Heo et al. not only clarified that expression of complex I proteins is significantly reduced in DJ-1 null dopaminergic neuronal cells, but also showed that basal respiration was decreased by 23 % in those cells in comparison with cells treated with rotenone

(Heo et al., 2012). DJ-1 null cells also showed a decrease in mitochondrial membrane potential, which taken together with the other data suggested a disruption of ATP production in the mitochondrial respiratory chain (Heo et al., 2012). It has also been determined that DJ-1 deficiency causes impairment in mitochondrial connectivity, fusion rates, membrane potential, respiratory capacity and ROS buffering in non-astrocytic cell *in vitro* (Ved et al., 2005, Blackinton et al., 2009, Hao et al., 2010, Irrcher et al., 2010, Krebiehl et al., 2010, Thomas et al., 2011). However, the mitochondrial function of DJ-1 and how it could be relevant to PD pathogenesis needs to be further evaluated.

1-3-5-2-2 DJ-1 and oxidative stress

Several studies have demonstrated that a lack of DJ-1 increases the sensitivity of cells to ROS (Thomas et al., 2011). Although the precise role of DJ-1 in oxidative stress is unclear, the translocation of wild type DJ-1 to the outer mitochondrial membrane in response to oxidative stress is believed to be neuroprotective (Canet-Aviles et al., 2004). Furthermore, accumulation of the acidic isoform of DJ-1 (pI 5.8) following oxidative stress, leads to speculation that DJ-1 is protective under oxidative stress (Canet-Aviles et al., 2004). Mitsumoto et al. have hypothesized that DJ-1 might be directly oxidized by free radicals (Mitsumoto and Nakagawa, 2001). This hypothesis was supported by Kinumi et al. who showed that the pI of DJ-1 shifts (from 6.2 to 5.8) after oxidation which is consistent with cysteine sulfinic acid formation (Kinumi et al., 2004). Canet-Aviles et al. demonstrated that only the cysteine residue at position 106 (C106) in DJ-1 is oxidized to form cysteine sulfinic acid, with C106A mutations preventing the formation of the oxidized isoform formation of DJ-1 in cells (Canet-Aviles et al., 2004, Kinumi et al., 2004). Indeed, DJ-1 plays a role in response to oxidative stress by regulating signal transduction associated with oxidative stress response and cell death (Saito, 2014). However, recent studies also indicated that DJ-1 functions as an oxidative stress sensor to change expression level of genes associated with anti-oxidative defense (Kahle et al., 2009, Wilson, 2011, Ariga et al., 2013). For instance, it has been reported DJ-1 is able to control oxidative stress insults by directly regulating expression of Cu/Zn superoxide desmutase (SOD1) which is a metalloenzyme that catalyzes the disproportionation of superoxide via ErK1/2-ELK1 pathway (Wang et al.,

2011). Taken together, DJ-1 exposes its anti-oxidative function through regulating various signalling pathways that will be explained in more details in following sections of this chapter.

1-3-5-2-3 DJ-1 and autophagy

DJ-1 was initially shown to influence autophagy during hypoxia by regulating microtubule-associated protein light chain 3 (LC3-I) processing and Sequestosome 1 (SQSTM1/p62) turnover (Vasseur et al., 2009). Silencing of DJ-1 in U2OS cells (human osteosarcoma) causes early stages of autophagy to occur spontaneously, and decreases the stability of both LC3-I and LC3-II upon exposure to hypoxia (Vasseur et al., 2009). However, the impact of these changes on autophagy as a whole is still unclear (Vasseur et al., 2009). Silencing of DJ-1 in U2OS cells also reduces the autophagy-associated clearance of p62 during hypoxia, while DJ-1 over-expression reduces p62 levels in neuronal cell. As p62 is involved in the formation of cytoplasmic proteinaceous inclusions such as LBs in PD, it has been suggested that changes in its turnover due to altered DJ-1 expression/activity may contribute to disease pathologenesis (Pursiheimo et al., 2009, Vasseur et al., 2009, Ichimura and Komatsu, 2010, Gao et al., 2012). In addition, DJ-1 has been reported to be neuroprotective by enhancing autophagy resulting in a more efficient clearance of damaged mitochondria and decreasing apoptosis in dopaminergic neuron cells (MN9D) (Gao et al., 2012). DJ-1 impacts upon autophagy by triggering the ERK1/2 pathway and repressing mTOR (Gao et al., 2012). It also has been shown that DJ-1 over-expression in neuronal cells decreased phospho-mTOR, a negative autophagy regulator, up-regulated beclin 1 which is involved in autophagosomes formation, and augmented the ratio of LC3II, autophagic marker to the inactive precursor LC3I (Gao et al., 2012). Gao et al. have observed that over-expression of DJ-1 in SN of rats lead to long-term reduction in PD symptoms such as depressive-like behaviour (Gao et al., 2012). Indeed, recent work by Miller-Fleming et al. has found deletion of *Hsp31* gene (a yeast DJ-1 homolog) impairs autophagy induction upon carbon starvation in yeast (Miller-Fleming et al., 2014).

1-3-5-2-4 DJ-1 as protease

DJ-1 belongs to the DJ-1/ThiJ/Pfp superfamily and thus shows sequence homology to proteins that contain a ThiJ domain, including protein chaperones, catalyses, proteases and the ThiJ kinases (Halio et al., 1996, Mizote et al., 1999, Du et al., 2000, Horvath and Grishin, 2001). The structure of DJ-1 is similar to the monomeric subunit of protease I, a cysteine protease from *Pyrococcus horikoshii,* but possesses an additional α-helix at the C-terminal region that functions to suppress the DJ-1 catalytic domain (Honbou et al., 2003, Lee et al., 2003). Interestingly, it has been reported that the C-terminal region of DJ-1 is cleaved in response to oxidative stress in *vitro* and in cultured cells (Ooe et al., 2006, Chen et al., 2010). The c-abl oncogene product 1 (ABL1), kinesin family member 1B (KIF1B) and Transthyretin, a causative protein in several amyloidoses, are three proteins that have been investigated as targets for the DJ-1 protease activity (Koide-Yoshida et al., 2007, Mitsugi et al., 2013). Work by Koide-Yoshida et al. has revealed that DJ-1 α-helix 9 and residue C106 are critical for this protease activity (Koide-Yoshida et al., 2007).

1-3-5-2-5 DJ-1 as a chaperone protein

Several studies on DJ-1 biological function have investigated its redox-sensitive chaperone activity (Olzmann et al., 2004, Deeg et al., 2010, Sajjad et al., 2014). Work by Shendelman et al. showed that DJ-1 effectively prevents α-Syn aggregation into protofibrils and neurofilament light subunit (NFL) with the PD causative mutation L166P in DJ-1 abolishing this activity (Shendelman et al., 2004). Additionally, a highly conserved and reactive cysteine residue at position 53 located at the dimer interface of DJ-1 plays a critical role in this reaction (Shendelman et al., 2004). Zondler et al. have revealed for the first time that DJ-1 can directly interact with monomeric α-Syn in vitro and living cells which supports the notion that interaction of these two proteins is an early event in the α-Syn aggregation process (Zondler et al., 2014). In this work they also demonstrated that DJ-1 decreases α-Syn dimerization, while familial PD mutations of DJ-1 abrogate this interaction and consequently fail to antagonise α-Syn dimerization (Zondler et al., 2014). Furthermore, DJ-1 chaperone activity is able to modulate mutant huntingtin aggregation in vitro and in vivo in various Huntington's disease models (Saj-

jad et al., 2014). Work by Yamashita et al. postulated that complex formation between mutant SOD1 and DJ-1 might imply oxidative stress induced chaperone activity of DJ-1 to prevent SOD1 aggregation (Yamashita et al., 2010). The idea of copper chaperone activity of DJ-1 is supported by Girotto et al. that found DJ-1 is able to activate SOD1 catalytic function through transferring copper ions from its C106 residue (Girotto et al., 2014). They also suggested under critical conditions DJ-1 may act as a copper chaperone for SOD1 as a backup and in an independent pathway from copper chaperone for SOD1 (CCS) (Girotto et al., 2014). However, although extensive evidence indicate that chaperone-like activity of DJ-1 is dependent on its oxidation, work by Zondler has also suggested that DJ-1 SUMOylation may play a role on its chaperone function (Shendelman et al., 2004, Zhou et al., 2006, Zondler et al., 2014).

1-3-5-2-6 DJ-1 and transcriptional regulation

DJ-1 acts as a cofactor for a subset of transcription factors, repressing or stimulating their target gene expression (Yamaguchi et al., 2012). DJ-1 influences diverse cell functions through regulating various transcription factors including androgen receptor, p53, polypyrimidine tract-binding protein associated splicing factor (PSF), Keap 1 and inhibitor for nuclear factor erythroid-2 related factor 2 (Nrf2) (Takahashi et al., 2001, Niki et al., 2003, Shinbo et al., 2005, Clements et al., 2006, Zhong et al., 2006, Fan et al., 2008b). Regulation of Nrf2, p53, PSF by DJ-1 is important in controlling dopamine synthesis and the response to oxidative stress (Ariga et al., 2013). Nrf2 is a master transcription factor participating in the cells response to oxidative stress and detoxification (Clements et al., 2006). In oxidative stress conditions DJ-1 stimulates the expression of antioxidative stress genes by translocating Nfr2 from the cytoplasm to the nucleus (Clements et al., 2006).

DJ-1 also elicits a neuroprotective role in oxidative stress by negatively regulating p53 which is a tumour suppressor involved in apoptosis and mitochondrial homeostasis (Shinbo et al., 2005, Fan et al., 2008b, Kato et al., 2013). Work by Giaime et al. indicated that DJ-1 physically interacts with p53, and this interaction is abrogated by pathogenic DJ-1 mutants (Giaime et al., 2010). Interestingly, DJ-1 protein levels are

post-transcriptionally negatively regulated by p53 while its dimerization is independent of p53 status (Vasseur et al., 2012).

DJ-1 stimulates human tyrosine hydroxylase (TH), which is one of two critical enzymes required for dopamine synthesis, by sequestering the PSF transcription factor (a negative regulator of TH gene expression) away from the human TH gene promoter (Zhong et al., 2006). Furthermore, DJ-1 triggers the enzymatic activity of both enzymes involved in dopamine synthesis, TH and L-DOPA carboxylase (DDC), through direct interactions, dependent upon oxidative stress levels (Ishikawa et al., 2012). This process may be disease relevant as over-expression of DJ-1 in the rat SN attenuates the effect of the rotenone (mitochondria complex 1 inhibitor) treatment by increasing levels of the TH (Gao et al., 2012). DJ-1 also up-regulates vesicular monoamine transporter 2 (VMAT2) gene expression, which packs dopamine into synaptic vesicles, and stimulates its activity via protein-protein interactions (Ishikawa et al., 2012). As VMAT2 can protect neurons from oxidized dopamine-induced damage by re-uptaking excess dopamine into synaptic vesicles, DJ-1 could exert its neuroprotective feature by contributing to this reaction (Ariga et al., 2013). Recent work by Yamagushi et al. has established that low-density lipoprotein receptor (LDLR) gene is another target for DJ-1 as a transcriptional regulator (Yamaguchi et al., 2012). This was the first time DJ-1 was reported to be involved in fatty acid synthesis metabolism.

1-3-5-2-7 DJ-1 and survival pathways

In 2005 DJ-1 was reported to play a role in the phosphatidylinositol-3 kinase (PI3K) survival pathway (Kim et al., 2005a). Activation of PI3K by epidermal growth factor (EGF) triggers phosphorylation of phosphatidylinositol (4,5)-bisphosphate (PIP2) to form phosphatidylinositol (3,4,5)-trisphosphate (PIP3), which recruits PIP3-dependent kinase (PDK) (Burgering and Coffer, 1995, Fruman et al., 1998). PDK consequently phosphorylates and activates the survival kinase, protein kinase B (PKB/Akt) (Alessi et al., 1997, Stokoe et al., 1997). The tumor suppressor PTEN negatively regulates PI3K pathway by dephosphorylating PIP3 (.Maehama and Dixon, 1998, Myers et al., 1998, Stambolic et al., 1998, Sun et al., 1999). Gain-of-function screens for PTEN modifiers in *Drosophila melanogaster* found that DJ-1 promotes the Akt pathway by suppressing

PTEN function (Kim et al., 2005a). DJ-1 has been shown to play a central role in Akt phosphorylation and to modulate Akt translocation to membranous fractions following oxidative stress (Aleyasin et al., 2010) (Figure 1.3.2).

DJ-1 has also been shown to implement its cytoprotective role in oxidative stress by sequestering Daxx and ASK1 (apoptosis signal-regulating kinase 1) and consequently inhibiting the Daxx/ASK1 cell-death signalling pathway (Junn et al., 2005). Activated ASK1 triggers c-Jun NH2-terminal kinase (JNK) and p38, consequently leading to cell apoptosis through mitochondria-dependent caspase activation (Ichijo et al., 1997, Saitoh et al., 1998, Hatai et al., 2000, Tobiume et al., 2001). ASK1 is activated in response to different cytotoxic stresses including TNF, Fas and ROS and leads to JNK activation which causes proteasome dysfunction and ER-stress-induced cell death, ultimately contributing to neurodegenerative diseases (Tobiume et al., 2001, Nishitoh et al., 2002).

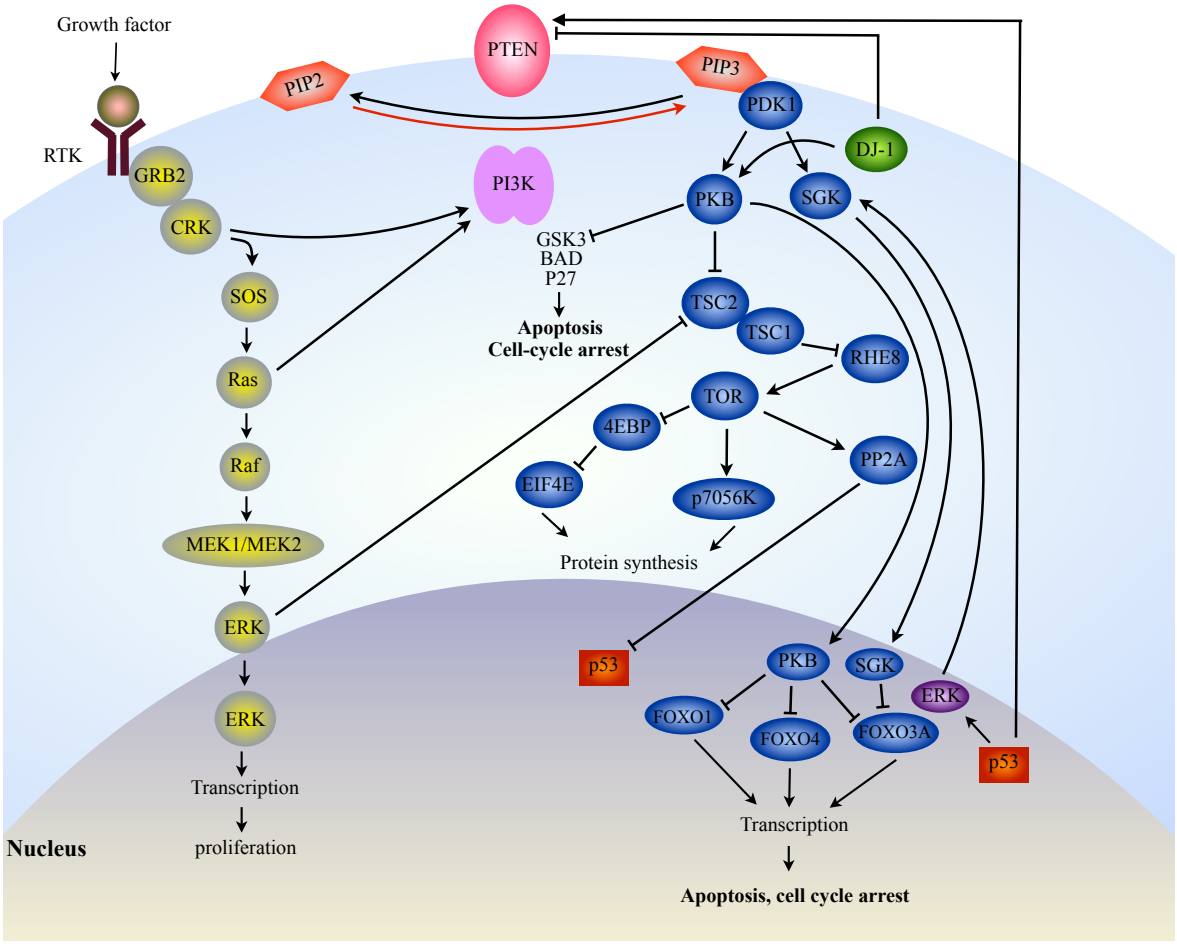

Figure 1.3.2 Model for the influence of DJ-1 on PI3K and PKB (also known as AKT) through the tumor suppressor PTEN. DJ-1 plays a direct role in cell survival and apoptosis through phosphorylation of PKB, indirectly effecting PI3K function (adapted from (Cully et al., 2006)).

1-3-5-2-8 DJ-1 and inflammation

The anti-inflammatory function of DJ-1 might be another prominent neuroprotective facet of this protein that is associated with PD since brain inflammation through astrocytes and microglia has been reported to be a PD risk factor (Drouin-Ouellet and Cicchetti, 2012, Kim et al., 2013). Interestingly, several studies revealed DJ-1 is strongly up-regulated in reactive astrocytes in PD brain that suggests a role in glia (Bandopadhyay et al., 2004, Neumann et al., 2004). Moreover, astroglial DJ-1 up-regulation has been observed in chronic neurodegenerative diseases and in an α-Synuclein mouse model of PD (Neumann et al., 2004). Work has also shown that DJ-1 regulates astrocyte neuroinflammatory response in a ROS and p38 ^{MAPK} dependent manner (Waak et al., 2009). Kim et al. demonstrated that DJ-1 plays a role as a scaffold protein and by promoting SHP-1 (Src-homology 2 [SH2] domain-containing protein tyrosine phosphatase-1) interaction with phosphorylated and unphosphorylated STAT1 (signal-transducer and activator of transcription) restricts excessive and prolonged STAT1 phosphorylated status and consequently attenuates IFN-γ (interferon-gamma)-induced inflammation (Kim et al., 2013). Thus, DJ-1 can act as neuroprotectant by repressing excessive brain inflammation in injured brain (Kim et al., 2013).

1-3-5-2-9 DJ-1 and caspases

Sequence analysis of the human DJ-1 protein has shown it harbours two putative caspase-6 recognition sites at positions Asp149 (D149) and Asp60 (D60) (Giaime et al., 2010). Caspase 6, which plays an important role in the cleavage of the huntingtin protein in Huntington's disease (HD), cleaves DJ-1 in TSM1 neurons (Telencephalon Specific Mouse 1) and a neuroblastoma cell line undergoing staurosporin (STS) (a protein kinase inhibitor) or 6-hydroxydopamine-mediated apoptosis (Graham et al., 2006, Robert et al., 2012). Although D149A mutations in DJ-1 completely abolish its proteolysis by caspase-6, L166P DJ-1 mutations increase its susceptibility to the caspase-6 cleavage (Giaime et al., 2010). It has been found that cleaved DJ-1, but not the full-length DJ-1, accumulates in the nucleus in various cell lines and this seems to be critical for its pro-apoptotic function (Robert et al., 2012). Furthermore, data using ROS dye dichloro-dihydrofluorescein diacetate (DCFDA) followed by cytometry has clarified the

protective role of WT DJ-1 in reduction of ROS in cells over-expressing WT DJ-1 treated with 1-methyl-4-phenylpyridinium (MPP+), in contrast with cells over-expressing cleaved DJ-1 (DJ-1 Nt) in the identical condition (Robert et al., 2012). Surprisingly, the percentage of oxidised DJ-1 versus total DJ-1 in cells stably over-expressing DJ-1 Nt is approximately 3 times higher than cells over-expressing WT DJ-1 in MPP+ treatment conditions (Robert et al., 2012). In contrast, cells over-expressing DJ-1 Ct not only significantly decreased caspase-3 activation in non-stimulated and stimulated cells by STS and natural toxin 6OHDA which is frequently utilised to mimic PD pathology but also reduced p53 transcriptional activity (Giaime et al., 2010). As DJ-1 levels are increased by inhibiting its cleavage utilising a caspase inhibitor (zVAD-fmk), it is speculated that DJ-1 exhibits a constitutive turnover depending on caspase activation (Robert et al., 2012). Furthermore, analysis of sporadic PD patients and control group brains has found an inverse correlation between DJ-1 and caspase-6 levels in normal and affected brains (Giaime et al., 2010).

1-3-5-2-10 DJ-1 and metal cytotoxicity

A recent study by Bjorkblom and et al. has explored new human DJ-1 cytoprotective features against metal induced toxicity (Bjorkblom et al., 2013). There is ample evidence that various metals such as zinc, copper and mercury may play a role in PD pathogenesis (Bjorkblom et al., 2013). It has been reported that levels of zinc, copper and iron in the basal ganglia and SN of PD patients are altered compared to controls (Dexter et al., 1991). Since iron is involved in oxidative stress and accumulates in the SN of PD patients, it could be hypothesized that iron plays role in PD (Dexter et al., 1987, Dexter et al., 1991). Moreover, increased levels of mercury in the blood and urine are a risk factor for developing PD (Ngim and Devathasan, 1989). Bjorkblom and et al. have shown that human DJ-1 binds to both copper and mercury and consequently protects cells from copper and mercury induced cytotoxicity, while some PD-linked mutations of DJ-1 (A104T and D149A) lose this ability (Bjorkblom et al., 2013). In addition to binding copper, DJ-1 promotes SOD1 activity by supplying its copper cofactor (Xu et al., 2010, Puno et al., 2013). Moreover, biochemical studies of the DJ-1 structure demonstrated that the stable homodimer is critical for its function as a copper carrier

(Puno et al., 2013). Accordingly, these findings validate the assumption that genetic factors may increase susceptibility of the individuals to environmental toxin induced cell death, and the ensuing development of PD.

1-3-5-3 PD familial and functional mutations of DJ-1

PD-linked mutations in the DJ-1 gene alter the sequence of the intact protein and consequently change the physicochemical properties which are fundamental to its functions (Malgieri and Eliezer, 2008). Approximately 28 mutants of DJ-1 have been discovered but only some of them have a clear pathogenetic nature (Bonifati et al., 2003). Thirteen mutations in DJ-1 gene have been identified in PD patients (Bonifati et al., 2003, Annesi et al., 2005). L166P, (Bonifati et al., 2003), M26I and D149A (Abou-Sleiman et al., 2003), A104T (Hague et al., 2003), and E64D (Hering et al., 2004), are DJ-1 point mutations suggested to be associated with familial forms of PD. In addition, Bonifati et al. in 2003 identified a large genomic deletion encompassing exons 1-5 of the DJ-1 gene in a Dutch kindred. Interestingly, some of these mutations, such as L166P, significantly decrease DJ-1 stability through the ubiquitin-proteasome pathway, while E64D which is a highly conserved DJ-1 mutation on the surface of the protein is highly stable (Miller et al., 2003, Hering et al., 2004). In vitro studies on L166P demonstrated that this point mutation severely perturbed DJ-1 secondary structure, as L166P DJ-1 only exists as a monomer in solution, and causes loss of protease and chaperone activity of DJ-1 (Tao and Tong, 2003, Olzmann et al., 2004, Shendelman et al., 2004). Moreover, the L166P DJ-1 mutant also is not able to protect cells from oxidative stress induced cell death (Gorner et al., 2004, Martinat et al., 2004, Taira et al., 2004, Kim et al., 2005b).

In contrast, the E64D DJ-1 mutant is the only DJ-1 mutation in which the crystal structure of the protein is identical to the wild type, although its turnover rate seems to be slightly higher than wild type protein (Gorner et al., 2004, Hering et al., 2004). Indeed, it has been reported that this mutation is located in a side chain at the exposed surface of the protein and does not alter the CD spectrum or melting curve of DJ-1 (Malgieri and Eliezer, 2008). A recent study by Repici et al. has shown that E64D DJ-1 mutant dimerization in living cells is comparable to the WT DJ-1 although this mutant

behaves differently from WT protein in response to oxidative stress conditions (Repici et al., 2013). E64D, M26I, D149A and A104T mutants bear the capacity to form homodimers and to heterodimerise with wild type DJ-1 (Blackinton et al., 2005). Even though some studies have reported M26I is able to dimerize, recent work by Repici et al. has revealed that the M26I mutant behaves similarly to L166P DJ-1 mutant in living cells (Repici et al., 2013). In this study they also showed that the decrease in M26I dimerization is due to a very low level of the M26I protein (Repici et al., 2013).

Causative DJ-1 mutations have been conjectured to abrogate DJ-1 function through two possible pathways: first, by disrupting or decreasing stability of DJ-1 dimerization such as L166P and M26I mutants (Hulleman et al., 2007, Malgieri and Eliezer, 2008, Repici et al., 2013), and secondly, like the D149A and A104T mutants, by interrupting the protein geometry around Cys106 which is fundamental for DJ-1 activities as a chaperone and anti-oxidant (Malgieri and Eliezer, 2008). However, the molecular basis of how these point mutations in DJ-1 change its function still requires investigation.

1-3-5-4 Post-translational modifications of DJ-1

DJ-1 is post-translationally modified by sumoylation, S-nitrosylation, and phosphorylation (Ito et al., 2006, Shinbo et al., 2006, Rahman-Roblick et al., 2008). Sumoylation is a fundamental post-translational modification involved in the pathogenesis of several neurodegenerative diseases such as Alzheimer's disease (AD) (Li et al., 2003, Fei et al., 2006, Fan et al., 2008a). Work by Takahashi et al. in 2001 showed DJ-1 is conjugated with SUMO-1, a small ubiquitin-like modifier, at Lys130 by PIASxα and PIASy and this modification is essential for DJ-1 functions in cell transformation and growth (Takahashi et al., 2001). Moreover, DJ-1 sumoylation also alters DJ-1 localization as non-sumoylated DJ-1 mutant (K130R) is mostly localized in the cytoplasm while WT DJ-1 distributes both in nucleus and cytoplasm (Fan et al., 2008a). Studies on DJ-1 sumoylation and its anti-oxidant activity showed that SUMO-1 conjugation occurs in an ROS level dependent manner, and sumoylated DJ-1 is active as a ROS scavenger (Shinbo et al., 2006). Interestingly, work has also indicated that L166P DJ-1 and K130RX DJ-1 (an artificial mutant in which three other amino acid residues, S57R,

E96G and H126Y were changed), are improperly sumoylated. These mutants result in DJ-1 misfolding and abnormal aggregation (Takahashi et al., 2001, Shinbo et al., 2006). In addition, the K130R mutation in DJ-1 abrogates its regulatory function on p53 transcriptional activity and its protective role against cell death (Fan et al., 2008a).

S-nitrosylation is a reversible post-translational protein modification obtained by the covalent attachment of a nitrogen monoxide group to the thiol group in Cys residues in proteins, thus modulating the function of a wide variety of proteins such as metalloprotease-9 and GAPDH (Stamler et al., 1992, Gu et al., 2002, Hara et al., 2005, Ito et al., 2006). Interestingly, protein S-nitrosylation is expedited under oxidative stress conditions (Chung et al., 2004, Yao et al., 2004). S-nitrosylation has been shown to be involved in PD by modulating Parkin ubiquitin ligase activities (Chung et al., 2004, Yao et al., 2004). Human DJ-1 harbours three Cys residues (Cys 46, Cys 53, Cys 106) that play a central role in DJ-1 structure and function (Ito et al., 2006). Work by Ito et al. indicated only the Cys 46 and Cys 53 residues in DJ-1 are susceptible to S-nitrosylation and the effects of this modification on DJ-1 structure and function require further investigation (Ito et al., 2006). Since Cys 46 contributes to preserving DJ-1 structure at the dimer interface, it is tempting to consider that S-nitrosylation plays a critical role in DJ-1 dimerization and subsequently in its function (Ito et al., 2006).

DJ-1 has recently been shown to be modified with 4-hydroxy-2-nonenal (4-HNE) at Lys-32 (isoforms 4 and 6) and Lys-62 (isoform 6) that is unique to PD diagnosis and severity and could be applied as a PD biomarker (Lin et al., 2012). 4-hydroxy-2-nonenal (HNE) is an α,β unsaturated aldehyde which is one of the main products of membrane peroxidation and is able to react with proteins to create stable adducts (Colton and Gilbert, 1987). An increase in concentration of HNE in the plasma, cerebrospinal fluid (CSF) and in nigral neurons in PD patients suggests HNE may be involved in the pathogenesis of PD (Yoritaka et al., 1996, Selley, 1998).

Even though the actual function of the 4-HNE modification in DJ-1 remains to be characterized it has been speculated that HNE-modified DJ-1 (indicative of damaged protein) is targeted for degradation by the proteasome or lysosome systems more readily (Ishimura et al., 2008, Lin et al., 2012). In 1997 Morikawa et al. revealed that HNE-modified proteins were localized in mitochondrial fractions of preeclamptic placenta

which were components of complex I (Morikawa et al., 1997). Furthermore, it has been demonstrated that activity of the complex I is decreased by HNE in a dose-dependent manner (Yoshino et al., 1997). Since DJ-1 is required for mitochondrial complex I assembly (Heo et al., 2012), HNE modified DJ-1 may have an effect on mitochondrial function.

Phosphorylation is one the most common protein modifications that modulates protein function (Rahman-Roblick et al., 2008). DJ-1 has been reported to be phosphorylated at 4 residues (T19, Y67, Y139, and Y141) (see PhosphoSite Plus database, http://www.phosphosite.org/proteinAction.do?id=4095), although the consequences of these modifications on DJ-1 functions, stability and localization are still unknown. Work by Rahman-Roblick et al. in 2008 showed DJ-1 is phosphorylated upon activation of p53, suggesting p53 negatively modulates DJ-1 activities by phosphorylation and subsequently facilitates apoptosis (Rahman-Roblick et al., 2008). Marcondes et al. have also indicated that DJ-1 phosphorylation is associated with p53 and apoptosis (Marcondes et al., 2010). In this study DJ-1 localization and its interaction with p53 have been considered in absence and presence of stroma, which revealed DJ-1 localization shifted from nucleus to the cytoplasm in presence of stroma and subsequently enhanced apoptosis sensitivity by increasing p53 activation (Marcondes et al., 2010). Indeed, in the absence of stroma in KG1a cells, proteins involved in cell survival, such as DJ-1, are highly phosphorylated which correlates with decreased mRNA and protein levels of p53 (Marcondes et al., 2010). Therefore, it could be speculated DJ-1 phosphorylation plays a role in apoptosis.

Studies on phosphorylation dynamics in human embryonic stem cell (hESC) differentiation revealed DJ-1 is phosphorylated at Thr-19 (Rigbolt et al., 2011). Interestingly, in 2012 Lin et al. reported DJ-1 phosphorylation at T19 and Y67 play a role in PD pathogenesis and could be used as a PD biomarker (Lin et al., 2012). Moreover, the Y139 and Y141 residues of DJ-1 have been identified by mass spectrometry (MS) studies aimed at identifying phosphotyrosine peptides, even though none of these phosphorylation sites have so far been studied in associated with DJ-1 function and localization (see PhosphoSite Plus database, http://www.phosphosite.org/proteinAction.do?id=4095).

DJ-1 has two other putative phosphorylation sites (T140 and S142) (see PhosphoSite Plus database, http://www.phosphosite.org/proteinAction.do?id=4095).

Lin et al. reported that in whole blood there are 7 isoforms of DJ-1 with various post-transcriptional modifications such as phosphorylation, oxidation and 4-HNE modifications, which alter the intrinsic protein charge (Lin et al., 2012). Interestingly, the expression level of each DJ-1 isoform vs. total DJ-1 is altered in AD and PD cases in comparison to controls, despite there being no clear correlation between level of any of these isoforms and PD severity (Lin et al., 2012). However, determining the physiological effects of post-translational modifications of DJ-1 on its function and as well as its role in PD pathogenesis, may shed light into the mechanisms underlying PD and also indicate novel therapeutic strategies for this devastating disorder.

1-4 Studying protein-protein interaction in living cells using Bimolecular fluorescence complementation (BiFC)

Several neurodegenerative diseases are characterised by protein misfolding and aggregation, ultimately leading to neurotoxicity. Despite the toxic nature of protein aggregates in these diseases being controversial, accumulation of misfolded proteins in those disorders are unavoidable. Studying protein-protein interaction in living cells is fundamental to elucidate protein dynamics, modulation by physiological changes, localization and function (Shin et al., 2009, Goncalves et al., 2010). The work in my thesis relies heavily on the bimolecular fluorescence complementation (BiFC) method in order to study protein-protein interactions. The development and use of BiFC, employing optical microscopy and live-cell imaging, has provided valuable insights into protein-protein interactions, and recently provided a mechanism by which to explore proteins associated with neurodegenerative disease. BiFC provides spatial and temporal resolution and can also be applied in a physiological relevant environment which is valuable in the context of neurodegenerative diseases by facilitating visualisation of dimeric and oligomeric species that are speculated to be toxic to neuronal cells in the brain (Goncalves et al., 2010).

The structure of fluorescent proteins like green fluorescent protein (GFP) comprises 11 antiparallel β-strands that creates a β-barrel, an α-helix which is located inside of this structure and harbours chromophore and several short helical structures (Figure 1.4.1) (Yang et al., 1996). It has been demonstrated by several studies that fluorescent proteins can be split at a loop or within a β-strand to generate non-fluorescent fragments that can be fused to proteins of interest (Kodama and Hu, 2012). The BiFC assay is based on the fusion of two non-fluorescent fragments of a fluorescent protein (reporters) to the proteins of interest (putative interaction partners). As the proteins of interest interact, the reporter fragments are brought together, fold into a quasi-native structure and re-establish the activity of the fluorescent protein (Chen et al., 2006, Kerppola, 2006). GFP (green), CFP (cyan), YFP (yellow) and RFP (red) are among the diverse reporter proteins which have been successfully employed in BiFC studies (Chu et al., 2009).

Circular permutation of proteins is an approach to change the order of amino acids in a protein sequence in which the original N-terminus and C-terminus of a protein are ligated and a new N-terminus and C-terminus are generated via splitting the circularized protein in internal structural regions (Yu and Lutz, 2011). One of the applications of this technique is to assess insertion position in the proteins without perturbing the overall structure of the protein (Yu and Lutz, 2011, Kodama and Hu, 2012).

Circular permutation studies on GFP showed that this protein could be split at positions in the loop between the 6^{th} and 7^{th} β-strands, in the 7^{th} β-strand, in the loop between the 7^{th} and 8^{th} β-strands, in the 8^{th} β-strand, and in the loop between the 8^{th} and 9^{th} β-strands (Baird et al., 1999). These positions were successfully employed to split several fluorescent proteins for the development of BiFC. In this project I used DJ-1 BiFC constructs: each construct consists of full length WT or mutant DJ-1, a short linker $(4Gly\text{-}ser)_2$ and N-terminal GFP fragment (amino acids 1-173, split in the loop between the 8^{th} and 9^{th} β-strands) or C terminal CFP fragment (amino acids 155-238, split in the loop between the 7^{th} and 8^{th} β-strands.

BiFC was first introduced in 2002 when it was used to characterize protein-protein interactions between basic Leucine zipper and Rel family transcription factors

(Hu et al., 2002). BiFC has been exploited to study multiple protein-protein interactions, which provides a unique opportunity to investigate subcellular protein complex formation, dynamic changes in multiple protein complexes and the regulation of association between interacting proteins (Hu and Kerppola, 2003, Vidi et al., 2008, Gehl et al., 2009).

BiFC overcomes some of the disadvantages of several techniques that were previously utilized in protein-protein interaction studies such as the size of the protein complexes, and the optical resolution of microscopes. In the neurodegeneration field, the study of the protein interactions involved in the formation of inclusion bodies is vital for understanding the molecular pathways involved in neurodegenerative disorders including AD, PD and HD. Indeed, expansion and development of a novel tool such as BiFC paves the way for clarifying the molecular pathways involved in neurodegenerative diseases. Furthermore, BiFC is an extremely powerful tool in the discovery of interaction partners but also in the field of sub-cellular localization studies (Chen et al., 2006). Lastly, since BiFC can be used in a wide variety of model organisms, from bacteria to mammalian cell lines, it is a useful tool for high throughput genetic or chemical screens (Bracha-Drori et al., 2004, Chen et al., 2007, Gehl et al., 2009). Although the BiFC assay is a powerful tool to study protein-protein interactions in physiological condition, it has some limitations that deserve to be mentioned here. It has been shown that the formation of a BiFC complex occurs in a multistep pathway in vitro, initiated by the contact of the proteins fused to the non-fluorescent fragments. This is a reversible phenomenon and can be influenced and competed by alternative interaction partners. Once the complex is stabilized by the association of the fluorescent fragments, it becomes resistant to competition by alternative interaction partners. Although this characteristic of BiFC provides a detection of weak and transient complexes without interference of non-specific interaction, this irreversibility limits the application of the BiFC assay for studying dynamic interactions (Hu et al., 2002). However, some studies showed that the BiFC complex is reversible as they detected rapid changes in BiFC signal (Schmidt et al., 2003, Guo et al., 2005). Another limitation of this assay is that fluorescent fragments have an intrinsic ability to associate with each other independently from the interaction of the proteins fused to the same fragments, which could cause background signal

(Zhang et al., 2004, Cabantous et al., 2005). Finally, in this assay the time required for fluorophore maturation (chemical reactions required for fluorophore formation) prevents real-time detection of rapid changes in interactions (Kerppola et al., 2006).

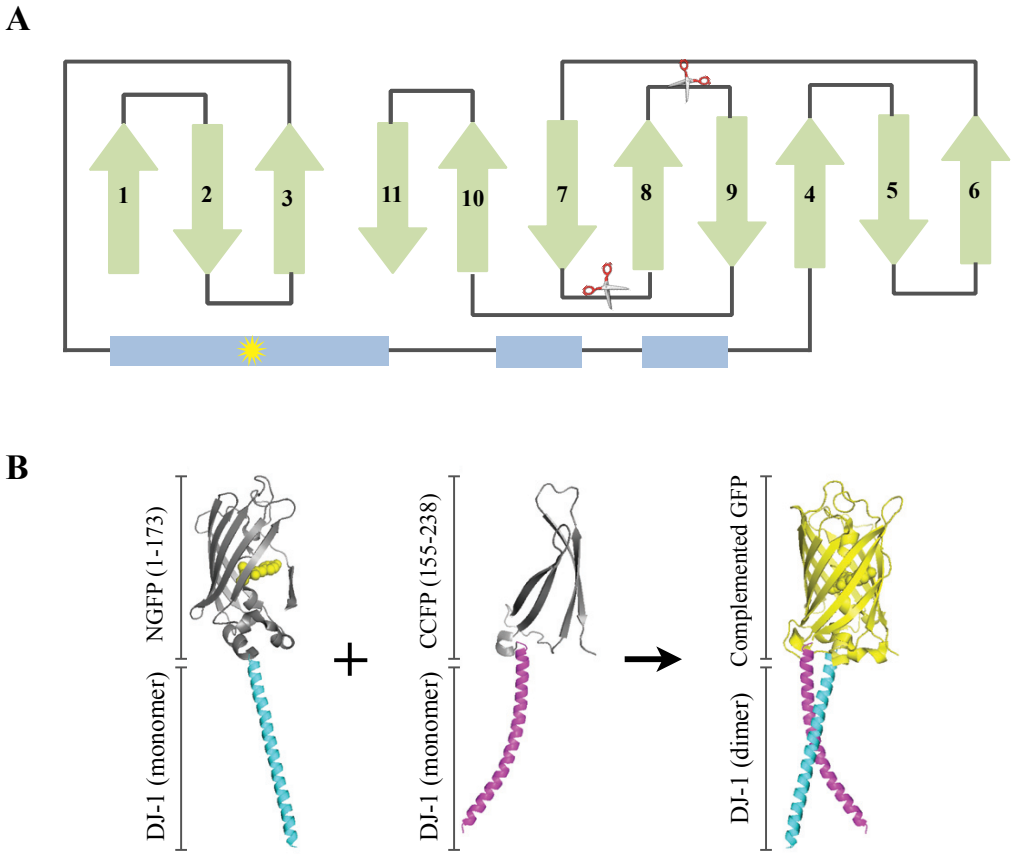

Figure 1.4.1 A) A folding topology diagram of the GFP protein. The numbered green arrows and blue boxes represent β-strands and α-helices respectively. The star symbol indicates a fluorophore. The two canonical split sites for generating our BiFC constructs are indicated by the scissors symbol. **B)** Schematic principle of BiFC to study DJ-1 dimerization. The left structure indicates DJ-1 NGFP (DJ-1 BiFC construct), middle structure represents DJ-1 CCFP (DJ-1 BiFC construct) and right structure shows DJ-1 dimerisation and the reconstituted GFP protein (adapted from (Kodama and Hu, 2012)).

1-5 Specific aims

As discussed earlier DJ-1 is a multifunctional protein involved in wide range of cellular pathways and linked to PD. To date, the precise role of DJ-1 dimerization and function in neurodegeneration is not clearly understood, and the role of protein interactions and protein modifications in dimerization and function has not been explored. As the function of DJ-1 is intimately linked to its dimerization, the identification of dimerization modifiers may represent a significant advance for the elucidation of novel therapeutic strategies for PD. To approach this aim, the main focus of this project was:

1) Screen for chemical modifiers of DJ-1 dimerization (Chapter 3)

In this first objective I initially established and optimised a BiFC based screen for chemical modifiers of DJ-1 dimerization (Chapter 3). A high throughput screen in 96 well plate format using BiFC and Cell^R Scan^R screen station was then performed. Kinase inhibitors and phosphatase inhibitors (134 kinase inhibitors, 34 phosphatase inhibitors) were tested in their ability to modify DJ-1 dimerization in living cells.

2) Investigate the role of DJ-1 phosphorylation in its dimerization and stability (Chapter 4)

The effects of DJ-1 phosphorylation at each potential residue upon its dimerization and stability were characterised by generating phosphomimetic DJ-1 mutants and analysing using BiFC and immunoblotting.

3) Investigate and characterise interactions between DJ-1 and tau (Chapter 5)

BiFC was used to identify direct interaction between DJ-1 and microtubule-associated protein tau in living cells. A panel of DJ-1 mutants were characterized in this context in normal and oxidative stress conditions.

Chapter 2

Materials and Methods

2-1 Materials

2-1-1 Plasmids and mammalian cell lines

pCDNA 3.1^{+} vectors (Invitrogen) containing Neomycin or Zeocin resistance genes were used in this study to generate DJ-1 BiFC constructs (Figure 2.1.1). All the mammalian cell lines, HEK 293T, HeLa, have been obtained from Dr. L. Miguel Martins (University of Leicester, MRC Toxicology Unit)

2-1-2 Chemical compounds

A kinase inhibitor library (http://www.selleckchem.com/screening/kinase-inhibitor-library.html) and a phosphatase inhibitor library (http://www.enzolifesciences.com/BML-2834/screen-well-phosphatase-inhibitor-library/) were obtained from Prof. Dr. Tiago Fleming Outeiro (University of Göttingen) (Appendix 1 and Appendix 2). Hydrogen peroxide 30% (W/W) was obtained from SIGMA.

2-1-3 Bacterial media and growth conditions

E.coli were grown in Luria agar broth (1 % Bacto-trytone, 0.5 % Bacto yeast extract, 0.5 % sodium chloride, pH 7.2). Solid media was made by supplementation with 2 % agar. To select for the presence of constructs media was supplemented with ampicillin (100 µg/ml; SIGMA). *E.coli* on plates were grown at 37°C while liquid cultures were grown at 37°C with continuous agitation at 220 rpm overnight. All the plasmid constructs were maintained in *E.coli* DH5-α (F– Φ80*lac*ZΔM15 Δ(*lac*ZYA-*arg*F) U169 *rec*A1 *end*A1 *hsd*R17 (rK–, mK+) *pho*A *sup*E44 λ– *thi*-1 *gyr*A96 *rel*A1).

2-1-4 Primers

Primers were designed to have a melting temperature > 60 °C with a CG content of > 50 %. All the primers were ordered from SIGMA and DJ-1 siRNA, was obtained from Ambion (136368). Sequences are listed in Table 2.1.1.

2-2-5 Antibodies

For immunoblotting experiments: anti-DJ-1 (C-16) goat polyclonal (1:1000 dilution, SANTA CRUZ Biotechnology, INC: sc-27006), anti-DJ-1 (D4) mouse monoclonal (1:1000 dilution, SANTA CRUZ Biotechnology, INC: sc-55572), anti-4E-BP1 rabbit polyclonal (1:1000, Cell Signaling), anti-GFP rabbit polyclonal (1:5000 to 1:20000 dilution, abcam), anti-α tubulin (TU-02) mouse monoclonal (1:1000 dilution, SANTA CRUZ), were utilised as a primary antibodies. Horseradish peroxidase-conjugated secondary antibodies were used for developing blots, which included horse anti-goat (1:10000 dilution, Vector Laboratories), horse anti mouse (1:10000 dilution, Vector Laboratories) and goat anti-rabbit (1:10000 dilution, Vector Laboratories).

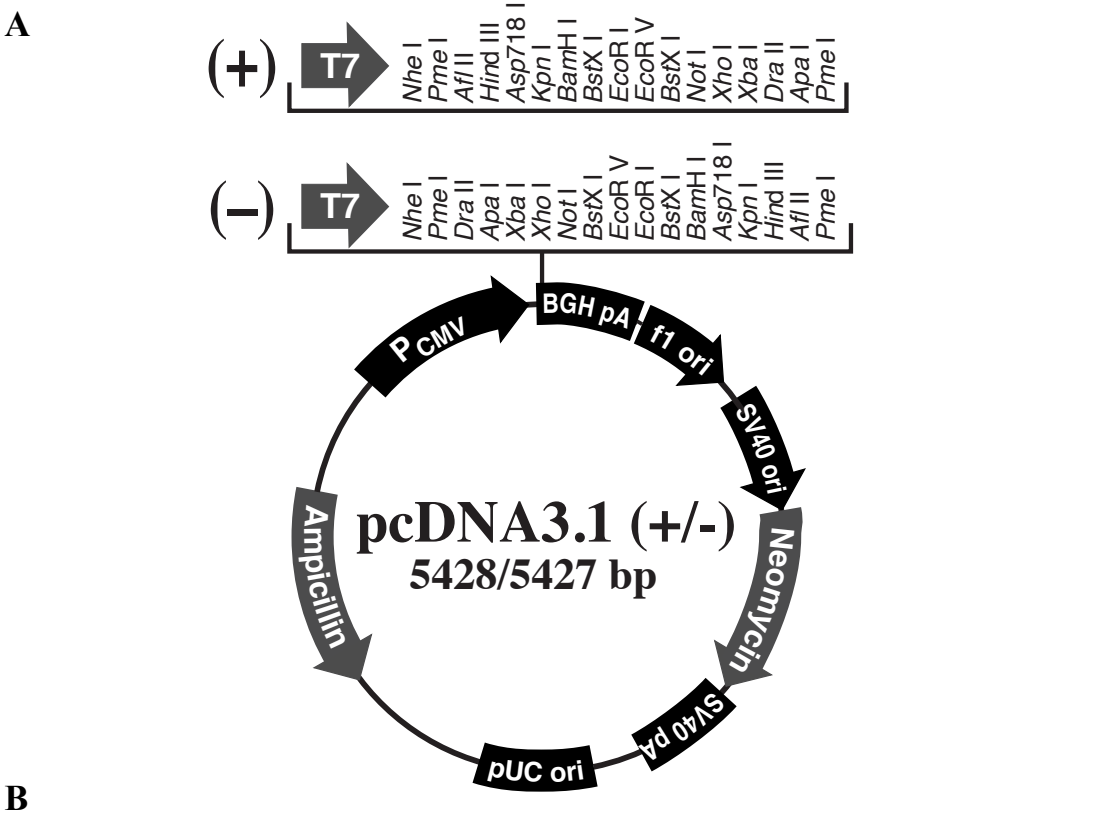

Figure 2.1.1 A) Schematic representation of the pCDNA 3.1^{+} vector that was used in this study. Expression of the DJ-1 BiFC constructs is under control of the CMV promoter that is located upstream of the *XbaI/NheI* restriction sites. **B)** A typical representation of two DJ-1 BiFC constructs used to co-transfect into the Hela/293T HEK cells.

Primer name	Sequence (5'-3')	Application
T7	TAAGCAGAGCTCTCTGGCTAACTA	pCDNA3.1 sequencing
BGH	TACTCAGACAATGCGATGCAA	pCDNA3.1 sequencing
Anti DJ-1 siRNA	GGUCAUUACACCUACUCUGTT	DJ-1 silencing
T19E-F	GGAGCAGAGGAAATGGAGGAGGTCATCCCTGTAGATGT	Site-Directed mutagenesis
T19E-R	ACATCTACAGGGATGACCTCCTCCATTTCCTCTGCTCC	Site-Directed mutagenesis
T19V-F	GGAGCAGAGGAAATGGAGGTGGTCATCCCTGTAGATGT	Site-Directed mutagenesis
T19V-R	ACATCTACAGGGATGACCACCTCCATTTCCTCTGCTCC	Site-Directed mutagenesis
Y67E-F	TGCAAAAAAAGAGGGACCAGAGGATGTGGTGGTTCTACCAG	Site-Directed mutagenesis
Y67E-R	CTGGTAGAACCACCACATCCTCTGGTCCCTCTTTTTTTGCA	Site-Directed mutagenesis
Y67F-F	TGCAAAAAAAGAGGGACCATTTGATGTGGTGGTTCTAC	Site-Directed mutagenesis
Y67F-R	GTAGAACCACCACATCAAATGGTCCCTCTTTTTTTGCA	Site-Directed mutagenesis

Table 2.1.1 List of oligonucleotides used in this study.

2-2 Methods

2-2-1 BiFC construct cloning

The pCDNA 3.1$^+$ vector Neomycin/Zeocin (Invitrogen) used in this study, was supplied as a linearized construct with the XbaI /NheI sticky ends allowing ligation of BiFC constructs (Figure 2.1.1). Expression of BiFC constructs in pCDNA 3.1$^+$ vector is under the control of the CMV promoter that is located upstream of the *XbaI/NheI* restriction site. This vector also contains Neomycin or Zeocin resistance genes for selection of stably transfected clones.

2-2-2 Generation of DJ-1 mutants constructs

2-2-2-1 QuikChange Lightning Multi Site-Directed Mutagenesis

All DJ-1 double mutants BiFC constructs were generated by PCR using a QuikChange Lightning Multi Site-Directed Mutagenesis Kit. Both WT DJ1-GN173 and wild type DJ1-CC155 BiFC constructs as templates (Repici et al., 2013). A typical 25 µl QuikChange Lightning Multi Site-Directed Mutagenesis reaction contained 100 ng of template DNA, 1 µl QuikChange Lightning Multi enzyme blend, 2.5 µl of 10X QuikChange Lightning Multi reaction buffer, 1 µl of dNTP mix (from QuikChange Lightning Multi Site-Directed Mutagenesis Kit), 100 ng of each primers, and 0.75 µl of QuikSolution. PCR was performed using a G-STORM PCR machine as follows: initial denaturation step for 2 minutes at 95°C, 30 cycles of denaturation at 95°C for 20 seconds, 30 seconds of annealing at 55°C (primer-depended temperature), followed by extension at 65°C for 30 seconds/kb (5 minutes) and a final extension step at 72°C for 5 minutes. PCR products were digested with 1 µl of the methylation specific restriction enzyme *Dpn-1* (QuikChange Lightning Multi Site-Directed Mutagenesis Kit) and incubated at 37°C for 2 hours to selectively digest the parental, methylated strand.

2-2-2-2 Site-Directed mutagenesis

All DJ-1 BiFC constructs containing single mutations were generated using PCR based site-directed mutagenesis (Thermo) utilising both WT DJ1-GN173 and WT DJ1-CC155 as templates. A typical 50 µl site-directed mutagenesis reaction consisted of 200 ng template DNA, 1U of Phusion High-Fidelity DNA polymerase, 0.5 µM of each

primer, 10 µl of 5X Phusion HF Buffer, 1 µl of 10 mM dNTPs mix. Typical cycling conditions included an initial denaturation step at 98°C, 25 cycles of denaturation at 98°C for 10 seconds, 30 seconds of annealing at 60°C, followed by extension at 72°C for time equaling 1 minute/kb (3.5 minutes) and a final extension step at 72°C for 10 minutes. PCR products were digested with 10 U of *Dpn-1* (New England Biolabs) and incubated for 2 hours at 37°C to selectively digest the parental, methylated DNA.

2-2-3 Transformation of XL10-Gold Ultracompetent cells

To transform XL10-Gold Ultracompetent cells, 2 µl of the β-ME mix provided with the QuikChange Lightning Multi Site-Directed Mutagenesis Kit was added to 50 µl of ultracompetent cells in prechilled 14-ml BD Falcon polypropylene round-bottom tubes. Cells were incubated on ice for 10 minutes with gently swirling every 2 minutes. 1.5 µl of *Dpn-1* treated DNA from each mutagenesis reaction was added into separate aliquots of ultracompetent cells and incubated on ice for 30 minutes. Cells were then heat shocked at 42°C for 30 seconds, and then immediately incubated on ice for 2 minutes. 500 µl of preheated (42°C) NZY^+ broth was then added into each tube and samples incubated at 37°C for 1 hour with shaking at 225-250 rpm. Cells were harvested at 13000 rpm for 1 minute using an Eppendorf 5424 centrifuge. The supernatant was decanted and the pellet suspended in the remaining liquid, and 1 µl, 10 µl and 100 µl of cells spread onto LB-Ampicillin (LUA-Amp) plates and incubated at 37°C overnight. 6 single colonies were picked and streaked onto fresh LUA-Amp plates and incubated as before. Samples were also transferred into 5 ml LUB-Amp for DNA extraction.

2-2-4 Transformation of competent *E.coli*

Plasmids were transformed into *DH5-α* cells (Bioline) as follows: 10 µl of ligated plasmid was added to 100 µl of competent cells and incubated on ice for 30 minutes. Cells were heat shocked at 42°C for 2 minutes followed by 2 minutes on ice. 1 ml LB was added and samples incubated for 60-90 minutes at 37°C before cells were harvested at 13000 rpm for 1 minute using a desktop Eppendrof 5424 centrifuge. The supernatant was decanted and the pellet suspended in the remaining liquid. Cells were

spread onto LB-Ampicillin (LUA-Amp) plates with glass beads and incubated at 37°C overnight. 6 single colonies were picked and streaked onto fresh LUA-Amp plates and incubated as before. Samples were also transferred into 5 ml LUB-Amp for DNA extraction.

2-2-5 Minipreps

Minipreps were performed utilising an Omega bio-tech E.Z.N.A plasmid mini kit I following manufacturer guidelines.

2-2-6 Agarose gel electrophoresis

Agarose gel electrophoresis was performed using gels made with Seakem LE agarose from Lonza dissolved in 1X TBE (90 mM Tris base, 90 mM boric acid, 2 mM EDTA, PH 8.0). Gels were supplemented with ethidium bromide (0.5 µg/ml) prior to casting and the percentage of the gels was specified by the DNA fragment to be separated. DNA samples were mixed with loading dye (10 % (W/V) Ficoll type 400, (W/V) 0.25 % bromophenol blue, 0.5 % (W/V) SDS), loaded into agarose gels, and separated by passing an electric field through 1X TBE buffer. Appropriate DNA markers (section 2.2.4) were used to determine the size of the DNA fragments. Gels were visualised using a Kodak 200L gel documentation system and processed using Kodak 1D Image analysis software.

2-2-7 Sequencing

Sequencing reactions included: 2µl of plasmid DNA (~500 ng), 2 pmol T7 or BGH sequencing primer, 1 µl BigDye Terminator 3.1, 1X sequencing buffer (Applied BioScience), and were made up to a final volume of 10 µl with distilled water. Sequencing was performed using G-STORM PCR machine as follows: 96°C for 1 minute, followed by 25 cycles of 30 seconds at 96°C, 5 seconds at 50°C, and 4 minutes at 60°C. Samples were purified using Edge purification columns following the manufacture's guidelines and provided to the Protein Nucleic Acid Chemistry Laboratory (PNACL), facility, University of Leicester.

2-2-8 Endofree minipreps and sample purification

Constructs were prepared for transfection by culturing cells overnight in 100 ml LB-Amp at 37°C with shaking. An Omega bio-tech E.Z.N.A endo free® plasmid mini kit II was used to prepare endotoxin free plasmid DNA following the manufacturer's guidelines. Samples were eluted in a final volume of 20 µl and purified further by phenol:chloroform extraction. A volume of phenol:chloroform:Isomyl alcohol (25:24:1) equal to the samples was added, gently mixed and centrifuged at 1200 rpm for 30 seconds using an Heraeus Sepatech Biofuge 13 centrifuge. The upper aqueous phase was transferred to a fresh tube and an equal volume of chloroform added and centrifuged as before. The upper aqueous phase was transferred to a new tube and twice the volume of 100 % ethanol and $1/10^{th}$ the volume of 3 M sodium acetate added before the samples were incubated at -20°C for 30 minutes. Samples were then centrifuged at 13000 rpm for 10 minutes and the pellet suspended in 200 µl 70 % ethanol, vortexed and re-centrifuged. The supernatant was removed and the pellet air dried and suspended in 20 µl of endo-free elution buffer. The DNA concentration was determined by measuring the absorbance at 260 nm in a nanodrop using the following constant for double-stranded DNA: 1 OD_{260} unit correlates to a DNA concentration of 50 ng/µl . Samples were diluted to a final concentration of 0.5 µg/µl using endo-free elution buffer.

2-2-9 Mammalian cell culture

HeLa cells were cultured in Dulbecco's Modified Eagles Medium (DMEM) (PAA) supplemented with 10 % fetal bovine serum (PAA), 2 mM L-glutamine (PAA) and 1 % Penicillin/Streptomycin (Sigma) at 37°C and 5 % CO_2. Cells were passaged 1 in 10 every 3-4 days and all experiments used sub-confluent cultures. Neomycin (G418) or Zeocin were used to select for stable transformants. In order to determine the effective concentration of the selection reagents for HeLa cell we determined the minimum inhibitory concentration. Cells were counted and seeded at a concentration of $1x10^5$ in 6 wells plates and incubated at 37°C in 5 % CO_2 for 24 hours. Cells were then treated with varying concentration of neomycin (100, 300, 500, 600, 700, 800, 1000, 2000 and 3000 µg/ml) or zeocin (50, 100, 150, 250, 350, 550, 650 and 800 µg/ml) with media be-

ing changed twice a week. The percentage of cell death in each well was considered every day by microscopy observation and recorded.

HEK 293T cells were cultured in Dulbecco's Modified Eagles Medium (DMEM (1X)+GlutaMAX^{TM}-1), high glucose, supplemented with 10 % fetal bovine serum (PAA) and 1 % Penicillin/Streptomycin (Sigma) at 37 °C and 5 % CO_2. Cells were passaged 1 in 10 twice a week and all experiments used sub-confluent cultures. In this study we used Zeocin to select for stable transformants. The effective concentration of Zeocin for HEK 293T cells was determined as previously described.

2-2-10 Lipofectamine LTX transfection

For transfection of HeLa cells with BiFC constructs cells were counted and $2x10^5$ cells seeded into 6 well plates containing 3 ml complete medium and incubated at 37°C in 5 % CO_2 for 24 hours. For each transfection reaction 1.25 µg of DNA was diluted in 500 µl of serum free medium and mixed completely. 1.25 µl PLUS reagent (Invitrogen) was added to the diluted DNA and incubated for 15 minutes at room temperature. 4.5 µl of LTX reagent (Invitrogen) was then added to the diluted DNA and PLUS reagent mixture and incubated for 25 minutes at room temperature. The medium was changed with fresh complete medium and the mixture of diluted DNA and transfection reagent was added to each well and incubated at 37°C in 5 % CO_2 for 24 hours . After 24 hours medium was changed, and twice a week over several weeks new medium was added with the addition of Neomycin selection at a final concentration of 800 µg/µl to select for stable transformants. Single colonies were picked into new plates and expanded for further analysis.

For transfection of HEK 293T cells with BiFC constructs cells were counted and seeded at a concentration of 6.25×10^5 cells/well in 6 well plates, precoated with 0.01 % poly-L-lysine solution, containing 2 ml complete medium and incubated at 37°C in 5 % CO_2 for 24 hours. For each transfection reaction 2.5 µg of DNA was diluted in 500 µl of serum free medium and mixed completely. 2.5 µl PLUS reagent (Invitrogen) was added to the diluted DNA and incubated for 5 minutes at room temperature. Then 6.25 µl LTX reagent (Invitrogen) was added to the diluted DNA and PLUS reagent mixture and incubated for 30 minutes at room temperature. The medium was changed with

fresh complete medium and the mixture of diluted DNA and transfection reagent was added to each well and incubated at 37°C in 5 % CO_2. After 24 hours medium was changed and twice a week over several weeks it was replaced with new medium containing Zeocin at a final concentration of 400 µg/ml to select for stable transformants. Single colonies were picked into new plates and expanded for further analysis.

HEK 293T cells were transfected with BiFC constructs using Lipofectamine LTX in 96 well plate format during screening. Cells were counted and seeded at a concentration of 2.5 x 10^4 cell/well in 96 well ibiTreat plate (Ibidi), precoated with 0.01 % poly-L-lysine solution, containing 200 µl complete medium and incubated at 37°C in 5 % CO_2 for 24 hours. For each transfection reaction 100 ng of DNA was diluted in 200 µl of serum free medium and mixed completely. 0.1 µl PLUS reagent (Invitrogen) was added to the diluted DNA and incubated for 15 minutes at room temperature. Then 0.25 µl LTX reagent (Invitrogen) was added into the diluted DNA and PLUS reagent mixture and incubated for 30 minutes at room temperature. The medium was changed with fresh complete medium and the mixture of diluted DNA and transfection reagent was added to each well and incubated at 37°C in 5 % CO_2. After 24 hours medium was changed with fresh medium. Cells were treated with drug compounds for 4 h and changes in fluorescent signal were analyzed using an Olympus Cell^R Scan^R screening station.

2-2-11 Lipofectamine 2000 transfection

For transfection of HEK 293T cells with BiFC constructs and anti DJ-1 siRNA, cells were counted and seeded at a concentration of 4 x 10^5 cells/well in 12 well plates, precoated with 0.01 % poly-L-lysine solution, containing 1 ml complete medium and incubated at 37°C in 5 % CO_2 for 24 hours. For each transfection reaction 0.3 µg of DNA and 12 pmol siRNA (Ambion 136368) (Table 2.1.1) were diluted in 100 µl of serum free medium and mixed completely. 3 µl Lipofectamine 2000 reagent (Invitrogen) were diluted in serum free medium, mixed completely and incubated for 5 minutes at room temperature. Then diluted DNA and siRNA mixture and Lipofectamine reagent mixture were combined, mixed gently and completely incubated for 20 minutes at room temperature. The medium was changed with fresh complete medium and the mixture of

diluted DNA, siRNA and transfection reagent was added to each well and incubated at 37°C in 5 % CO_2. After 24 hours medium was changed.

HEK 293T cells were transfected with BiFC constructs and anti DJ-1 siRNA using Lipofectamine 2000 in 96 well plates for screening. Cells were counted and seeded at a concentration of 1.5 x 10^4 cells/well in 96 well ibiTreat plate (Ibidi), precoated with 0.01 % poly-L-lysine solution, containing 200 µl complete medium and incubated at 37°C in 5 % CO_2 for 24 hours. For each transfection reaction 0.5 µg of DNA and 0.5 pmol of siRNA were diluted in 25 µl of serum free medium and mixed completely. 0.35 µl Lipofectamine 2000 reagent (Invitrogen) was diluted into the of serum free medium, mixed completely and incubated for 5 minutes at room temperature. Diluted DNA/siRNA and the Lipofectamine reagent mixture were combined, mixed gently and incubated for 20 minutes at room temperature. The medium was changed with fresh complete medium and the mixture of diluted DNA, siRNA and transfection reagent was added to each well and incubated at 37°C in 5 % CO_2. After 24 hours medium was changed with fresh medium. Changes in fluorescent signal were analysed using an Olympus Cell^R Scan^R screening station.

2-2-12 Protein extraction

Proteins were extracted from cells transiently transfected with desired plasmids. All the equipment and solutions were maintained on ice (4°C) to avoid protein degradation. To extract total proteins from cells in 6 well plate, 100 µl of lysis buffer (20 mM Trizma Acetate, 0.27 M Sucrose, 1 mM EDTA, 1 mM EGTA, 50 mM NaF, 5 mM Na pyrophosphate decahydrate, 1 mM Na Orthovanadate (Na_3-VO_4), 10 mM β-glycerophosphate disodium, 1 mM DTT, 1X Triton, 1X Cocktail Roche) was added to each well for 10 minutes, and cells transferred to prechilled 1.5 ml tubes and centrifuged at 13000 rpm for 10 minutes. Supernatant were transferred to fresh prechilled 1.5 ml tubes and 6 µl of the cleared protein lysates used to determine the protein concentration, and the rest of the protein lysates were kept at -80°C for future use.

Proteins concentration was determined using Bradford assays, which are based on the binding of protein to a dye that leads to a shift in the dye's absorbance. Bovine serum albumin was used as a protein standard to construct a standard curve (stock solu-

tion was diluted in distilled water to 0.125, 0.25, 0.50, 0.75, 1, 1.5, and 2 mg/ml). Each protein sample was diluted with distilled water to give a final volume of 15 µl 5 µl of each sample and protein standard were added to wells of a transparent 96 well plate (in duplicate) and 250 µl of Bradford reagent (1 X, BIO RAD) was added to the samples. Samples were incubated in the dark at room temperature for 5 minutes and mixed at 900 rpm using a Heidolph TITRAMAX 1000 shaker. The absorbance at 595 nm was then measured in BMG labtech FLUOstar Omega plate reader.

2-2-13 Immunoblotting

Samples for immunoblotting were prepared as described in section 2-1-12. Approximately 10-20 µg of protein was loaded per lane along with Precision Plus Protein™ Standards (BIO RAD) as a marker. Standard 10 % running gel (5 ml buffer SPA (1.5 M Tris.HCl (PH 8.8), 0.2 % (W/V) SDS), 6.7 ml 30 % (W/V) Acrylamide/methylene bisacrylamide solution (ProtoGel), 7.9 ml H_2O, 150 µl APS (10 %), 15 µl TEMED) and stacking gel (2 ml stacking buffer (0.5 M Tris.HCl (PH 6.8), 1360 µl 30 % (W/V) Acrylamide/methylene bisacrylamide solution (ProtoGel), 80 µl APS (10 %), 8 µl TEMED) were used for all the immunoblotting experiments. Electrophoresis was performed at a constant 40 mA in running buffer (250 mM Tric.HCl, 1.9 M Glycine, 0.5 % (W/V) SDS) until sufficient separation of protein fragments were achieved (~90 minutes). Gels were then transferred to blotting apparatus layered with a PVDF membrane (Millipore) treated with 100 % methanol and blotted for 2 hours at 100 V in blotting buffer (0.02 M Tric, 0.15 M Glycine, 12 % (V/V) methanol). Following blotting PVDF membranes were incubated in blocking solution (5 % (W/V) milk solution in 1 X TBS-T (20 mM Tris, 150 mM NaCl, 0.1 % Tween 20)) for 1 hour. Membranes were then incubated in primary antibody diluted in blocking solution and incubated overnight on a rocker at 4°C. Membranes were then washed three times for 15 minutes with 1 X TBS-T before being incubated with HRP conjugated secondary antibody diluted in blocking solution (1 % (W/V) milk solution in 1X TBS-T) for 1 hour at room temperature. After three washes with 1 X TBS-T for 15 minutes, proteins were visualised with ECL reagent (SuperSignal West Dura, Thermo Scientific Pierce) and X-ray film (Fujifilm).

2-2-14 Gel densitometry

Following immunoblot experiments changes in protein expression were quantified using Image J software. The intensity of individual protein bands from scanned X-ray film were evaluated, and the expression of the proteins of interest were normalized using α-tubulin as a loading control.

2-2-15 Immunocytochemistry (ICC)

To observe cells with confocal or Cell^R Scan^R microscopy cells were grown on coverslips (precoated with 0.01 % poly-L-lysine solution), and transfected with the desired plasmids. 24 or 48 hours after transfection cells were fixed with 4 % paraformaldehyde solution for 20 minutes at 37°C . Cells were washed three times with 1 X phosphate buffered saline (PBS) before being incubated in blocking solution (1 % bovine serum albumin (BSA), 0.2 % Triton X-100) for 30 minutes at room temperature. Primary antibodies were diluted in blocking solution incubated with the fixed cells overnight on a rocker at 4°C. Cells were then washed thrice with 1 X PBS for 5 minutes, then incubated for 2 minutes in diluted (1:2000) Hoechst 33342 trihyrochloride, trihydrate 10 mg/ml (Invitrogen) in 1 X PBS. Cells were washed three times with 1 X PBS for 5 minutes, before being incubating with secondary antibodies diluted in blocking solution for 1 hour at room temperature in the dark. Finally, cells were washed three times with 1 X PBS for 5 minutes before mounted. Fixed cells on coverslips were mounted with Mowiol (4.3 mM Mowiol 4-88 reagent (CALBIOCHEM), 3.62 M glycerol, 2 M Tris (PH 8.5), Sodium Azide (NaN3) 0.02 %). One drop of room temperature Mowiol was added to each coverslip and slides were incubated in the dark at room temperature for 2 hours to allow the Mowiol set. All slides were stored at 4°C until use.

2-2-16 DJ-1 phosphorylation assay

To check DJ-1 phosphorylation status in control and oxidative stress conditions HEK 293T cells were transfected with DJ-1 BiFC constructs as described in section 2-2-10 in 6 well plates. 48 hours after transfection cells were exposed to 1 mM hydrogen peroxide (H_2O_2) for 2 hours. Then, cells were washed 3 times with 1 X KREBS

buffer without phosphate (118.4 mM NaCl, 4.69 mM KCl, 4.17 mM $NaHCO_3$, 1.18 mM MgSO4 -7H2O, 11.7 mM Glucose, 9.99 mM HEPES, 1.29 mM $CaCl_2$ -$2H_2O$) before being incubated in 1 X KREBS buffer containing 100 µCi per/ml [P^{32}]orthophosphate at 37°C in 5 % CO_2 for 90 minutes. Cells were then lysed in lysis buffer as described in section 2-2-12, and the DJ-1 BiFC constructs co-immunoprecipitated using anti-GFP conjugated agarose beads following manufacturer's instructions (Chromotek GFP-Trap_A). 10 µl of conjugated beads were added to each sample and then incubated on a rocker at 4°C for 2 hours. Immunoprecipitated proteins were resolved by 10 % SDS-PAGE and visualised by autoradiography.

2-2-17 Scan^R microscopy

Fluorescence signals were acquired and analysed using the Olympus IX81 Scan^R screening station. Cells were grown in a 96 well ibiTreated plate (Ibidi) (2 x 10^4 cell/well), precoated with 0.01 % poly-L-lysine solution. 24 hours after transfection cells were treated with kinase inhibitors, phosphatase inhibitors or aggregation modifying compounds at a final concentration of 1, 5, 10, and 20 µM for 4 hours, and for oxidative stress treatment cells were exposed to 1 mM H_2O_2 for 2 hours. Cells were imaged (16 pictures/well) using an Olympus 20 X LUCPlanFLN/NA = 0.45 objective equipped with a Hamamatsu ORCA-AG CCD camera and Olympus MT20 light source. The following setting were applied for screening: BiFC signals excitation 459-481 nm, emission 510-560 nm, and RFP excitation 546-566 nm, emission 585-650 nm. For each position a DIC image was acquired to check cell viability. Cells with RFP were gated based on their size (area and perimeter) and checked for overexposure in the RFP and BiFC channels. BiFC efficiency was calculated as the ratio between the green BiFC signal and the red signal obtained from a full length RFP construct that was always transfected together with the BiFC constructs.

2-2-18 Confocal laser scanning microscopy

To observe and image cells with a confocal laser scanning microscope (CLSM), 4x10^5 cells were seeded in 60 µ-dish ibiTreat (Ibidi) dishes and transfected with the appropriate BiFC constructs. Cells were imaged using an Olympus FV1000

CLSM in sequential mode using an Olympus UPlanSAPO 60X/NA=1.35 objective, dwell time of 4 µs/Pixel, Kalman filter of 3, and a zoom of 3. For BiFC excitation the 488 nm laser was used and of the emitted fluorescence detected between 500-550 nm, and for RFP excitation the 559 nm laser was used and the fluorescent-emission was detected between 570-670 nm. The 488 nm laser was also utilised to collect differential interference contrast (DIC) images.

2-2-19 Lactate dehydrogenease (LDH) assay

The LDH assay was carried out in transparent 96 well plates. 50 µl of medium was removed from each sample of cultured cells and transferred into 96 well plates. 50 µl of reconstituted Substrate Mix (using procedures supplied by manufacturer (Promega)) was added to each well and incubated in the dark at room temperature for 30 minutes. 50 µl of stop solution (Promega) was added to each well, mixed, and the absorbance at 490-492 nm measured using a BMG labtech FLUOstar Omega platereader.

2-2-20 Statistical analysis

For quantifying the BiFC data, we normalised the GFP emissions by the emissions of RFP: the ratio between the BiFC signal and the RFP emission was quantified for every cell expressing RFP after subtraction of the background signal 24 or 48 hours post-transfection using Cell^R Scan^R screening station (Repici et al., 2013). The results obtained per each single well were then analysed with Prism 5 (GraphPad), applying Kruskal-Wallis tests followed by post hoc analysis and a Dunn test, with statistical significance set at $p < 0.05$ (as performed in Repici et al., 2013). All the data are expressed as means ± SEM.

Chapter 3

Screening for chemical modifiers of DJ-1 dimerization in living cells

3-1 Introduction

As discussed in Chapter 1, DJ-1 has been shown to be post-translationally modified by sumoylation, S-nitrosylation and phosphorylation. Although the effects of DJ-1 sumoylation and S-nitrosylation on its function and localization have been studied by several research groups, to our knowledge nobody has directly studied the effect of DJ-1 phosphorylation on its function and localization. However, recent work by Lin and colleagues has shown that DJ-1 phosphorylation (T19 and Y67) not only may play an important role in PD pathogenesis but also could be used as a biomarker for PD diagnosis and severity (Lin et al., 2012) (see Chapter 4). In order to characterize and clarify this point we decided to identify kinases and phosphatases that regulate DJ-1 phosphorylation status in living cells. Thus, we optimised the Olympus Scan^R screening station to perform screening using kinases and phosphatases chemical inhibitors for identification of novel DJ-1 dimerization modifiers. As the function of DJ-1 is intimately linked to its dimerization, the identification of kinases and phosphatases that modulate DJ-1 dimerization may represent a significant advance for the elucidation of DJ-1 phosphorylation role(s) in cellular pathways and in contribution with its role in PD pathogenesis.

To identify kinases or phosphates that modulate DJ-1 dimerization, we used a kinase inhibitor library (http://www.selleckchem.com/screening/kinase-inhibitor-library.html) and a phosphatase inhibitor library (http://www.enzolifesciences.com/BML-2834/screen-well-phosphatase-inhibitor-library/) extensively used by different research groups (Patel et al., 2012, Acquaviva et al., 2014b, Acquaviva et al., 2014a, Ketley et al., 2014).

3-2 Optimization of screening conditions

3-2-1 Generation of DJ-1 BiFC constructs

Since DJ-1 dimerization has primarily been studied biochemically, monitoring what happens in living cells could provide a great opportunity to clarify its dimerization and perhaps function, localization and potential modifying factors in living cells. To study DJ-1 dimerization modifiers I took advantage of BiFC. This method is based on the reconstruction of two halves of a fluorescence protein through interaction between two partners fused to the fluorescent fragments. In my project, the interaction between two proteins of interest (DJ-1 monomers), respectively fused with the N-terminal half of GFP and with the C-terminal half of CFP, was monitored in living cells transfected with both BiFC constructs using either confocal or fluorescence microscopy.

The dynamics of DJ-1 dimerization in living cells utilizing BiFC was extensively investigated by Dr. Repici in our laboratory (Repici et al., 2013). For identifying DJ-1 dimerization modifiers it was critical to generate cell lines (HEK 293T) that stably over-express DJ-1 BiFC constructs, as this would decrease variation in BiFC signal under screening conditions. We thus used two wild type DJ-1 BiFC constructs (DJ-1/NGFP 1-173 (DJ-1/GN173) and DJ-1/CCFP 155-238 (DJ-1/CC155)), available in our laboratory. As both constructs contained a Neomycin selection marker we cloned the DJ-1/CCFP (155-238) BiFC sequence into pcDNA 3.1^+ carrying a Zeocin selectable marker, allowing us to generate clones stably expressing both constructs as described in Chapter 2. To determine whether the pcDNA 3.1^+ cloning product contains the DJ-1 BiFC construct, isolated plasmids were digested with *SpeI*, which recognises new sites generated by insertion of DJ-1 into the vector (Figure 3.2.1).

To confirm the digestion data and verify if our DJ-1 BiFC construct was inserted in the correct orientation, we sequenced the constructs with the predicted DJ-1 insertion. Following the confirmation of clone 15 by sequencing (data not shown), we generated stable clones expressing both WT DJ-1 BiFC constructs with the two different selection markers (see below).

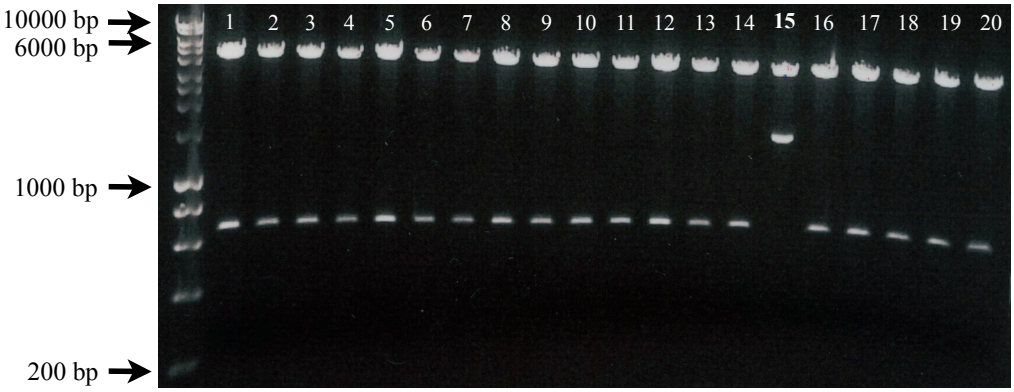

Figure 3.2.1 Restriction digestion of isolated pcDNA 3.1$^+$ plasmids by *Spe*I. This plasmid contains two restriction sites for *Spe*I. *Spe*I digests the empty pCDNA 3.1$^+$ into the two fragments 4340 and 686 bp, whereas it digests pCDNA 3.1$^+$ encoding the DJ-1 BiFC construct into 4340 and 1555 bp fragments. Plasmids containing the DJ-1 BiFC construct can thus easily be detected from plasmids without the DJ-1 BiFC construct.

3-2-2 Testing the sensitivity of HeLa and HEK 293T cells to neomycin and zeocin

To obtain stable clones over-expressing both DJ-1 BiFC constructs, we selected HeLa and HEK 293T cell lines as cellular models since they are easy to transfect, and used Neomycin and Zeocin as selection markers. We first monitored the sensitivity of HeLa cells to these two antibiotics by performing kill curve experiments to identify the effective concentration of antibiotics to be used to isolate stable clones, and we also repeated the same experiments after a high number of cell passages (32), to check whether HeLa cells sensitivity alters with time. I observed that 800 μg/ml of Neomycin and 150 μg/ml Zeocin are the concentrations needed for generating stable clones using HeLa cells (Figure 3.2.2 and 3.2.3).

We also examined HEK 293T sensitivity to only Zeocin since this cell line is Neomycin resistant. Kill curve experiments were carried out to verify the effective concentration of antibiotic to apply for generating stable clones. This test was performed thrice to investigate if HEK 293T cells sensitivity to Zeocin changes with time. Results of the HEK 293T cells kill curve experiment is shown in Figure 3.2.4. Our data showed that 500 μg/ml is the effective concentration of Zeocin to obtain HEK 293T stable clones.

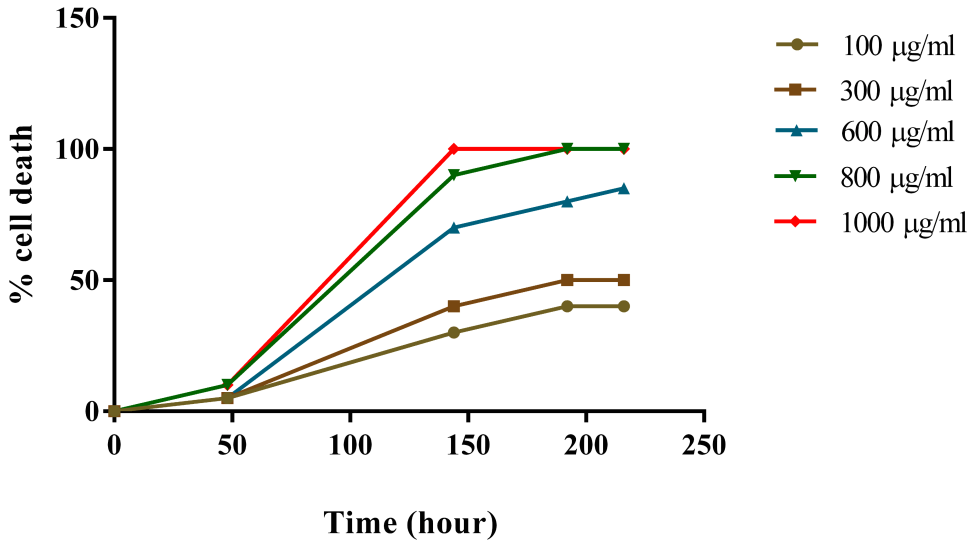

Figure 3.2.2 Neomycin kill curve to detect sensitivity of HeLa cells to this antibiotic. The final concentration to select stable clones in our experimental context was 800 µg/ml. Percentage of cell death was monitored. Cell medium was changed thrice a week over two weeks with medium containing appropriate concentrations of Neomycin selection to obtain the ideal concentration required to kill HeLa cells within approximately 168 hours (7 days).

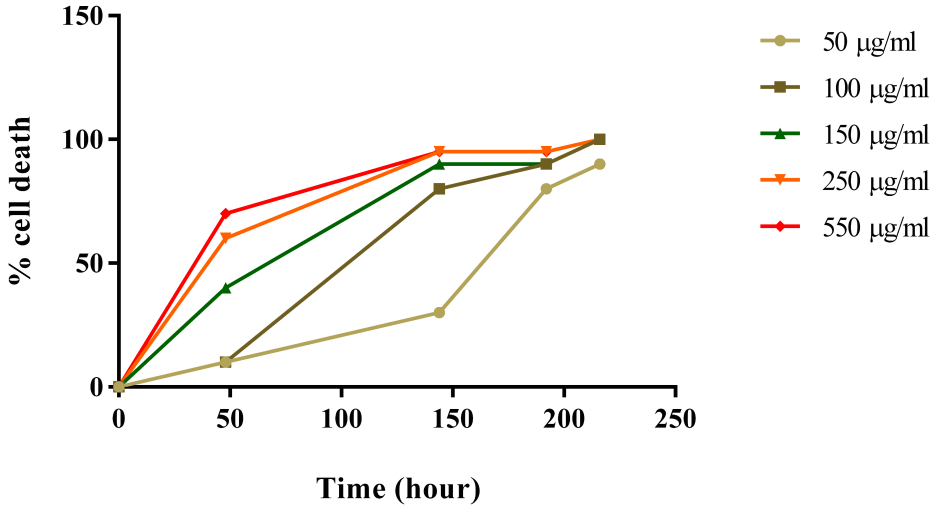

Figure 3.2.3 Zeocin kill curve for HeLa cells. The effective concentration of Zeocin for selecting stable clones is 150 µg/ml. Percentage of cell death was monitored. Cell medium was changed thrice a week over two weeks with medium containing appropriate concentrations of Zeocin to obtain the ideal concentration to kill HeLa cells within approximately 168 hours (7 days).

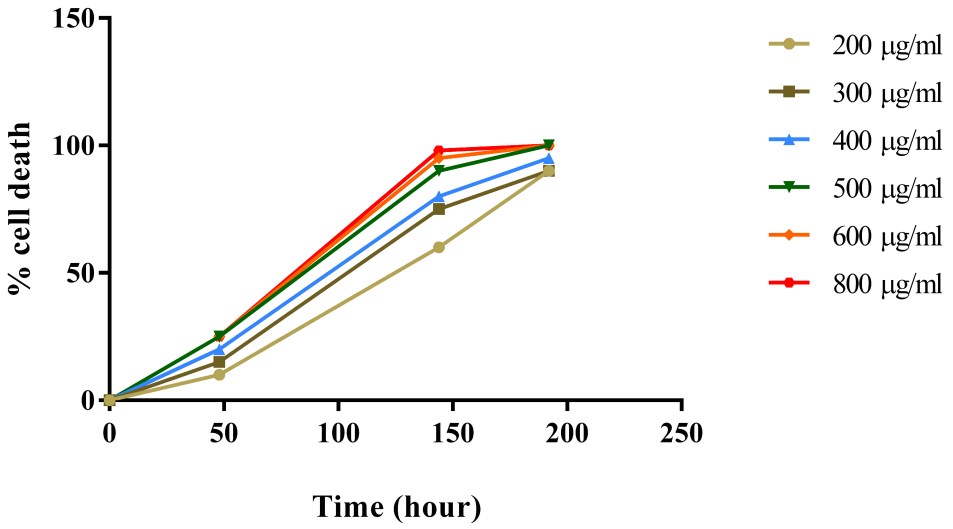

Figure 3.2.4 Zeocin kill curve for HEK 293T cells. The effective concentration of Zeocin for selecting stable clones is 500 µg/ml. Percentage of cell death was monitored. Cell medium was changed thrice a week over two weeks with medium containing appropriate concentrations of Zeocin selection to obtain the ideal concentration required to kill HEK 293T cells within approximately 168 hours (7 days).

3-2-3 Optimization of mammalian cell transfection conditions

To generate stable clones over-expressing both DJ-1 BiFC constructs, it was important to select a transfection reagent with high transfection efficiency and low level of toxicity to the cells. We therefore estimated the efficiency of a number of transfection reagents such as Lipofectamine-LTX (Invitrogen), Trans-IT (Mirus) and Effectene (QIAGEN). Cells were transfected with plasmids encoding DJ-1 BiFC constructs and RFP encoding plasmid as internal control, and transfection efficiency determined by selecting cells in the bright field and checking for RFP expression using a Scan^R microscope. We found that the Lipofectamine-LTX reagent was not toxic to both cell lines (HeLa and HEK 293T) and also that its transfection efficiency was approximately 90 %, thus making this a good reagent for our purposes. In contrast, the two other transfection reagents produced low transfection efficiencies.

3-2-4 Generating stable clonal cell lines over-expressing DJ-1 BiFC constructs

3-2-4-1 HeLa cell line clones

After testing HeLa cell sensitivity for both Neomycin and Zeocin, we turned our focus to making stable cell line clones over-expressing both DJ-1 BiFC constructs. HeLa cells were transfected using the lipofectamine-LTX method with the DJ-1/GN173 DJ-1/CC155 constructs using Neomycin and Zeocin as selection markers. This approach would therefore require the presence of both GFP-encoding fragments for the production of green fluorescence. We observed that even though our isolated clones were derived from individual green cells, not all the cells obtained from that clone presented a fluorescence signal. Indeed, in the majority of our isolated clones the green fluorescence signal was completely lost after 2-3 weeks. The reasons for this observation are unclear, I can however speculate that the expression level of one of the DJ-1 BiFC constructs in our stable clones was highly decreased over time or that our cells lost one of the DJ-1 BiFC constructs (Figure 3.2.5).

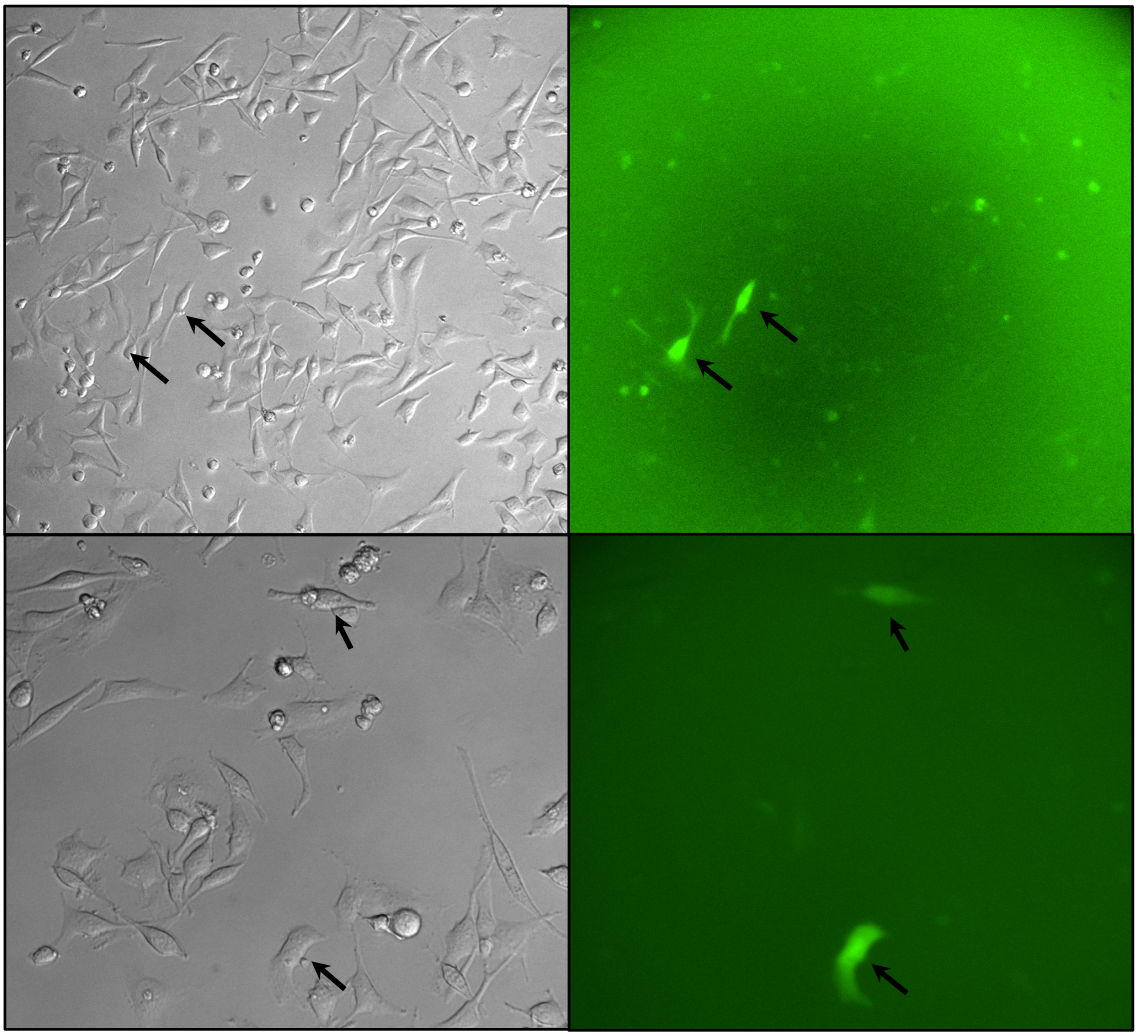

Figure 3.2.5 Picture of single clones obtained from HeLa cells stably co-transfected with both DJ-1 BiFC constructs. Images clearly show that although all cells came from one single cell, only a few cells within the clonal population present a green fluorescence signal.

3-2-4-2 HEK 293T cell line clones

The HEK 293T cell line was the other candidate I implemented for generating stable clones over-expressing DJ-1 BiFC constructs. After determining the effective concentration of Zeocin to be used for producing stable clones, HEK 293T cells were transfected using the lipofectamine-LTX method with the DJ-1/GN173 construct (with the Neomycin resistance marker) and the DJ-1/CC155 construct (containing the Zeocin selection marker). I isolated three single clones, and pooled other clones that survived after applying medium containing Zeocin for over several weeks. During this time I monitored the fluorescence signal by Cell^R microscopy twice a week (Figure 3.2.6).

For performing any experiments using stable clones over-expressing DJ-1 BiFC constructs, it is essential to detect constant GFP fluorescent signal from these cells through confocal or fluorescence microscopy. For this to occur, the constructs should be stably integrated in the genome and expressed at similar levels. We thus assayed protein levels of the DJ-1 BiFC constructs by immunoblotting using anti DJ-1 antibody (Figure 3.2.7). I found that in the three stable clones analyzed the expression levels of the two DJ-1 constructs was extremely variable. Only in the case of the pooled clones were equivalent levels of DJ-1 BiFC construct expression observed as a result of the average between low and high expression of BiFC constructs.

In addition, the morphology of these cells did not change in comparison with not-transfected HEK 293T cells (Figure 3.2.6). I thus selected the HEK 293T pooled clones stably over-expressing DJ-1 BiFC constructs for performing the screens described below using kinase inhibitors and phosphatase inhibitors.

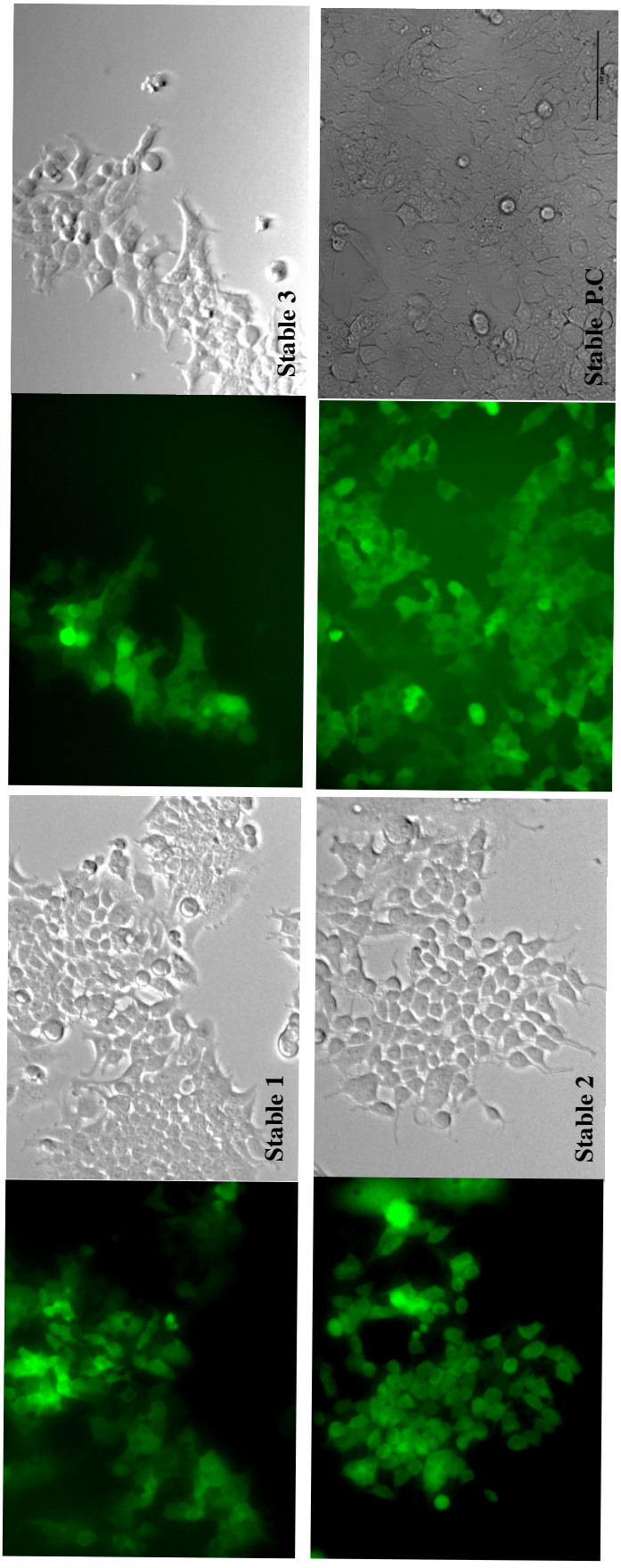

Figure 3.2.6 Images of three independent single clones and pool of clones generated by stably co-transfecting HEK293T cells with both DJ-1 BiFC constructs. Images clearly represent these clones are stably expressing both BiFC constructs. The pooled clone (PC) was selected for performing the screens. Scale bar = 100 µm.

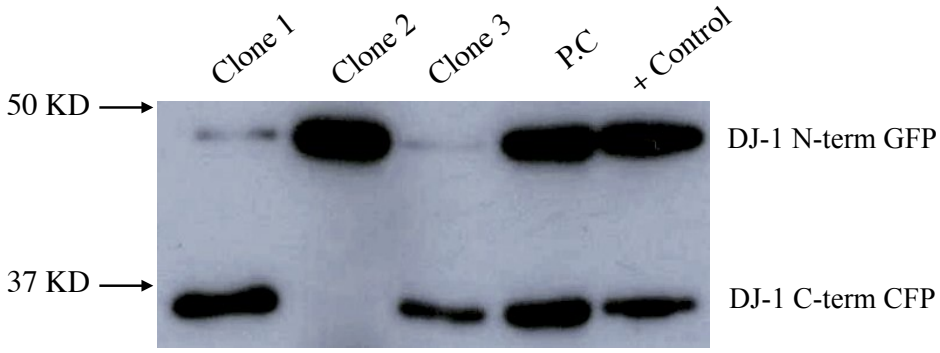

Figure 3.2.7 Expression levels of both DJ-1 BiFC constructs in the obtained stable clones. Anti DJ-1 immunoblots shows expression levels of both DJ-1 BiFC constructs, compared to a positive control (+Control) which was transiently transfected with DJ-1 BiFC constructs. In each lane the upper band corresponds to DJ-1/GN173 and the lower band corresponds to DJ-1/CC155. Our results clearly show that only in the pool of clones (PC) the expression levels of both DJ-1 BiFC constructs are equal and similar to the control.

3-2-5 Optimization of Olympus Scan^R screening station for 96 well plate format

In parallel with generating stable cells over-expressing DJ-1 BiFC constructs, I also focused on optimizing the Olympus Scan^R screening station for experiments using a 96 well plate format, which would permit more rapid screening than the standard BiFC approach used in the laboratory. The Scan^R system can be adjusted to take any number of images per well in order to maximize the number of cells being analyzed, though increasing the number of images takes additional time to run the screen (Figure 3.2.8). Various number of images per well were thus tested to determine the minimum possible amount of time needed to obtain a consistent signal from cells in each well, as the screen was to be conducted in living cells. I initially tested two different numbers of images per well (1 and 25 images per well) through pilot screening experiments in HeLa cells transiently transfected with both DJ-1 BiFC constructs and RFP. RFP was used as an internal control for selecting transfected cells and also for normalizing signals recorded from each well. I noted that even though the screening time when taking one image per well was short (~ 1.5 hours per plate), the fluorescent signal recorded showed high fluctuation (Figure 3.2.9 and Figure 3.2.10). On the other hand, I observed that despite obtaining a consistent fluorescent signal when taking 25 images per well, the screening time increased dramatically to approximately 7 hours per plate (Figure 3.2.9 and Figure 3.2.11).

For these reasons, when I obtained the stable HEK 293T clones over-expressing the DJ-1 BiFC constructs, I tested an intermediate number of images per well (16 images per well) in both these stable clones and HeLa/HEK 293T cell lines transiently transfected with WT DJ-1 BiFC constructs and RFP (Figure 3.2.9, Figure 3.2.12 and 3.2.15). As fluorescent signals recorded were constant with approximately 10-20 % variation between the highest and the lowest signal, and also the time of the screening was approximately 2.5 hours per plate, I used this condition for the screening discussed below.

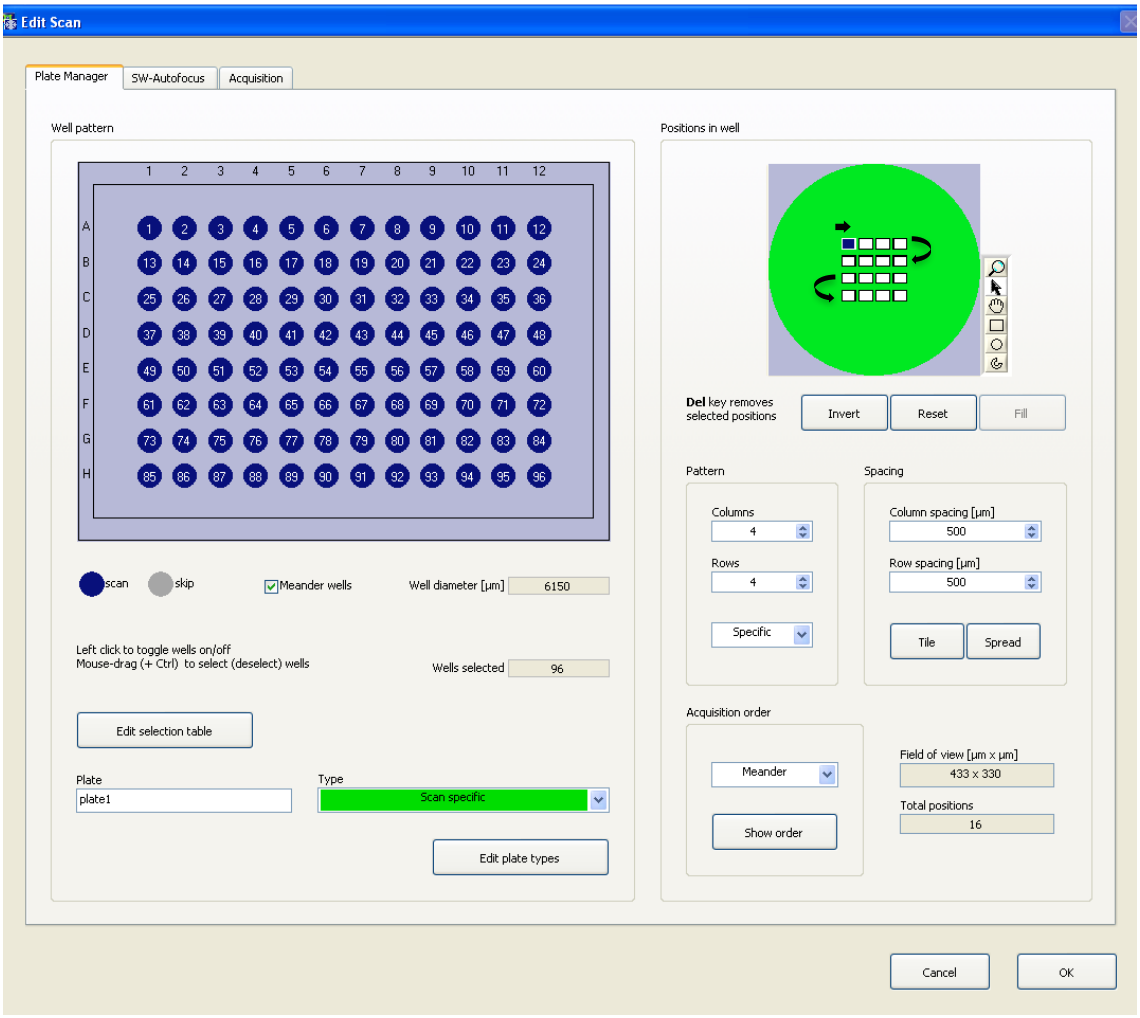

Figure 3.2.8 Schematic model showing selected areas from each well for imaging in 16 images per well format. Arrows indicate imaging direction in each well. Software was set up to find the auto fine, Coarse and Hardware focus in the first area of imaging as well as auto fine focus for the other areas of imaging in each individual well.

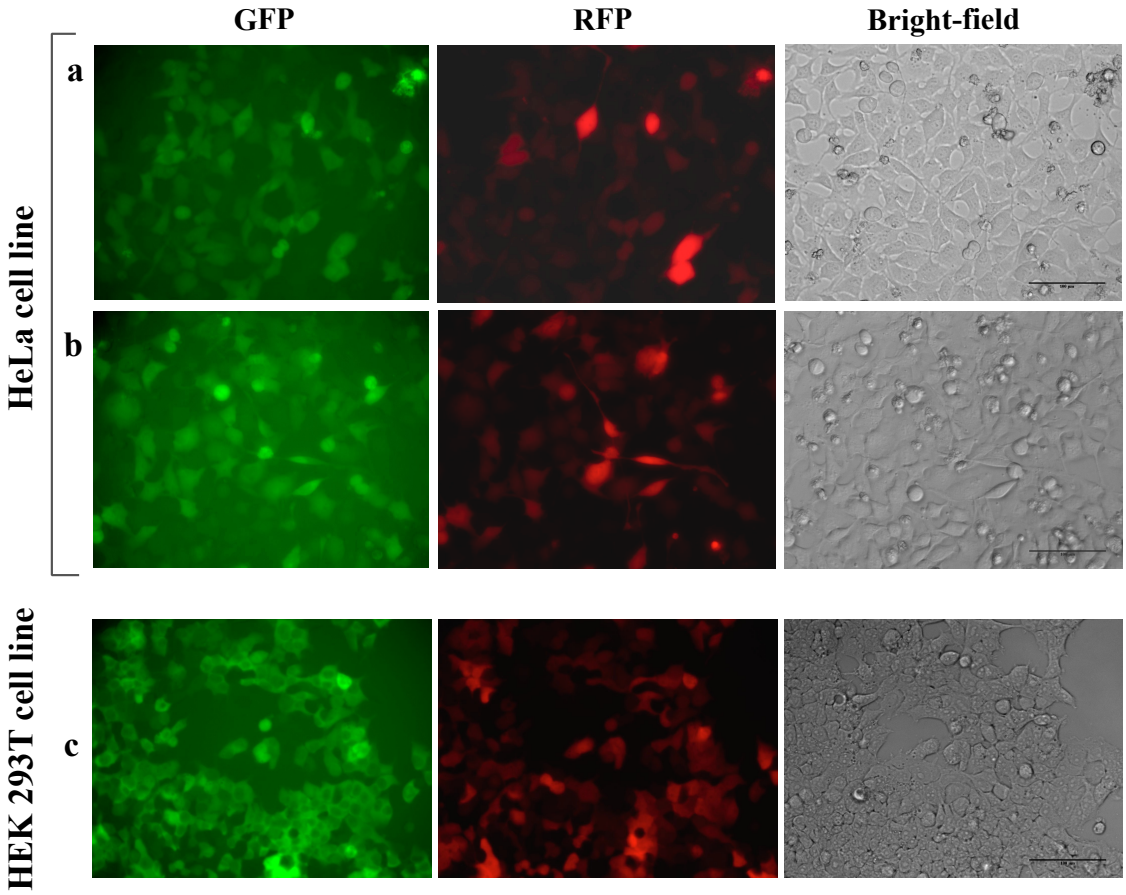

Figure 3.2.9 Sample of images taken during pilot screening experiments. a) images from the first pilot screen (HeLa cells transiently transfected with DJ-1 BiFC constructs and RFP), in which 1 image was taken per well (Figure 3.2.10). b) images taken in the second pilot screen (HeLa cells transiently transfected with DJ-1 BiFC constructs and RFP) in which 25 images were taken per well (Figure 3.2.11). c) images taken using HEK 293T transiently transfected with DJ-1 BiFC constructs and RFP (16 images per well) (Figure 3.2.12). Scale bar = 100 μm

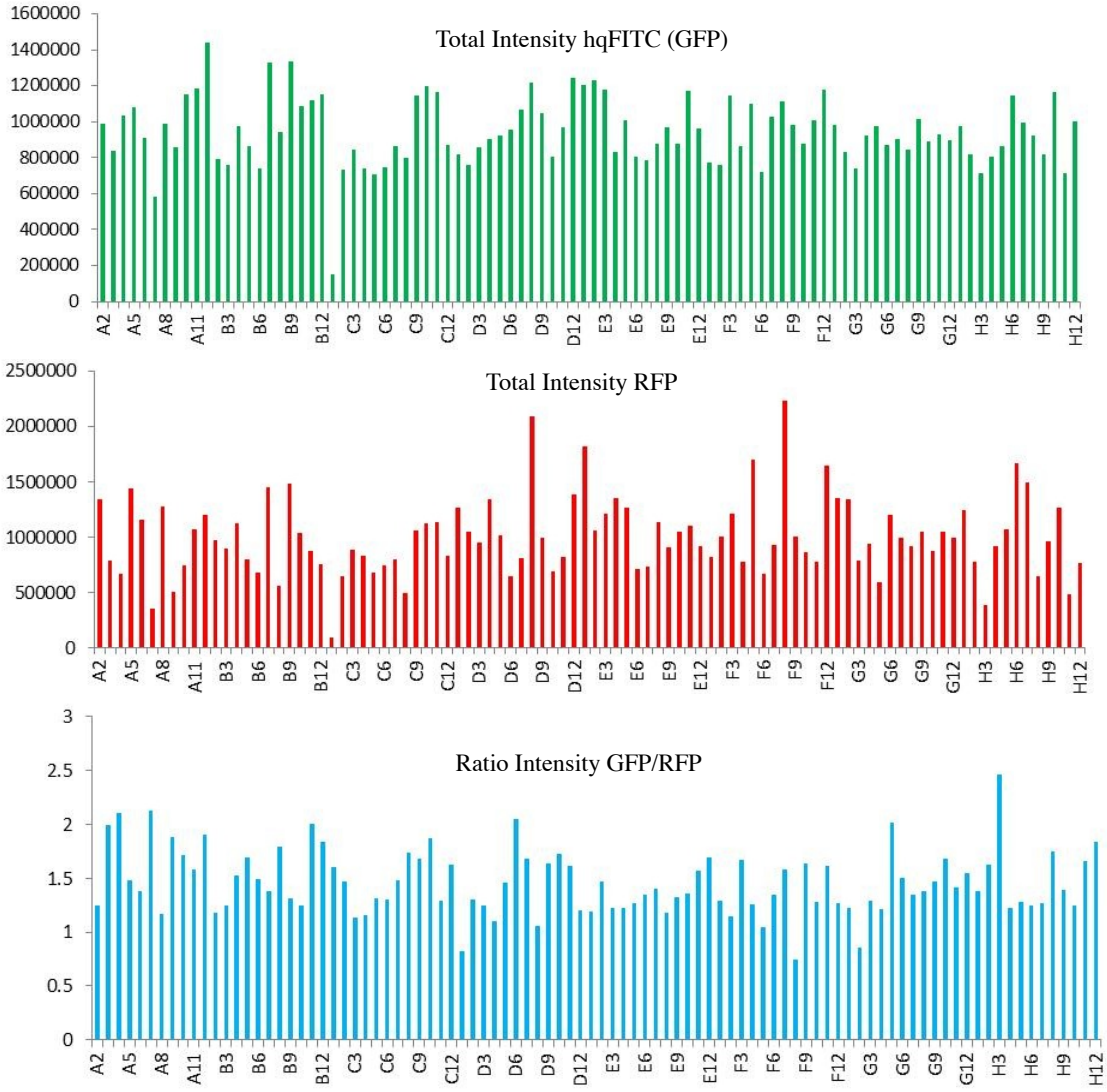

Figure 3.2.10 WT DJ-1 BiFC constructs fluorescence complementation (green graph) and RFP signals (red graph) were recorded taking one picture per well in 96 well plates 48 hours post-transfection. The blue graph shows the average ratio intensity (green/red). Emission intensities were corrected for background fluorescence. HeLa cells were used as a cellular model, and cotransfected with plasmids encoding WT DJ-1 BiFC constructs (20 ng of each construct) and a plasmid encoding RFP (10 ng). High fluctuation of signal was observed from well to well.

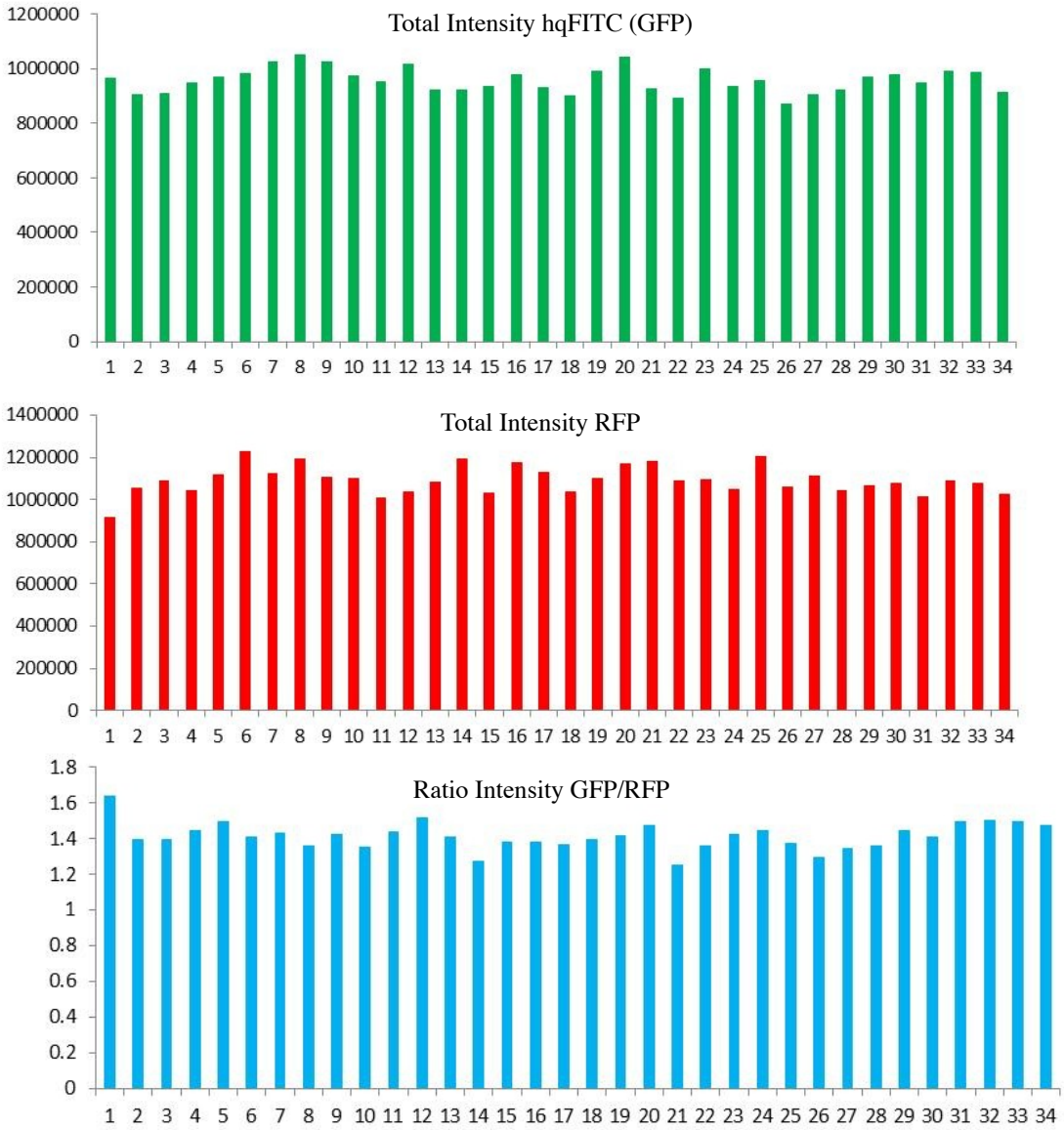

Figure 3.2.11 WT DJ-1 BiFC constructs fluorescence complementation and RFP signals were recorded by taking 25 images per well in a 96 well plate 48 hours post-transfection. The blue graph shows the average ratio intensity (green/red) per picture for each well. Emission intensities were corrected for background fluorescence. Hela cells and the same transfection conditions as in the previous experiment were used. Even though signal fluctuation in each well decreased and constant signals were recorded, time of screening highly increased.

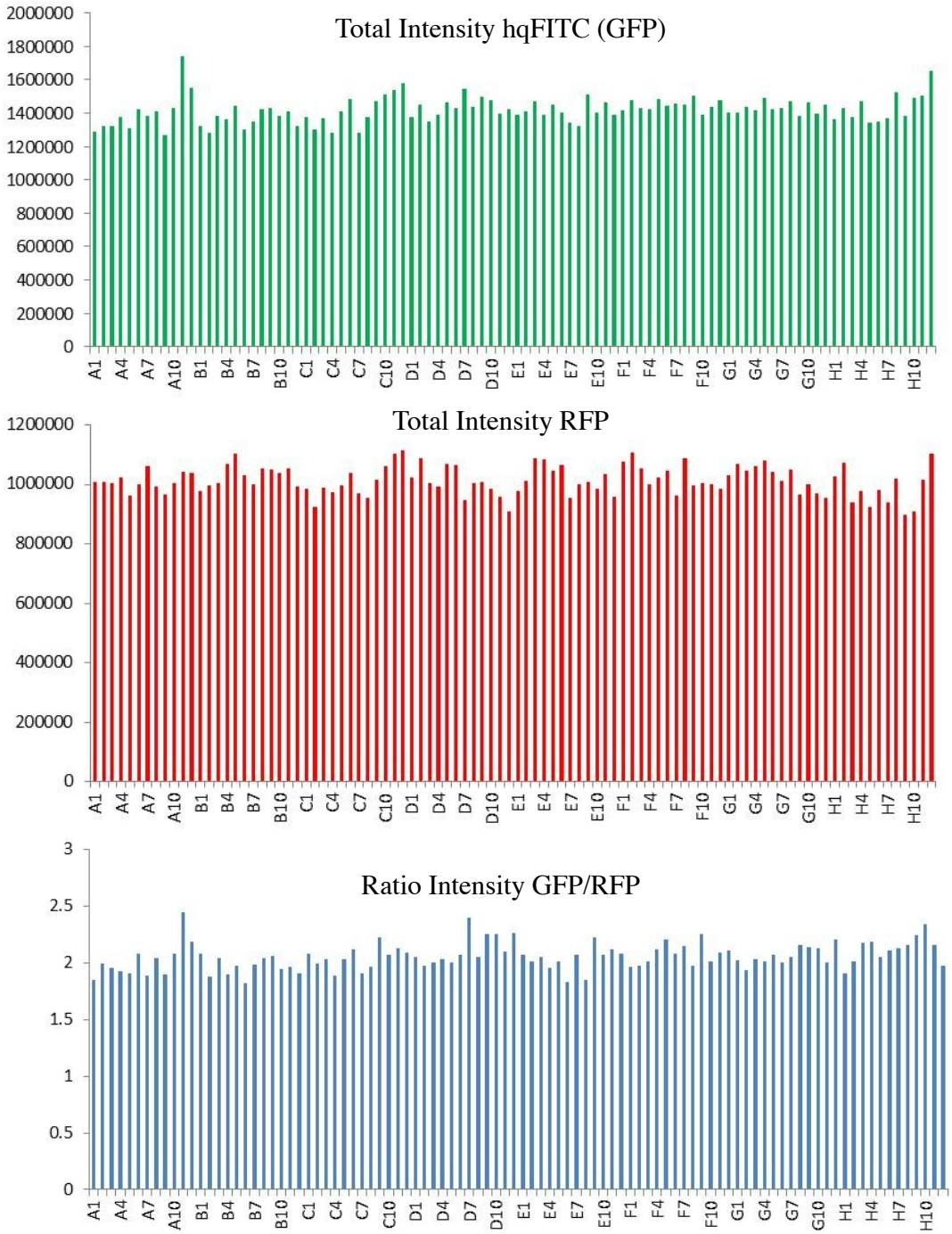

Figure 3.2.12 Further optimization of BiFC screening conditions for 96 well plate format. HEK 293T cells were transiently transfected with plasmids encoding both DJ-1 BiFC constructs and RFP as a reporter. Fluorescence complementation signals was recorded taking 16 images per well 48 hours post-transfection. The blue graph shows the average ratio intensity (green/red) for each well. Emission intensities were corrected for background fluorescence.

To verify the robustness of our model I next tested if the DJ-1 BiFC signal could be modulated by knocking down the DJ-1 gene using an anti DJ-1 siRNA, and also whether or not this possible change could be recorded through the Cell^R Scan^R screen station. In order to address this aim, HEK 293T cells were transiently co-transfected with plasmids for both DJ-1 BiFC constructs, RFP and anti DJ-1 siRNA in a 12 well plate, and cells were imaged 72 hours after transfection. Two different amounts of anti DJ-1 siRNA (12 pmol and 14 pmol) were tested to obtain optimal DJ-1 knock down following Lipofectamine 2000 transfection. Results from this experiment clearly showed that DJ-1 BiFC was significantly decreased (~ 50 %) compared to the control (cells transiently transfected with WT DJ-1 BiFC constructs and RFP) (Figure 3.2.13).

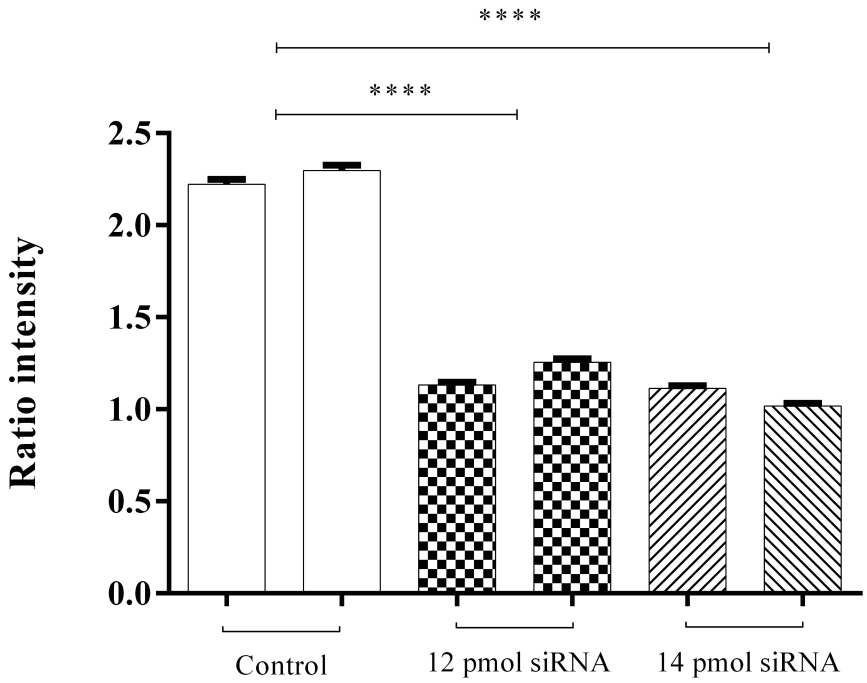

Figure 3.2.13 DJ-1 BiFC signal can be modulated by knocking down DJ-1 gene using anti DJ-1 siRNA. To test if any changes in DJ-1 BiFC signal could be recorded through the Cell^R Scan^R screen station, signals recorded from HEK 293T cells transiently transfected with WT DJ-1 BiFC constructs, RFP and anti DJ-1 siRNA (two wells per condition) were compared to signal from HEK cells transiently transfected with WT DJ-1 BiFC constructs and RFP as a control (each bar represents single well), 72 hours after transfection. DJ-1 BiFC signal was significantly decreased (~ 50-60 %) with RNAi knockdown of the *PARK7* gene. **** $P < 0.001$.

To check if the observed decrease in BiFC signals in cells transfected with anti DJ-1 siRNA was due to a decrease in DJ-1 protein levels, we performed DJ-1 immunoblotting from the same cell lysates and we found that the decreased DJ-1 BiFC signal indeed corresponded to decreased DJ-1 protein levels in those cells (Figure 3.2.14).

To confirm if the optimized conditions for screening in transiently transfected cells could be applied to HEK 293T stable clones, we performed pilot experiments as described before (taking 16 images per well in 96 well plate format) using HEK 293T stable pooled clones over-expressing WT DJ-1 BiFC constructs. Since detecting consistent BiFC signal is critical for screening, we were interested in 1) determining whether or not the BiFC signal of this stable clone was constant and 2) understanding if BiFC changes in this cell line could be recorded without normalizing BiFC signal with RFP. We thus seeded the HEK 293T stable clone (PC) in a 96 well plate, and 24 hours later 6 wells (H6-H12) were transfected with anti DJ-1 siRNA, and the BiFC signal analysed 48 hours after transfection. Our results show that BiFC signal is observed at consistent levels in these cells and alteration in DJ-1 BiFC signal after DJ-1 siRNA could be detected by the Cell^R Scan^R screen station (Figure 3.2.13). Indeed, our screening data in this experiment indicate that although a decrease in DJ-1 levels due to siRNA treatment can be detected by our Cell^R Scan^R screen station, this reduction is not consistent with our previous results (~ 30 % versus ~ 50%). We speculated that our observation might be due to the anti DJ-1 siRNA behaving differently in transiently transfected cells compared with stable clones, or it could be a consequence of the lack of an internal normalisation signal (RFP) in the stable cell lines.

In parallel with the pilot screen for stable clones, and in order to verify whether or not our results from anti DJ-1 siRNA experiment using PC (Figure 3.2.15) correspond to decrease in DJ-1 protein levels, we selected the stable clone 1 cell line as its morphology was more similar to the HEK 293T control to verify reduction in DJ-1 protein level through knocking down its gene by anti DJ-1 siRNA for 48 hours. We carried out an immunoblotting experiment using anti DJ-1 antibody that detects both DJ-1 BiFC constructs, and found that RNAi knockdown of DJ-1 decreases protein levels by ~ 50 %, similar to what was obtained with transiently transfected cells. Results from the

pilot screen and immunoblot experiments suggested that for accurate detection of DJ-1 BiFC alterations, BiFC signal must be normalized with RFP (Figure 3.2.15 and Figure 3.2.16).

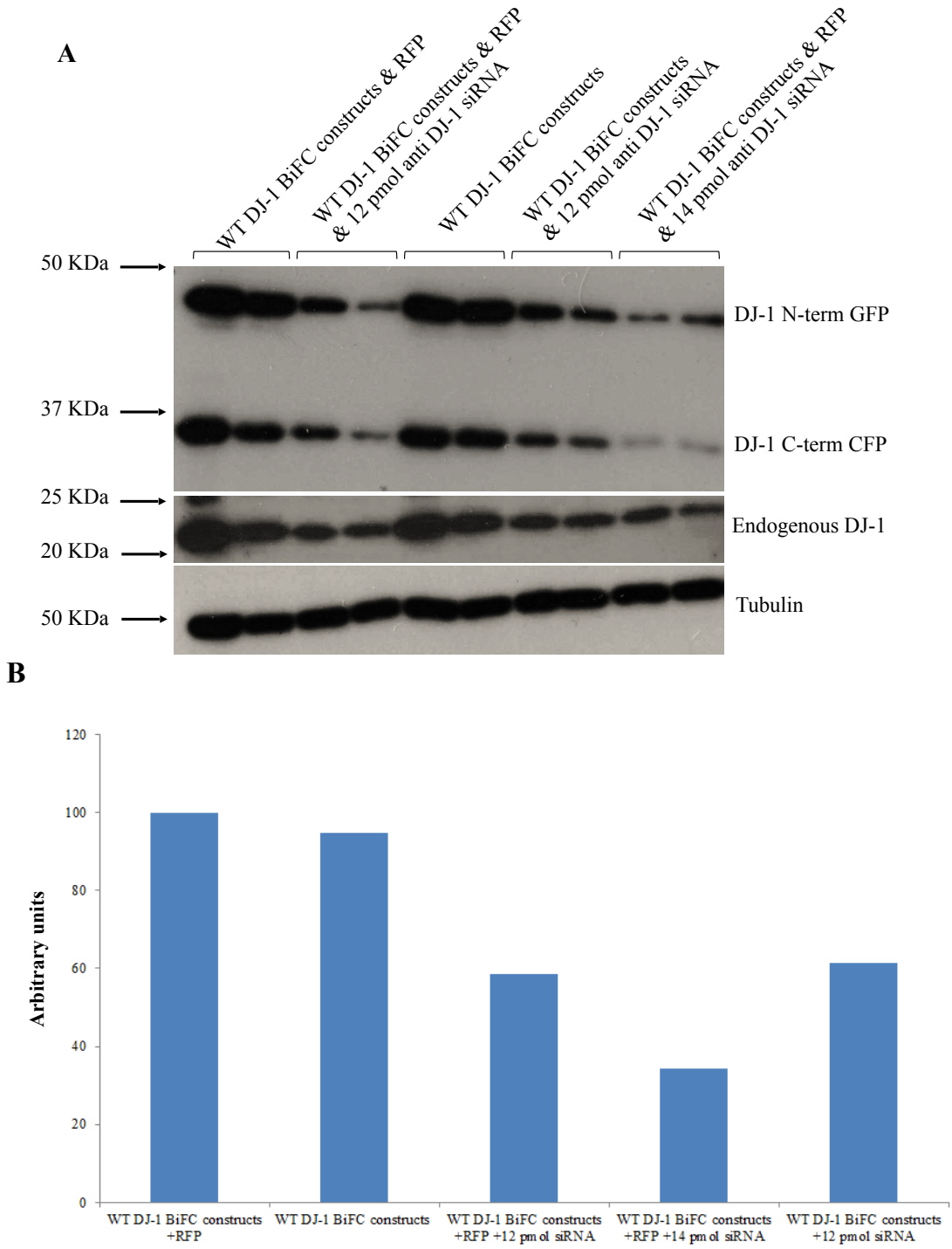

Figure 3.2.14 **A)** Immunoblots of the lysates obtained from the transfected cell populations used in pilot screen for verifying whether or not the DJ-1 siRNA modulates BiFC signals (Figure 3.2.13). Anti DJ-1 antibody was used in this experiment to detect DJ-1 BiFC constructs. In each lane, the upper band corresponds to DJ-1 GN173 and the intermediate band represents DJ-1 CC155. **B)** Gel densitometry to quantify DJ-1 protein levels.

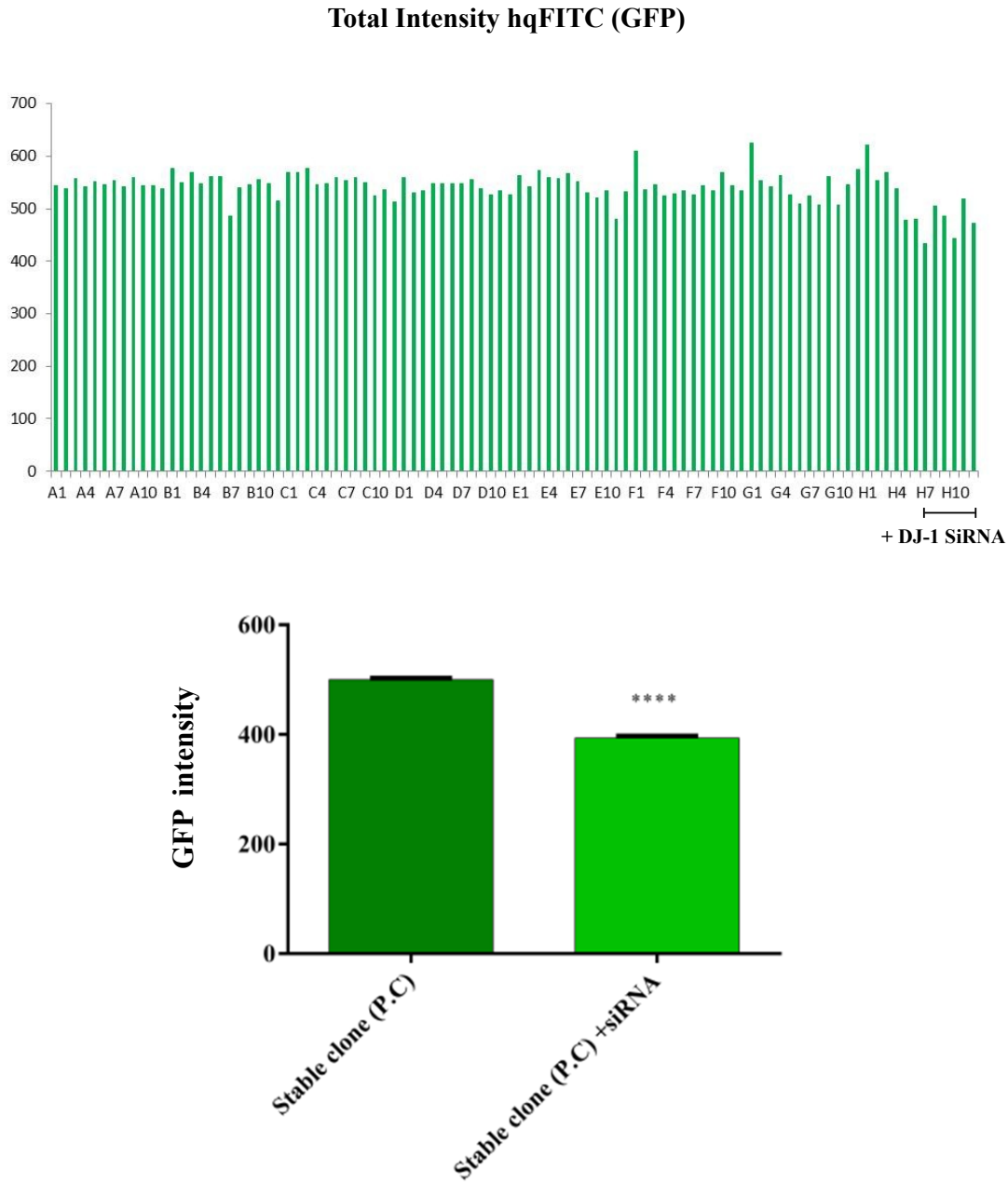

Figure 3.2.15 Optimizing conditions for 96 well plate format BiFC screen. HEK 293T stable clone cells over-expressing DJ-1 BiFC constructs were transfected with a RFP encoding plasmid and imaged 24 hours post-transfection. The last 6 wells (H6-H12) were transfected as well with anti DJ-1 siRNA for 48 hours. Fluorescence complementation between WT DJ-1 BiFC constructs was recorded taking 16 images per well in a 96 well plate. DJ-1 BiFC signal is consistent between wells in this cell line, but for accurate detection the BiFC signal must be normalized to RFP signal. **** $P < 0.001$.

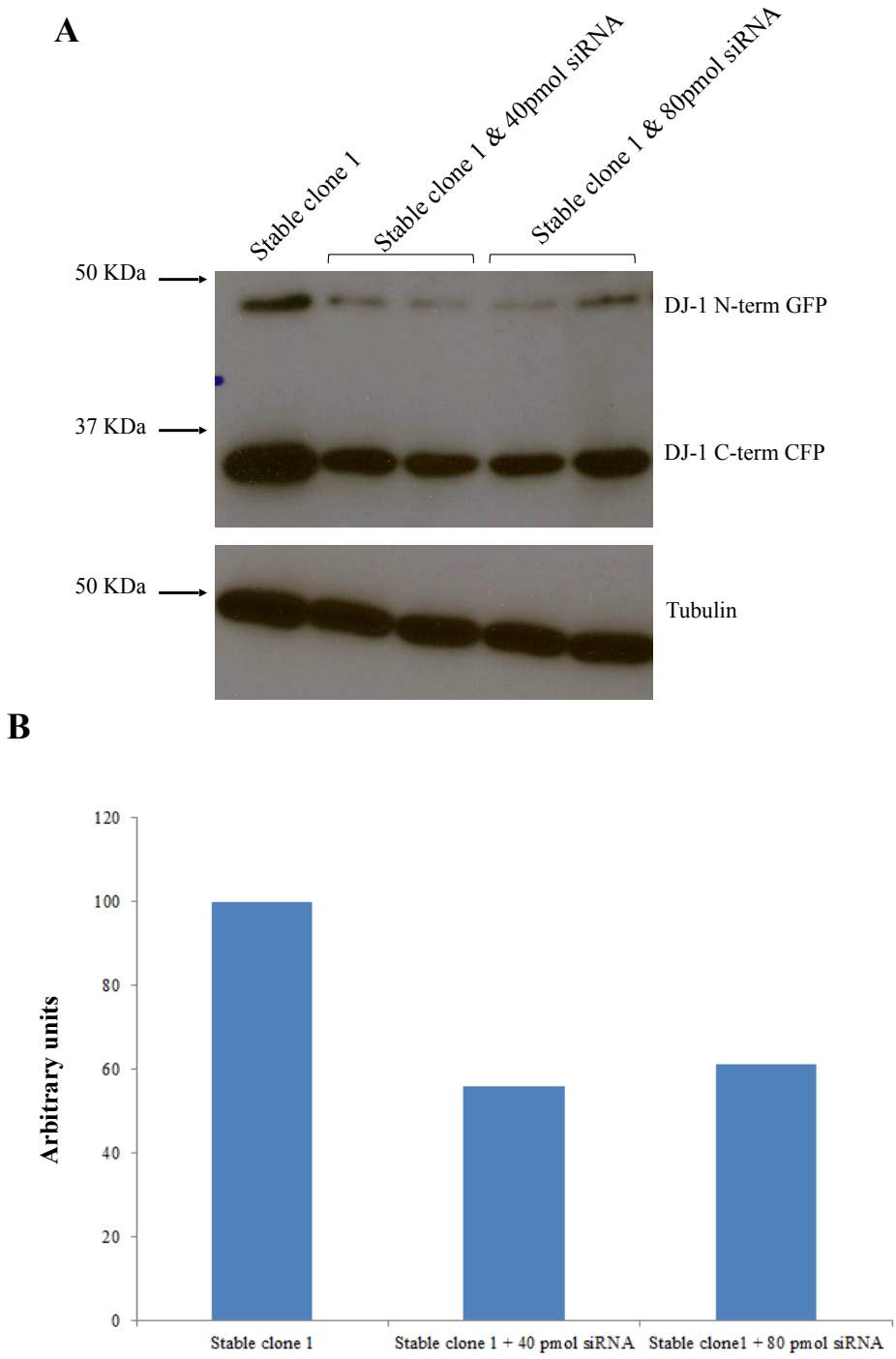

Figure 3.2.16 A) Immunoblots of the lysates obtained from the HEK 293T stable clone cells transfected with anti DJ-1 siRNA for 48 hours. DJ-1 was detected using anti DJ-1 antibody. In each lane, the upper band corresponds to DJ-1 GN173 and the intermediated band represents DJ-1 CC155. **B)** Gel densitometry quantification of DJ-1 protein levels.

3-3 Cell-based screen for modulators of DJ-1 dimerization

3-3-1 Screening protocol

After having optimized conditions to perform high throughput screening on a 96 well plate, we chose to perform a pharmacological screen for identifying kinases and phosphatases able to modify DJ-1 dimerization. We focused on identifying the best conditions for the screening procedure such as concentration of the compounds, interval time between transfection and compound treatment, and treatment length.

The screening steps are summarized in Figure 3.3.1. The HEK 293T stable DJ-1 BiFC clone was transiently transfected with the control construct encoding RFP, and 24 hours post-transfection the cell medium was changed and cells treated with test compounds. Screening was performed 4 hours after treatment, and fluorescence was analyzed via the Cell^R Scan^R screen station. To analyze fluorescence signals, cells were selected in the red channel, and gated for overexposed RFP and GFP. GFP emissions were normalized by the emissions of RFP. In each experimental plate we set up three different control conditions: 1) cells transfected with RFP and treated with the same concentration of dimethyl sulfoxide (DMSO) used to dissolve the screening compounds, 2) cells transfected with RFP but not treated with DMSO and 3) cells not transfected with RFP. Since we observed a DMSO effect on DJ-1 BiFC signal, cells transfected with RFP and treated with the same required concentration of DMSO were used as controls in each experiment.

A total of 194 kinase inhibitors and 33 phosphatase inhibitors were screened. During the primary screen cells were treated with kinase inhibitors at 5 μM or phosphatase inhibitors at 1 and 5 μM, with a single biological replicate for each compound. After 4 hours DJ-1 dimerization was measured, and cellular toxicity determined based on cellular morphology (Appendix 3 and Appendix 4). Analysis of the images showed that test compounds did not cause significant levels of cellular toxicity at the concentrations used. Compounds which decreased DJ-1 BiFC signal less than the lowest DMSO control signal or increased DJ-1 BiFC signal more than the highest DMSO control signal were selected as initial candidates for further study. Using this approach we identified 42 kinase inhibitors and 13 phosphatase inhibitors that altered DJ-1 dimerisation.

To validate the candidates identified in the primary screen compounds were retested in quadruplicate. All the images were again analysed for morphological changes that could indicate cellular toxicity. Compounds that decreased the BiFC signal in three out of four replicates compared with the lowest control signal were selected for further analyses. We used the same selection approach to validate compounds that increased DJ-1 dimerization. This secondary screen revealed that 15 of the candidate kinase inhibitors and 10 of the phosphatase inhibitors were able to consistently modify DJ-1 dimerization (Appendix 5). However, as the compounds induced relatively small changes in DJ-1 BiFC signal we repeated the validation process.

We found that out of the 13 phosphatase inhibitors identified in the primary screen none was validated in the next screen. Moreover the percentages of change in DJ-1 BiFC signals obtained with these compounds were too low (less that 10 %) to be considered as relevant. Thus, we did not continue further studies on these compounds. All the images taken during this screen were monitored for morphological study of the cells to check the possible toxic effect of these compounds, and none was observed.

The 15 kinase inhibitors identified in the primary and secondary screens were also re-tested at concentrations of 5 μM in quadruplicate to verify whether or not results from the primary and secondary screens were valid (Figure 3.3.2). Out of 15 kinase inhibitors that decreased DJ-1 dimerization in the primary and secondary screens, 10 kinase inhibitors significantly alter DJ-1 dimerisation in the tertiary screen. Identification of these potential DJ-1 modifiers was followed by their functional classification (Table 3.3.1). Interestingly, almost all of the kinases whose inhibition affected DJ-1 dimerization have been reported to be implicated in neurodegenerative disorders (i.e. c-Abl, Akt and GSK3β).

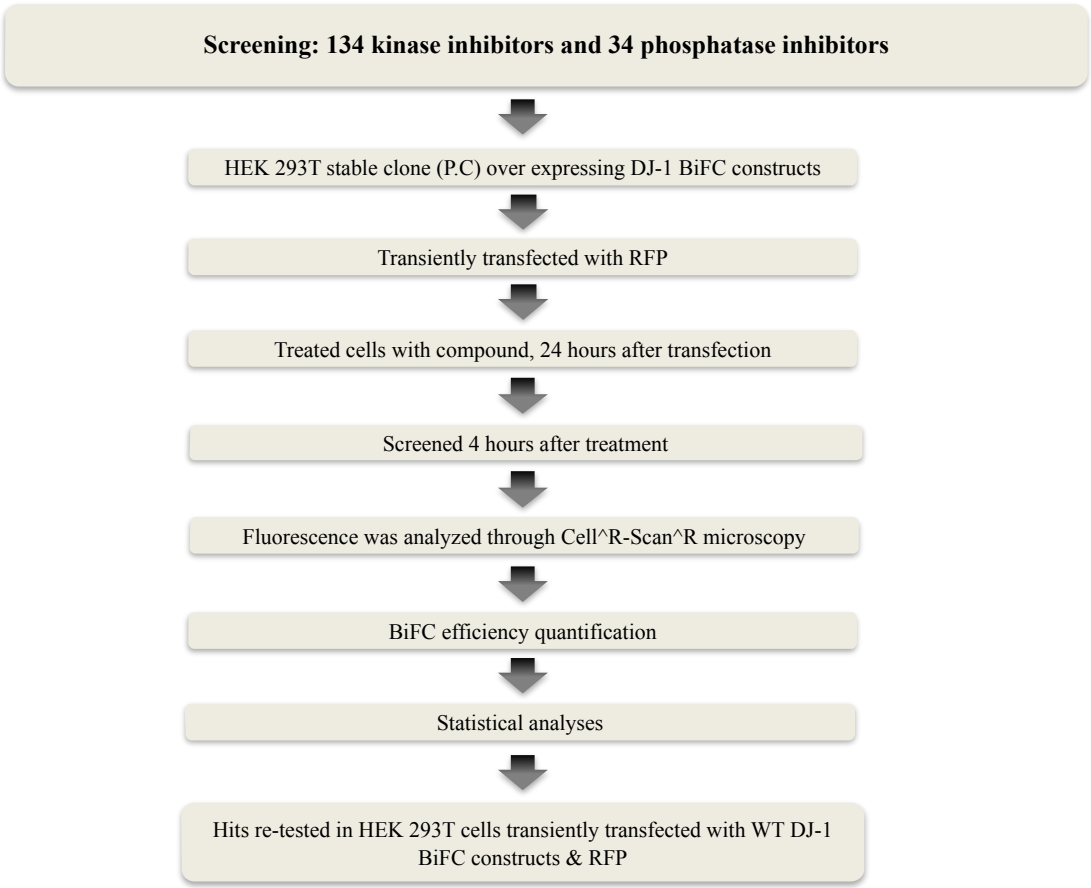

Figure 3.3.1 Overview of the high throughput screen for DJ-1 dimerization modifying compounds. In the first step, HEK 293T stable clone cells were transiently transfected with RFP as an internal control, and 24 hours post-transfection cells were treated with compounds or DMSO as control for 4 hours. The Cell^R Scan^R screening station was used to analyze fluorescence signal and quantify BiFC efficiency. Compounds which showed statistically significant decreases or increases in DJ-1 BiFC signal were re-screened in HEK 293T cells transiently transfected with WT DJ-1 BiFC constructs and RFP.

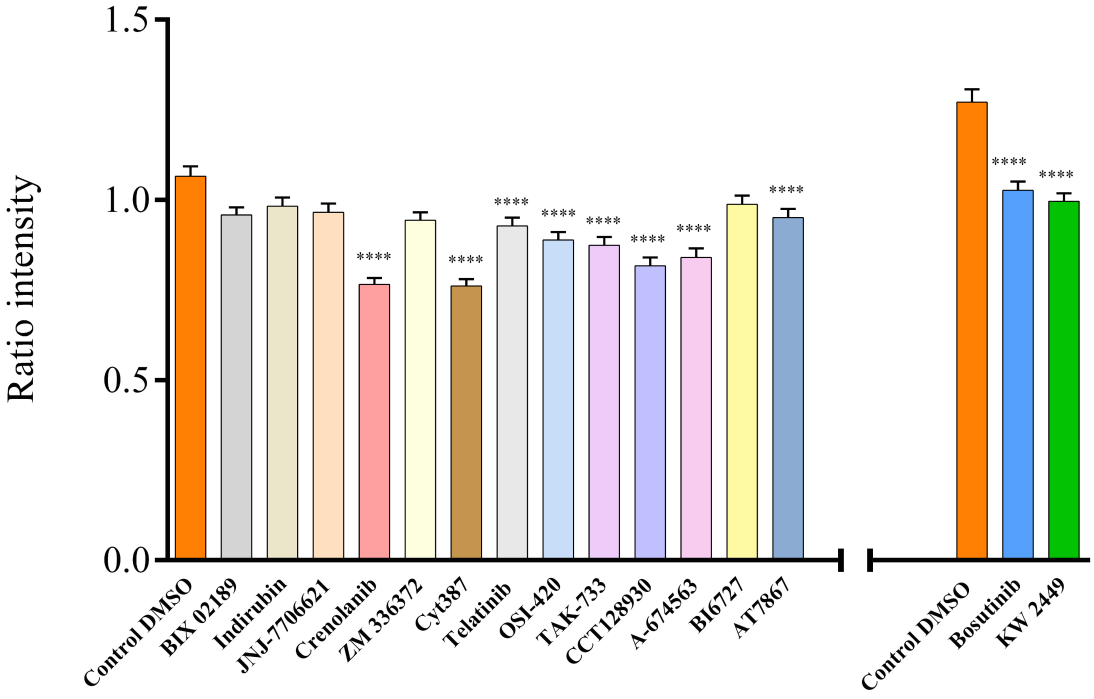

Figure 3.3.2 Kinase inhibitors identified in the secondary screen were validated in a tertiary screen. Cells were treated with kinase inhibitors at 5 μM concentration in quadruplicate for 4 hours and DJ-1 BiFC signal was analyzed, and quantified through the Cell^R Scan^R screening station. Graph shows average ratio intensity (GFP/RFP) per condition and error bars represent SEM. ****P<0.0001.

Compound Name	Kinase inhibited
AT7867	Akt 1, Akt2 and Akt3
A-674563	Akt1
CCT128930	Akt2
BIX 02189	MEK5, ERK5
TAK-733	MEK1
Crenolanib	PDGFRα, PDGFRβ
Telatinib	VEGFR2, VEGFR3,PDGFRα, and c-Kit
OSI-420	EGFR
Bosutinib	Src, Abl
KW2449	FLT3, Abl, Aurora A, JAK2, FGFR1
Cyt387	JAK1, JAK2, JAK3
ZM336372	c-Raf
BI6727	PIK1
Indirubin	CDK1,CDK2, CDK5 , GSK3β, Src
JNJ-7706621	CDK1/Cyclin B, CDK2/Cyclin A,CDK2/Cyclin E, Aurora-A, Aurora-B

Table 3.3.1 Kinase inhibitor compounds that modulate DJ-1 dimerization and their targets kinases.

To confirm our data from the primary, secondary and tertiary screens, and also to check whether or not the effect of the compounds is dose dependent, we re-tested again all these 10 hits at three different concentrations (100 nM, 1 and 5 μM) in quadruplicate in two independent experiments. We decided to verify what was the effect of a much lower concentration (100 nM), as the IC50s of these compounds are low (between 2-50 nM) in comparison with the concentrations we used in primary, secondary and tertiary screens. We observed that only 5 out of the 10 kinase inhibitors significantly modulated DJ-1 dimerization in this experiment and as shown in Figure 3.3.3 none of these hits could modulate DJ-1 dimerization at the lowest concentration (100 nM). Surprisingly, in the new screens the kinase inhibitors Telatinib and TAK-733 showed a different result from the first three screens, as they increased DJ-1 dimerization at both 1 and 5 μM concentrations. More importantly, we were able to confirm that Bosutinib, KW2449, and Crenolanib decreased DJ-1 dimerization, validating our previous results. Interestingly, Bosutinib and KW2449 not only caused a constant decrease in DJ-1 dimerization (~ 13-18 %) in all the screens, but also they target the same tyrosine kinase, c-Abl (Figure 3.3.3 and Table 3.3.1). c-Abl has been reported to be implicated in neurodegenerative disorders such as AD and PD. Even though there is no evidence to indicate a direct effect of c-Abl on DJ-1, these results suggest that c-Abl directly or indirectly modulates DJ-1 dimerization.

We decided to further explore the potential role of c-Abl in DJ-1 dimerization and the screen was re-performed using only Bosutinib and KW2449 kinase inhibitors with a wide range of concentrations (1-50 μM), to check whether or not this reduction in DJ-1 dimerization is a dose dependent phenomenon. To this end, we used HEK 293T cells transiently transfected with WT DJ-1 BiFC constructs and RFP, and 24 hours post-transfection cells were treated with kinase inhibitors in quadruplicate. The screen was carried out 4 hours after treatment and all the images from the screen were monitored for the cellular morphology to check any toxic effects of these compounds. The 50 μM concentration of both compounds was toxic to the cells (data not shown), and we also observed 20 μM is a threshold concentration for cell toxicity effect of both compounds, as DJ-1 dimerization increases at this concentration due to cell death (data not shown).

Our results from this experiment show Bosutinib and KW2449 decrease DJ-1 dimerization in a dose dependent manner at 1, 5 and 10 μM treatments (Figure 3.3.4).

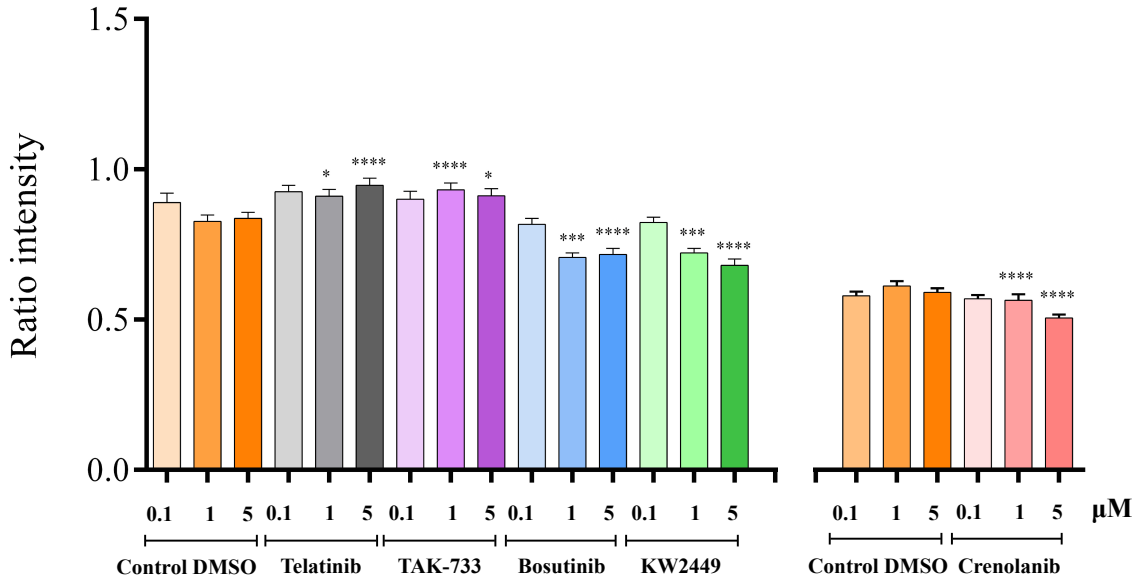

Figure 3.3.3 The kinase inhibitors Telatinib and TAK-733 increased DJ-1 dimerization at 1 and 5 µM, while Bosutinib, KW2449 and Crenolanib decreased dimerization. Each condition was tested in quadruplicate. The histogram shows the average ratio intensity (green/red) per well ±SEM. ****P<0.0001.

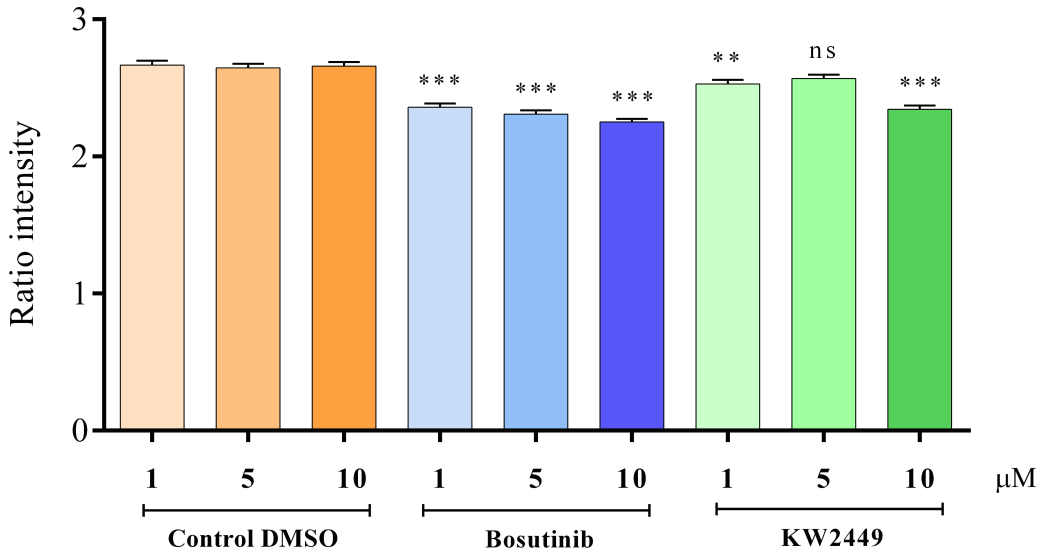

Figure 3.3.4 Bosutinib and KW2449 dose-dependently decrease DJ-1 dimerization in living cells. Conditions were tested in quadruplicate. The histogram shows the average ratio intensity (green/red) per well ±SEM. ***P<0.0001.

3-3-2 The effect of Bosutinib and KW2449 treatment on DJ-1 dimerization in oxidative stress conditions

Since one of the main cellular roles of DJ-1 is protection from oxidative stress and our laboratory previously showed that WT DJ-1 dimerization increases in response to oxidative stress (Repici et al., 2013), we next used the same screening procedure to check if treatment with these hits could influence DJ-1 dimerization under oxidative stress conditions. To approach this aim, we used HEK 293T cells transiently transfected with WT DJ-1 BiFC constructs and RFP, treated with compounds 24 hours after transfection for 4 hours, and subjected to oxidative stress by exposure to 1 mM H_2O_2 treatment for 2 hours. The screen was carried out using the same procedure as described earlier in Section 3.3.1 with a 96 well plate format, each condition was tested in 4 different wells (quadruplicate).

I found that treatment with Bosutinib and KW2449 dose dependently decreases DJ-1 dimerization in both normal and oxidative stress conditions (Figure 3.3.5 and 3.3.6). Interestingly, I observed that Bosutinib decreases the effect of H_2O_2 treatment on DJ-1 dimerization in a dose dependent manner, and at 10 μM it completely prevented the increase of WT DJ-1 dimerization due to oxidative stress (blue vs pink) (Figure 3.3.5). In contrast KW2449 did not influence the effect of H_2O_2 treatment on DJ-1 dimerization (green vs orange) (Figure 3.3.6).

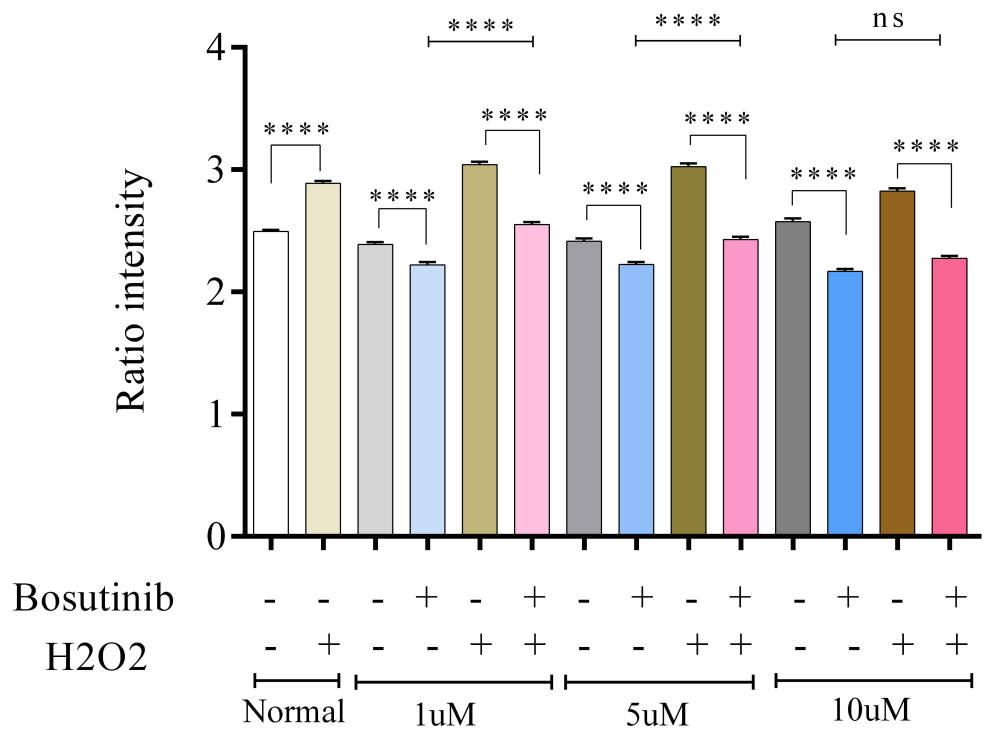

Figure 3.3.5 The effects of Bosutinib on DJ-1 dimerization in normal and oxidative stress conditions. Despite oxidative stress stabilizing WT DJ-1 dimerization, Bosutinib dose dependently decreases this increase in DJ-1 dimerization and at 10 μM completely prevents it (blue vs pink). Conditions were tested in quadruplicate. The histogram shows the average ratio intensity (green/red) per well ±SEM. ****P<0.0001.

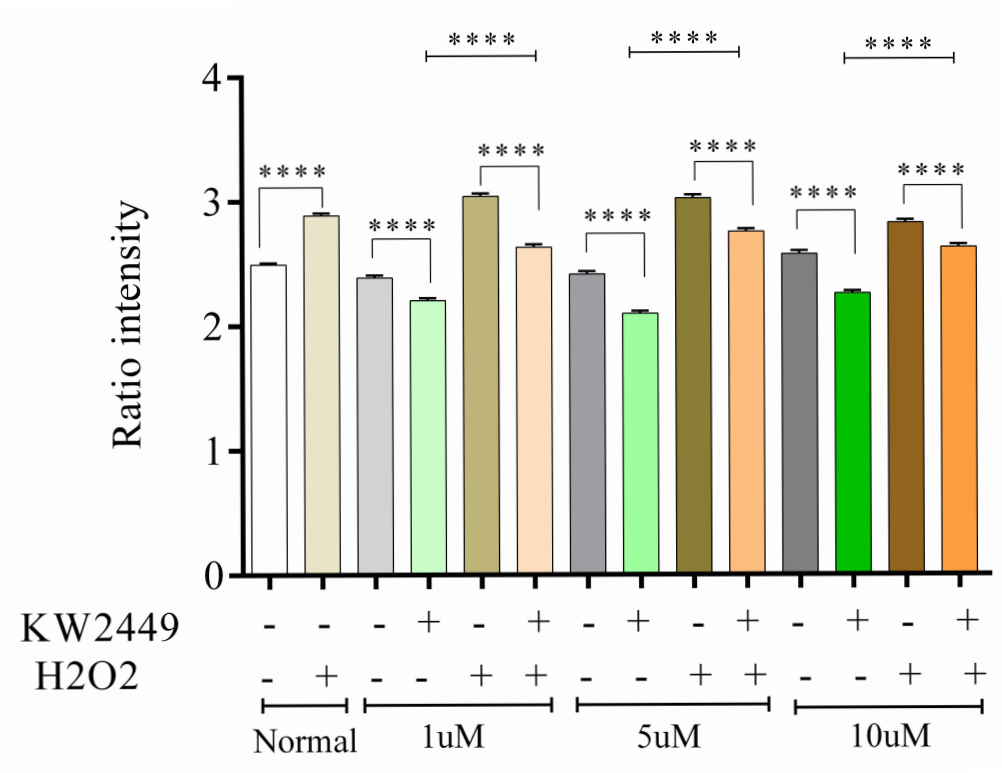

Figure 3.3.6 KW2449 decreases DJ-1 dimerization in normal and oxidative stress conditions. KW2449 does not influence the effect of H_2O_2 treatment on DJ-1 dimerisation (green vs orange). Each condition was tested in quadruplicate. The graph displays the average ratio intensity (green/red) per well ±SEM. ****P<0.0001.

3-3-3 Bosutinib and KW2449 treatment modulate E64D DJ-1 dimerization

To further elucidate the role of our hits in DJ-1 dimerization and function, we extended our work and tested the effect of these kinase inhibitors on the dimerization of E64D DJ-1. Indeed, biochemical approaches have shown that the E64D mutant form of DJ-1 is able to dimerize as WT, and these results were recently validated in living cells by Dr. Repici in our laboratory (Gorner et al., 2004, Hulleman et al., 2007, Malgieri and Eliezer, 2008, Repici et al., 2013). However, despite oxidative stress conditions stabilizing WT DJ-1 dimerization, it does not have any effect on E64D DJ-1 dimerization, which may have implications for its role in PD pathogenesis (Repici et al., 2013). To explore this aim, we transiently transfected cells with E64D BiFC constructs and our RFP control construct. 24 hours post-transfection cells were treated with compounds for 4 hours, and then with 1 mM H_2O_2 for 2 hours in quadruplicate and screened as above (Figure 3.3.7 and Figure 3.3.8).

Data from this screen demonstrated that Bosutinib decreases E64D DJ-1 dimerization both in normal and oxidative stress conditions. The effect of the Bosutinib treatment on E64D DJ-1 dimerization disappeared at 10 μM in normal conditions (gray vs blue). This treatment also dose dependently decreases the oxidative stress effect on E64D DJ-1 dimerization similar to the manner which occurs with WT DJ-1 (blue vs pink) (Figure 3.3.7). I also noticed treatment with KW2449 decreased E64D DJ-1 dimerization in normal conditions, but this reduction disappears by increasing compound concentration (gray vs green). In contrast, we observed KW2449 treatment stabilizes E64D dimerization in oxidative stress conditions (green vs orange). Interestingly, we also observed that DMSO effects E64D dimerization in oxidative stress. Although recent work by Repici et al. has shown that the E64D dimer does not react to oxidative stress (Repici et al., 2013), I observed that E64D dimerization decreases in presence of DMSO (Figure 3.3.7 and Figure 3.3.8).

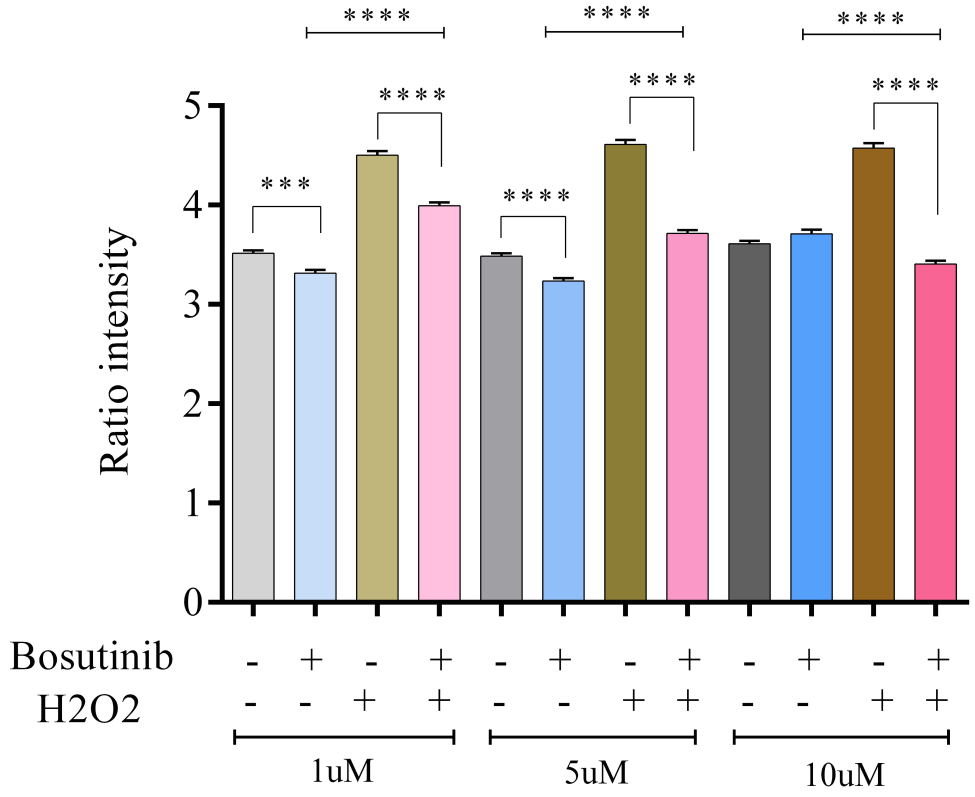

Figure 3.3.7 Bosutinib modulates E64D dimerization in normal and oxidative stress conditions. In control conditions Bosutinib decreases E64D DJ-1 dimerization similarly to WT DJ-1 at low concentration but this reduction disappears with increasing concentrations (gray vs blue). Although treatment with Bosutinb stabilizes E64D DJ-1 dimerization in oxidative stress at the lower concentration, this effect completely disappeared at 10 μM (blue vs pink). Conditions were tested in quadruplicate. The histogram shows the average ratio intensity (green/red) per well ±SEM. ****P<0.0001.

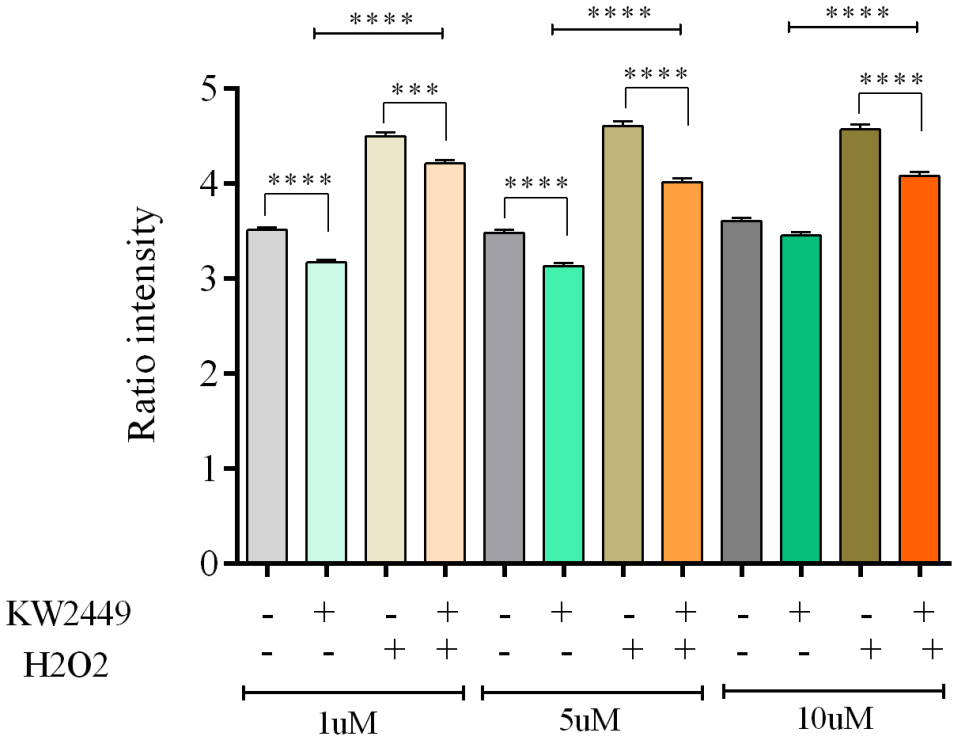

Figure 3.3.8 KW2449 modulates E64D dimerization in normal and oxidative stress conditions. KW2449 decreases E64D DJ-1 dimerization similar to WT DJ-1 at low concentrations, but this reduction diminishes with increasing concentration (gray vs green). Treatment with KW2449 stabilizes E64D DJ-1 dimerization in oxidative stress. Each condition was tested in quadruplicate. The histogram shows the average ratio intensity (green/red) per well ±SEM. ****P<0.0001.

3-3-4 The effects of Bosutinib and KW2449 treatment on DJ-1 protein levels

As it was possible that the reductions observed in DJ-1 dimerization after treatment with Bosutinib and KW2449 were due to changes in DJ-1 protein expression or stability, we used immunoblotting to check DJ-1 protein levels after treatment with these compounds. Thus, we transiently transfected cells with WT and E64D DJ-1 BiFC constructs, and 24 hours post-transfection cells were treated with compounds for 4 hours and exposed to 1 mM H_2O_2 for 2 hours. Immunoblotting analysis revealed that there was no difference in DJ-1 levels in cells treated with Bosutinib and KW2449 compared to cells treated with DMSO as a control (Figure 3.3.9, 3.3.10, 3.3.11, 3.3.12). These results indicate that the changes observed above are most likely due to alterations in DJ-1 dimerization, though the sensitivity of immunoblotting may mean that small changes in protein levels are not detected.

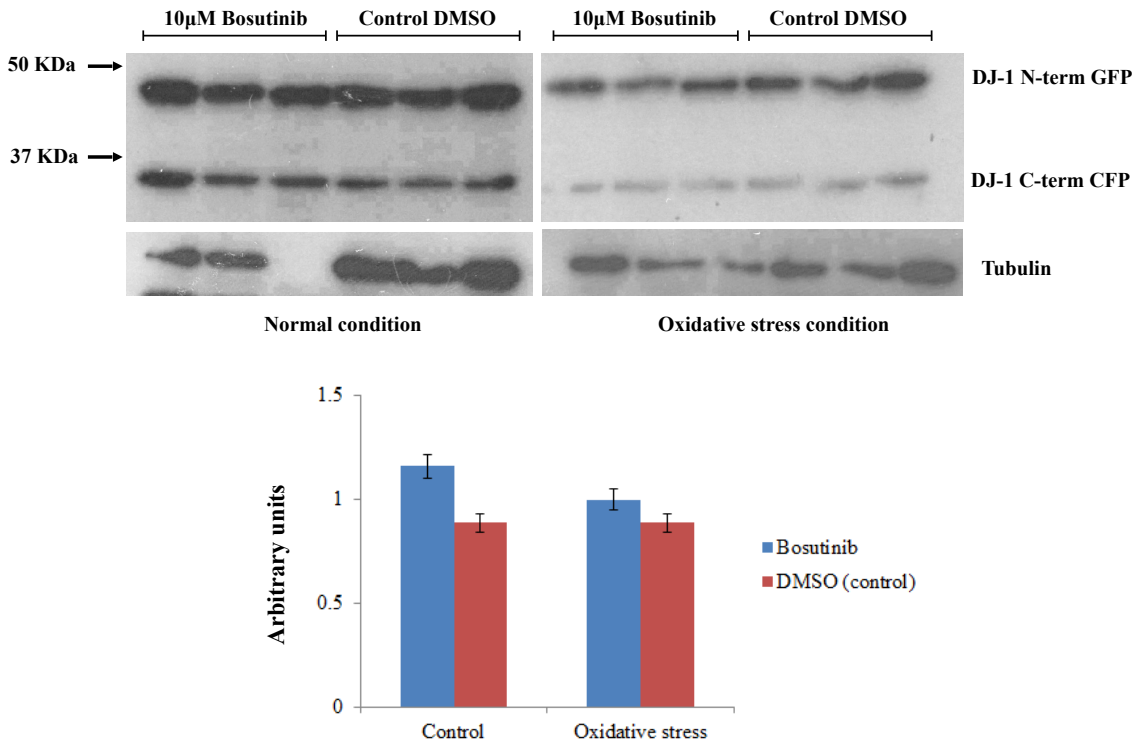

Figure 3.3.9 Bosutinib treatment did not affect protein DJ-1 levels in normal and oxidative stress conditions. 24 hours after transfection cells were treated with 10 µM Bosutinib for 4 hours (with or without 1mM H_2O_2 for 2 hours). DJ-1 protein was detected by immunoblotting using antibodies against DJ-1. Immunoblot results show that DJ-1 levels are not altered upon treatment with Bosutinib in normal and oxidative stress. Tubulin was used as a loading control. In each lane, the upper band corresponds to DJ-1-GN173 and the lower band corresponds to DJ-1-CC155. Gel densitometry was performed using the average of three replicates (3 wells per condition) for each condition.

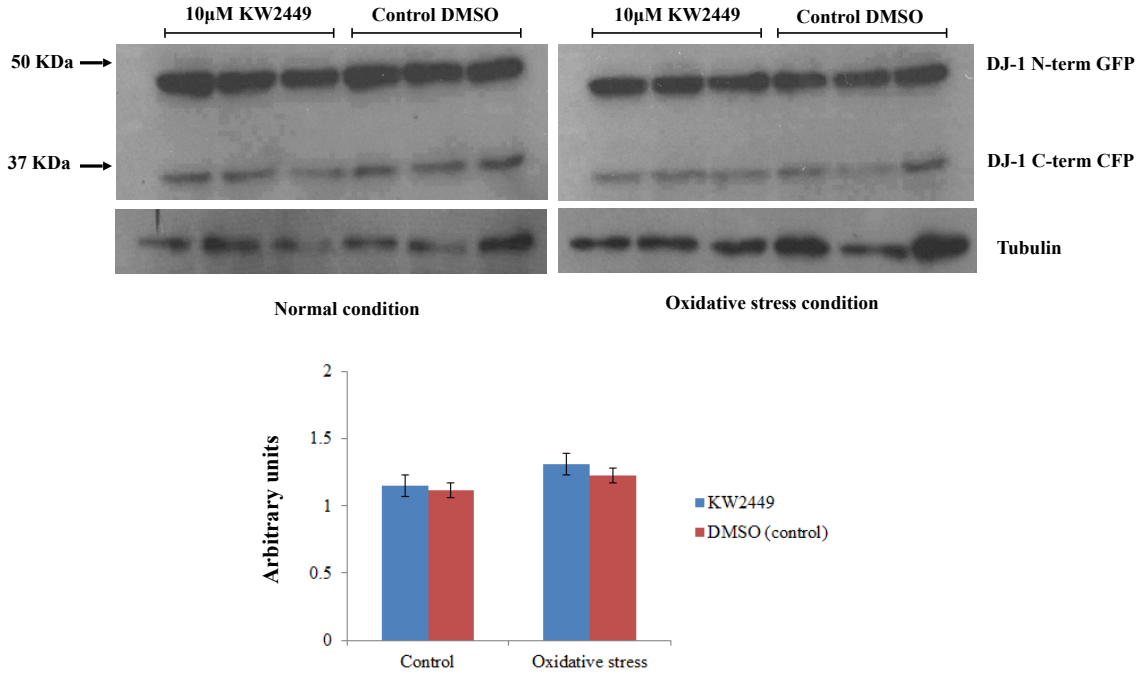

Figure 3.3.10 KW2449 treatment does not affect DJ-1 levels in normal and oxidative stress conditions. 24 hours after transfection cells were treated with 10 µM KW2449 for 4 hours, with or without 1mM H_2O_2 for 2 hours. DJ-1 was detected by immunoblotting using antibodies against DJ-1. Immunoblot data showed that DJ-1 levels are not altered upon treatment with KW2449 in normal and oxidative stress conditions. Tubulin was used as a loading control. In each lane, the upper band corresponds to DJ-1-GN173 and the lower band corresponds to DJ-1-CC155. Gel densitometry was performed using average of three technical repeats (3 wells) for each condition.

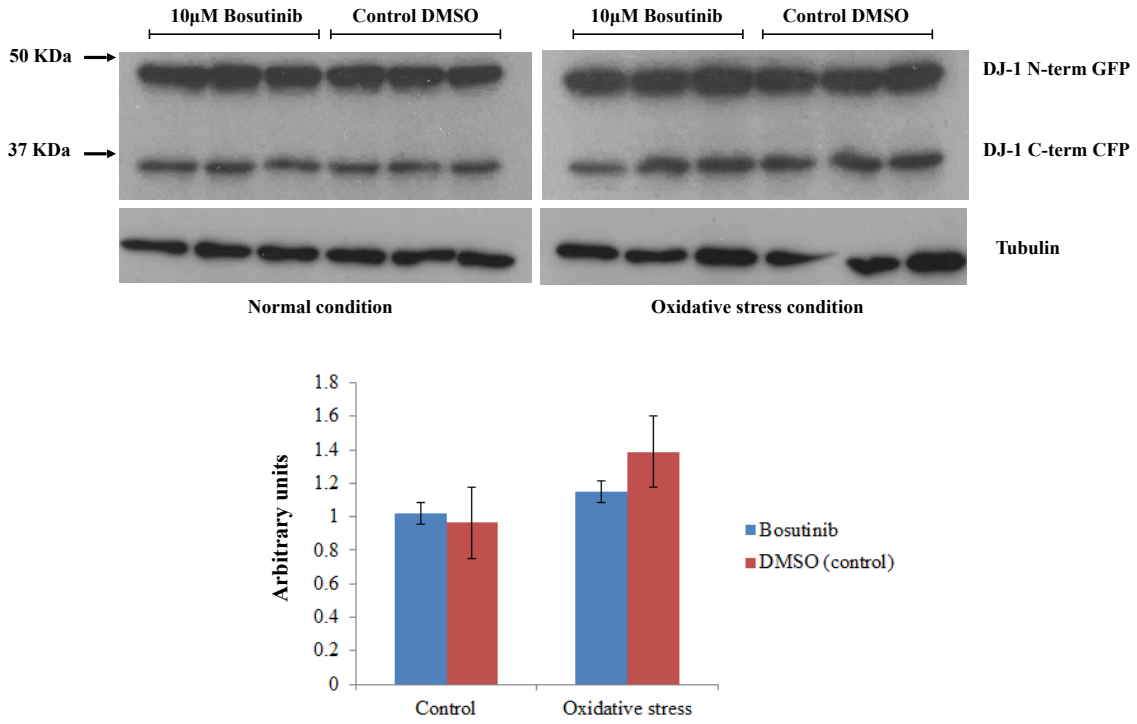

Figure 3.3.11 Bosutinib treatment does not affect E64D DJ-1 levels in normal and oxidative stress conditions. 24 hours after transfection cells were treated with 10 μM Bosutinib for 4 hours, with or without 1 mM H_2O_2 for 2 hours. Immunoblot results show DJ-1 levels are not altered upon treatment with Bosutinib in normal and oxidative stress conditions. Tubulin was used as a loading control. In each lane, the upper band corresponds to DJ-1-GN173 and the lower band corresponds to DJ-1-CC155. Gel densitometry was performed using average of three technical repeats (3 wells) for each condition.

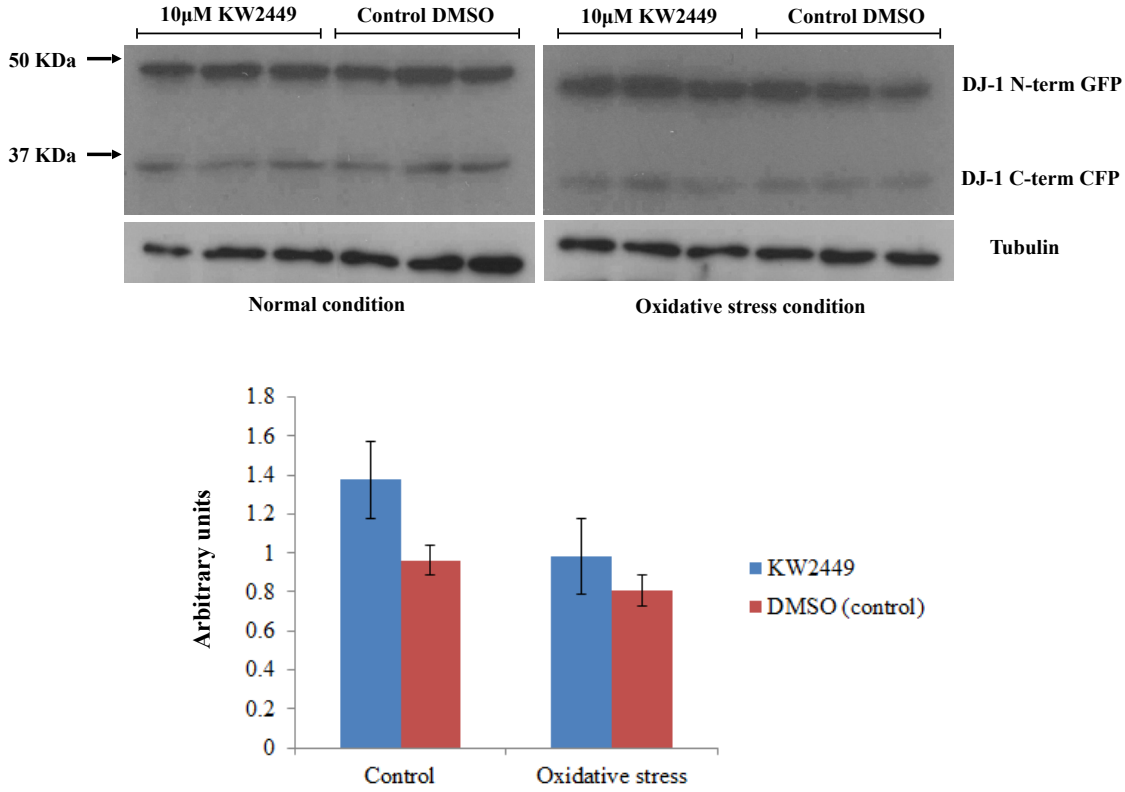

Figure 3.3.12 KW2449 treatment does not influence E64D DJ-1 protein levels in normal and oxidative stress conditions. 24 hours after transfection cells were treated with 10 μM KW2449 for 4 hours and with or without 1mM H_2O_2 for 2 hours. Immunoblot data showed DJ-1 protein levels are not altered upon treatment with KW2449 in normal and oxidative stress conditions. Tubulin was used as a loading control. In each lane, the upper band corresponds to DJ-1-GN173 and the lower band corresponds to DJ-1-CC155. Gel densitometry was performed using average of three technical repeats (3 wells) for each condition.

3-3-5 Treatment with Bosutinib and KW2449 does not have toxic effects on cells

Another imperative criterion that should be considered to validate our results is cell viability. Indeed, we needed to check whether a decrease in DJ-1 dimerization upon treatment with Bosutinib and KW2449 was really due to c-Abl inhibition and not to cytotoxic effects of the treatment leading to a decreased number of fluorescent cells due to compound toxicity, and thus less signal. To this end, we used the lactate dehydrogenease (LDH) toxicity assay to test cytotoxicity after cell treatment with Bosutinib and KW2449. The LDH assay is based upon quantifying LDH activity which is a stable cytosolic enzyme released upon cell death. Medium from cells whose lysates were used for immunoblotting in Section 3.3.4 was used for the LDH assay. No toxic effect due to Bosutinib or KW2449 treatment in cells transfected with WT or E64D DJ-1 was observed (Figure 3.3.13, 3.3.14).

However, these data suggest that none of the concentrations of either compounds (Bosutinib & KW2449) were toxic to our cellular model, thus indicating that decrease in DJ-1 BiFC fluorescence upon treatment with these compounds is likely due to decrease in DJ-1 dimerization and not to the cytotoxicity effects of the treatments. Interestingly, we also observed that although H_2O_2 treatment is toxic to the cells transfected with WT DJ-1, this cytotoxicity effect is completely eliminated upon treatment with kinase inhibitors Bosutinib and KW2449 (Figure 3.3.13). Our results also indicated that Bosutinib treatment ameliorates the cytotoxic effect of H_2O_2 treatment on cells over-expressing E64D DJ-1 BiFC constructs similar to the WT DJ-1. On the other hand, KW2449 treatment on those cells showed some cytotoxicity upon H_2O_2 treatment that was significantly lower than control condition (Figure 3.3.14).

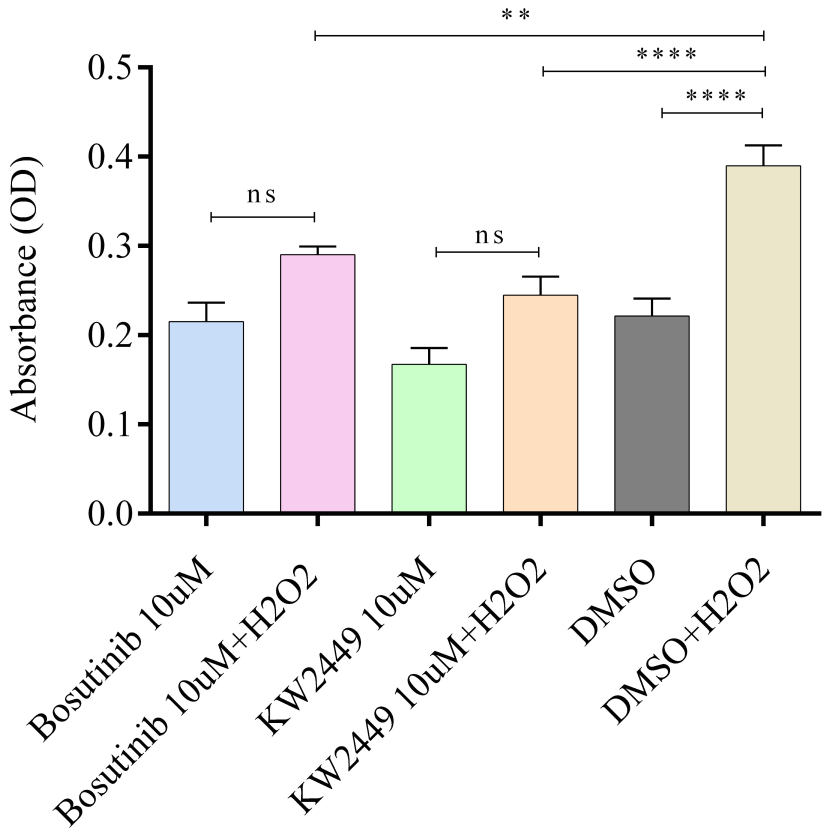

Figure 3.3.13 LDH toxicity test for Bosutinib and KW2449 treatment on WT DJ-1 BiFC transfected cells. The histogram displays the level of released LDH in the medium for each condition. Treatment with Bosutinib and KW2449 not only are not toxic to the cells but also ameliorate the cytotoxic effect of hydrogen peroxide. Data is Mean ±SEM. ****P<0.0001.

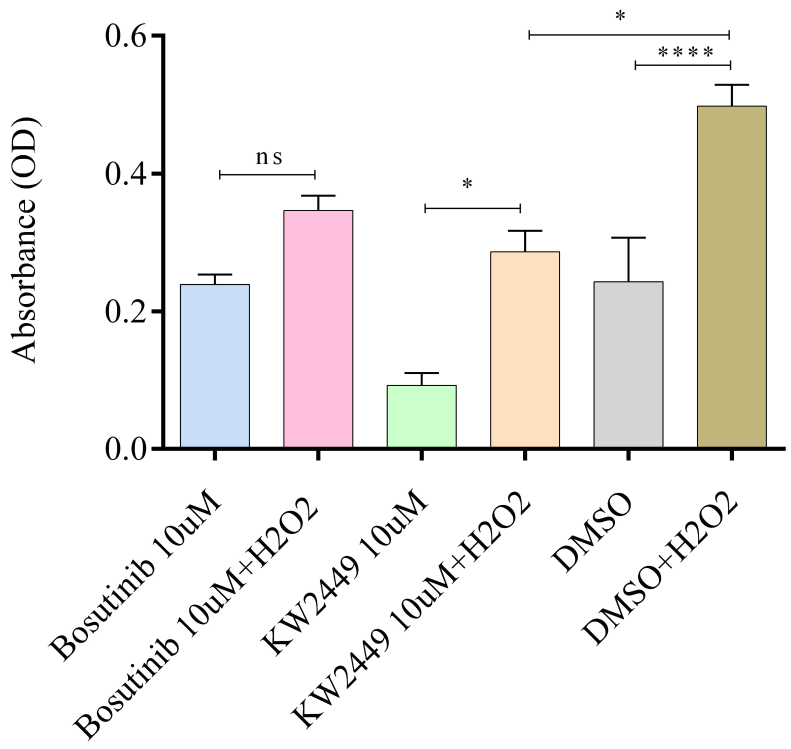

Figure 3.3.14 Analysis of the cytotoxic effects of Bosutinib and KW2449 treatment on cells over-expressing E64D DJ-1 BiFC constructs. Histogram shows LDH released in the medium for each condition. Similarly to the WT DJ-1, treatment with Bosutinib ameliorates the cytotoxic effect of H_2O_2 treatment. Although cells treated with KW2449 showed some cytotoxicity upon H_2O_2 treatment this was significantly lower than control conditions. Data shows Mean ±SEM. ****P<0.0001.

3-4 Discussion

Investigating the complex role of DJ-1 modifications and its effects on DJ-1 stability, function and localization is vital for clarifying DJ-1 role in various cellular pathways, especially in response to oxidative stress, as well as its pathological role in PD. Screen such as that described above with kinase and phosphatase inhibitors serve not only to examine the vast majority of kinases and phosphatases and their signaling networks that might directly or indirectly influence DJ-1 function, but also to provide a unique opportunity to test promising drug targets.

As discussed in more detail in the introduction, BiFC has been widely employed to study protein-protein interactions particularly in the neuroscience field since this technique allows the visualisation of the formation of dimeric and oligomeric species by aggregation-prone proteins. Indeed, the BiFC approach is relatively quick and accurate and allows to visualise what happens in living cells. In this study we selected this method to carry out screens to investigate kinases and phosphatases able to modulate DJ-1 dimerization as a metric of DJ-1 function. To our knowledge nobody has ever studied DJ-1 phosphorylation status nor its correlation with DJ-1 dimerization.

In order to implement the screen, our first step was to generate DJ-1 BiFC constructs with two different selection markers for obtaining stable clones over-expressing DJ-1 BiFC constructs. To this end, we measured the concentration of antibiotics (zeocin and neomycin) needed for selecting cells that stably over-express both DJ-1 BiFC constructs by performing kill curve experiments. One of the major concerns in this study was selecting suitable cells for generating stable clones that are not only easy to transfect, but also morphologically appropriate for studying DJ-1 localization after treatment. The HeLa cell line was selected as our first candidate for generating stable clones over-expressing DJ-1 BiFC constructs as this cell line fulfills both criteria. We observed this cell line is not able to stably over-express DJ-1 BiFC constructs. The reason why fluorescence complementation between DJ-1 BiFC constructs disappeared after two weeks despite both selection markers (Neomycin and Zeocin) were applied twice a week after transfection was not clear, but clearly indicated these cells were not applicable for our screening experiment. One possible explanation for this phenomenon might be that DJ-

1 genomic insertion in HeLa cells occurs in a way that leads to DJ-1 expression being silenced.

The HEK 293T cell line was also used for generating stable clones over-expressing the DJ-1 BiFC constructs. Although this cell line is easy to transfect and is morphologically suitable for our studies, one of its major disadvantages is its resistance to Neomycin, which is one of our selection markers for generating stable clones. However, we observed that despite the fact that we were not able to use Neomycin to select stable clones, fluorescence complementation signal in these cells could be detected by Cell^R Scan^R microscopy after a month, suggesting that both constructs were stably integrated into the genome of these cells.

To exploit the HEK 293T stable clone over-expressing the DJ-1 BiFC constructs in our high throughput screening system, it was necessary to confirm that both DJ-1 BiFC constructs were expressed in those cells by immunoblot. Also, it was very relevant to check whether or not the BiFC signal of this clone is constant, and also whether this same signal could be modulated by knocking down DJ-1 expression, as a proof of concept that we could detect variation in DJ-1 BiFC levels. We found that both DJ-1 BiFC constructs are equally expressed in our stable clone and that the fluorescence complementation signal is consistent. Importantly, the BiFC signal could be modulated by altering expression of DJ-1 BiFC constructs.

We next focused on optimizing the BiFC screening on 96 well plate format. One of the main concerns related to this point is that for selecting cells and normalizing fluorescence signal emission through Cell^R Scan^R screening station the RFP signal is essential, and this requires a transfection step which can be toxic to the cells. We then first tested whether Cell^R Scan^R screening station is able to accurately detect all the changes in DJ-1 BiFC signal without normalizing fluorescence signal emission by the emission of RFP. To this aim, we knocked down DJ-1 expression through anti DJ-1 siRNA, and we checked if the reduction in the DJ-1 BiFC signal was recorded by Cell^R Scan^R screening station as corresponding to the decrease in DJ-1 protein level. Unfortunately, the Cell^R Scan^R screening station is not able to detect any changes in DJ-1 BiFC signal without normalising the GFP emission by the emission of RFP. Thus, we had to transiently transfect BiFC stable clone cells with RFP 24 hours before treating

with compounds for an accurate detection of DJ-1 BiFC signal. Additionally, following the screening, all the taken images were checked to certify changes in DJ-1 BiFC signal are neither due to toxicity upon transfection nor toxicity due to chemical compounds treatment. We then tested varying number of images per well to obtain a constant BiFC signal from each individual well in the minimum time, important as our screen was planned to be carried out in living cells. This optimized condition enabled us to perform our screens using 194 kinase inhibitors and 33 phosphatase inhibitors compounds to identify novel DJ-1 dimerisation modifiers.

Our BiFC data show that Boutinib and KW2449 constantly decrease DJ-1 dimerization (~ 15-18 %). Interestingly, despite these two kinase inhibitors targeting different kinases (Table 3.3.1), c-Abl tyrosine kinase is a common target for both inhibitors which suggests c-Abl could be involved in the decrease of DJ-1 dimerization upon treatment with these compounds. In addition, although STI-571 is the most common c-Abl inhibitor that has been used by different research groups (Cancino et al., 2008, Ko et al., 2010), it has been reported that Bosutinib can inhibit c-Abl more potently than STI-571 (http://www.selleckchem.com/products/Bosutinib.html). Therefore, the effect of STI-571 could also be tested on DJ-1 dimerization to further validate our screen results.

Inhibition of the c-Abl tyrosine kinase by either Bosutinib or KW2449 decreased DJ-1 dimerization in normal and oxidative stress conditions. This suggests that c-Abl may directly or indirectly influence DJ-1 dimerization. We also observed that Bosutinib completely reversed the oxidative stress effect on DJ-1 dimerization. Additionally, we tested these two compounds on E64D which is the only DJ-1 mutant structurally identical to the WT protein, and we observed similar results to the ones observed with the WT protein.

Abelson tyrosine kinase (c-Abl) is a nonreceptor tyrosine kinase that localizes in cytoplasm, and the nucleus as well, since it bears a nuclear localization signal (Hubbard and Till, 2000). Abundant evidence has shown that c-Abl plays distinct roles based on its subcellular localization and is involved in multiple interconnected pathways, thus acting as an arbiter of neuronal survival and neuronal death (Gonfloni et al., 2012). For instance, although the nuclear form of c-Abl is activated in response to genotoxic stress,

cytoplasmic c-Abl is involved in the apoptotic response of cells to oxidative stress (Kharbanda et al., 1995, Sun et al., 2000). Indeed, cytochrome c release and apoptosis in response to oxidative stress were shown to be c-Abl dependent mechanism (Sun et al., 2000). Kumar et al. showed that in response to oxidative stress, cytoplasmic c-Abl translocates into mitochondria leading to mitochondria dysfunction and cell death (Kumar et al., 2001). Subcellular fractionation studies by Ito et al. have identified that ~20 % of c-Abl is also detectable in the endoplasmic reticulum (ER) (Ito et al., 2001). In response to ER stress, the ER-associated c-Abl fraction translocates to mitochondria leading to release of cytochrome c and apoptosis (Ito et al., 2001).

More importantly, c-Abl is involved in central nervous system development and its activation is increased in neurodegenerative disorders such as AD and PD. Indeed, nonspecific post-translational modifications induced by c-Abl may contribute to mitochondrial dysfunction, oxidative stress response and protein aggregation that are typical features of neurodegenerative disorders (Gonfloni et al., 2012). In the AD context, phosphorylated c-Abl at residue T735 has been shown to colocalize with amyloid plaques, neurofibrillary tangles (NFTs) and granulovacuolar degeneration (GVD) in the entorhinal cortex, hippocampus and brain of AD patients (Yoshida et al., 2005, Jing et al., 2009, Schlatterer et al., 2011). Moreover, c-Abl/p73 proapoptotic signaling has been shown to be induced by Amyloid β (Aβ) fibrils in primary neurons, while pharmacological inhibition of c-Abl suppresses Aβ-dependent toxicity (Alvarez et al., 2004, Cancino et al., 2008). Notably, further AD-related work has found that c-Abl directly phosphorylates microtubule-associated protein (MAP) tau at residue Y394, and also indirectly mediates its phosphorylation through activation of Cdk5 and GSK3β kinases (Alvarez et al., 2004, Derkinderen et al., 2005, Cancino et al., 2008). It has recently been shown that c-Abl is activated in Parkinson's disease (Ko et al., 2010, Schlatterer et al., 2011). Parkinson’s related protein Parkin which is an ubiquitin E3 ligase involved in mitochondria function and autophagy is negatively regulated by c-Abl (Gonfloni et al., 2012). Notably, phosphorylation of Parkin at residue Y143 by c-Abl is a main Parkin post-translational modification that leads to Parkin inactivation and disease progression in sporadic forms of PD (Ko et al., 2010). Treatment of mice with the dopaminergic toxin MPTP stimulated ABL kinase and Parkin tyrosine phosphorylation. Interestingly,

MPTP-induced Parkin tyrosine phosphorylation was not observed in mice with the neuronal knockout of Abl1, and this phosphorylation defect correlated with a reduction in MPTP-induced neuronal cell death in the Abl1-deficient mouse brain (Ko et al., 2010). More recently, a brain-penetrant ABL kinase inhibitor was shown to also protect mice from the MPTP-induced loss of TH+ neurons (Imam et al., 2013).

The effect of Bosutinib and KW2449 on DJ-1 dimerization may be explained by a direct or an indirect effect of c-Abl on DJ-1 protein. Investigation of c-Abl targets association with DJ-1 in absence and presence of c-Abl by coIP, immunohistochemistry or MS may help to clarify precise mechanisms behind the reduction in DJ-1 dimerization upon c-Abl inhibition. On the other hand, as c-Abl is a key player in the response of cells to oxidative stress, and we know from our previous studies that oxidative stress increases DJ-1 dimerization, the decrease in dimerization could thus be an indirect effect of the reduction of oxidative stress as a consequence of c-Abl inhibition.

Thus, in this study I have established and optimized a high throughput BiFC screening that will permit further identification of DJ-1 interaction partners in living cells for a better understanding of DJ-1 role associated with PD pathogenesis. Furthermore, I have identified c-Abl as a novel DJ-1 dimerization modifier that may shed more light on DJ-1 functions (Figure 3.4.1).

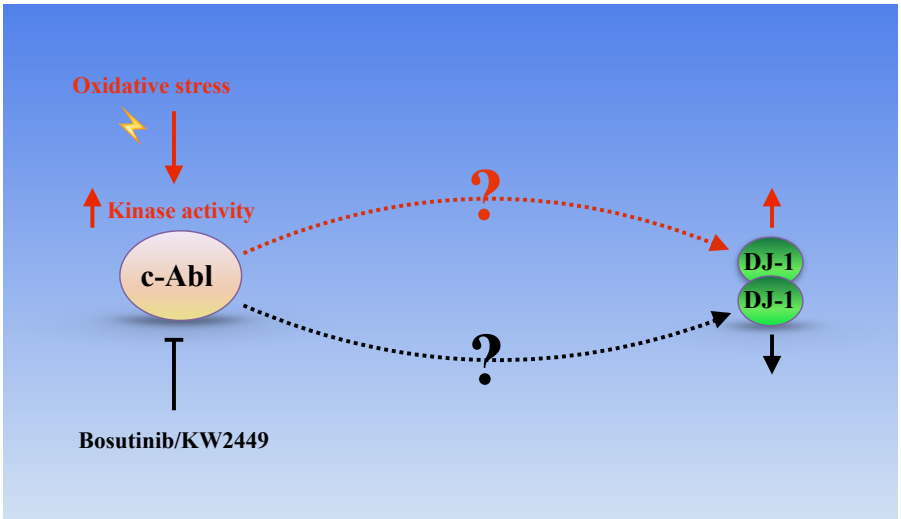

Figure 3.4.1 Model for the possible influence of c-Abl on DJ-1 dimerization. c-Abl is up-regulated upon oxidative stress and this correlates with the increase in DJ-1 dimerization in oxidative stress conditions there. This correlation may be mediated by a direct or indirect effect of c-Abl on DJ-1 protein.

Chapter 4

Exploring the functional implications of DJ-1 phosphorylation

4-1 Introduction

Protein post-translational modifications (PTMs) contribute to a wide range of cellular processes from enzymatic activation, regulation of signal transduction to cell cycle control by directly influencing the structure, dynamics and interaction networks of their targets (Petrov et al., 2013). Proteins in the cell are covalently modified in two distinct ways: 1) by non regulated mechanisms that mainly occur in response to oxidative stress and are predominantly associated with protein damage, and are thus linked to age-related diseases such as neurodegenerative disorders and cancers; and 2) enzymatic post-translational modifications that are implicated in large number of cellular processes (Berlett and Stadtman, 1997, Walsh et al., 2005, van Rossum et al., 2012).

Protein phosphorylation is the most common post-translational modification and influences ~ 30 % of eukaryotic proteins, hence pathological dysregulation of kinase activity has been reported in vast majority of human diseases including neurodegenerative diseases and most of cancers (Cohen, 2000, Blume-Jensen and Hunter, 2001, Mann et al., 2002, Manning et al., 2002, Liachko et al., 2013). Proteins can be phosphorylated at multiple residues by different protein kinases leading to altered protein functions in various cellular pathways (Manning et al., 2002, Moorhead et al., 2007). Indeed, modified residues can contribute to fine-tuning of molecular interactions, and can also alter activity and stability of proteins rather than modulating individual functions (Zhou et al., 2007).

The identification of phosphorylated residues in proteins associated with neurodegenerative diseases, and understanding how such modifications can influence conformation, localization and function of a target protein can provide a better understanding of the molecular mechanisms underlying the complex pathogenesis processes of these disorders. Interestingly, global phosphoproteomic approaches exploiting MS have recently been used for the elucidation of neurodegenerative diseases (Bahk et al., 2013). This technique provides several analytical strategies for the identification of phospho-

proteins and characterization of the location of the phosphorylated sites on these proteins (Ashman and Villar, 2009, Piggee, 2009).

As discussed earlier (see Section 1.3.5.6) Parkinson's related protein DJ-1 is post-translationally modified by sumoylation, S-nitrosylation, and phosphorylation (Ito et al., 2006, Shinbo et al., 2006, Rahman-Roblick et al., 2008). Lin and colleagues found that two novel DJ-1 post-translational modifications - phosphorylation at T19 and Y67 and HEN adduction of DJ-1 - are not only associated with PD pathogenesis, but could also be used as PD biomarkers (Lin et al., 2012). Focusing on phosphorylation data obtained from MS in different studies associated with cancer and PD have revealed that DJ-1 is phosphorylated at residues T19, Y67, Y139, Y141 as well as potentially at T140, S142 sites via in silica analysis. However, to our knowledge, the effects of DJ-1 phosphorylation on its function, localization, dimerization and stability have never been studied.

To characterize DJ-1 phosphorylation, I first verified whether or not we were able to detect phosphorylated DJ-1 in normal conditions or in response to oxidative stress. Next, to study the effect of DJ-1 phosphorylation on specific residues, I generated DJ-1 phosphomimetic and phosphoblocking mutant BiFC constructs for the all the possible residues in the DJ-1 protein structure and I characterized the effects of these mutants on DJ-1 in normal and oxidative stress condition.

4-2 Investigating the role of phosphorylation in DJ-1 function

4-2-1 Detection of DJ-1 phosphorylation in normal and oxidative stress conditions in HEK 293T cells

HEK 293T cells were used to investigate whether or not we were able to detect DJ-1 phosphorylation in our cellular model. Thus, HEK 293T cells were transiently transfected with DJ-1 BiFC constructs and 48 hours post-transfection the medium was changed and cells were incubated in KREBS buffer containing radiolabelled P^{32*} for 90 minutes. After cell lysis GFP trap beads were used to pull down the GFP tagged DJ-1 BiFC constructs and phosphorylation was revealed by autoradiography, while DJ-1 expression via immunoblotting with an anti-DJ-1 antibody (Figure 4.2.1). We did not observe any protein corresponding to the size of the DJ-1 BiFC constructs, thus indicating that DJ-1 phosphorylation was not detected in our experimental context. This could be due to decreased stability or low levels of phosphorylated DJ-1. Indeed, in past work a large volume of sample was necessary to detect phosphorylated DJ-1 (Lin et al., 2012). It is also possible that phosphorylated DJ-1 is not present in normal conditions in these cells (Figure 4.2.1).

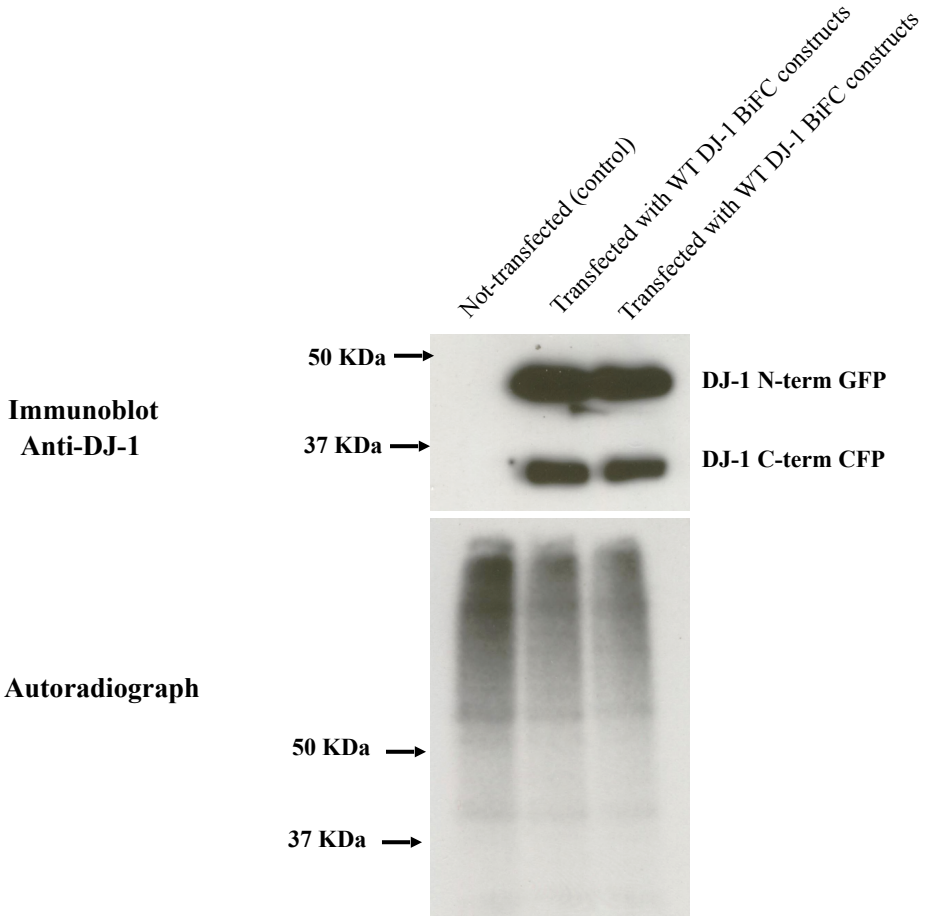

Figure 4.2.1 DJ-1 phosphorylation could not be detected in HEK 293T cells in normal conditions. Top panel, anti-DJ-1 immunoblotting performed as a control for loading samples (12 % of total sample was used). Bottom panel autoradiography that clearly shows DJ-1 phosphorylation could not be detected in normal conditions.

As ample evidence indicates that one of the main functions of DJ-1 is cellular protection from oxidative stress, we hypothesized that this protein could be phosphorylated in oxidative stress conditions, and we thus repeated the above experiment in oxidative stress. We first validated our oxidative stress paradigm by treating cells with two different oxidants and analyzing 4E-BP1 isoforms as a metric of oxidative stress response in the treated cells. Eukaryotic translocation initiation factor 4E-binding protein 1 (4E-BP1) is a key component of the mTOR signalling pathway that has been shown to be dephosphorylated in response to oxidative stress (Pham et al., 2000, Flynn et al., 2012). 4E-BP1 is detectable as 3 bands (α, β and γ) in immunoblots in which α has the greatest mobility (least-phosphorylated form), while γ is least mobile and is the most highly phosphorylated form (Pham et al., 2000). We thus used this protein in our immunoblotting experiments as a marker of oxidative stress condition.

HEK 293T cells were exposed to either paraquat (200 μM and 500 μM) for 24 hours or H_2O_2 (1 mM for 2 hours, and 2 mM for an hour). Cell lysates were immunoblotted using anti DJ-1 and anti 4E-BP1 antibodies. Our results clearly show that both paraquat and H_2O_2 induce oxidative stress in HEK 293T cells, as a shift in 4E-BP1 protein isoforms was observed (Figure 4.2.2). Interestingly, we did not detect any change in mobility of endogenous DJ-1 (Figure 4.2.2).

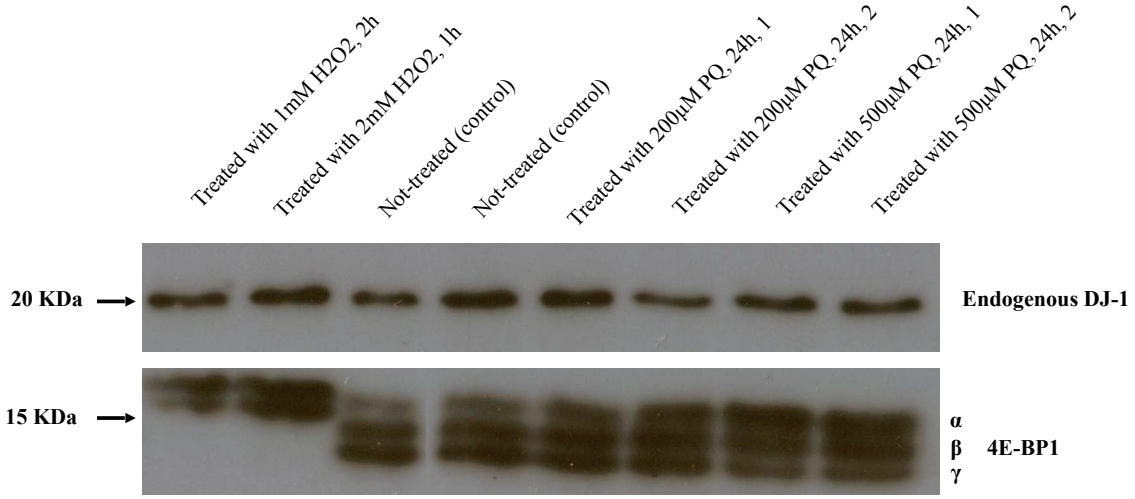

Figure 4.2.2 Anti DJ-1 and 4E-BP1 immunoblots of the lysates obtained from HEK 293T cells treated with oxidants. Paraquat and H_2O_2 induce oxidative stress at both concentrations used as a shift is clearly observed for 4E-BP1. However, no change in size of endogenous DJ-1 that corresponding to its phosphorylation was observed.

With stress conditions thus optimized, the autoradiograph experiment using HEK 293T was repeated as described above. Cells transiently transfected with WT DJ-1 BiFC constructs were treated with 2 mM H_2O_2 for one hour 48 hours post-transfection. Our results are shown in Figure 4.2.3 and they clearly indicate that DJ-1 was not phosphorylated in oxidative stress conditions. The fact that we could not observe DJ-1 phosphorylation in normal and oxidative stress conditions could be due to either technical or biological reasons. For instance, autoradiography may not be sensitive enough to detect DJ-1 phosphorylation, or the time of incubation/labelling with KREBS buffer containing phosphoric acid P^{32*} was not sufficient. It may also be that a very small subset of DJ-1 is phosphorylated at any given time, or that phosphorylated DJ-1 may exhibit reduced stability. To further investigate the potential functional consequences of DJ-1 phosphorylation, we chose to generate phosphomimetic and phosphoblocking DJ-1 BiFC constructs for all possible phosphorylation sites to explore their effect upon DJ-1 dimerization and stability.

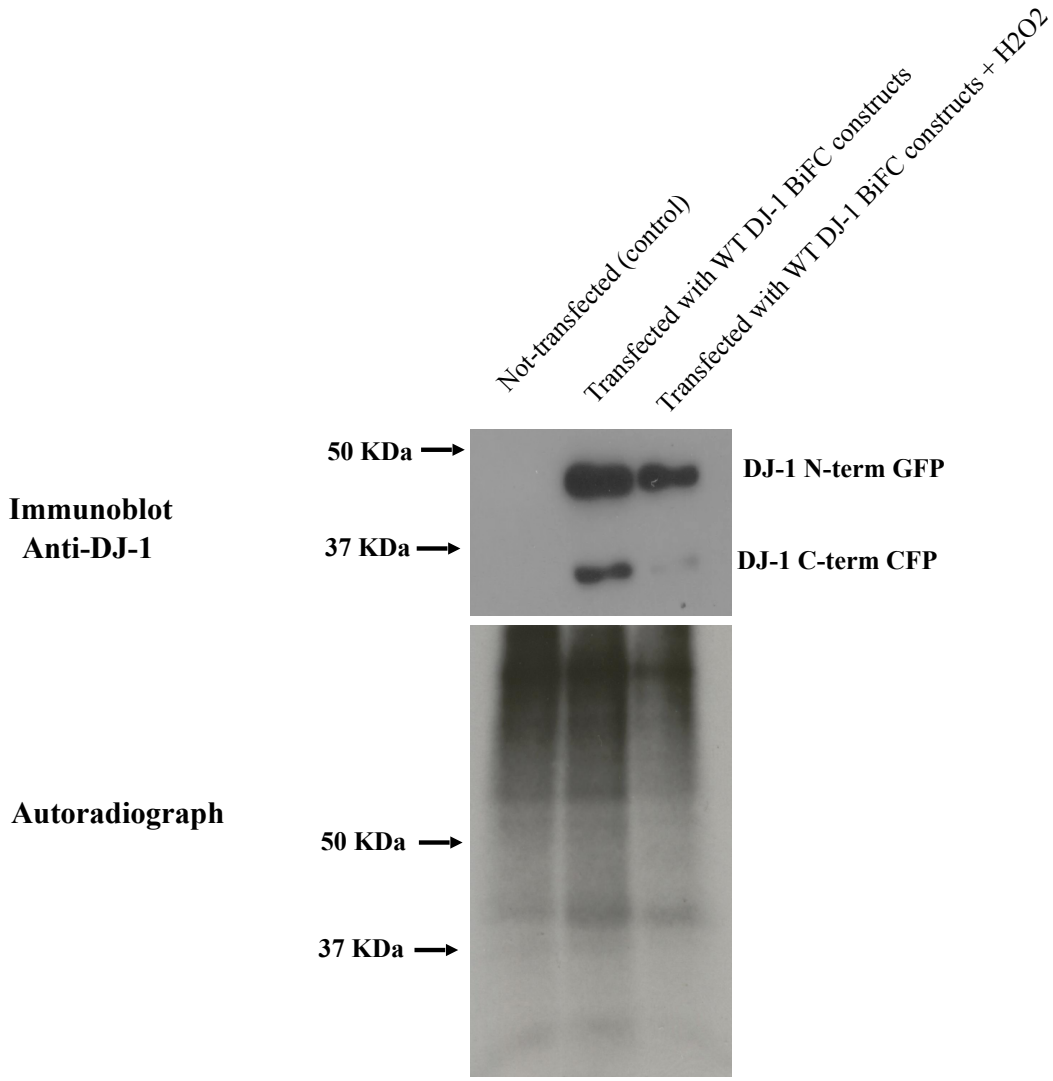

Figure 4.2.3 DJ-1 phosphorylation could not be detected in the HEK 293T cell line in oxidative stress conditions. Top panel: anti DJ-1 immunoblotting performed as a control for loading samples (12 % of total sample was used). DJ-1 protein levels decrease in oxidative stress conditions. Bottom panel: DJ-1 phosphorylation could not be detected in oxidative conditions.

4-2-2 DJ-1 phosphostatus modulates its stability

Constructing phosphomimetic and phosphoblocking mutants is a common approach to investigate the functional effects of phosphorylation on a specific protein. Since a recent study suggested DJ-1 phosphorylation at T19 and Y67 residues is potentially linked to PD (Lin et al., 2012), and these two sites are conserved through evolution from rat to human, we selected these two sites as the first ones to be mutated to glutamate or aspartate by site-directed mutagenesis for our phosphomimetic studies (double phosphomimetic mutant). We also generated DJ-1 BiFC constructs with phosphoblocking mutations (threonine substituted with valine; tyrosine with phenylalanine) to elucidate whether or not these mutations reverse the potential effects of phosphorylation at those sites.

The double phosphomimetic and phosphoblocking DJ-1 mutants BiFC constructs were transfected into HEK 293T cells and analyzed with the Cell^R Scan^R screening station to study their dimerization compared to WT DJ-1 in normal and oxidative stress conditions in quadruplicate. In this experiment we also transfected HEK 293T cells with E64D and C106A mutant versions of the DJ-1 BiFC constructs as a control since: 1) E64D DJ-1 has been shown to have comparable protein level to WT DJ-1 though its dimerization is not stabilized in response to oxidative stress similar to WT DJ-1 (Repici et al., 2013), 2) C106A is a redox-sensitive DJ-1 mutant. 24 hours after transfections cells were treated with 1mM H_2O_2 for 2 hours. Our results show that although the DJ-1 double phosphoblocking mutant is able to dimerize in a manner similar to WT, dimerization of phosphomimetic mutant is dramatically decreased (Figure 4.2.4). In addition, we also tested the ability of the double phosphomimetic DJ-1 mutant to form heterodimers with WT DJ-1. We observed a reduction in fluorescence complementation signal similar to what observed for the cells transfected with the two phosphomimetic DJ-1 BiFC constructs, thus suggesting that this DJ-1 mutant is not able to dimerize with itself or with the WT protein (data not shown).

We speculated that phosphorylation might affect protein dimerization directly by altering protein conformation or indirectly via reduction of DJ-1 protein levels, as a result of a decrease in phosphorylated DJ-1 stability. To clarify this point we performed immunoblotting using anti DJ-1 antibody to assess protein levels of the DJ-1 phospho-

mutants (Figure 4.2.5). We found that DJ-1 phosphomimetic mutant protein levels are dramatically decreased in comparison with either WT DJ-1 or the phosphoblocking mutant DJ-1. Notably, under oxidative stress conditions, the phosphomimetic mutations completely eliminated DJ-1 protein levels.

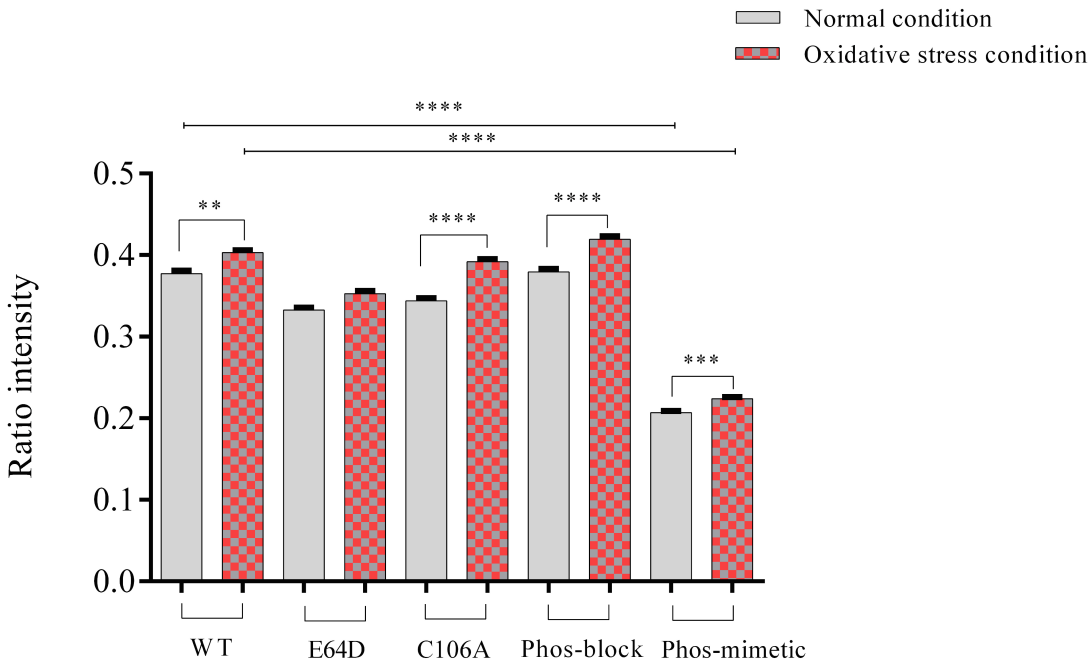

Figure 4.2.4 Effect of DJ-1 double phosphomimetic and phosphoblocking mutants on its dimerization. The DJ-1 double phosphoblocking mutant (T19 and Y67) dimerizes similarly to the WT DJ-1 in normal and oxidative stress (1mM H_2O_2 for 2 hours) conditions although phosphomimetic mutations of the same residues dramatically decreases DJ-1 dimerization in both conditions. Conditions were tested in quadruplicate. The graph shows the average ratio intensity (green/red) per well ±SEM. ****P<0.0001.

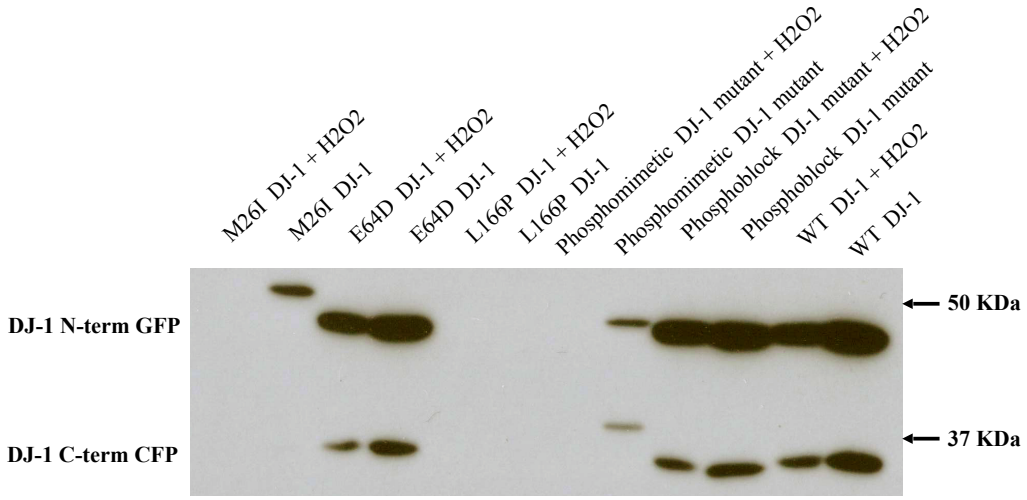

Figure 4.2.5 Effect of DJ-1 double phosphomimetic and phosphoblocking mutants on DJ-1 stability in normal and oxidative stress conditions. DJ-1 protein levels were analysed 48 hours after transfection by immunoblotting using anti DJ-1 antibody. The immunoblot clearly shows that DJ-1 double phosphomimetic mutants (T19 and Y67) dramatically decrease DJ-1 stability in both conditions, thus indicating the decrease observed in DJ-1 BiFC signal was likely due to a reduction in protein level. In contrast, the double phosphoblocking DJ-1 mutant showed similar stability as the WT protein.

The results from the BiFC experiment (Figure 4.2.4) and immunoblotting (Figure 4.2.5) suggest that DJ-1 phosphorylation at T19 and Y67 residues influences its stability and therefore its dimerization. To further investigate whether the reduced dimerization we observed is entirely dependent on protein levels, we attempted to normalize phosphomimetic mutant protein levels by transfecting cells with increased DNA concentrations of the BiFC constructs. To this end, we transiently transfected HEK 293T cells with 0.3 μg DNA of WT DJ-1 BiFC constructs, and three different concentrations (0.6, 3.5 and 5.5 μg) of phosphomimetic DJ-1 mutant with two biological replicates in two distinct experiments. Dimerization signal was quantified 48 hours post-transfection with the Cell^R Scan^R screening station using a 24 well plate format. For oxidative stress condition, 48 hours after transfection cells were treated with 1mM H_2O_2 for 2 hours (Figure 4.2.7). We then assessed WT and phosphomimetic mutant DJ-1 protein levels in each condition by anti GFP immunoblotting of cell lysates obtained from cell populations used in the BiFC experiment (Figure 4.2.6).

Immunoblotting data did not show an increase in protein levels when we used increasing amount of phosphomimetic DJ-1 mutant DNA. We speculated by increasing the amount of DNA, transfection efficiency was decreased. To overcome this impediment, we repeated the first experiment by changing the amount of DNA used in the transfection (Figure 4.2.8, 4.2.9). However, this finding supports our previous data on the dramatic effect of DJ-1 phosphorylation at T19 and Y67 on DJ-1 stability, and accordingly dimerization.

Our data from the second experiment showed that the dimerization signal in cells transiently transfected with double phosphomimetic mutant BiFC constructs slightly increases by increasing the amount of DNA but did not reach the WT DJ-1 levels which indicates the BiFC approach is more sensitive than immunoblotting. However, in this experiment we did not observe an increase in WT DJ-1 BiFC signal in oxidative stress conditions compared to control conditions as we would expect (Repici et al., 2013) (Figure 4.2.9).

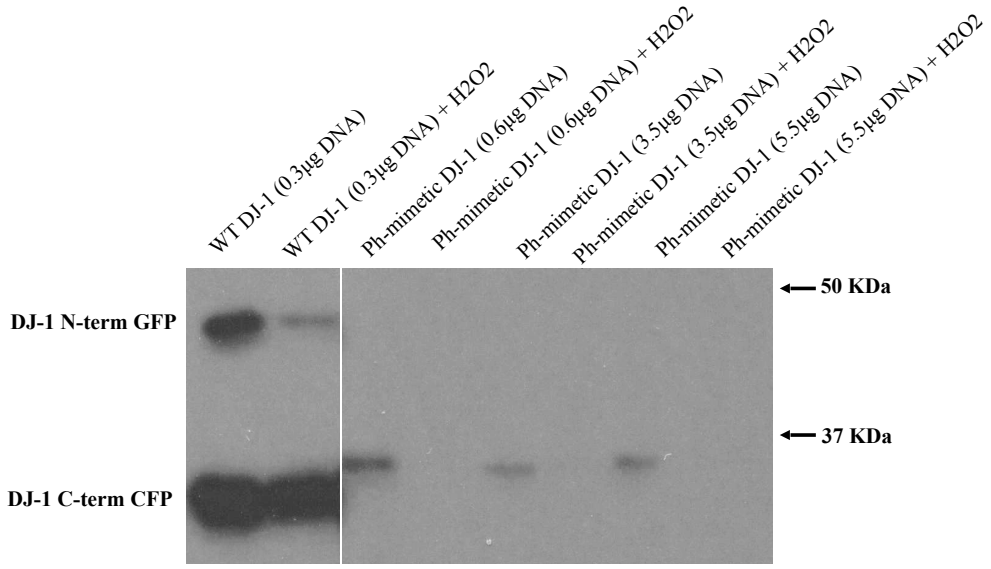

Figure 4.2.6 Anti GFP immunoblot of the lysates obtained from transfected cells used in the BiFC experiment (Figure 4.2.7). In each lane the upper band corresponds to the DJ-1-N-teriminal GFP construct and lower band to the DJ-1-C-terminal CFP construct. The immunoblot data shows that the DJ-1 phosphomimetic mutant highly influences protein stability as we were not able to normalize protein levels of this mutant relative to WT protein.

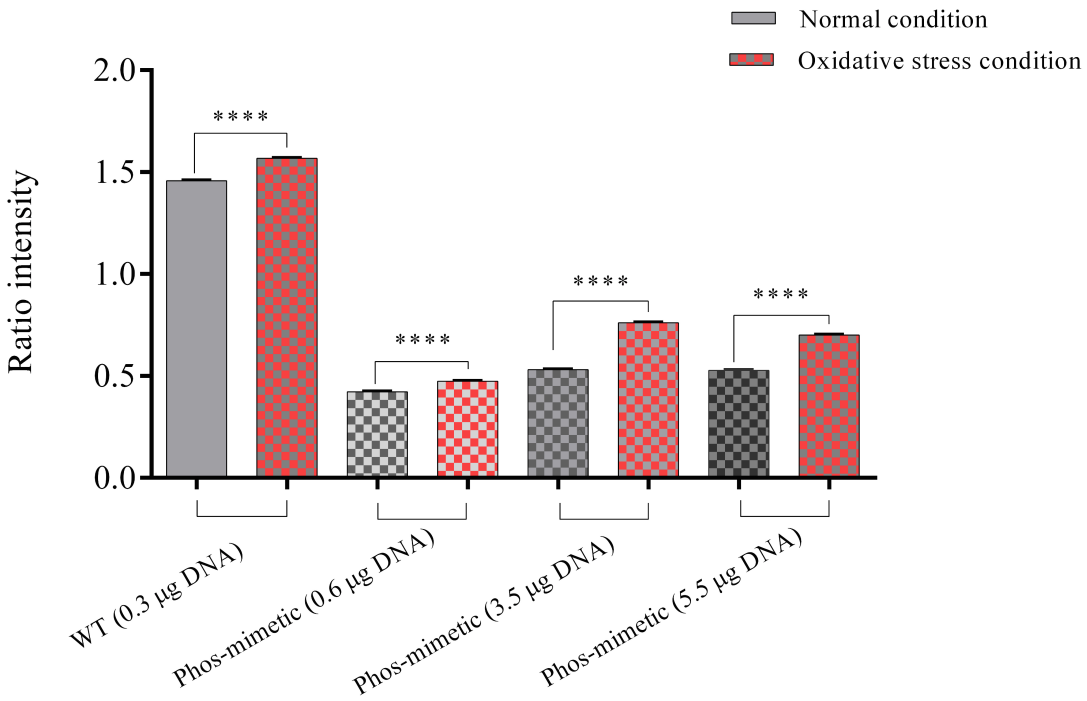

Figure 4.2.7 Dimerization signal of WT and phosphomimetic DJ-1 mutants in normal and oxidative stress (1mM H_2O_2 for 2 hours) conditions 48 hours post-transfection (different transfection conditions). BiFC signal in the cells transfected with the phosphomimetic DJ-1 mutant constructs did not reach WT DJ-1 levels. Conditions were tested in two biological replicates. Graph shows average ratio intensity (GFP/RFP) per condition ±SEM. ****P<0.0001.

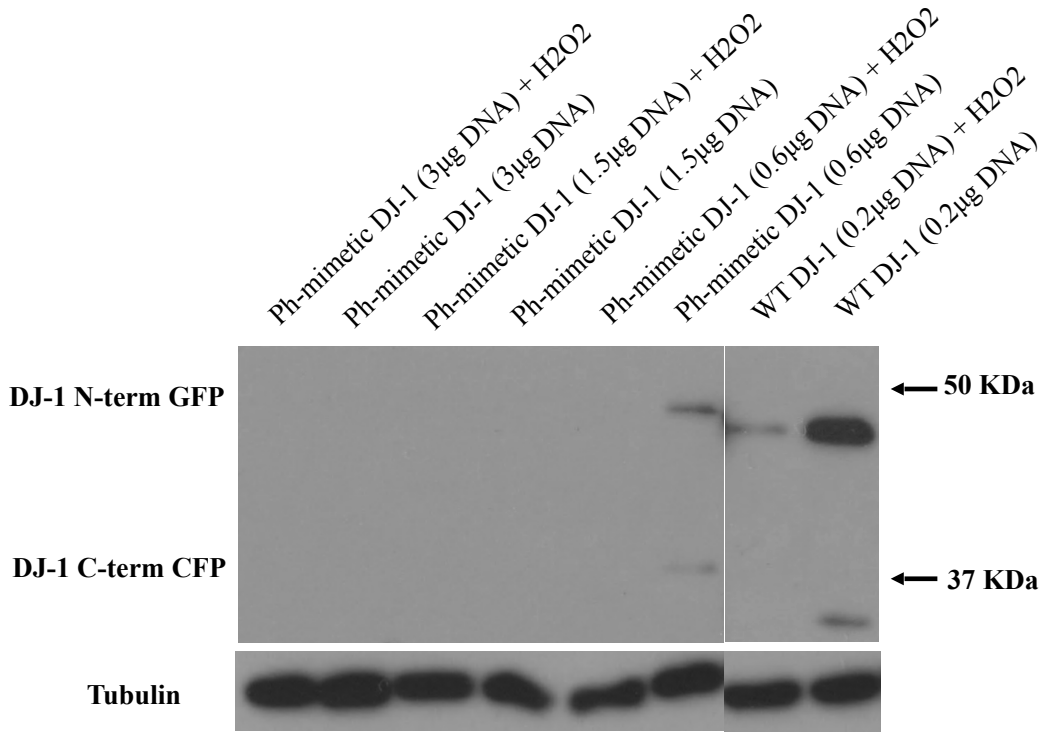

Figure 4.2.8 Anti GFP immnunoblot of the lysates obtained from transfected cells used in BiFC experiment (Figure 4.2.9) in normal and oxidative stress conditions. In each lane the upper band corresponds to DJ-1-N-terminal GFP and the middle band to DJ-1-C-terminal CFP. Immunoblot data indicate the DJ-1 phosphomimetic mutant highly influences protein stability as again we were not able to normalize protein level of this mutant to WT protein.

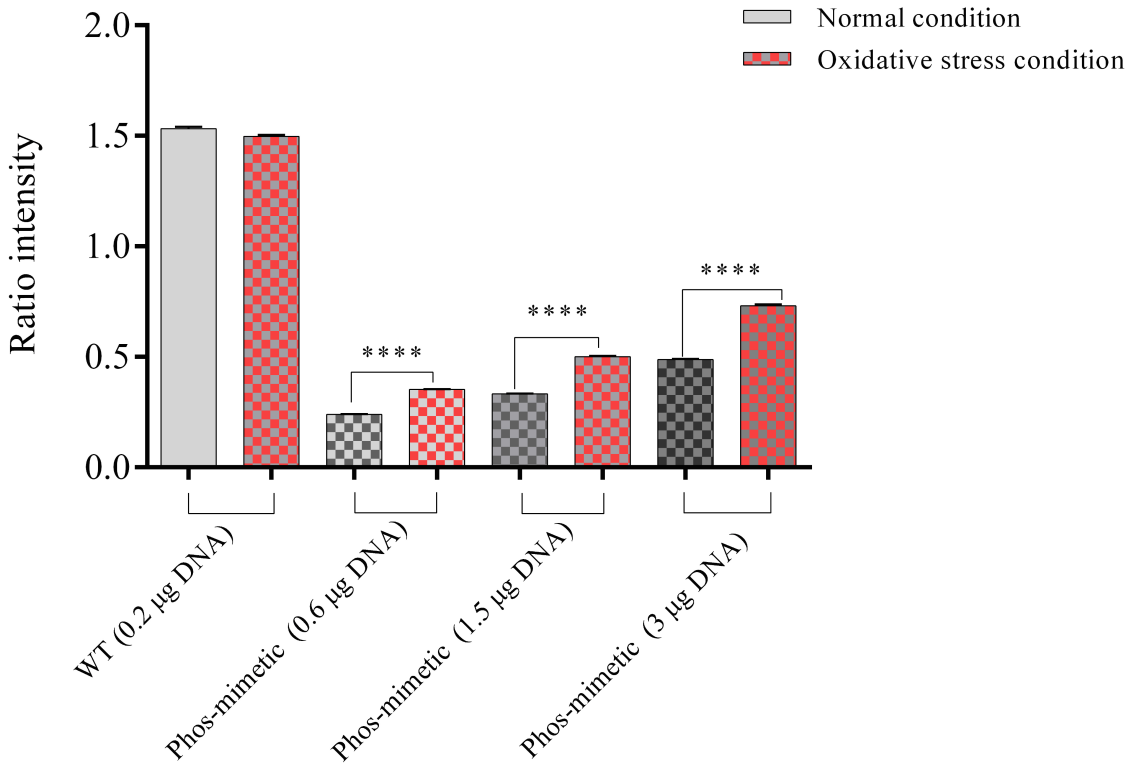

Figure 4.2.9 DJ-1 phosphorylation at T19 and Y67 residues decreases DJ-1 dimerization. HEK 293T cells were transiently transfected with increased amounts of the phosphomimetic DJ-1 mutant BiFC constructs, 48 hours after transfection cells were treated with 1mM H_2O_2 for 2 hours. In this experiment intermediate DNA concentrations were used to avoid a reduction in transfection efficiency. Our data show that despite the increase in the DNA encoding the DJ-1 phosphomimetic mutant, the BiFC remained very low compared to the WT signal. Each condition was tested in two biological replicates. Histogram shows average ratio intensity (GFP/RFP) per condition ±SEM. ****P<0.0001.

Our results with the double T19 and Y67 phosphomimetic mutants clearly show an effect of phosphorylation on protein stability and that phosphoblocking mutants do not affect DJ-1 levels or dimerization. We thus decided to next study all the potential phosphorylation sites in DJ-1 by generating single phosphomimetic mutant versions of the DJ-1 BiFC constructs (T19E, Y67E, Y139E, Y141E, T140D and S142D) using site-directed mutagenesis (see PhosphoSite Plus database, http://www.phosphosite.org/proteinAction.do?id=4095) and we repeated the experiments as discussed above.

When we analyzed BiFC complementation 24 hours post-transfection, cells expressing T19E, Y67E, Y139E mutant DJ-1 BiFC constructs revealed a very low BiFC signal, while cells expressing Y141E and S142D exhibited an intermediate complementation signal. However, all of these five phosphomimetic DJ-1 mutants significantly decreased DJ-1 dimerization compared to WT DJ-1. In contrast, the T140D phosphomimetic mutant and the double phospho-block mutant in T19 and Y67 sites (as already found before) behaved similarly to WT DJ-1 (Figure 4.2.10). Interestingly, we observed that in all cases dimerization is increased under oxidative stress (1mM H_2O_2 for 2 hours) conditions. Each condition was tested in quadruplicate. Immunoblotting experiments indicated a lower level of protein in all the DJ-1 phosphomimetic mutants except T140D. Furthermore, the protein levels of the DJ-1 mutants exhibiting intermediate BiFC signal (i.e. Y141E and S142D) were intermediate between the WT and Y67 and T19, protein levels suggesting that differences in proteins levels may explain most of the differences in dimerization observed. Nonetheless, when comparing T19E with S142D for example, similar protein levels are observed in normal conditions, though BiFC signal is much lower with the T19E - suggesting that the modification at this site may directly impair dimerization. Notably, our results suggest DJ-1 phosphorylation at several potential sites leads the protein to be rapidly degraded in living cells. Furthermore, our data also show that mimicking DJ-1 phosphorylation at Y67E residue changes the band position (higher molecular weight) of both DJ-1 BiFC constructs in comparison with WT and other phosphomimetic mutants (Figure 4.2.11, 4.2.12) (Table 4.2.1).

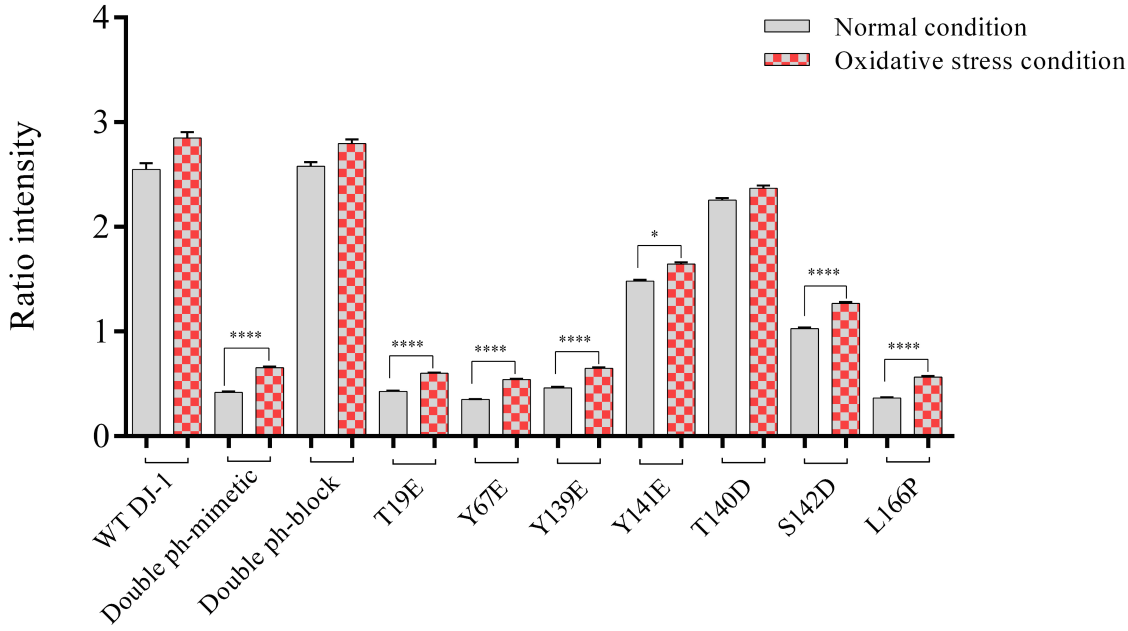

Figure 4.2.10 Effect of DJ-1 phosphomimetic mutants on the efficiency of fluorescence complementation between DJ-1 BiFC constructs in normal and oxidative stress (1mM H_2O_2 for 2 hours) conditions. All the DJ-1 phosphomimetic mutants highly decrease fluorescence signal compared with WT DJ-1 in normal and oxidative stress conditions except T140D DJ-1 mutant. Graph displays average ratio intensity (GFP/RFP) per condition ±SEM. ****P<0.0001.

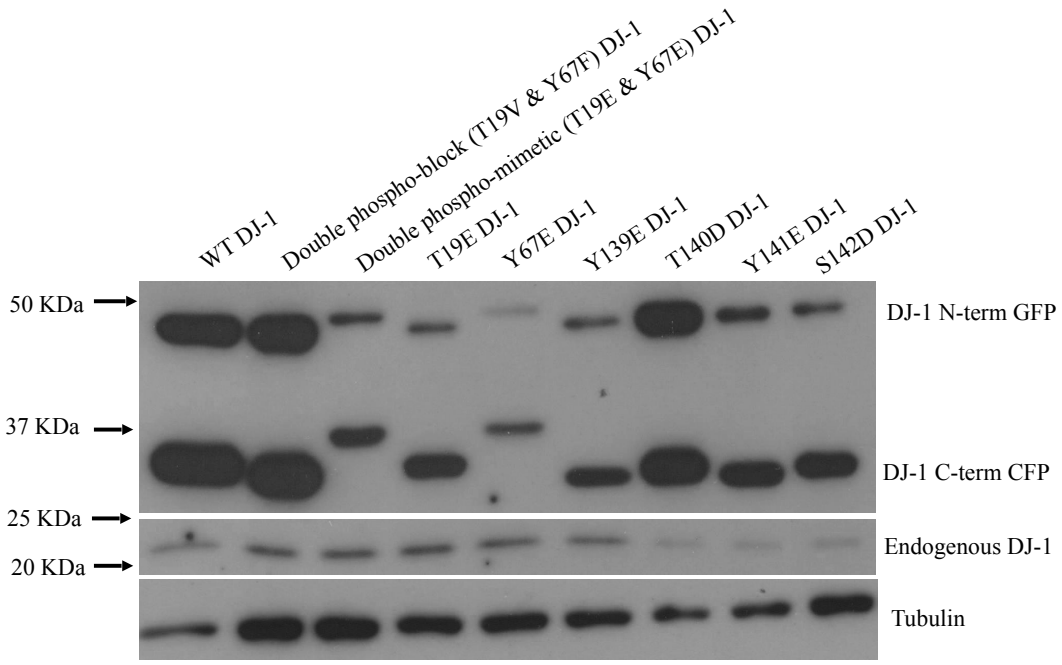

Figure 4.2.11 Effects of DJ-1 phosphorylation on its stability in normal conditions. Lysates were obtained from transiently transfected HEK 293T cell populations with WT, double phospho-block, double phosphomimetic and all the single phosphomimetic BiFC constructs (T19E, Y67E, Y139E, T140D, Y141E, S142D) 24 hours post-transfection. In each lane the upper band corresponds to the DJ-1-GN173 construct, the intermediate band corresponds to the DJ-1-CC155 construct, and the lower band corresponds to endogenous DJ-1. DJ-1 modification at any of potential phosphorylation site highly decreases DJ-1 stability except for T140D mutation.

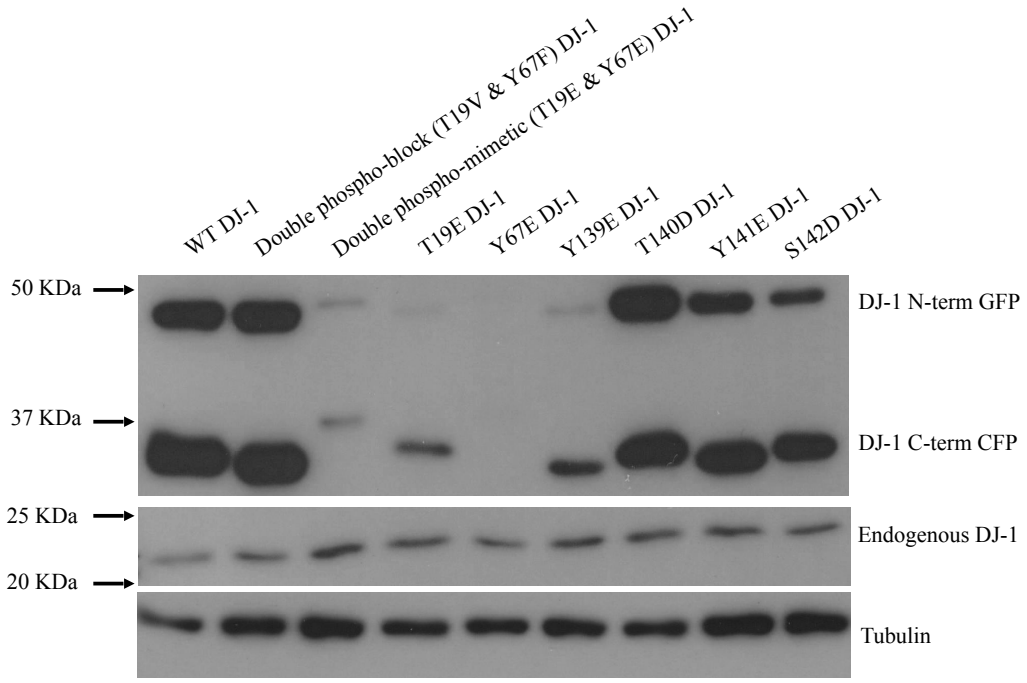

Figure 4.2.12 Effects of DJ-1 phosphorylation at all the potential phosphorylation sites on its stability in oxidative stress conditions. Lysates were obtained from transiently transfected HEK 293T cells with WT, double phospho-block, double phosphomimetic and all the single phosphomimetics BiFC constructs (T19E, Y67E, Y139E, T140D, Y141E, S142D) 24 hours post-transfection and subjected to oxidative stress by exposure to 1 mM H_2O_2 for 2 hours. DJ-1 phosphorylation at any of the potential phosphorylation sites highly decreases DJ-1 stability except for T140D.

DJ-1 mutants	Dimerization compared with WT DJ-1	Protein stability compared with WT DJ-1
Double phosphomimetic (T19E & Y67E)	~ 16 %	~ 12 %
T19E	~ 16 %	~ 13 %
Y67E	~ 16 %	~ 9 %
Y139E	~ 16 %	~ 17 %
T140D	~ 90 %	~ 88 %
Y141E	~ 60 %	~ 33 %
S142D	~ 40 %	~ 19 %

Table 4.2.1 DJ-1 phosphomimetic mutants influence its dimerization and stability.

4-3 Discussion

In the previous chapter we performed high throughput screening to identify novel kinases that modulate DJ-1 dimerization. Despite this kind of screen providing a unique opportunity to investigate novel phosphorylation modifications that could play a central role on function, stability and localization of DJ-1 protein, molecular mechanisms underlying these changes require further investigation. To this end, we decided to take an alternative approach to study DJ-1 phosphorylation and the effects of phosphorylation on DJ-1 function.

First, we examined whether or not DJ-1 is phosphorylated in normal or oxidative stress conditions by autoradiography. While over-expressed DJ-1 BiFC constructs could be easily detected after the pull-down assay by immunoblotting, autoradiography analysis revealed no DJ-1 phosphorylation. We hypothesised that the incubation time of cells with KREBS buffer containing phosphoric acid P^{32*} may not have been sufficient for DJ-1 phosphorylation or, alternatively this technique is not sensitive enough to detect DJ-1 phosphorylation. However, since our studies on DJ-1 phosphorylation show that this post-translational modification drastically decreases DJ-1 stability, we can hypothesize that low levels of phosphorylated DJ-1 in our cellular model is the major obstacle to study DJ-1 phosphorylation using this approach.

We next generated double phosphomimetic and phosphoblocking BiFC DJ-1 mutants for the first two phosphorylation sites (T19 and Y67) of DJ-1 which have been reported to be linked to PD. Indeed, DJ-1 phosphorylation at T19 and Y67 residues could not only play a role in PD pathogenesis but also could be used as PD biomarkers (Lin et al., 2012). Moreover, phosphorylation of DJ-1 at Y67 residue (Rush et al., 2005) and a p53 dependent DJ-1 phosphorylation was previously investigated in cancer studies (Rahman-Roblick et al., 2008). Since detection of DJ-1 phosphorylation through radiolabelling was not feasible, these phosphomimetic/blocking DJ-1 BiFC constructs serve as a powerful tool to characterize the potential role that phosphorylation of DJ-1 has on its stability, localization, dimerization and function. BiFC analysis showed that the DJ-1 phosphomimetic mutant highly decreased the complementation signal compared to WT DJ-1, while there was no difference between the phosphoblocking mutant and WT protein BiFC signal. Thus, the phosphoblocking mutant served as a critical

control showing that mutation of these residues per se is not sufficient to modulate BiFC dimerization signal of DJ-1. Interestingly, immunoblotting data using lysates obtained from cell populations used in the BiFC experiments exhibited a low level of expression of phophomimetic DJ-1 mutant compared to WT DJ-1 while phosphoblocking DJ-1 mutant showed a similar expression level to WT DJ-1.

Our findings from BiFC and respective immunoblot experiments strongly suggest DJ-1 phosphorylation at T19 and Y67 highly decreases DJ-1 stability. This suggests that DJ-1 phosphorylated at these positions is rapidly degraded in living cells and further experiments are needed to clarify the pathway responsible for this degradation. The potential future directions for studying DJ-1 phosphorylation are discussed in Chapter 6.

As we showed DJ-1 phosphorylation in the first two potential sites highly decreases DJ-1 stability, we were prompted to investigate the effect of a single phosphorylation event at all the potential phosphorylation positions on this protein. BiFC and immunoblotting results on the single phosphomimetic mutants indicated DJ-1 phosphorylation at any potential site highly decreases protein stability and as a result reduces its dimerization. This is in agreement with the study by Lin et al. where they showed that more sample was required for detecting DJ-1 phosphorylation using MS (Lin et al., 2012).

Thus, this work has provided for the first time new insights into DJ-1 phosphorylation effect on its stability and dimerization. Despite normal dimerization and stability occurring when potential phosphorylation sites were blocked, the substitution of predicted phosphorylation sites with glutamate or aspartate highly decreases DJ-1 dimerization and stability in living cells. We thus hypothesize that DJ-1 phosphorylation might contribute to its turnover. We also interrogated DJ-1 phosphorylation effects on its dimerization and stability in oxidative stress conditions. Our results revealed that for all the phosphomimetic studied the dimerization increases in oxidative stress similarly to the WT DJ-1. These findings indicate that DJ-1 phosphorylation does not affect its normal reaction to the oxidative stress conditions. However, further studies are required for clarifying whether or not DJ-1 phosphorylation plays a role in normal conditions or in response to oxidative stress. However, as DJ-1 phosphorylation has been reported to be associated with PD (Lin et al., 2012) and also based on our findings that DJ-1 phos-

phorylation effects its stability, it could be postulated that abnormal phosphorylation of DJ-1 may play a role in PD pathogenesis by highly decreasing its stability and levels in the cells, thereby reducing its protective function.

In summary, in this chapter we provided evidence that DJ-1 phosphorylation influences its stability and dimerization in comparison with WT protein in living cells. This will enable us to uncover role of this modification in DJ-1 function and pathogenesis of PD in our in progress and future work.

Chapter 5
Exploring the relationship between DJ-1 and tau
5-1 Introduction

It has long been demonstrated that neurodegenerative diseases display overlapping clinical and pathological features (Rizzu et al., 2004). Indeed, protein misfolding and oxidative stress are implicated in several neurodegenerative disorders such as AD, PD and HD. Recent studies in our group have shown DJ-1 is able to modulate α-Syn and huntingtin aggregation through its oxidation-sensitive chaperone activity (See Chapter 1) (Sajjad et al., 2014, Zondler et al., 2014).

The alteration, dysfunction and abnormal accumulation of microtubule associated protein tau has long been associated with several neurodegenerative disorders such as AD, frontotemporal dementia and parkinsonism linked to chromosome 17 (FTDP-17) (Shahani et al., 2006). In all the neurodegenerative diseases associated with tau, collectively called tauopathies, this protein is abnormally hyperphosphorylated and accumulates as intracellular neurofibrillary tangles (NFTs) reported to play a central role in the neurodegenerative process (Lee et al., 2001, Shahani and Brandt, 2002, Brandt et al., 2005). The human tau gene is mapped to the long arm of chromosome 17 at band position 17q21(Neve et al., 1986) and spans a genomic region of > 100 kb, containing 16 exons (Kolarova et al., 2012). Primary sequence analysis revealed the presence in the protein structure of an acidic N-terminal (pI 3.8) followed by a proline-rich region (pI 11.4) and a basic C-terminal tail (pI 10.8), resulting in dipole structure with two domains of opposite charge (Kolarova et al., 2012).

Tau is a prototypical natively unfolded protein with six known isoforms with varying numbers of tubulin binding domains at its C-terminus. Also, an insertion of 29 amino acids (N1 copy, N2 copies or no insertion) at its N-terminus has been identified (von Bergen et al., 2005, Jeganathan et al., 2008, Kolarova et al., 2012) (Figure 5.1.1). Ample evidence has indicated that each of these isoforms plays a specific physiological roles and that they are differentially expressed during brain development (Kolarova et al., 2012).

Tau binds to microtubules via its C-terminus that consists of several repeated domains encoded by exons 9-12 (Brandt and Lee, 1993). Indeed, the main cellular function of tau protein, promoting tubulin polymerization and stability, mostly depends on these repeats that are known as microtubules binding repeats (MTBR) (Brandt and Lee, 1993, Mandell and Banker, 1996). Since tau phosphorylation regulates its affinity for microtubules, phosphorylated and dephosphorylated status of the protein influences diverse cellular processes microtubules are involved in, such as intracellular trafficking (Trinczek et al., 1999, Kolarova et al., 2012). For instance, over-expression or mislocalization of tau stimulates its intracellular connections: slows down exocytosis and disrupts mitochondria distribution through inhibition of microtubule-based organelle transport (Ebneth et al., 1998, Kolarova et al., 2012).

Tau protein interacts with cytoskeletal components including spectrin and actin filaments, the neuronal plasma membrane and with intracellular membranous components such as mitochondria through its N-terminal part, known as the projection domain (Jung et al., 1993, Brandt et al., 1995, Kolarova et al., 2012). Tau also interacts with the Src-homology 3 (SH3) domain of several proteins including Fyn (tyrosine kinase from Src family), which is involved in protein trafficking (Reynolds et al., 2008, Kolarova et al., 2012). The tau and Fyn interaction regulates N-methyl-D-aspartic acid (NMDA) receptor signalling in dendritic spines, and the outgrowth of cytoplasmic processes in oligodendrocytes which influences neuronal plasticity (Klein et al., 2002, Ittner et al., 2010, Pritchard et al., 2011).

Although actual mechanisms by which tau develops into a nonfunctional and pathogenesis-linked protein are not clearly understood, abnormal post-translational modifications are hypothesized to be a main cause of this defeat (Kolarova et al., 2012). Indeed, while normal phosphorylation of this protein is essential for its optimal function, abnormal tau phosphorylation and its consequent aggregation or amyloid formation is one the earliest symptoms of neuronal degeneration in AD (Braak et al., 1994, Kolarova et al., 2012). For instance, peptidyl-prolyl cis/trans isomerase (Pin1) binds to the tau protein after its phosphorylation on the Thr^{231} residue and modulates its phosphorylation status by making it accessible for protein phosphatase 2A, consequently regulating its function (Kolarova et al., 2012). In the cytosol of neurons the population

of either phosphorylated or dephosphorylated tau are maintained in equilibrium by kinases and phosphatases cooperation, this being essential for tau protein interactions (Arrasate et al., 2000, Maas et al., 2000, Kolarova et al., 2012).

Despite 80 potential serine or threonine phosphorylation sites having been described in the longest variant of tau, the contribution of tau modification and aggregation to neuronal death remains unclear (Sergeant et al., 2005, Shahani et al., 2006). Various studies have found that glycogen synthase kinase 3 β (GSK-3β), cyclin-dependent kinase 5 (cdk5), cAMP-dependent protein kinase (PKA), and calcium/calmodulin-dependent kinase II (CaMK-II) are the kinases that play a fundamental role in tau phosphorylation in the brain (Gong and Iqbal, 2008).

It has been shown that tau and α-Syn pathology coexist (in the same or separate lesions) in neurons and oligodendrocytes of many neurodegenerative disorders (Hansen et al., 1990, McKeith et al., 1996). Expression of pathogenic mutants of α-Syn (A53T) produces α-Syn filamentous inclusions which are associated with fibrillar tau lesions formation in human and mice (Giasson et al., 2003). Moreover, pathological forms of tau and α-Syn coexist in familial forms of PD cases that in spectrum diagnosis between AD and PD are referred as dementia with Lewy bodies (DLBs) (Hansen et al., 1990, McKeith et al., 1996, Duda et al., 2002, Giasson et al., 2003). Pathological forms of tau have also been detected in brains of PD patients with LRRK2 mutations (Gaig et al., 2008). A recent study revealed that over-expression of the LRRK2-I2020T mutation in cultured cells increased the level of phosphorylated tau protein (Taymans and Cookson, 2010).

In 2003 Rizzu et al. found DJ-1 colocalization in neurofibrillary tangles (NFTs) and neuropil threads (NTs) within the substantia nigra, caudate, putamen and temporal cortex of several patients with DLB (Rizzu et al., 2004). This was the first report of a link between DJ-1 and tau inclusions in degenerative tauopathies. Recent work by Wang et al. has also demonstrated that PD-related DJ-1 mutations L166P and D149A, extensively studied as loss of function mutants associated with early onset familial forms of PD, increase abnormal phosphorylation of tau protein in mouse neuroblastoma (N2a) cells through Akt/GSK-3β pathway (Wang et al., 2013). Specifically, it was found that

the pathological L166P or D149A DJ-1 mutants significantly decreased phosphorylation levels of Akt at Thr308, which inhibits Akt function (Wang et al., 2013).

These findings prompted us to investigate tau and DJ-1 interactions in living cells and also to elucidate whether mutations of DJ-1 modulate any potential tau/DJ-1 interactions in normal and oxidative stress conditions.

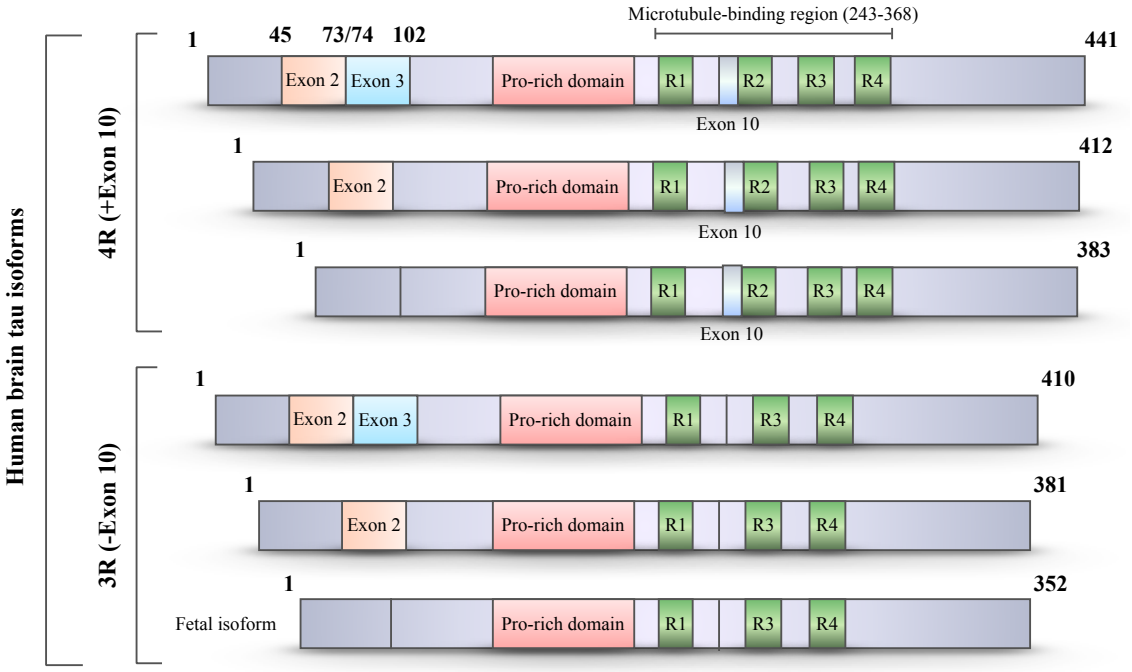

Figure 5.1.1 Human brain tau isoforms. The isoforms vary by the inclusion or exclusion of exons 2, 3 and 10, and also by the number of microtubule binding domains. In this study we used the longest tau isoform (tau-441) (adapted from (Vingtdeux et al., 2012)).

5-2 WT and mutant versions of DJ-1 directly interact with WT tau in physiological conditions

5-2-1 Investigation of the interaction between DJ-1 and tau in living cells

To investigate tau and DJ-1 direct interactions in living cells we used BiFC, as our lab had already generated DJ-1 BiFC constructs and we received tau BiFC constructs from our collaborator Dr. Outeiro. Tau BiFC constructs consist of tau protein (tau-441) tagged with either the N-terminal or the C-terminal of Venus (Figure 5.2.1). As already discussed in Chapter 3 it has been shown that fluorophore reconstitution is able to occur for the combination of Venus and GFP or CFP (Hu et al., 2002). Thus, if WT DJ-1 is able to interact with WT tau in living cells the two non fluorescent fragments will be brought together, and refold into a fluorescent complex easily visualised by fluorescent microscopy.

To this end, HEK 293T cells were transiently transfected with different combinations of WT DJ-1 and WT tau BiFC constructs (VN-tau & DJ-1 CCFP, or Tau-VC & DJ-1-NGFP) to determine whether or not we are able to observe any fluorescent signal. The L166P DJ-1 BiFC constructs were used as a negative control. Confocal laser scanning microscopy (CLSM) xy images show that a fluorescent signal was clearly visible for one of the WT DJ-1/WT tau BiFC constructs combinations (VN-tau & DJ-1 CCFP) (Figure 5.2.2), thus indicating an interaction between DJ-1 and tau in living cells. For the combination of tau-VC & DJ-1-NGFP no fluorescent signal was observed, indicating interaction between DJ-1 and tau can only be detected if the tags are present in a specific orientation, as has been previously reported by different studies in BiFC experiments (Outeiro et al., 2008, Zondler et al., 2014) (Figure 5.2.2).

Interestingly, our primary CLSM data shows that the WT DJ-1 and WT tau complex mainly localizes to microtubule-like structures in comparison with the WT DJ-1 dimer that localises mainly in cytoplasm with a small portion in nucleus, which suggest tau may recruit DJ-1 to the microtubule-like structures. Further experiments are needed to confirm the co-localization of WT DJ-1/WT tau complex with microtubules, (check whether the BiFC signal colocalizes with an anti Beta-tubulin ICC signal). In

contrast, we did not observe any changes in localization of WT tau dimer in comparison with the WT DJ-1 and WT tau complex.

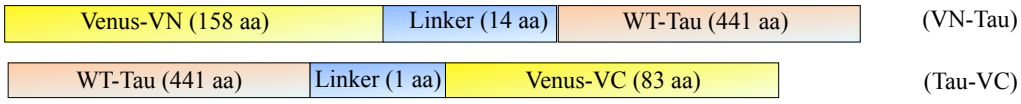

Figure 5.2.1 Schematic representation of the tau BiFC constructs used in this study. We received these constructs from our collaborator Prof. Dr. Tiago Fleming Outeiro (University of Göttingen).

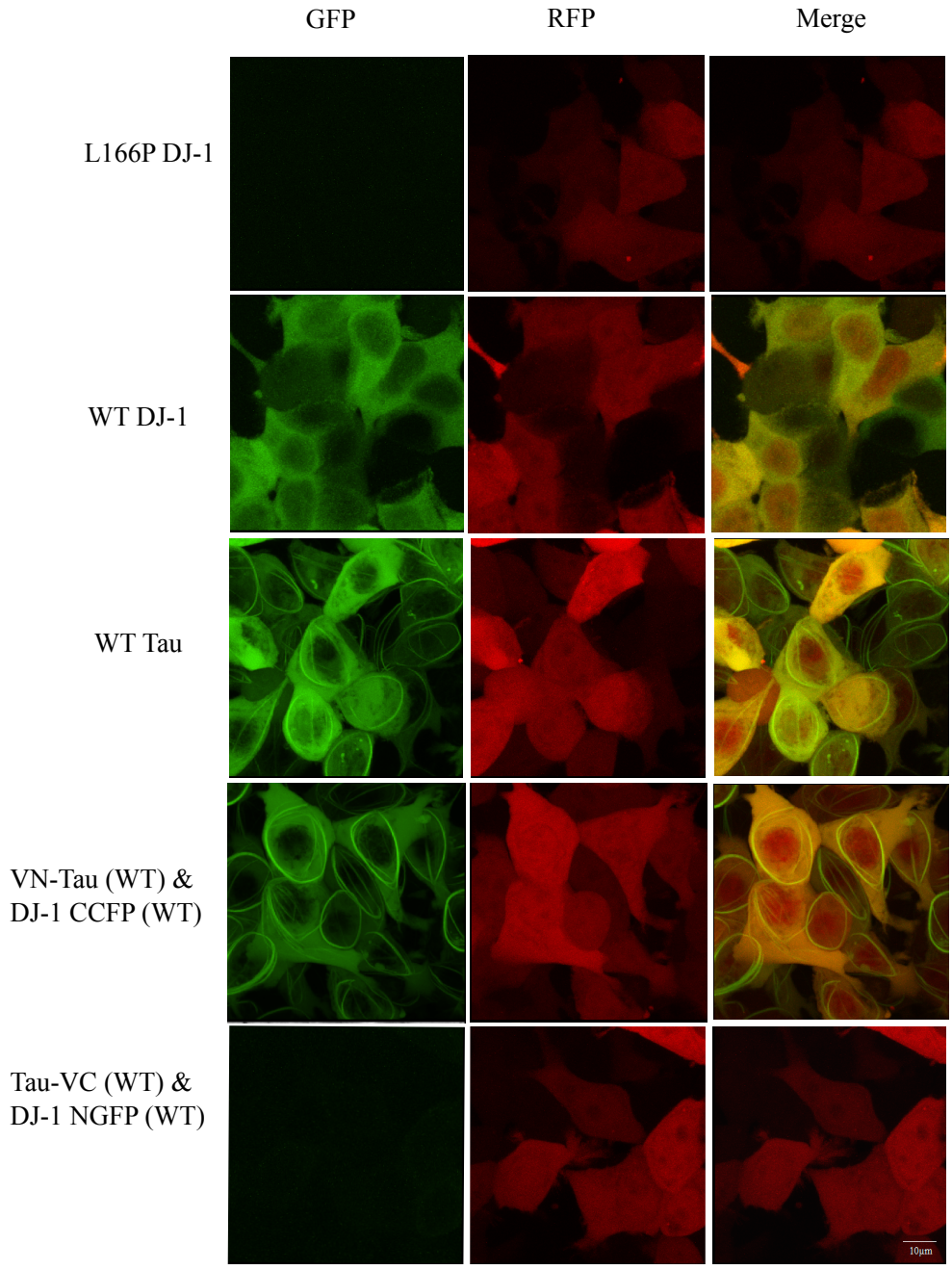

Figure 5.2.2 WT DJ-1 and WT tau directly interact in living HEK 293T cells. Confocal laser scanning microscopy (CLSM) xy images represent complementation driven by WT DJ-1 and WT tau interactions in living HEK 293T cells 24 hours after transfection. L166P DJ-1 BiFC constructs that completely prevent DJ-1 dimerization were used as a negative control. Interestingly, the DJ-1 and tau interaction can be detected in one BiFC combination (VN-tau & DJ-1 CCFP). In all the conditions cells were cotransfected with a plasmid encoding RFP to allow for normalization of the BiFC signal. Scale bar = 10 μm.

We next employed a panel of DJ-1 mutant BiFC constructs E64D, M26I, L10P, C106A, K130R, ΔP158, L166P, double phosphomimetic (T19E, Y67E) and double phosphoblocking (T19V, Y67F) mutants to test whether or not mutations in DJ-1 influence its interaction with the tau protein. Surprisingly, we observed all the DJ-1 mutants are able to interact with WT tau to same degree in living cells (data not shown), despite some of these mutants such as L166P and M26I have been previously shown in our laboratory to prevent DJ-1 dimerization and to be rapidly degraded (Repici et al., 2013).

Confocal analysis showed that microtubule-like structures labelling present in HEK 293T cells over-expressing either WT tau BiFC constructs or WT VN-tau + WT DJ-1 CCFP disappeared in cells over-expressing WT VN-tau + L166P DJ-1 CCFP (Figure 5.2.3). We also observed HEK 293T cells transfected with WT VN-tau + L10P DJ-1 CCFP exhibited a more cytoplasmic distribution of the complementation signal. Cells transfected with WT VN-tau + ΔP158 DJ-1 CCFP mostly exhibited cytoplasmic and nuclear fluorescence, rather than a microtubule-like structures localization. In contrast, cells over-expressing WT VN-tau + double phosphomimetic (T19E & Y67E) DJ-1 CCFP BiFC combination were characterised by a strong microtubule-like structures localization of the complementation signal (Figure 5.2.3). Other DJ-1 mutants in combination with WT VN-tau showed localization similar to the WT DJ-1/WT VN-tau (data not shown).

Taken together, the data from CLSM analysis suggest some of the DJ-1 mutations tested affect the interaction between tau and DJ-1, as well as the localization of this interaction complex. However, these data required further investigation to confirm and validate our initial results.

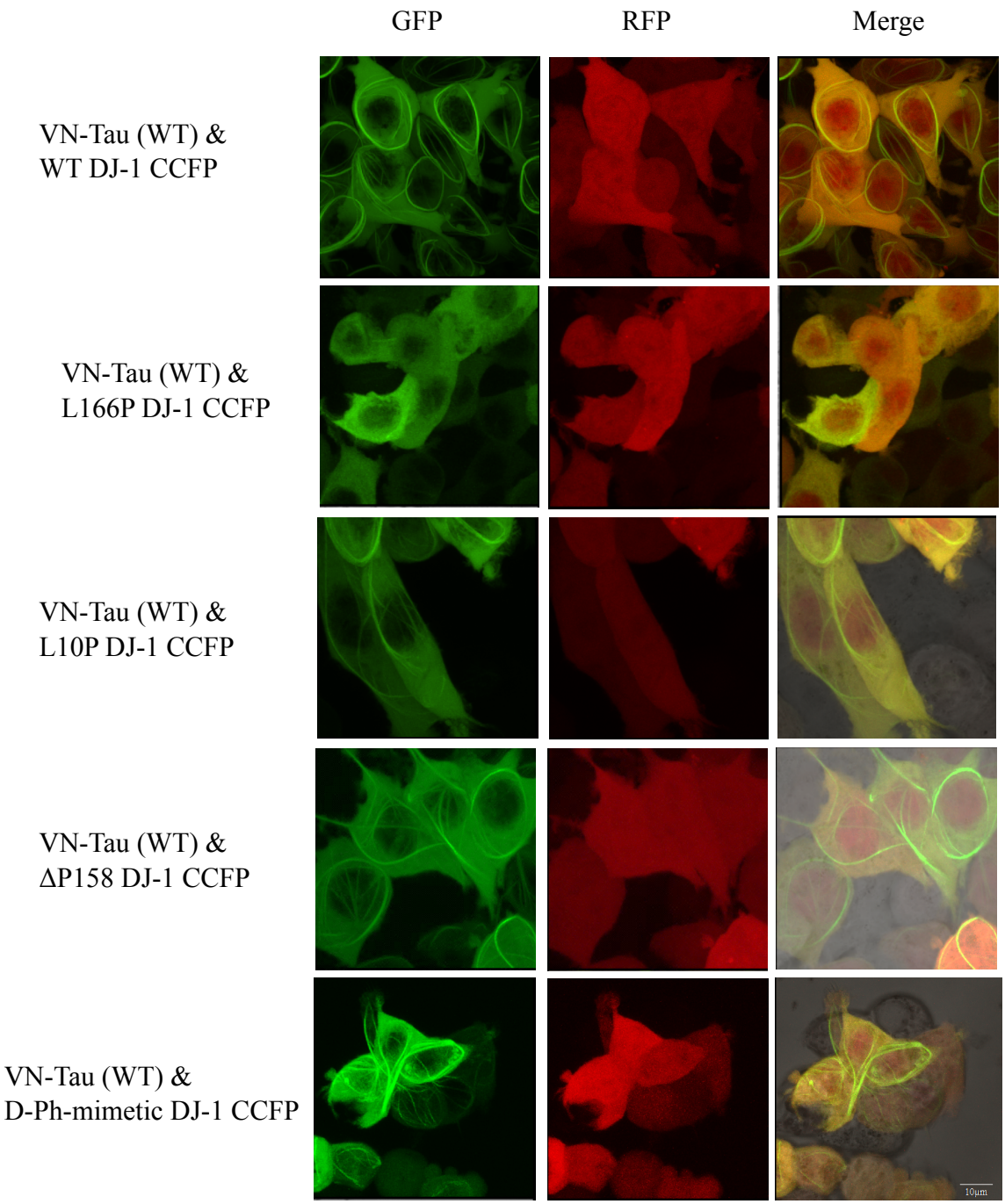

Figure 5.2.3 Effect of L166P, L10P, ΔP158 and double phosphomimetic (T19E, Y67E) DJ-1 mutants on its interaction with WT tau protein. CLSM xy images represent complementation reaction driven by WT DJ-1 or subset of its mutations and WT tau interaction in living HEK 293T cells 24 hours post-transfection. Mutant versions of the DJ-1 BiFC construct (DJ-1 CCFP) interact with WT tau differently from WT DJ-1, based upon localisation and distribution of the complementation signal. Scale bar = 10 µm.

As the main role of DJ-1 in PD context is the protection from oxidative stress, we next tested the effect of oxidative stress on the WT DJ-1/WT tau interaction. In this first experiment we also looked at C106A and DJ-1 double phosphomimetic (T19E & Y67E) DJ-1 mutants. These two DJ-1 mutants were chosen since the cysteine residue at position 106 is responsible for DJ-1 self oxidation in response to oxidative stress and we speculated that DJ-1 phosphorylation might play a role during oxidative stress conditions. HEK 293T cells were transiently transfected with a combination of WT VN-tau BiFC construct and either WT DJ-1 CCFP, C106A CCFP or double-phosphomimetic CCFP DJ-1 BiFC construct. 24 hours after transfection cells were subjected to oxidative stress by exposure to 1 mM H_2O_2 for 2 hours before imaging. CLSM analysis indicated that although no differences between normal and oxidative stress condition were detected in cells transfected with WT VN-tau/WT DJ-1 CCFP and WT VN-tau/C106A CCFP, the BiFC complementation signal of cells over-expressing WT VN-tau + double-phosphomimetic DJ-1 CCFP was more strongly localized to microtubule-like structures (Figure 5.2.4). We also observed tau localization alone become more diffuse with oxidative stress (Figure 5.2.4) which supports previous studies on tau localization upon H_2O_2 treatment that has shown tau accumulates in the nuclei in oxidative stress conditions (Sultan et al., 2011). However, our localization data in normal and oxidative stress conditions must be further validated by quantification.

Figure 5.2.4 Effect of oxidative stress on DJ-1 and tau interactions. CLSM images show the BiFC complementation reaction driven by WT, C106A and double phosphomimetic (T19E, Y67E) DJ-1 and WT tau interactions in living HEK 293T cells. 24 hours post-transfection cells were subjected to oxidative stress by exposure to 1 mM H_2O_2 for 2 hours before CLSM analysis. No difference in fluorescence complementation signal was detected for cells over-expressing WT-VN-tau/ WT DJ-1 CCFP and WT-VN-tau/C106A CCFP in oxidative stress compared to normal conditions. On the contrary, the interaction of double phosphomimetic (T19E, Y67E) mutant DJ-1 with WT VN-tau was more localized to microtubule-like structures in oxidative stress conditions. Scale bar = 10 μm.

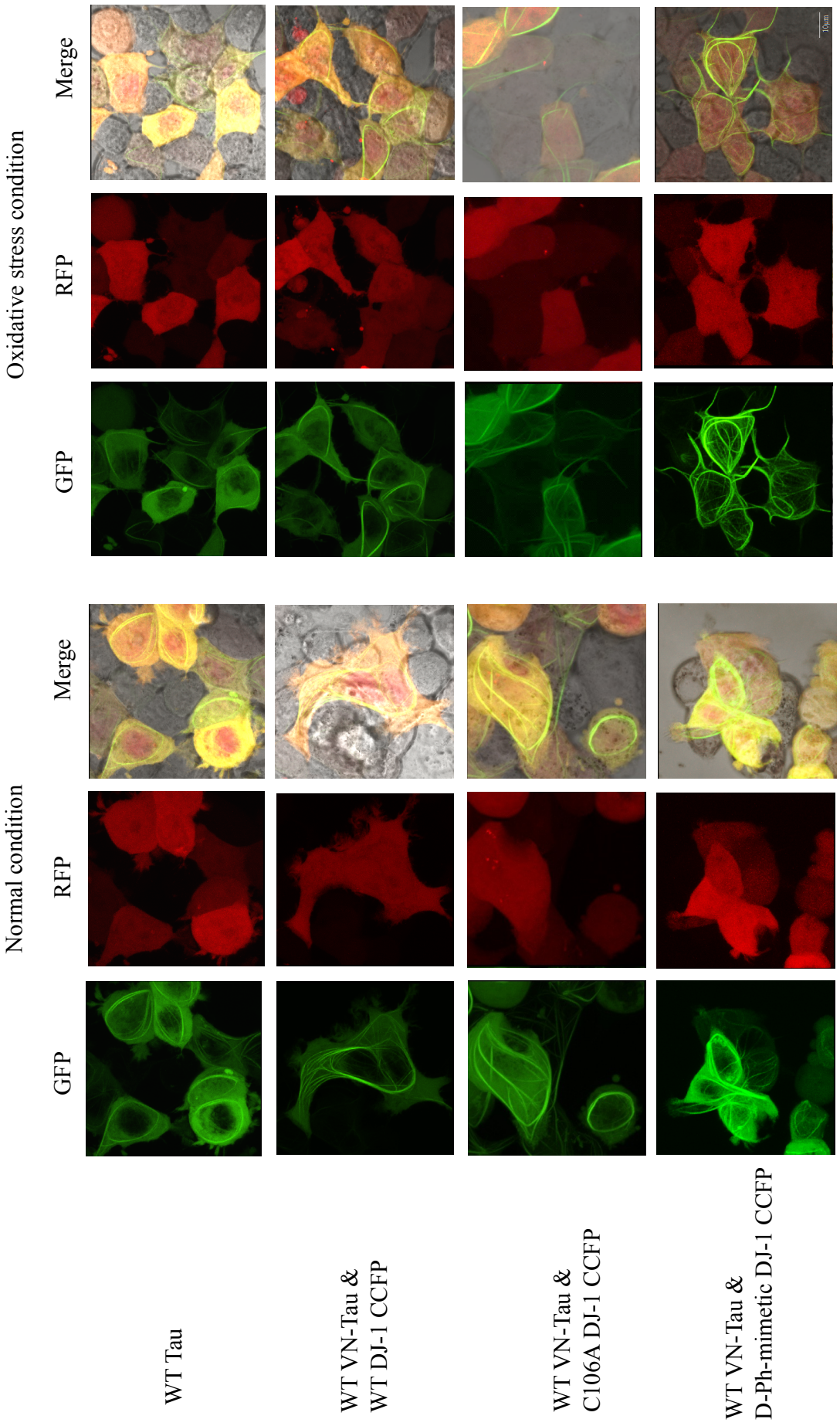
Normal condition
Oxidative stress condition
GFP
RFP
Merge
WT Tau
WT VN-Tau &
WT DJ-1 CCFP
WT VN-Tau &
C106A DJ-1 CCFP
WT VN-Tau &
D-Ph-mimetic DJ-1 CCFP

Next we decided to quantify the fluorescence signal for all the conditions analysed. This approach would provide a better understanding of the effects of any DJ-1 mutations on its interaction with WT tau in normal and oxidative stress conditions. To approach this aim, we transiently transfected HEK 293T cells with the WT VN-tau BiFC construct and WT or a panel of DJ-1 mutant versions of DJ-1 CCFP BiFC constructs (E64D, C106A, K130R, ΔP158, M26I, L10P, L166P, E18A, E163K, A104T, T19E, Y67E, Y139E, T140D, Y141E, S142D) in 24 well plate format with a single biological replicate for each combination. BiFC signals were analysed 48 hours after transfection through the Cell^R Scan^R screening station, to allow for a higher expression of the BiFC constructs. Quantification of the complementation signal clearly revealed most of the mutations in DJ-1 influence its interaction with WT tau (Figure 5.2.5). Indeed, while BiFC fluorescence for C106A, A104T and K130R DJ-1 mutants were not altered from WT DJ-1, a significant decrease in the BiFC signal of WT tau plus Y141E, T140D, E64D, E18A, E163K and S142D DJ-1 mutants and an even higher decrease for L10P, M26I, T19E, ΔP158, Y139E, Y67E and L166P was observed (Figure 5.2.5).

For exploring the effects of oxidative stress on tau/DJ-1 interactions we next repeated the BiFC experiment by imaging cells before and after treatment with 1 mM H_2O_2 for 2 hours. In this context, as our results can be influenced by the time of screening for different DJ-1 mutants based on their position on the plate (approximately 2 hours), we transfected the cells in the first and last well of the experimental plate with WT DJ-1 BiFC constructs as controls for H_2O_2 treatment. Quantification of the BiFC signal obtained from cells over-expressing WT tau and WT DJ-1 revealed fluorescence significantly decreases in response to oxidative stress, thus indicating a destabilization of the WT tau and WT DJ-1 interaction in this condition. This was true as well for the interaction between WT tau and most of the DJ-1 mutants tested (for the S142D mutant a decrease was observed but it was not significant). In contrast, the DJ-1 mutants E64D, M26I, T19E, ΔP158, Y139E, L10P, Y67E and L166P did not show any influence in interaction with WT tau in oxidative stress conditions (Figure 5.2.6). Interestingly, except for E64D, the other DJ-1 mutants that did not show any effect on the BiFC signal in oxidative stress have low protein stability. No difference in fluorescence complementation signal of the controls was detected between the first and the last well in the plate in

normal and oxidative stress conditions, proving that screening time did not have any effect on the BiFC signal obtained during this experiment (Figure 5.2.7).

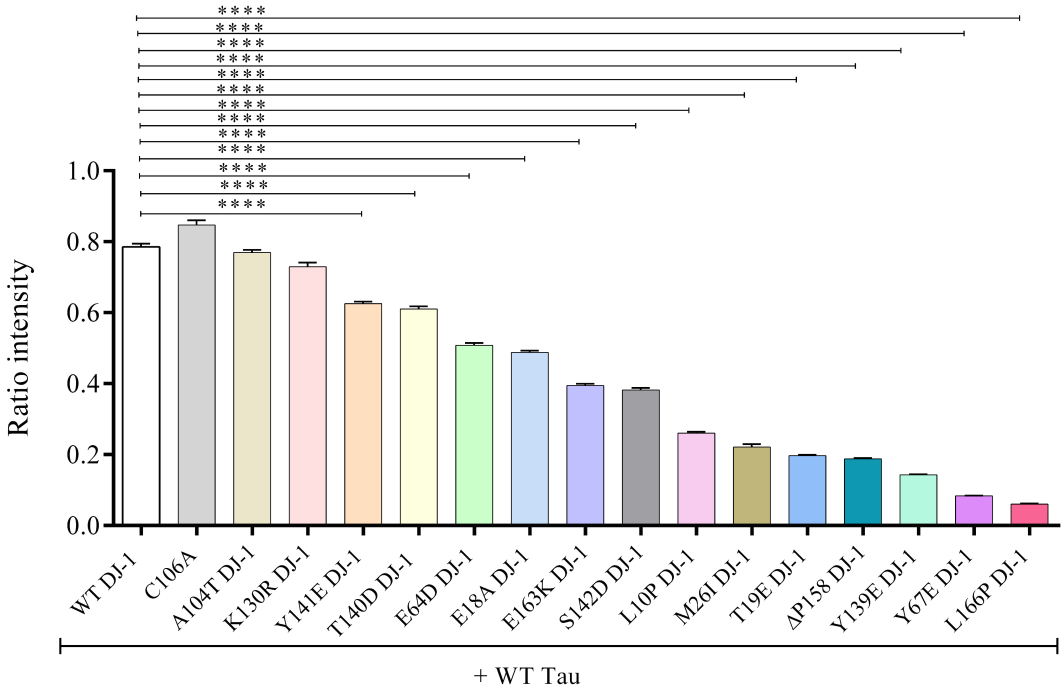

Figure 5.2.5 Effect of the DJ-1 mutants on fluorescence complementation efficiency between WT tau (VN-tau) and DJ-1 (CCFP). Mutations in DJ-1 influence its interaction with WT tau in normal conditions. This graph shows the average ratio intensity (green/ red) per well ±SEM. ****P<0.0001.

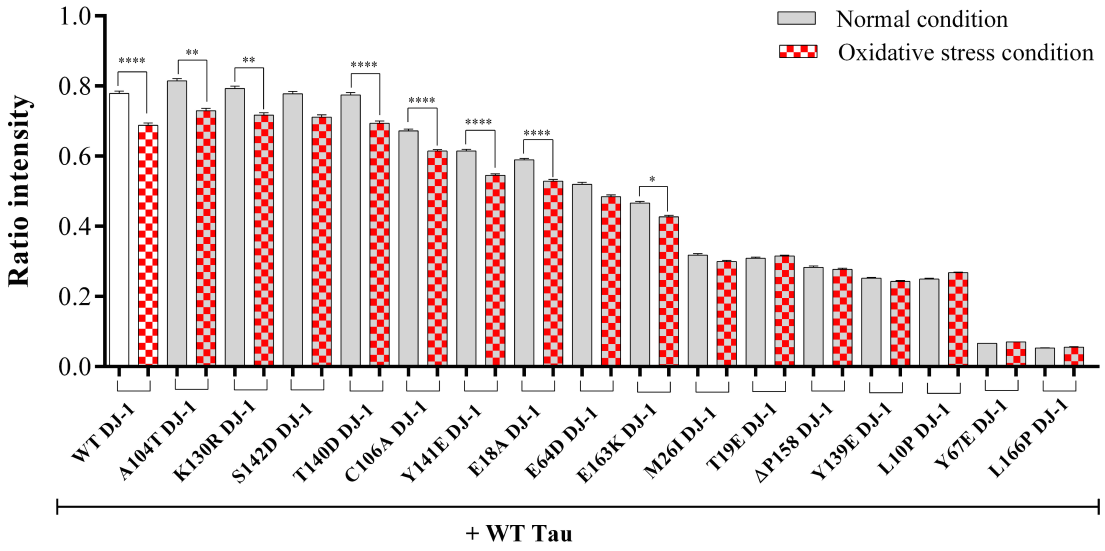

Figure 5.2.6 Oxidative stress destabilizes the tau/DJ-1 interaction (VN-tau + DJ-1 CCFP). BiFC signal of WT tau/WT DJ-1 transfected cells decreases in response to H_2O_2 treatment (1 mM for 2 hours). All the conditions were tested in a single biological replicate. The histogram displays the average ratio intensity (green/red) per well ±SEM. ****P<0.0001.

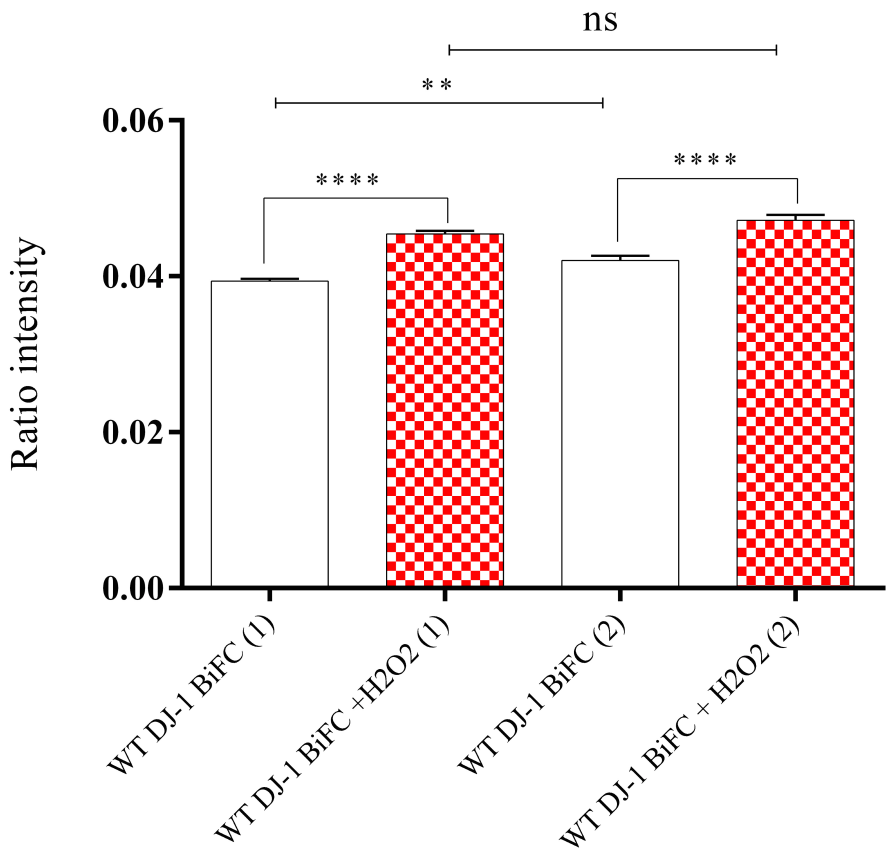

Figure 5.2.7 Screening time did not influence BiFC signal. HEK 293T cells in the first (1) and last (2) wells of the 24 well plate were transfected with WT DJ-1 BiFC constructs as a control to check if position of the well influences H_2O_2 treatment effect on BiFC fluorescence signal. The histogram shows the average ratio intensity (green/red) per well ±SEM. ****P<0.0001.

To confirm our BiFC data and to elucidate if the observed effects of the DJ-1 mutants on the tau/DJ-1 interaction were entirely due their mutated sites or to an effect of the mutation on protein levels, we repeated the BiFC experiments in 6 well plate format with a single biological replicate, followed by immunoblotting to check the protein level of the selected DJ-1 mutants. For this objective, five DJ-1 mutants were used: 1) E64D which has been shown in our laboratory to have comparable expression levels to WT DJ-1 while it had ~ 33 % less interaction with WT tau compared with WT DJ-1; 2) C106A due to its importance in DJ-1 response to oxidative stress; 3) L166P which has exhibited no alteration in interaction with WT tau in response to oxidative stress and also because this DJ-1 mutant changes localization of the WT tau/WT DJ-1 complex from microtubule-like structures to the cytoplasm; 4) Y67E as our immunoblotting analysis has shown this phosphomimetic mutation increases DJ-1 gel migration and it is the most unstable DJ-1 phosphomimetic mutant; and 5) Y141E. This DJ-1 phosphomimetic mutant was selected because although our immunoblotting data indicated a lower level of this mutant compared to the WT protein (see Chapter 4), it has more propensity to interact with WT tau in comparison with E64D DJ-1 mutant that has comparable protein levels to the WT DJ-1 (Figure 5.2.6).

When we looked at the BiFC signal from the 6 well plate experiment we found that our results were in accordance with our previous BiFC data (Figure 5.2.8 compared to Figure 5.2.6). Only the C106A DJ-1 interaction with WT tau was different, as we observed it was slightly lower than WT DJ-1 as opposed to slightly higher (Figure 5.2.5), thus indicating there is no significant difference between this DJ-1 mutant and WT DJ-1 in their interactions with WT tau. Moreover, in agreement with the BiFC signal, immunoblotting analysis using anti GFP antibody indicated that level of C106A DJ-1 protein was comparable to WT DJ-1, while lower levels of E64D DJ-1 protein was observed. Interestingly, we observed although Y141E protein level is ~ 70 % lower than WT DJ-1, its interaction with WT tau is decreased by only 26 % in comparison with WT DJ-1 (Figure 5.2.9). Overall, our data indicate that most of the DJ-1 mutants influence DJ-1/tau interactions in normal and oxidative stress conditions, and suggest that protein stability of each of these DJ-1 mutants plays an important role in this interaction.

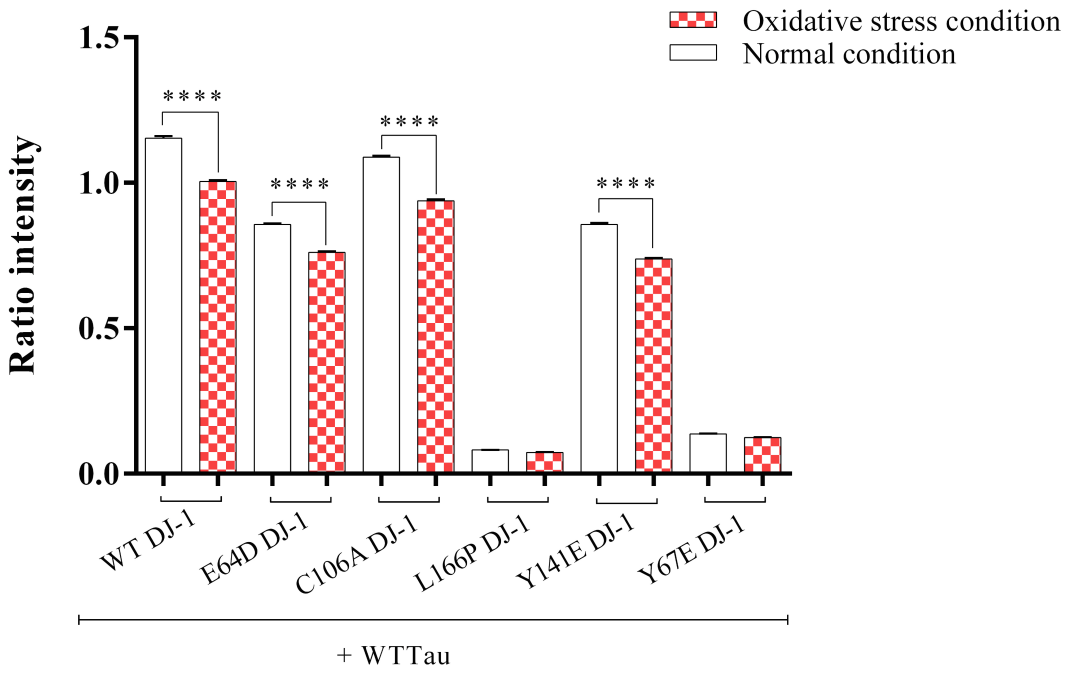

Figure 5.2.8 Effect of the E64D, C106A, L166P, Y141E and Y67E DJ-1 mutations on the efficiency of fluorescence complementation between DJ-1 and WT tau BiFC constructs 48 hours after transfection in normal and oxidative stress (1 mM H_2O_2 for 2 hours) conditions with a single biological replicate. The histogram displays the average ratio intensity (green/red) per well ±SEM. ****P<0.0001.

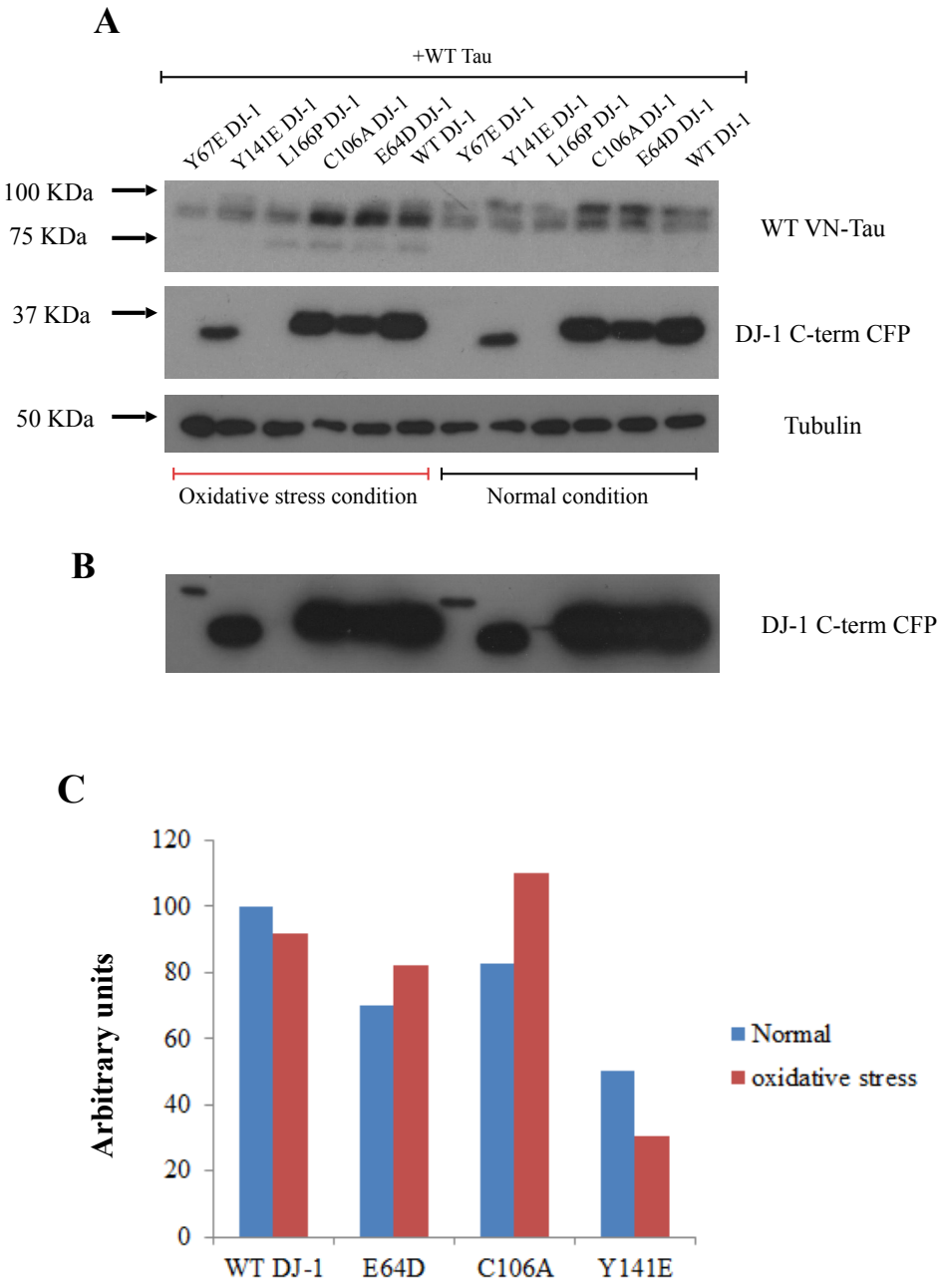

Figure 5.2.9 **A)** Anti-GFP immunoblots of the lysates obtained from transfected cell populations used in the BiFC experiment (Figure 5.2.8) showing the expression levels of the different DJ-1 mutants in comparison to the WT DJ-1. **B)** Anti-GFP immunoblots (A, mid-panel) with higher exposure time to detect L166P and Y67E DJ-1 mutants. **C)** Gel densitometry to measure expression levels of the different DJ-1 mutants in comparison with WT DJ-1 (data are not shown for Y67E and L166P as DJ-1 is not detected in Figure A).

5-2-2 Exploring tau toxicity in the BiFC cell model

Our data so far indicate that DJ-1 likely directly interacts with tau in physiological conditions. Although the reason for this interaction is unclear, it may be related to the function of DJ-1 as a protein chaperone (Sajjad et al., 2014, Zondler et al., 2014). In order to validate our results we next checked if tau over-expression in our cell model could cause cell toxicity, as it is imperative to exclude any toxic effect that could cause a change in the BiFC signal per se (as described in Chapter 3). To this end, we evaluated cell death in cells transiently co-transfected with WT DJ-1 CCFP and WT VN-tau. In order to conclude on our results we needed all the proper controls, and we thus looked at cells transfected with WT DJ-1 BiFC constructs and WT tau BiFC constructs. In addition, we also transfected cells with only WT DJ-1 CCFP, only WT VN-tau, only the RFP construct, only pcDNA 3.1^+ construct, WT DJ-1 CCFP and RFP construct, WT VN-tau and RFP construct and pcDNA 3.1^+ as control conditions in a 96 well plate format. 0.05 µg of each plasmid was used for transfection (0.1 µg of DNA in cells transfected with two plasmids and 0.05 µg of DNA in cells transfected with only one plasmid were used). In this experiment we also assessed the cell viability of not transfected cells (N-Transfected), and cells only treated with transfection reagent without DNA (T-reagent) as negative controls. 48 hours after transfection cells were subjected to LDH (see Chapter 3) cell viability assay (Figure 5.2.10). LDH analysis clearly showed that WT tau over-expression does not have any toxicity effects on our BiFC cell model which indicates that our BiFC data on tau/DJ-1 interactions is not influenced by toxicity effects of tau over-expression.

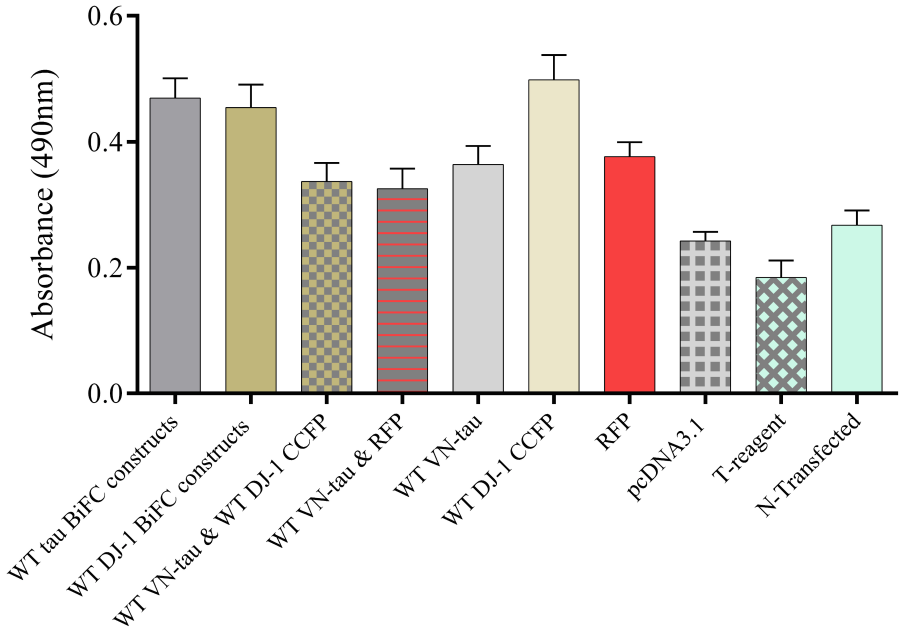

Figure 5.2.10 Effect of tau over-expression on HEK 293T cell viability determined via LDH release assay 48 hours post-transfection. 0.1 µg of DNA in cells transfected with two plasmids and 0.05 µg of DNA in cells transfected with only one plasmid were utilized to transfect HEK 293T cells. Not transfected HEK 293T (N-Transfected) and cells only treated with transfection reagent (T-reagent) were used as a negative control. As the histogram illustrates there is no statistically significant difference in LDH release between cells transfected with various plasmids. Data are expressed as mean ±SEM.

5-2-3 Exploring tau/DJ-1 interactions in the presence of c-Abl inhibitors

Previous work found that amyloid-β-peptide (Aβ) promotes c-Abl activity in rat hippocampal neurons, which contributes to Aβ-induced apoptosis and neurodegeneration (Alvarez et al., 2004). Moreover, other studies observed that mRNA and protein levels of c-Abl are increased in AD models (Alvarez et al., 2004, Cancino et al., 2008, Cancino et al., 2011). Interestingly, it was observed that inhibition of c-Abl via chemical compounds or RNAi ameliorated several AD features, including tau phosphorylation, apoptosis and behavioural impairments both in vivo and in vitro (Alvarez et al., 2004, Cancino et al., 2008, Cancino et al., 2011). Alteration of c-Abl kinase activity and its distribution in AD brain has been shown to be associated with its role in Aβ signal transduction and tau pathology (Jing et al., 2009). Considering these data, we hypothesized that if inhibition of c-Abl by Bosutinib and KW2449 (our hits from screening) decreases tau phosphorylation, and tau phosphorylation regulates the ability of tau to interact with protein partners, this could affect tau/DJ-1 interaction in our cellular model. To examine this hypothesis, we transiently co-transfected the HEK 293T cells with WT VN-tau, WT DJ-1 CCFP and RFP. 24 hours after transfection, cells were treated with Bosutinib and KW2449 at concentrations of 1 and 5 μM in quadruplicate for 4 hours. To check oxidative stress effects on tau and DJ-1 upon c-Abl inhibition, 2 hours after treatment with Bosutinib or KW2449 a subset of the cells were subjected to 1 mM H_2O_2 for 2 hours before imaging.

We observed that WT tau and WT DJ-1 interactions increased upon treatment with 1 μM Bosutinib (blue) compared to DMSO control (gray) (Figure 5.2.11). Furthermore, this increase diminished upon treatment with 5 μM concentration of this compound. Interestingly we found that treatment with Bosutinib dose dependently reversed the effect of the oxidative stress on WT tau and WT DJ-1 interaction (brown vs pink) (Figure 5.2.11).

In addition, we found that the WT tau + WT DJ-1 interaction in normal conditions decreases with KW2449 treatment in a dose dependent manner (Figure 5.2.12). Our data also revealed that KW2449 treatment completely eliminates the H_2O_2 dependent reduction of WT tau and WT DJ-1 interactions at 5 μM treatment (Figure 5.2.12). Altogether, our data suggest that inhibition of c-Abl eliminates the oxidative stress effect on WT tau/WT DJ-1 interactions.

As a further approach to assess tau and DJ-1 interactions, we next explored the potential effect of c-Abl inhibition on WT tau interaction with DJ-1 mutants. Thus, we repeated the BiFC experiment using several mutant versions of DJ-1 CCFP BiFC constructs (E64D, C106A, L166P, L10P, M26I, K130R, ΔP158). We observed that almost all of the DJ-1 mutants behaved similarly to WT DJ-1 in interaction with WT tau in the presence of these two c-Abl inhibitors (data not shown).

Furthermore, our BiFC data also demonstrated that the WT tau interaction with the L166P DJ-1 mutant dramatically increases in response to Bosutinib treatment, and this effect is much more pronounced than that observed with WT DJ-1. In addition, we also observed that oxidative stress does not have any effects on WT tau and L166P DJ-1 mutant interaction (Figure 5.2.13).

Analyses of fluorescence complementation signal between WT tau and L166P DJ-1 mutant with KW2449 treatment showed that this compound does not alter interactions between these two proteins in normal conditions. Moreover, although the aforementioned interaction of WT tau and L166P DJ-1 mutant did not change in response to oxidative stress, KW2449 significantly increased their interaction in oxidative stress conditions (Figure 5.2.14).

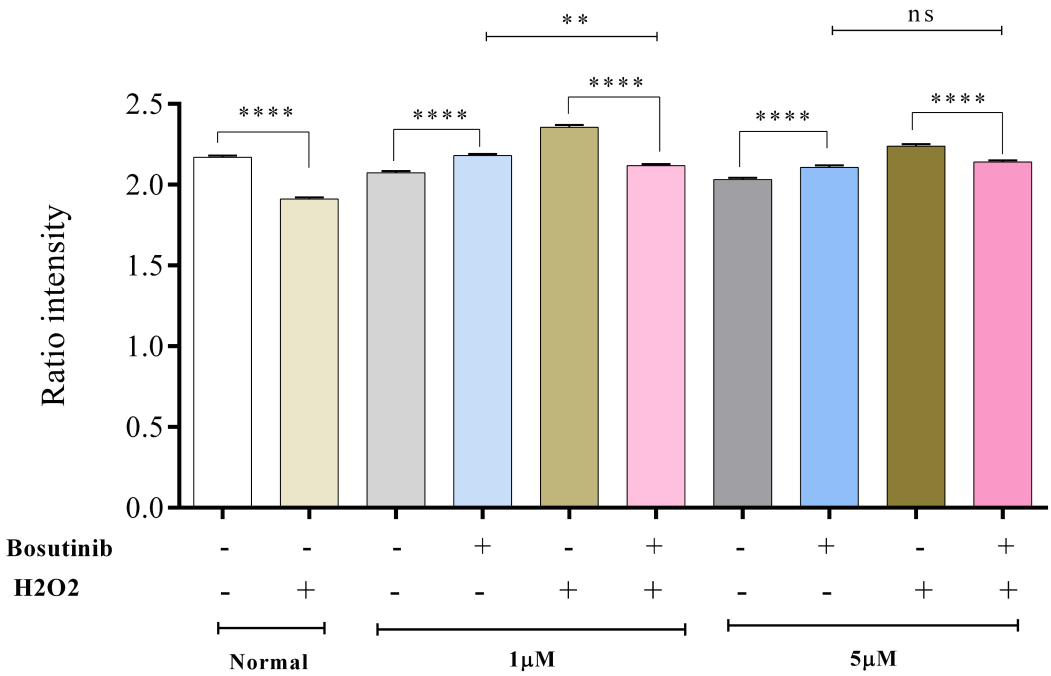

Figure 5.2.11 Effect of Bosutinib treatment on WT tau and WT DJ-1 interaction in normal and oxidative stress (1 mM H_2O_2 for 2 hours) conditions. Oxidative stress destabilizes WT tau and WT DJ-1 interaction, and this effect is decreased upon treatment with the c-Abl inhibitor Bosutinib. Bosutinib treatment also increases WT tau and WT DJ-1 interactions in normal conditions. Conditions were tested in quadruplicate. The histogram displays the average ratio intensity (green/red) per well ±SEM. ****P<0.0001.

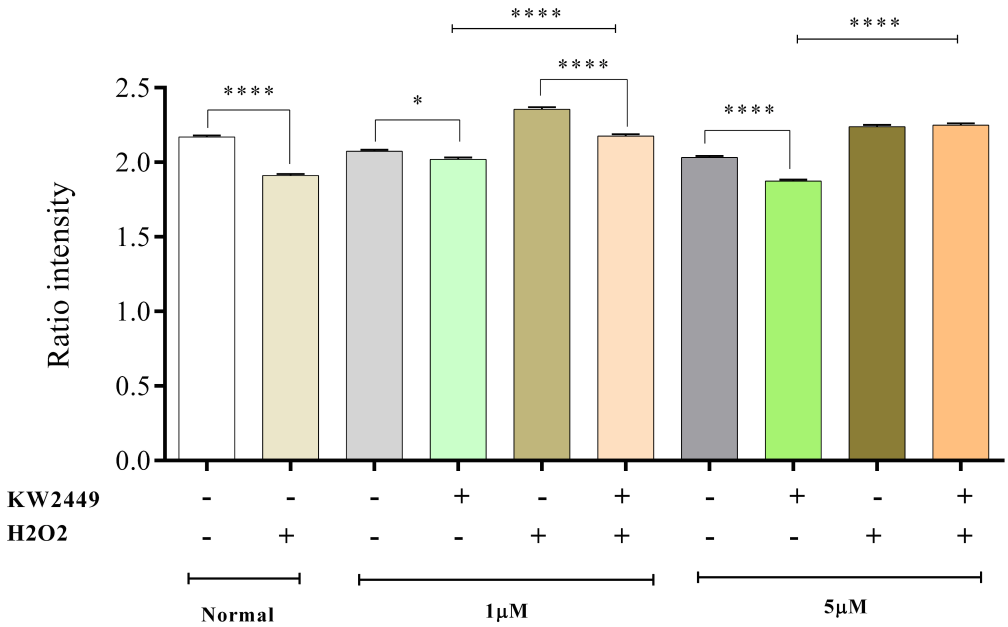

Figure 5.2.12 Effect of KW2449 treatment on WT tau and WT DJ-1 interactions in normal and oxidative stress (1 mM H_2O_2 for 2 hours) conditions. KW2449 dose dependently decreases WT tau + WT DJ-1 interactions in normal conditions, while this treatment increases this interaction in oxidative stress conditions compared with the DMSO control. Conditions were tested in quadruplicate. The histogram displays the average ratio intensity (green/red) per well ±SEM. ****P<0.0001.

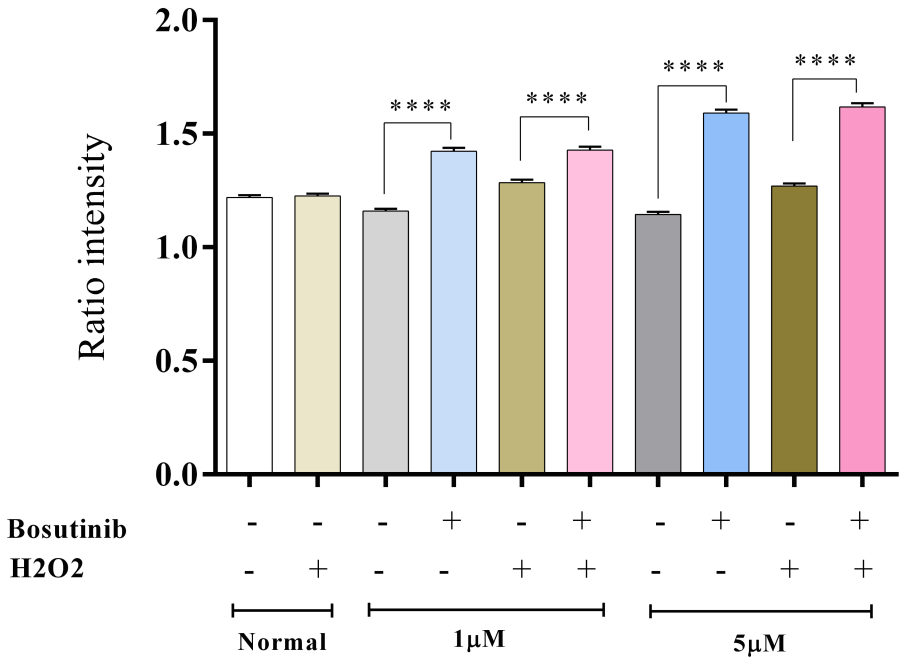

Figure 5.2.13 Effect of Bosutinib treatment on WT tau and L166P DJ-1 mutant interaction in normal and oxidative stress (1 mM H_2O_2 for 2 hours) conditions. Bosutinib treatment significantly increases WT tau and L166P DJ-1 mutant interaction in normal conditions. Oxidative stress has not influenced WT tau and L166P DJ-1 interaction in absence or in presence of Bosutinib. Each condition was tested in quadruplicate. The histogram displays the average ratio intensity (green/red) per well ±SEM. ****P<0.0001.

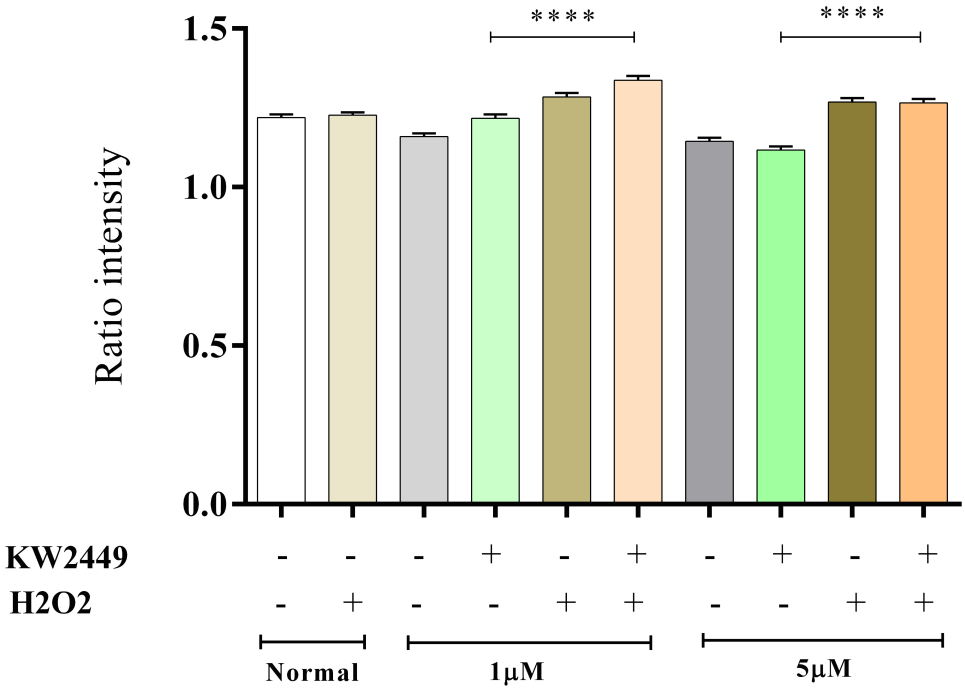

Figure 5.2.14 Effect of the KW2449 treatment on WT tau and L166P DJ-1 mutant interaction in normal and oxidative stress (1 mM H_2O_2 for 2 hours) conditions. KW2449 treatment has not altered WT tau and L166P DJ-1 mutant interaction in normal conditions. As graph shows KW2449 treatment increases these two protein interaction in oxidative stress conditions. Conditions were tested in quadruplicate. The histogram displays the average ratio intensity (green/red) per well ±SEM. ****P<0.0001.

5-3 Discussion

Hyperphosphoryled tau is a major component of neurofibrillary tangles in AD (Yancopoulou and Spillantini, 2003). The gene encoding the tau protein, which normally stabilizes microtubules, has recently been linked to PD in association studies (Tobin et al., 2008, Simon-Sanchez et al., 2009). In addition, co-localization of tau and a-Syn has been observed in LBs (Ishizawa et al., 2003) and increased tau phosphorylation found in the synaptic enriched fraction from PD brains (Muntane et al., 2008). Interestingly, while it is not known whether DJ-1-associated PD brains have LB pathology, studies have found that DJ-1 co-localizes with tau inclusions in AD, Pick's disease and progressive supranuclear palsy (Neumann et al., 2004, Rizzu et al., 2004). Kumaran and colleagues (Kumaran et al., 2007) broadly examined DJ-1 immunoreactivity in a variety of neurodegenerative disorders and found that in AD and frontotemporal lobar degeneration with Pick bodies, DJ-1 was enriched in the sarkosyl-insoluble fractions of frozen brain tissue containing insoluble hyperphosphorylated tau, thus underlying DJ-1 association with tau pathology. It has also been shown that two PD-related DJ-1 mutants L166P and D149A, increase abnormal phosphorylation of tau (Wang et al., 2013). However, a direct interaction of DJ-1 and tau in physiological conditions had never been studied.

My initial step in this chapter was to test both combinations of DJ-1 BiFC constructs and tau BiFC constructs (Tau-VC + DJ-1 NGFP or VN-Tau + DJ-1 CCFP) in our cellular model. Interestingly, we only observed a tau/DJ-1 interaction in cells co-transfected with DJ-1 CCFP and VN-tau. This is not surprising as it has previously been shown that for fluorophore reconstitution the tags of the fluorescent proteins must be present in a specific orientation (Outeiro et al., 2008, Zondler et al., 2014). We next explored the potential effect of mutations in DJ-1 upon its interactions with tau. We found that several different DJ-1 mutants are able to interact with WT tau in living cells in physiological conditions. Strikingly, we observed despite some of the DJ-1 mutants such as L166P, M26I, L10P and ΔP158 that prevent DJ-1 dimerization in physiological conditions (Repici et al., 2013), are able to dimerize with WT tau in our cellular model. Additionally, we also found that different DJ-1 mutants affect localization of the DJ-1/tau complex. For instance, WT tau/L166P DJ-1 mostly localized in the cytoplasm, and

WT tau/DJ-1double phosphomimetic (T19E, Y67E) was more strongly localized to microtubules upon H_2O_2 treatment (see section 5.2.1). These data suggest that though these familial DJ-1 mutants retain tau/DJ-1 interactions, they have an influence on tau/DJ-1 complex localization, which may have implications for their roles in PD pathogenesis.

To quantify the effects of the different DJ-1 mutants on tau/DJ-1 interactions, cells were cotransfected with VN-tau and different mutant versions of DJ-1 CCFP and fluorescence complementation signals were analyzed and quantified via the Cell^R Scan^R screen station. Most of the DJ-1 mutants reduced BiFC signal , thus indicating a reduced interaction with tau compared with WT DJ-1 while the C106A, A104T and K130R mutations did not significantly alter tau/DJ-1 interactions (Figure 5.2.5). However, as the oxidation-sensitive chaperone activity of DJ-1 reduces both huntingtin and α-Syn aggregation (Sajjad et al., 2014, Zondler et al., 2014), we speculate that tau/DJ-1 interaction may occur to modulate tau aggregation (see Chapter 6). Thus, our data also suggest that direct interaction between tau and DJ-1 may play a role in PD pathogenesis as familial DJ-1 mutants decrease this interaction.

Notably, the efficiency of fluorescence complementation between WT tau and different DJ-1 mutants appears to depend predominantly on the protein stability of DJ-1 mutants, as shown by immunoblotting analysis using anti GFP antibody. Interestingly, both immunoblotting and BiFC results showed interactions between WT tau and L166P or Y67E DJ-1 mutants, which have very low protein levels, did not significantly alter upon H_2O_2 treatment. Interestingly, the phosphomimetic Y141E DJ-1 mutant exhibiting ~ 70 % less protein stability showed a higher propensity to interact with tau (only ~ 30 % decrease in the BiFC signal compared to WT DJ-1), in comparison with other DJ-1 mutants such as E64D DJ-1 that have comparable expression levels with WT DJ-1.

One of the caveats in studying protein stability of the various DJ-1 mutants using immunoblotting anti DJ-1, is that different DJ-1 antibodies may not recognize all the DJ-1 mutants since each antibody recognizes a different epitope of DJ-1, which may be altered by the mutations. Although protein stability of the panel of DJ-1 mutants and their ability to dimerize has been extensively studied in our laboratory by Dr. Repici, one of the major limitations in our project was that the anti DJ-1 antibody (DJ-1 (C-16),

Santa Cruz Biotechnology, INC: sc-27006)- which was shown to detect all DJ-1 mutants with the same quality of recognition- was no longer available. We then needed to employ multiple antibodies, the anti DJ-1 antibody (DJ-1 (D4), Santa Cruz Biotechnology, INC: sc-55572) and anti-GFP antibody (abcam, ab6556). Indeed, DJ-1 antibody D4 from Santa Cruz Biotechnology showed a different affinity for the WT vs E64D mutant while the anti DJ-1 antibody C-16, equally regonized both WT and E64D. Moreover, D4 antibody was not able to detect L166P DJ-1. We overcome this problem by using an anti GFP antibody able to detect L166P DJ-1, that showed protein stability of E64D DJ-1 is ~ 30 % less than WT DJ-1, not consistent with our previous results. Overall, our immunoblotting data suggests that various DJ-1 and GFP antibodies could be tested to reduce bias when evaluating protein stability of DJ-1 mutants.

Following the investigation of DJ-1 and tau interaction in physiological conditions, the cytotoxicity effects of over-expression of WT tau in HEK 293T cells were also tested. Notably, we did not observe any toxic effect in cells over-expressing WT tau by LDH assay. We speculate this occurs because HEK 293T cells tolerate high levels of tau over-expression without serious toxicity (Li et al., 2004, Bandyopadhyay et al., 2007, Gohar et al., 2009). However, further approaches are needed to better explore the effect of WT or mutant versions of tau over-expression in living cells and the influence of WT DJ-1 on it. This could be interrogated by studying the cellular localization of these two proteins and by detecting the presence of cytoplasmic tau inclusions by immunocytochemical studies and CLSM, and the effect of the various versions of DJ-1 upon these structures using neuronal cells. Indeed, determination of DJ-1 effect on tau aggregation using biochemical approaches may shed light into the function of tau/DJ-1 dimer (Schafer et al., 2013). For instance, as tau aggregation can be induced by octadecyl sulfate (ODS), we could study effect of DJ-1 over-expression on tau aggregation by dot blot, mass spectrometry and sedimentation in this model.

Last step in this chapter, we used a 96 well plate format to interrogate WT tau interactions with WT DJ-1 and our panel of DJ-1 mutants in the presence of c-Abl chemical inhibitors Bosutinib and KW2449, which we identified in our first screen (see Chapter 3) in normal and oxidative stress conditions. This is relevant to our work as c-Abl was shown not only to directly phosphorylate tau at residue Y394, but also to indi-

rectly mediate its phosphorylation through activation of Cdk5 and GSK3β kinases (Alvarez et al., 2004, Derkinderen et al., 2005, Cancino et al., 2011).

This screen thus served as an opportunity to investigate how inhibition of c-Abl influences the tau/DJ-1 interaction and also whether mutant versions of DJ-1 behave differently from WT DJ-1 in this context. We observed that Bosutinib slightly increased WT tau and WT DJ-1 interactions in normal conditions. Conversely, KW2449 has a stronger effect in modulating WT tau and WT DJ-1 interactions in a dose dependent manner. Thus, one possible explanation for the effect of c-Abl inhibition on tau/DJ-1 interaction is that c-Abl directly modulates tau phospho status thereby exerting its effect on tau/DJ-1 interactions. Interestingly, inhibition of c-Abl with both compounds reversed the oxidative stress effect on WT tau and WT DJ-1 interactions. Effect of the c-Abl inhibition on tau/DJ-1 interaction in oxidative stress conditions is interesting in the PD context as oxidative stress is prevalent in PD brain and it has been shown that c-Abl is activated by various oxidative stressors (Sun et al., 2000). Finally, we did not observed any significant differences in the interaction between tau and our panel of DJ-1 mutants in the presence of c-Abl chemical inhibitors compared with WT DJ-1.

Thus, in this chapter we provide evidence that WT tau is able to directly interact with WT DJ-1 in physiological conditions and that this interaction is destabilized under oxidative stress conditions. We also find that pathogenic mutations in DJ-1 partially constrain interactions with tau, suggesting a potential novel pathway in PD pathogenesis. Lastly, we showed that the likely inhibition of c-Abl by chemical compounds affects tau/DJ-1 interactions in normal and oxidative stress conditions. However, for a better understanding of the role of this interaction in the cell and how this is related to neurodegenerative diseases and specially PD pathogenesis further investigations are required (see Chapter 6).

Chapter 6

Discussion and future directions

Although complete understanding of the actual function of DJ-1 has been an area of extreme interest for researchers with regards to its implication on PD pathogenesis and cancers, little is known about its exact role in the cells. In this study, I focused on DJ-1 phosphorylation using DJ-1 dimerization as a metric for its function with the aim of achieving a more clear understanding of physiological role of DJ-1 phosphorylation in response to oxidative stress. This approach provided a unique opportunity to clarify the consequence of DJ-1 phosphorylation on it function and protein stability, which may help to shed more light into pathological basis of PD and perhaps other neurodegenerative disease.

I developed a BiFC high throughput screen for DJ-1 dimerization modifiers using Olympus Scan^R screening station which to our knowledge is the first time a screening methodology has been developed to identify kinases and phosphatases that directly or indirectly play a role in DJ-1 function. I identified two kinase inhibitors with the same target (c-Abl) out of 168 compounds screened that showed a consistent decrease in DJ-1 dimerisation (~ 13-18 %) in all the re-test experiments. Interestingly, as was discussed in more detail in Chapter 3, ample evidence has shown that this kinase plays a critical role in neurodegenerative diseases. Investigation of c-Abl targets may shed more light into precise mechanisms and cellular pathways by which this kinase influences DJ-1 dimerization and function .

I then studied DJ-1 phosphorylation in living cells in normal conditions or in response to oxidative stress, but no signal was detected by a common phosphorylation assay, which is extensively used to interrogate protein phosphorylation. To overcome this problem, phosphomimetic and phosphoblocking mutations of DJ-1 were generated using site-directed mutagenesis that allowed us to obtain a picture of the effects of these post-translational modifications on DJ-1 dimerization, function and stability. I found evidence showing that DJ-1 phosphorylation at all potential phosphorylation sites on DJ-1 protein except T140D, drastically decrease DJ-1 stability and dimerization in living cells.

In the third part of our work I interrogated direct interaction of DJ-1 and tau in living cells in normal and oxidative stress conditions. My results clearly indicate for the first time that DJ-1 and tau interact in living cells and that the tau/DJ-1 interaction and tau/DJ-1 complex localization are affected by various DJ-1 mutations. These data strongly suggest tau/DJ-1 interaction as a new direction to be explored in PD and further studies are needed to better explore the relevance of such an interaction.

6-1 Future directions

One of the first steps for future directions will be to study if c-Abl function can modulate DJ-1 dimerization. Investigation of proteins and cellular pathways regulated by c-Abl activity may help to clarify the precise mechanisms behind the reduction of DJ-1 dimerization upon c-Abl inhibition. We will first take advantage of immunoblotting technique using phospho-specific antibodies against different c-Abl targets such as tau, Parkin and Cdk5 to verify whether inhibition of c-Abl by both hits from our screen, Bosutinib and KW2449, decreases phosphorylation of its targets. Such experiment could provide the launching pad for mechanistic characterization of linkage between c-Abl and DJ-1 dimerization and function. In parallel, experiments will be performed by triggering proteins downstream of c-Abl and monitoring their effect on DJ-1 dimerization and function. For example, effect of the knocking down and/or over-expression of these proteins on DJ-1 dimerization can be examined. Also CoIP analysis can be exploited for investigation of potential direct interaction of DJ-1 with those proteins. Though this an interesting area to contemplate for future studies, the effect size we observed was rather modest. Thus, it may be worth concentrating efforts on the work discussed below.

While our high throughput kinase inhibitor and phosphatase inhibitor screen aimed to investigate novel kinases or phosphatases that modulate DJ-1 dimerization, there is limitation on how much information these type of high throughput screen can provide. Another powerful tool that will help in a further characterization of DJ-1 phosphorylation in physiological conditions is studying the DJ-1 phosphomimetic mutants developed during this study. As BiFC and immunoblotting analyses have shown that DJ-1 mimicking phosphorylation at all its potential sites drastically decrease DJ-1 stabi-

lity, one of the future directions for clarifying DJ-1 phosphorylation role in cellular pathway(s) is the identification of the degradation pathway responsible for phosphorylated DJ-1 degradation in living cells. Indeed, in the next step of this study we plan to block using chemical inhibitors blocking proteasome, calpain and lysosome function, which are three main protein degradation systems, in cells over-expressing DJ-1 phosphomimetic mutants, and then perform immunoblotting analysis using anti DJ-1 and anti ubiquitin antibody to investigate the protein degradation pathway involved in phosphorylated DJ-1 turnover. This study will provide vital information on how this post-translational modification modulates DJ-1 function, and may help for investigating the role of DJ-1 phosphorylation in the familial PD cases.

In this study we also provided evidence that WT DJ-1 is able to directly interact with WT tau in physiological conditions which prompted us to verify whether or not different DJ-1 mutants influence its interaction with WT tau. As aforementioned, our primary data showed some of the DJ-1 mutants can affect localization of the WT tau/DJ-1 complex in normal and oxidative stress conditions, and the primary future direction of this study will be to validate our results by quantifying changes in DJ-1 and tau localization upon DJ-1 mutation exploiting immunocytochemistry followed by CLSM analysis. Another perspective for clarifying consequences of DJ-1 and tau interaction in living cells is investigating whether or not phospho status of tau influences its interaction with DJ-1 by using phospho tau specific antibodies in immunocytochemistry. Additionally, as DJ-1 has been shown to function as redox-sensitive chaperone (Sajjad et al., 2014, Zondler et al., 2014), it would be interesting to study the effect of this protein on tau aggregation (see section 5-3). However, as HEK 293T cells tolerate tau over-expression toxicity (Li et al., 2004, Bandyopadhyay et al., 2007, Gohar et al., 2009) they do not represent a good model for this aim, and we would rather use neuronal cells (SH-SY5Y neuroblastoma cell line or primary neurons). We could then study if DJ-1 over-expression can rescue proaggregant ΔK280 tau toxicity (Khlistunova et al., 2006) by using LDH and MTT assays and if DJ-1 can reduce ΔK280 aggregates by performing a Thioflavin staining (Khlistunova et al., 2006). A better characterization of DJ-1 and tau interaction will aid for a better understanding of their role(s) in neurodegenerative disorders.

6-2 Conclusions

Thus in conclusion, although role of DJ-1 in several cellular pathways and processes including cellular survival, cellular transformation, RNA binding and response to oxidative stress has long been established, the precise function of this protein is still unknown. I identified two kinase inhibitors that act upon c-Abl which may modulate DJ-1 dimerization. Additionally, we showed for the first time that DJ-1 phosphorylation strongly decreases its stability, further supporting the hypothesis that DJ-1 phosphorylation may play a central role in its function. Interestingly, it has been previously shown that DJ-1 phosphorylation may be associated with PD pathogenesis (Lin et al., 2012). This study may thus represent the first step towards a significant understanding of the role of DJ-1 phosphorylation and its contribution to PD pathogenesis. We also investigated direct interaction between tau and DJ-1 in living cells. It is of interest to note that, though the role of tau/DJ-1 interaction in cellular pathways or its contribution to neurodegenerative diseases is not clear, our results indicate that PD causative mutant versions of DJ-1 influence tau/DJ-1 interactions and localization.

ABOU-SLEIMAN, P. M., HEALY, D. G., QUINN, N., LEES, A. J. & WOOD, N. W. 2003. The role of pathogenic DJ-1 mutations in Parkinson's disease. Ann Neurol, 54, 283-6.

ACQUAVIVA, J., HE, S., SANG, J., SMITH, D. L., SEQUEIRA, M., ZHANG, C., BATES, R. C. & PROIA, D. A. 2014a. mTOR inhibition potentiates HSP90 inhibitor activity via cessation of HSP synthesis. Mol Cancer Res, 12, 703-13.

ACQUAVIVA, J., SMITH, D. L., JIMENEZ, J. P., ZHANG, C., SEQUEIRA, M., HE, S., SANG, J., BATES, R. C. & PROIA, D. A. 2014b. Overcoming acquired BRAF inhibitor resistance in melanoma via targeted inhibition of Hsp90 with ganetespib. Mol Cancer Ther, 13, 353-63.

AGAMANOLIS, D. Available: http://neuropathology-web.org/chapter9/chapter9d-PD.html.

ALEGRE-ABARRATEGUI, J. & WADE-MARTINS, R. 2009. Parkinson disease, LRRK2 and the endocytic-autophagic pathway. Autophagy, 5, 1208-10.

ALESSI, D. R., JAMES, S. R., DOWNES, C. P., HOLMES, A. B., GAFFNEY, P. R., REESE, C. B. & COHEN, P. 1997. Characterization of a 3-phosphoinositide-dependent protein kinase which phosphorylates and activates protein kinase Balpha. Curr Biol, 7, 261-9.

ALEYASIN, H., ROUSSEAUX, M. W., MARCOGLIESE, P. C., HEWITT, S. J., IRRCHER, I., JOSELIN, A. P., PARSANEJAD, M., KIM, R. H., RIZZU, P., CALLAGHAN, S. M., SLACK, R. S., MAK, T. W. & PARK, D. S. 2010. DJ-1 protects the nigrostriatal axis from the neurotoxin MPTP by modulation of the AKT pathway. Proc Natl Acad Sci U S A, 107, 3186-91.

ALEYASIN, H., ROUSSEAUX, M. W., PHILLIPS, M., KIM, R. H., BLAND, R. J., CALLAGHAN, S., SLACK, R. S., DURING, M. J., MAK, T. W. & PARK, D. S. 2007. The Parkinson's disease gene DJ-1 is also a key regulator of stroke-induced damage. Proc Natl Acad Sci U S A, 104, 18748-53.

ALVAREZ, A. R., SANDOVAL, P. C., LEAL, N. R., CASTRO, P. U. & KOSIK, K. S. 2004. Activation of the neuronal c-Abl tyrosine kinase by amyloid-beta-peptide and reactive oxygen species. Neurobiol Dis, 17, 326-36.

ANNESI, G., SAVETTIERI, G., PUGLIESE, P., D'AMELIO, M., TARANTINO, P., RAGONESE, P., LA BELLA, V., PICCOLI, T., CIVITELLI, D., ANNESI, F., FIERRO, B., PICCOLI, F., ARABIA, G., CARACCIOLO, M., CIRO CANDIANO, I. C. & QUATTRONE, A. 2005. DJ-1 mutations and parkinsonism-dementia-amyotrophic lateral sclerosis complex. Ann Neurol, 58, 803-7.

ARIGA, H., TAKAHASHI-NIKI, K., KATO, I., MAITA, H., NIKI, T. & IGUCHI-ARIGA, S. M. 2013. Neuroprotective function of DJ-1 in Parkinson's disease. Oxid Med Cell Longev, 2013, 683920.

ARRASATE, M., PEREZ, M. & AVILA, J. 2000. Tau dephosphorylation at tau-1 site correlates with its association to cell membrane. Neurochem Res, 25, 43-50.

ASHMAN, K. & VILLAR, E. L. 2009. Phosphoproteomics and cancer research. Clin Transl Oncol, 11, 356-62.

BAHK, Y. Y., AHSAN-UL-BARI, M. & KIM, Y. J. 2013. Biomedical application of phosphoproteomics in neurodegenerative diseases. J Microbiol Biotechnol, 23, 279-88.

BAIRD, G. S., ZACHARIAS, D. A. & TSIEN, R. Y. 1999. Circular permutation and receptor insertion within green fluorescent proteins. Proc Natl Acad Sci U S A, 96, 11241-6.

BANDOPADHYAY, R., KINGSBURY, A. E., COOKSON, M. R., REID, A. R., EVANS, I. M., HOPE, A. D., PITTMAN, A. M., LASHLEY, T., CANET-AVILES, R., MILLER, D. W., MCLENDON, C., STRAND, C., LEONARD, A. J., ABOU-SLEIMAN, P. M., HEALY, D. G., ARIGA, H., WOOD, N. W., DE SILVA, R., REVESZ, T., HARDY, J. A. & LEES, A. J. 2004. The expression of DJ-1 (PARK7) in normal human CNS and idiopathic Parkinson's disease. Brain, 127, 420-30.

BANDYOPADHYAY, B., LI, G., YIN, H. & KURET, J. 2007. Tau aggregation and toxicity in a cell culture model of tauopathy. J Biol Chem, 282, 16454-64.

BANDYOPADHYAY, U. & CUERVO, A. M. 2007. Chaperone-mediated autophagy in aging and neurodegeneration: lessons from alpha-synuclein. Exp Gerontol, 42, 120-8.

BERLETT, B. S. & STADTMAN, E. R. 1997. Protein oxidation in aging, disease, and oxidative stress. J Biol Chem, 272, 20313-6.

BERMAN, S. B. & HASTINGS, T. G. 1999. Dopamine oxidation alters mitochondrial respiration and induces permeability transition in brain mitochondria: implications for Parkinson's disease. J Neurochem, 73, 1127-37.

BISKUP, S., GERLACH, M., KUPSCH, A., REICHMANN, H., RIEDERER, P., VIEREGGE, P., WULLNER, U. & GASSER, T. 2008. Genes associated with Parkinson syndrome. J Neurol, 255 Suppl 5, 8-17.

BJORKBLOM, B., ADILBAYEVA, A., MAPLE-GRODEM, J., PISTON, D., OKVIST, M., XU, X. M., BREDE, C., LARSEN, J. P. & MOLLER, S. G. 2013. Parkinson disease protein DJ-1 binds metals and protects against metal-induced cytotoxicity. J Biol Chem, 288, 22809-20.

BLACKINTON, J., AHMAD, R., MILLER, D. W., VAN DER BRUG, M. P., CANET-AVILES, R. M., HAGUE, S. M., KALEEM, M. & COOKSON, M. R. 2005. Ef-

fects of DJ-1 mutations and polymorphisms on protein stability and subcellular localization. Brain Res Mol Brain Res, 134, 76-83.

BLACKINTON, J., LAKSHMINARASIMHAN, M., THOMAS, K. J., AHMAD, R., GREGGIO, E., RAZA, A. S., COOKSON, M. R. & WILSON, M. A. 2009. Formation of a stabilized cysteine sulfinic acid is critical for the mitochondrial function of the parkinsonism protein DJ-1. J Biol Chem, 284, 6476-85.

BLIN, O., DESNUELLE, C., RASCOL, O., BORG, M., PEYRO SAINT PAUL, H., AZULAY, J. P., BILLE, F., FIGARELLA, D., COULOM, F., PELLISSIER, J. F. & ET AL. 1994. Mitochondrial respiratory failure in skeletal muscle from patients with Parkinson's disease and multiple system atrophy. J Neurol Sci, 125, 95-101.

BLUME-JENSEN, P. & HUNTER, T. 2001. Oncogenic kinase signalling. Nature, 411, 355-65.

BONIFATI, V., RIZZU, P., VAN BAREN, M. J., SCHAAP, O., BREEDVELD, G. J., KRIEGER, E., DEKKER, M. C., SQUITIERI, F., IBANEZ, P., JOOSSE, M., VAN DONGEN, J. W., VANACORE, N., VAN SWIETEN, J. C., BRICE, A., MECO, G., VAN DUIJN, C. M., OOSTRA, B. A. & HEUTINK, P. 2003. Mutations in the DJ-1 gene associated with autosomal recessive early-onset parkinsonism. Science, 299, 256-9.

BOON, J. Y., DUSONCHET, J., TRENGROVE, C. & WOLOZIN, B. 2014. Interaction of LRRK2 with kinase and GTPase signaling cascades. Front Mol Neurosci, 7, 64.

BRAAK, E., BRAAK, H. & MANDELKOW, E. M. 1994. A sequence of cytoskeleton changes related to the formation of neurofibrillary tangles and neuropil threads. Acta Neuropathol, 87, 554-67.

BRACHA-DRORI, K., SHICHRUR, K., KATZ, A., OLIVA, M., ANGELOVICI, R., YALOVSKY, S. & OHAD, N. 2004. Detection of protein-protein interactions in plants using bimolecular fluorescence complementation. Plant J, 40, 419-27.

BRANDT, R., HUNDELT, M. & SHAHANI, N. 2005. Tau alteration and neuronal degeneration in tauopathies: mechanisms and models. Biochim Biophys Acta, 1739, 331-54.

BRANDT, R. & LEE, G. 1993. Functional organization of microtubule-associated protein tau. Identification of regions which affect microtubule growth, nucleation, and bundle formation in vitro. J Biol Chem, 268, 3414-9.

BRANDT, R., LEGER, J. & LEE, G. 1995. Interaction of tau with the neural plasma membrane mediated by tau's amino-terminal projection domain. J Cell Biol, 131, 1327-40.

BRAVO, J., MATE, M. J., SCHNEIDER, T., SWITALA, J., WILSON, K., LOEWEN, P. C. & FITA, I. 1999. Structure of catalase HPII from Escherichia coli at 1.9 A resolution. Proteins, 34, 155-66.

BUELER, H. 2009. Impaired mitochondrial dynamics and function in the pathogenesis of Parkinson's disease. Exp Neurol, 218, 235-46.

BURBULLA, L. F., KREBIEHL, G. & KRUGER, R. 2010. Balance is the challenge--the impact of mitochondrial dynamics in Parkinson's disease. Eur J Clin Invest, 40, 1048-60.

BURGERING, B. M. & COFFER, P. J. 1995. Protein kinase B (c-Akt) in phosphatidylinositol-3-OH kinase signal transduction. Nature, 376, 599-602.

CABANTOUS, S., TERWILLIGER, T. C. & WALDO, G. S. 2005. Protein tagging and detection with engineered self-assembling fragments of green fluorescent protein. Nat Biotechnol, 23, 102-7.

CANCINO, G. I., PEREZ DE ARCE, K., CASTRO, P. U., TOLEDO, E. M., VON BERNHARDI, R. & ALVAREZ, A. R. 2011. c-Abl tyrosine kinase modulates tau pathology and Cdk5 phosphorylation in AD transgenic mice. Neurobiol Aging, 32, 1249-61.

CANCINO, G. I., TOLEDO, E. M., LEAL, N. R., HERNANDEZ, D. E., YEVENES, L. F., INESTROSA, N. C. & ALVAREZ, A. R. 2008. STI571 prevents apoptosis, tau phosphorylation and behavioural impairments induced by Alzheimer's beta-amyloid deposits. Brain, 131, 2425-42.

CANET-AVILES, R. M., WILSON, M. A., MILLER, D. W., AHMAD, R., MCLENDON, C., BANDYOPADHYAY, S., BAPTISTA, M. J., RINGE, D., PETSKO, G. A. & COOKSON, M. R. 2004. The Parkinson's disease protein DJ-1 is neuroprotective due to cysteine-sulfinic acid-driven mitochondrial localization. Proc Natl Acad Sci U S A, 101, 9103-8.

CARBALLO-CARBAJAL, I., WEBER-ENDRESS, S., ROVELLI, G., CHAN, D., WOLOZIN, B., KLEIN, C. L., PATENGE, N., GASSER, T. & KAHLE, P. J. 2010. Leucine-rich repeat kinase 2 induces alpha-synuclein expression via the extracellular signal-regulated kinase pathway. Cell Signal, 22, 821-7.

CHAN, D., CITRO, A., CORDY, J. M., SHEN, G. C. & WOLOZIN, B. 2011. Rac1 protein rescues neurite retraction caused by G2019S leucine-rich repeat kinase 2 (LRRK2). J Biol Chem, 286, 16140-9.

CHARTIER-HARLIN, M. C., KACHERGUS, J., ROUMIER, C., MOUROUX, V., DOUAY, X., LINCOLN, S., LEVECQUE, C., LARVOR, L., ANDRIEUX, J., HULIHAN, M., WAUCQUIER, N., DEFEBVRE, L., AMOUYEL, P., FARRER, M. & DESTEE, A. 2004. Alpha-synuclein locus duplication as a cause of familial Parkinson's disease. Lancet, 364, 1167-9.

CHEN, B., LIU, Q., GE, Q., XIE, J. & WANG, Z. W. 2007. UNC-1 regulates gap junctions important to locomotion in C. elegans. Curr Biol, 17, 1334-9.

CHEN, C. D., OH, S. Y., HINMAN, J. D. & ABRAHAM, C. R. 2006. Visualization of APP dimerization and APP-Notch2 heterodimerization in living cells using bimolecular fluorescence complementation. J Neurochem, 97, 30-43.

CHEN, J., LI, L. & CHIN, L. S. 2010. Parkinson disease protein DJ-1 converts from a zymogen to a protease by carboxyl-terminal cleavage. Hum Mol Genet, 19, 2395-408.

CHEN, X., DE SILVA, H. A., PETTENATI, M. J., RAO, P. N., ST GEORGE-HYSLOP, P., ROSES, A. D., XIA, Y., HORSBURGH, K., UEDA, K. & SAITOH, T. 1995. The human NACP/alpha-synuclein gene: chromosome assignment to 4q21.3-q22 and TaqI RFLP analysis. Genomics, 26, 425-7.

CHU, J., ZHANG, Z., ZHENG, Y., YANG, J., QIN, L., LU, J., HUANG, Z. L., ZENG, S. & LUO, Q. 2009. A novel far-red bimolecular fluorescence complementation system that allows for efficient visualization of protein interactions under physiological conditions. Biosens Bioelectron, 25, 234-9.

CHUNG, K. K., THOMAS, B., LI, X., PLETNIKOVA, O., TRONCOSO, J. C., MARSH, L., DAWSON, V. L. & DAWSON, T. M. 2004. S-nitrosylation of parkin regulates ubiquitination and compromises parkin's protective function. Science, 304, 1328-31.

CLARK, I. E., DODSON, M. W., JIANG, C., CAO, J. H., HUH, J. R., SEOL, J. H., YOO, S. J., HAY, B. A. & GUO, M. 2006. Drosophila pink1 is required for mitochondrial function and interacts genetically with parkin. Nature, 441, 1162-6.

CLEMENTS, C. M., MCNALLY, R. S., CONTI, B. J., MAK, T. W. & TING, J. P. 2006. DJ-1, a cancer- and Parkinson's disease-associated protein, stabilizes the antioxidant transcriptional master regulator Nrf2. Proc Natl Acad Sci U S A, 103, 15091-6.

COHEN, P. 2000. The regulation of protein function by multisite phosphorylation--a 25 year update. Trends Biochem Sci, 25, 596-601.

COLTON, C. A. & GILBERT, D. L. 1987. Production of superoxide anions by a CNS macrophage, the microglia. FEBS Lett, 223, 284-8.

CONWAY, K. A., HARPER, J. D. & LANSBURY, P. T. 1998. Accelerated in vitro fibril formation by a mutant alpha-synuclein linked to early-onset Parkinson disease. Nat Med, 4, 1318-20.

CONWAY, K. A., ROCHET, J. C., BIEGANSKI, R. M. & LANSBURY, P. T., JR. 2001. Kinetic stabilization of the alpha-synuclein protofibril by a dopamine-alpha-synuclein adduct. Science, 294, 1346-9.

COOKSON, M. R. 2010. The role of leucine-rich repeat kinase 2 (LRRK2) in Parkinson's disease. Nat Rev Neurosci, 11, 791-7.

COOPER, J. M., MANN, V. M., KRIGE, D. & SCHAPIRA, A. H. 1992. Human mitochondrial complex I dysfunction. Biochim Biophys Acta, 1101, 198-203.

CORTI, O., LESAGE, S. & BRICE, A. 2011. What genetics tells us about the causes and mechanisms of Parkinson's disease. Physiol Rev, 91, 1161-218.

CULLY, M., YOU, H., LEVINE, A. J. & MAK, T. W. 2006. Beyond PTEN mutations: the PI3K pathway as an integrator of multiple inputs during tumorigenesis. Nat Rev Cancer, 6, 184-92.

DANZER, K. M., RUF, W. P., PUTCHA, P., JOYNER, D., HASHIMOTO, T., GLABE, C., HYMAN, B. T. & MCLEAN, P. J. 2011. Heat-shock protein 70 modulates toxic extracellular alpha-synuclein oligomers and rescues trans-synaptic toxicity. FASEB J, 25, 326-36.

DAVIDSON, B., HADAR, R., SCHLOSSBERG, A., STERNLICHT, T., SLIPICEVIC, A., SKREDE, M., RISBERG, B., FLORENES, V. A., KOPOLOVIC, J. & REICH, R. 2008. Expression and clinical role of DJ-1, a negative regulator of PTEN, in ovarian carcinoma. Hum Pathol, 39, 87-95.

DAVIDSON, W. S., JONAS, A., CLAYTON, D. F. & GEORGE, J. M. 1998. Stabilization of alpha-synuclein secondary structure upon binding to synthetic membranes. J Biol Chem, 273, 9443-9.

DAWSON, T. M. & DAWSON, V. L. 2014. Parkin plays a role in sporadic Parkinson's disease. Neurodegener Dis, 13, 69-71.

DE LAU, L. M. & BRETELER, M. M. 2006. Epidemiology of Parkinson's disease. Lancet Neurol, 5, 525-35.

DEEG, S., GRALLE, M., SROKA, K., BAHR, M., WOUTERS, F. S. & KERMER, P. 2010. BAG1 restores formation of functional DJ-1 L166P dimers and DJ-1 chaperone activity. J Cell Biol, 188, 505-13.

DERKINDEREN, P., SCALES, T. M., HANGER, D. P., LEUNG, K. Y., BYERS, H. L., WARD, M. A., LENZ, C., PRICE, C., BIRD, I. N., PERERA, T., KELLIE, S., WILLIAMSON, R., NOBLE, W., VAN ETTEN, R. A., LEROY, K., BRION, J. P., REYNOLDS, C. H. & ANDERTON, B. H. 2005. Tyrosine 394 is phosphorylated in Alzheimer's paired helical filament tau and in fetal tau with c-Abl as the candidate tyrosine kinase. J Neurosci, 25, 6584-93.

DEXTER, D. T., CARAYON, A., JAVOY-AGID, F., AGID, Y., WELLS, F. R., DANIEL, S. E., LEES, A. J., JENNER, P. & MARSDEN, C. D. 1991. Alterations in the levels of iron, ferritin and other trace metals in Parkinson's disease

and other neurodegenerative diseases affecting the basal ganglia. Brain, 114 (Pt 4), 1953-75.

DEXTER, D. T., WELLS, F. R., AGID, F., AGID, Y., LEES, A. J., JENNER, P. & MARSDEN, C. D. 1987. Increased nigral iron content in postmortem parkinsonian brain. Lancet, 2, 1219-20.

DIAS, V., JUNN, E. & MOURADIAN, M. M. 2013. The role of oxidative stress in Parkinson's disease. J Parkinsons Dis, 3, 461-91.

DORSEY, E. R., CONSTANTINESCU, R., THOMPSON, J. P., BIGLAN, K. M., HOLLOWAY, R. G., KIEBURTZ, K., MARSHALL, F. J., RAVINA, B. M., SCHIFITTO, G., SIDEROWF, A. & TANNER, C. M. 2007. Projected number of people with Parkinson disease in the most populous nations, 2005 through 2030. Neurology, 68, 384-6.

DROUIN-OUELLET, J. & CICCHETTI, F. 2012. Inflammation and neurodegeneration: the story 'retolled'. Trends Pharmacol Sci, 33, 542-51.

DU, X., CHOI, I. G., KIM, R., WANG, W., JANCARIK, J., YOKOTA, H. & KIM, S. H. 2000. Crystal structure of an intracellular protease from Pyrococcus horikoshii at 2-A resolution. Proc Natl Acad Sci U S A, 97, 14079-84.

DUDA, J. E., GIASSON, B. I., MABON, M. E., LEE, V. M. & TROJANOWSKI, J. Q. 2002. Novel antibodies to synuclein show abundant striatal pathology in Lewy body diseases. Ann Neurol, 52, 205-10.

EBNETH, A., GODEMANN, R., STAMER, K., ILLENBERGER, S., TRINCZEK, B. & MANDELKOW, E. 1998. Overexpression of tau protein inhibits kinesin-dependent trafficking of vesicles, mitochondria, and endoplasmic reticulum: implications for Alzheimer's disease. J Cell Biol, 143, 777-94.

EL-AGNAF, O. M., SALEM, S. A., PALEOLOGOU, K. E., CURRAN, M. D., GIBSON, M. J., COURT, J. A., SCHLOSSMACHER, M. G. & ALLSOP, D. 2006. Detection of oligomeric forms of alpha-synuclein protein in human plasma as a potential biomarker for Parkinson's disease. FASEB J, 20, 419-25.

FAN, J., REN, H., FEI, E., JIA, N., YING, Z., JIANG, P., WU, M. & WANG, G. 2008a. Sumoylation is critical for DJ-1 to repress p53 transcriptional activity. FEBS Lett, 582, 1151-6.

FAN, J., REN, H., JIA, N., FEI, E., ZHOU, T., JIANG, P., WU, M. & WANG, G. 2008b. DJ-1 decreases Bax expression through repressing p53 transcriptional activity. J Biol Chem, 283, 4022-30.

FEI, E., JIA, N., YAN, M., YING, Z., SUN, Q., WANG, H., ZHANG, T., MA, X., DING, H., YAO, X., SHI, Y. & WANG, G. 2006. SUMO-1 modification in-

creases human SOD1 stability and aggregation. Biochem Biophys Res Commun, 347, 406-12.

FLYNN, J. M., CZERWIENIEC, G. A., CHOI, S. W., DAY, N. U., GIBSON, B. W., HUBBARD, A. & MELOV, S. 2012. Proteogenomics of synaptosomal mitochondrial oxidative stress. Free Radic Biol Med, 53, 1048-60.

FORTIN, D. L., TROYER, M. D., NAKAMURA, K., KUBO, S., ANTHONY, M. D. & EDWARDS, R. H. 2004. Lipid rafts mediate the synaptic localization of alpha-synuclein. J Neurosci, 24, 6715-23.

FRUMAN, D. A., MEYERS, R. E. & CANTLEY, L. C. 1998. Phosphoinositide kinases. Annu Rev Biochem, 67, 481-507.

GAIG, C., EZQUERRA, M., MARTI, M. J., VALLDEORIOLA, F., MUNOZ, E., LLADO, A., REY, M. J., CARDOZO, A., MOLINUEVO, J. L. & TOLOSA, E. 2008. Screening for the LRRK2 G2019S and codon-1441 mutations in a pathological series of parkinsonian syndromes and frontotemporal lobar degeneration. J Neurol Sci, 270, 94-8.

GANDHI, S., WOOD-KACZMAR, A., YAO, Z., PLUN-FAVREAU, H., DEAS, E., KLUPSCH, K., DOWNWARD, J., LATCHMAN, D. S., TABRIZI, S. J., WOOD, N. W., DUCHEN, M. R. & ABRAMOV, A. Y. 2009. PINK1-associated Parkinson's disease is caused by neuronal vulnerability to calcium-induced cell death. Mol Cell, 33, 627-38.

GAO, H., YANG, W., QI, Z., LU, L., DUAN, C., ZHAO, C. & YANG, H. 2012. DJ-1 protects dopaminergic neurons against rotenone-induced apoptosis by enhancing ERK-dependent mitophagy. J Mol Biol, 423, 232-48.

GEHL, C., WAADT, R., KUDLA, J., MENDEL, R. R. & HANSCH, R. 2009. New GATEWAY vectors for high throughput analyses of protein-protein interactions by bimolecular fluorescence complementation. Mol Plant, 2, 1051-8.

GIAIME, E., SUNYACH, C., DRUON, C., SCARZELLO, S., ROBERT, G., GROSSO, S., AUBERGER, P., GOLDBERG, M. S., SHEN, J., HEUTINK, P., POUYSSEGUR, J., PAGES, G., CHECLER, F. & ALVES DA COSTA, C. 2010. Loss of function of DJ-1 triggered by Parkinson's disease-associated mutation is due to proteolytic resistance to caspase-6. Cell Death Differ, 17, 158-69.

GIASSON, B. I., FORMAN, M. S., HIGUCHI, M., GOLBE, L. I., GRAVES, C. L., KOTZBAUER, P. T., TROJANOWSKI, J. Q. & LEE, V. M. 2003. Initiation and synergistic fibrillization of tau and alpha-synuclein. Science, 300, 636-40.

GIROTTO, S., CENDRON, L., BISAGLIA, M., TESSARI, I., MAMMI, S., ZANOTTI, G. & BUBACCO, L. 2014. DJ-1 is a copper chaperone acting on SOD1 activation. J Biol Chem, 289, 10887-99.

GOHAR, M., YANG, W., STRONG, W., VOLKENING, K., LEYSTRA-LANTZ, C. & STRONG, M. J. 2009. Tau phosphorylation at threonine-175 leads to fibril formation and enhanced cell death: implications for amyotrophic lateral sclerosis with cognitive impairment. J Neurochem, 108, 634-43.

GONCALVES, S. A., MATOS, J. E. & OUTEIRO, T. F. 2010. Zooming into protein oligomerization in neurodegeneration using BiFC. Trends Biochem Sci, 35, 643-51.

GONFLONI, S., MAIANI, E., DI BARTOLOMEO, C., DIEDERICH, M. & CESARENI, G. 2012. Oxidative Stress, DNA Damage, and c-Abl Signaling: At the Crossroad in Neurodegenerative Diseases? Int J Cell Biol, 2012, 683097.

GONG, C. X. & IQBAL, K. 2008. Hyperphosphorylation of microtubule-associated protein tau: a promising therapeutic target for Alzheimer disease. Curr Med Chem, 15, 2321-8.

GORNER, K., HOLTORF, E., ODOY, S., NUSCHER, B., YAMAMOTO, A., REGULA, J. T., BEYER, K., HAASS, C. & KAHLE, P. J. 2004. Differential effects of Parkinson's disease-associated mutations on stability and folding of DJ-1. J Biol Chem, 279, 6943-51.

GRAHAM, D. G., TIFFANY, S. M., BELL, W. R., JR. & GUTKNECHT, W. F. 1978. Autoxidation versus covalent binding of quinones as the mechanism of toxicity of dopamine, 6-hydroxydopamine, and related compounds toward C1300 neuroblastoma cells in vitro. Mol Pharmacol, 14, 644-53.

GRAHAM, R. K., DENG, Y., SLOW, E. J., HAIGH, B., BISSADA, N., LU, G., PEARSON, J., SHEHADEH, J., BERTRAM, L., MURPHY, Z., WARBY, S. C., DOTY, C. N., ROY, S., WELLINGTON, C. L., LEAVITT, B. R., RAYMOND, L. A., NICHOLSON, D. W. & HAYDEN, M. R. 2006. Cleavage at the caspase-6 site is required for neuronal dysfunction and degeneration due to mutant huntingtin. Cell, 125, 1179-91.

GREENBAUM, E. A., GRAVES, C. L., MISHIZEN-EBERZ, A. J., LUPOLI, M. A., LYNCH, D. R., ENGLANDER, S. W., AXELSEN, P. H. & GIASSON, B. I. 2005. The E46K mutation in alpha-synuclein increases amyloid fibril formation. J Biol Chem, 280, 7800-7.

GU, Z., KAUL, M., YAN, B., KRIDEL, S. J., CUI, J., STRONGIN, A., SMITH, J. W., LIDDINGTON, R. C. & LIPTON, S. A. 2002. S-nitrosylation of matrix metalloproteinases: signaling pathway to neuronal cell death. Science, 297, 1186-90.

GUO, Y., REBECCHI, M. & SCARLATA, S. 2005. Phospholipase Cbeta2 binds to and inhibits phospholipase Cdelta1. J Biol Chem, 280, 1438-47.

HAAS, R. H., NASIRIAN, F., NAKANO, K., WARD, D., PAY, M., HILL, R. & SHULTS, C. W. 1995. Low platelet mitochondrial complex I and complex II/III activity in early untreated Parkinson's disease. Ann Neurol, 37, 714-22.

HAGUE, S., ROGAEVA, E., HERNANDEZ, D., GULICK, C., SINGLETON, A., HANSON, M., JOHNSON, J., WEISER, R., GALLARDO, M., RAVINA, B., GWINN-HARDY, K., CRAWLEY, A., ST GEORGE-HYSLOP, P. H., LANG, A. E., HEUTINK, P., BONIFATI, V., HARDY, J. & SINGLETON, A. 2003. Early-onset Parkinson's disease caused by a compound heterozygous DJ-1 mutation. Ann Neurol, 54, 271-4.

HALIO, S. B., BLUMENTALS, II, SHORT, S. A., MERRILL, B. M. & KELLY, R. M. 1996. Sequence, expression in Escherichia coli, and analysis of the gene encoding a novel intracellular protease (PfpI) from the hyperthermophilic archaeon Pyrococcus furiosus. J Bacteriol, 178, 2605-12.

HALLIWELL, B. 1992. Reactive oxygen species and the central nervous system. J Neurochem, 59, 1609-23.

HANSEN, L., SALMON, D., GALASKO, D., MASLIAH, E., KATZMAN, R., DE-TERESA, R., THAL, L., PAY, M. M., HOFSTETTER, R., KLAUBER, M. & ET AL. 1990. The Lewy body variant of Alzheimer's disease: a clinical and pathologic entity. Neurology, 40, 1-8.

HAO, L. Y., GIASSON, B. I. & BONINI, N. M. 2010. DJ-1 is critical for mitochondrial function and rescues PINK1 loss of function. Proc Natl Acad Sci U S A, 107, 9747-52.

HARA, M. R., AGRAWAL, N., KIM, S. F., CASCIO, M. B., FUJIMURO, M., OZEKI, Y., TAKAHASHI, M., CHEAH, J. H., TANKOU, S. K., HESTER, L. D., FERRIS, C. D., HAYWARD, S. D., SNYDER, S. H. & SAWA, A. 2005. S-nitrosylated GAPDH initiates apoptotic cell death by nuclear translocation following Siah1 binding. Nat Cell Biol, 7, 665-74.

HASTINGS, T. G., LEWIS, D. A. & ZIGMOND, M. J. 1996. Role of oxidation in the neurotoxic effects of intrastriatal dopamine injections. Proc Natl Acad Sci U S A, 93, 1956-61.

HATAI, T., MATSUZAWA, A., INOSHITA, S., MOCHIDA, Y., KURODA, T., SAKAMAKI, K., KUIDA, K., YONEHARA, S., ICHIJO, H. & TAKEDA, K. 2000. Execution of apoptosis signal-regulating kinase 1 (ASK1)-induced apoptosis by the mitochondria-dependent caspase activation. J Biol Chem, 275, 26576-81.

HEO, J. Y., PARK, J. H., KIM, S. J., SEO, K. S., HAN, J. S., LEE, S. H., KIM, J. M., PARK, J. I., PARK, S. K., LIM, K., HWANG, B. D., SHONG, M. & KWEON, G. R. 2012. DJ-1 null dopaminergic neuronal cells exhibit defects in mitochon-

drial function and structure: involvement of mitochondrial complex I assembly. PLoS One, 7, e32629.

HERING, R., STRAUSS, K. M., TAO, X., BAUER, A., WOITALLA, D., MIETZ, E. M., PETROVIC, S., BAUER, P., SCHAIBLE, W., MULLER, T., SCHOLS, L., KLEIN, C., BERG, D., MEYER, P. T., SCHULZ, J. B., WOLLNIK, B., TONG, L., KRUGER, R. & RIESS, O. 2004. Novel homozygous p.E64D mutation in DJ1 in early onset Parkinson disease (PARK7). Hum Mutat, 24, 321-9.

HIRSCH, E. C., GRAYBIEL, A. M. & AGID, Y. 1989. Selective vulnerability of pigmented dopaminergic neurons in Parkinson's disease. Acta Neurol Scand Suppl, 126, 19-22.

HOD, Y. 2004. Differential control of apoptosis by DJ-1 in prostate benign and cancer cells. J Cell Biochem, 92, 1221-33.

HOD, Y., PENTYALA, S. N., WHYARD, T. C. & EL-MAGHRABI, M. R. 1999. Identification and characterization of a novel protein that regulates RNA-protein interaction. J Cell Biochem, 72, 435-44.

HONBOU, K., SUZUKI, N. N., HORIUCHI, M., NIKI, T., TAIRA, T., ARIGA, H. & INAGAKI, F. 2003. The crystal structure of DJ-1, a protein related to male fertility and Parkinson's disease. J Biol Chem, 278, 31380-4.

HORVATH, M. M. & GRISHIN, N. V. 2001. The C-terminal domain of HPII catalase is a member of the type I glutamine amidotransferase superfamily. Proteins, 42, 230-6.

HSU, C. H., CHAN, D. & WOLOZIN, B. 2010. LRRK2 and the stress response: interaction with MKKs and JNK-interacting proteins. Neurodegener Dis, 7, 68-75.

HU, C. D., CHINENOV, Y. & KERPPOLA, T. K. 2002. Visualization of interactions among bZIP and Rel family proteins in living cells using bimolecular fluorescence complementation. Mol Cell, 9, 789-98.

HU, C. D. & KERPPOLA, T. K. 2003. Simultaneous visualization of multiple protein interactions in living cells using multicolor fluorescence complementation analysis. Nat Biotechnol, 21, 539-45.

HUAI, Q., SUN, Y., WANG, H., CHIN, L. S., LI, L., ROBINSON, H. & KE, H. 2003. Crystal structure of DJ-1/RS and implication on familial Parkinson's disease. FEBS Lett, 549, 171-5.

HUBBARD, S. R. & TILL, J. H. 2000. Protein tyrosine kinase structure and function. Annu Rev Biochem, 69, 373-98.

HULLEMAN, J. D., MIRZAEI, H., GUIGARD, E., TAYLOR, K. L., RAY, S. S., KAY, C. M., REGNIER, F. E. & ROCHET, J. C. 2007. Destabilization of DJ-1 by fa-

milial substitution and oxidative modifications: implications for Parkinson's disease. Biochemistry, 46, 5776-89.

HWANG, O. 2013. Role of oxidative stress in Parkinson's disease. Exp Neurobiol, 22, 11-7.

ICHIJO, H., NISHIDA, E., IRIE, K., TEN DIJKE, P., SAITOH, M., MORIGUCHI, T., TAKAGI, M., MATSUMOTO, K., MIYAZONO, K. & GOTOH, Y. 1997. Induction of apoptosis by ASK1, a mammalian MAPKKK that activates SAPK/JNK and p38 signaling pathways. Science, 275, 90-4.

ICHIMURA, Y. & KOMATSU, M. 2010. Selective degradation of p62 by autophagy. Semin Immunopathol, 32, 431-6.

IMAM, S. Z., TRICKLER, W., KIMURA, S., BINIENDA, Z. K., PAULE, M. G., SLIKKER, W., JR., LI, S., CLARK, R. A. & ALI, S. F. 2013. Neuroprotective efficacy of a new brain-penetrating C-Abl inhibitor in a murine Parkinson's disease model. PLoS One, 8, e65129.

INDEN, M., KITAMURA, Y., TAKAHASHI, K., TAKATA, K., ITO, N., NIWA, R., FUNAYAMA, R., NISHIMURA, K., TANIGUCHI, T., HONDA, T., TAIRA, T. & ARIGA, H. 2011. Protection against dopaminergic neurodegeneration in Parkinson's disease-model animals by a modulator of the oxidized form of DJ-1, a wild-type of familial Parkinson's disease-linked PARK7. J Pharmacol Sci, 117, 189-203.

IRRCHER, I., ALEYASIN, H., SEIFERT, E. L., HEWITT, S. J., CHHABRA, S., PHILLIPS, M., LUTZ, A. K., ROUSSEAUX, M. W., BEVILACQUA, L., JAHANI-ASL, A., CALLAGHAN, S., MACLAURIN, J. G., WINKLHOFER, K. F., RIZZU, P., RIPPSTEIN, P., KIM, R. H., CHEN, C. X., FON, E. A., SLACK, R. S., HARPER, M. E., MCBRIDE, H. M., MAK, T. W. & PARK, D. S. 2010. Loss of the Parkinson's disease-linked gene DJ-1 perturbs mitochondrial dynamics. Hum Mol Genet, 19, 3734-46.

ISHIKAWA, S., TANAKA, Y., TAKAHASHI-NIKI, K., NIKI, T., ARIGA, H. & IGUCHI-ARIGA, S. M. 2012. Stimulation of vesicular monoamine transporter 2 activity by DJ-1 in SH-SY5Y cells. Biochem Biophys Res Commun, 421, 813-8.

ISHIMURA, A., ISHIGE, K., TAIRA, T., SHIMBA, S., ONO, S., ARIGA, H., TEZUKA, M. & ITO, Y. 2008. Comparative study of hydrogen peroxide- and 4-hydroxy-2-nonenal-induced cell death in HT22 cells. Neurochem Int, 52, 776-85.

ISHIZAWA, T., MATTILA, P., DAVIES, P., WANG, D. & DICKSON, D. W. 2003. Colocalization of tau and alpha-synuclein epitopes in Lewy bodies. J Neuropathol Exp Neurol, 62, 389-97.

ITO, G., ARIGA, H., NAKAGAWA, Y. & IWATSUBO, T. 2006. Roles of distinct cysteine residues in S-nitrosylation and dimerization of DJ-1. Biochem Biophys Res Commun, 339, 667-72.

ITO, S., KATO, T. & FUJITA, K. 1988. Covalent binding of catechols to proteins through the sulphydryl group. Biochem Pharmacol, 37, 1707-10.

ITO, Y., PANDEY, P., MISHRA, N., KUMAR, S., NARULA, N., KHARBANDA, S., SAXENA, S. & KUFE, D. 2001. Targeting of the c-Abl tyrosine kinase to mitochondria in endoplasmic reticulum stress-induced apoptosis. Mol Cell Biol, 21, 6233-42.

ITTNER, L. M., KE, Y. D., DELERUE, F., BI, M., GLADBACH, A., VAN EERSEL, J., WOLFING, H., CHIENG, B. C., CHRISTIE, M. J., NAPIER, I. A., ECKERT, A., STAUFENBIEL, M., HARDEMAN, E. & GOTZ, J. 2010. Dendritic function of tau mediates amyloid-beta toxicity in Alzheimer's disease mouse models. Cell, 142, 387-97.

JEGANATHAN, S., VON BERGEN, M., MANDELKOW, E. M. & MANDELKOW, E. 2008. The natively unfolded character of tau and its aggregation to Alzheimer-like paired helical filaments. Biochemistry, 47, 10526-39.

JING, Z., CALTAGARONE, J. & BOWSER, R. 2009. Altered subcellular distribution of c-Abl in Alzheimer's disease. J Alzheimers Dis, 17, 409-22.

JUNG, D., FILLIOL, D., MIEHE, M. & RENDON, A. 1993. Interaction of brain mitochondria with microtubules reconstituted from brain tubulin and MAP2 or TAU. Cell Motil Cytoskeleton, 24, 245-55.

JUNN, E., TANIGUCHI, H., JEONG, B. S., ZHAO, X., ICHIJO, H. & MOURADIAN, M. M. 2005. Interaction of DJ-1 with Daxx inhibits apoptosis signal-regulating kinase 1 activity and cell death. Proc Natl Acad Sci U S A, 102, 9691-6.

KAHLE, P. J., WAAK, J. & GASSER, T. 2009. DJ-1 and prevention of oxidative stress in Parkinson's disease and other age-related disorders. Free Radic Biol Med, 47, 1354-61.

KATO, I., MAITA, H., TAKAHASHI-NIKI, K., SAITO, Y., NOGUCHI, N., IGUCHI-ARIGA, S. M. & ARIGA, H. 2013. Oxidized DJ-1 inhibits p53 by sequestering p53 from promoters in a DNA-binding affinity-dependent manner. Mol Cell Biol, 33, 340-59.

KERPPOLA, T. K. 2006. Visualization of molecular interactions by fluorescence complementation. Nat Rev Mol Cell Biol, 7, 449-56.

KETLEY, A., CHEN, C. Z., LI, X., ARYA, S., ROBINSON, T. E., GRANADOS-RIVERON, J., UDOSEN, I., MORRIS, G. E., HOLT, I., FURLING, D., CHAOUCH, S., HAWORTH, B., SOUTHALL, N., SHINN, P., ZHENG, W.,

AUSTIN, C. P., HAYES, C. J. & BROOK, J. D. 2014. High-content screening identifies small molecules that remove nuclear foci, affect MBNL distribution and CELF1 protein levels via a PKC-independent pathway in myotonic dystrophy cell lines. Hum Mol Genet, 23, 1551-62.

KHARBANDA, S., REN, R., PANDEY, P., SHAFMAN, T. D., FELLER, S. M., WEICHSELBAUM, R. R. & KUFE, D. W. 1995. Activation of the c-Abl tyrosine kinase in the stress response to DNA-damaging agents. Nature, 376, 785-8.

KHLISTUNOVA, I., BIERNAT, J., WANG, Y., PICKHARDT, M., VON BERGEN, M., GAZOVA, Z., MANDELKOW, E. & MANDELKOW, E. M. 2006. Inducible expression of Tau repeat domain in cell models of tauopathy: aggregation is toxic to cells but can be reversed by inhibitor drugs. J Biol Chem, 281, 1205-14.

KIM, J. H., CHOI, D. J., JEONG, H. K., KIM, J., KIM, D. W., CHOI, S. Y., PARK, S. M., SUH, Y. H., JOU, I. & JOE, E. H. 2013. DJ-1 facilitates the interaction between STAT1 and its phosphatase, SHP-1, in brain microglia and astrocytes: A novel anti-inflammatory function of DJ-1. Neurobiol Dis, 60, 1-10.

KIM, R. H., PETERS, M., JANG, Y., SHI, W., PINTILIE, M., FLETCHER, G. C., DELUCA, C., LIEPA, J., ZHOU, L., SNOW, B., BINARI, R. C., MANOUKIAN, A. S., BRAY, M. R., LIU, F. F., TSAO, M. S. & MAK, T. W. 2005a. DJ-1, a novel regulator of the tumor suppressor PTEN. Cancer Cell, 7, 263-73.

KIM, R. H., SMITH, P. D., ALEYASIN, H., HAYLEY, S., MOUNT, M. P., POWNALL, S., WAKEHAM, A., YOU-TEN, A. J., KALIA, S. K., HORNE, P., WESTAWAY, D., LOZANO, A. M., ANISMAN, H., PARK, D. S. & MAK, T. W. 2005b. Hypersensitivity of DJ-1-deficient mice to 1-methyl-4-phenyl-1,2,3,6-tetrahydropyrindine (MPTP) and oxidative stress. Proc Natl Acad Sci U S A, 102, 5215-20.

KINUMI, T., KIMATA, J., TAIRA, T., ARIGA, H. & NIKI, E. 2004. Cysteine-106 of DJ-1 is the most sensitive cysteine residue to hydrogen peroxide-mediated oxidation in vivo in human umbilical vein endothelial cells. Biochem Biophys Res Commun, 317, 722-8.

KITADA, T., ASAKAWA, S., HATTORI, N., MATSUMINE, H., YAMAMURA, Y., MINOSHIMA, S., YOKOCHI, M., MIZUNO, Y. & SHIMIZU, N. 1998. Mutations in the parkin gene cause autosomal recessive juvenile parkinsonism. Nature, 392, 605-8.

KLEIN, C., KRAMER, E. M., CARDINE, A. M., SCHRAVEN, B., BRANDT, R. & TROTTER, J. 2002. Process outgrowth of oligodendrocytes is promoted by interaction of fyn kinase with the cytoskeletal protein tau. J Neurosci, 22, 698-707.

KLIONSKY, D. J., CUERVO, A. M., DUNN, W. A., JR., LEVINE, B., VAN DER KLEI, I. & SEGLEN, P. O. 2007. How shall I eat thee? Autophagy, 3, 413-6.

KNOTT, A. B. & BOSSY-WETZEL, E. 2008. Impairing the mitochondrial fission and fusion balance: a new mechanism of neurodegeneration. Ann N Y Acad Sci, 1147, 283-92.

KO, H. S., LEE, Y., SHIN, J. H., KARUPPAGOUNDER, S. S., GADAD, B. S., KOLESKE, A. J., PLETNIKOVA, O., TRONCOSO, J. C., DAWSON, V. L. & DAWSON, T. M. 2010. Phosphorylation by the c-Abl protein tyrosine kinase inhibits parkin's ubiquitination and protective function. Proc Natl Acad Sci U S A, 107, 16691-6.

KODAMA, Y. & HU, C. D. 2012. Bimolecular fluorescence complementation (BiFC): a 5-year update and future perspectives. Biotechniques, 53, 285-98.

KOIDE-YOSHIDA, S., NIKI, T., UEDA, M., HIMENO, S., TAIRA, T., IGUCHI-ARIGA, S. M., ANDO, Y. & ARIGA, H. 2007. DJ-1 degrades transthyretin and an inactive form of DJ-1 is secreted in familial amyloidotic polyneuropathy. Int J Mol Med, 19, 885-93.

KOLAROVA, M., GARCIA-SIERRA, F., BARTOS, A., RICNY, J. & RIPOVA, D. 2012. Structure and pathology of tau protein in Alzheimer disease. Int J Alzheimers Dis, 2012, 731526.

KREBIEHL, G., RUCKERBAUER, S., BURBULLA, L. F., KIEPER, N., MAURER, B., WAAK, J., WOLBURG, H., GIZATULLINA, Z., GELLERICH, F. N., WOITALLA, D., RIESS, O., KAHLE, P. J., PROIKAS-CEZANNE, T. & KRUGER, R. 2010. Reduced basal autophagy and impaired mitochondrial dynamics due to loss of Parkinson's disease-associated protein DJ-1. PLoS One, 5, e9367.

KUMAR, S., BHARTI, A., MISHRA, N. C., RAINA, D., KHARBANDA, S., SAXENA, S. & KUFE, D. 2001. Targeting of the c-Abl tyrosine kinase to mitochondria in the necrotic cell death response to oxidative stress. J Biol Chem, 276, 17281-5.

KUMARAN, R., KINGSBURY, A., COULTER, I., LASHLEY, T., WILLIAMS, D., DE SILVA, R., MANN, D., REVESZ, T., LEES, A. & BANDOPADHYAY, R. 2007. DJ-1 (PARK7) is associated with 3R and 4R tau neuronal and glial inclusions in neurodegenerative disorders. Neurobiol Dis, 28, 122-32.

KURODA, Y., MITSUI, T., KUNISHIGE, M., SHONO, M., AKAIKE, M., AZUMA, H. & MATSUMOTO, T. 2006. Parkin enhances mitochondrial biogenesis in proliferating cells. Hum Mol Genet, 15, 883-95.

LARSEN, K. E., SCHMITZ, Y., TROYER, M. D., MOSHAROV, E., DIETRICH, P., QUAZI, A. Z., SAVALLE, M., NEMANI, V., CHAUDHRY, F. A., EDWARDS, R. H., STEFANIS, L. & SULZER, D. 2006. Alpha-synuclein overexpression in PC12 and chromaffin cells impairs catecholamine release by interfering with a late step in exocytosis. J Neurosci, 26, 11915-22.

LARSEN, N. J., AMBROSI, G., MULLETT, S. J., BERMAN, S. B. & HINKLE, D. A. 2011. DJ-1 knock-down impairs astrocyte mitochondrial function. Neuroscience, 196, 251-64.

LAVOIE, M. J. & HASTINGS, T. G. 1999. Dopamine quinone formation and protein modification associated with the striatal neurotoxicity of methamphetamine: evidence against a role for extracellular dopamine. J Neurosci, 19, 1484-91.

LAVOIE, M. J., OSTASZEWSKI, B. L., WEIHOFEN, A., SCHLOSSMACHER, M. G. & SELKOE, D. J. 2005. Dopamine covalently modifies and functionally inactivates parkin. Nat Med, 11, 1214-21.

LEE, C. S., HAN, J. H., JANG, Y. Y., SONG, J. H. & HAN, E. S. 2002. Differential effect of catecholamines and MPP(+) on membrane permeability in brain mitochondria and cell viability in PC12 cells. Neurochem Int, 40, 361-9.

LEE, J. Y., SONG, J., KWON, K., JANG, S., KIM, C., BAEK, K., KIM, J. & PARK, C. 2012. Human DJ-1 and its homologs are novel glyoxalases. Hum Mol Genet, 21, 3215-25.

LEE, S. J., KIM, S. J., KIM, I. K., KO, J., JEONG, C. S., KIM, G. H., PARK, C., KANG, S. O., SUH, P. G., LEE, H. S. & CHA, S. S. 2003. Crystal structures of human DJ-1 and Escherichia coli Hsp31, which share an evolutionarily conserved domain. J Biol Chem, 278, 44552-9.

LEE, V. M., GOEDERT, M. & TROJANOWSKI, J. Q. 2001. Neurodegenerative tauopathies. Annu Rev Neurosci, 24, 1121-59.

LEV, N., RONCEVIC, D., ICKOWICZ, D., MELAMED, E. & OFFEN, D. 2006. Role of DJ-1 in Parkinson's disease. J Mol Neurosci, 29, 215-25.

LI, G., YIN, H. & KURET, J. 2004. Casein kinase 1 delta phosphorylates tau and disrupts its binding to microtubules. J Biol Chem, 279, 15938-45.

LI, Y., WANG, H., WANG, S., QUON, D., LIU, Y. W. & CORDELL, B. 2003. Positive and negative regulation of APP amyloidogenesis by sumoylation. Proc Natl Acad Sci U S A, 100, 259-64.

LIACHKO, N. F., MCMILLAN, P. J., GUTHRIE, C. R., BIRD, T. D., LEVERENZ, J. B. & KRAEMER, B. C. 2013. CDC7 inhibition blocks pathological TDP-43 phosphorylation and neurodegeneration. Ann Neurol, 74, 39-52.

LIM, K. L., CHEW, K. C., TAN, J. M., WANG, C., CHUNG, K. K., ZHANG, Y., TANAKA, Y., SMITH, W., ENGELENDER, S., ROSS, C. A., DAWSON, V. L. & DAWSON, T. M. 2005. Parkin mediates nonclassical, proteasomal-independent ubiquitination of synphilin-1: implications for Lewy body formation. J Neurosci, 25, 2002-9.

LIN, X., COOK, T. J., ZABETIAN, C. P., LEVERENZ, J. B., PESKIND, E. R., HU, S. C., CAIN, K. C., PAN, C., EDGAR, J. S., GOODLETT, D. R., RACETTE, B. A., CHECKOWAY, H., MONTINE, T. J., SHI, M. & ZHANG, J. 2012. DJ-1 isoforms in whole blood as potential biomarkers of Parkinson disease. Sci Rep, 2, 954.

LIU, F., NGUYEN, J. L., HULLEMAN, J. D., LI, L. & ROCHET, J. C. 2008a. Mechanisms of DJ-1 neuroprotection in a cellular model of Parkinson's disease. J Neurochem, 105, 2435-53.

LIU, W., VIVES-BAUZA, C., ACIN-PEREZ, R., YAMAMOTO, A., TAN, Y., LI, Y., MAGRANE, J., STAVARACHE, M. A., SHAFFER, S., CHANG, S., KAPLITT, M. G., HUANG, X. Y., BEAL, M. F., MANFREDI, G. & LI, C. 2009. PINK1 defect causes mitochondrial dysfunction, proteasomal deficit and alpha-synuclein aggregation in cell culture models of Parkinson's disease. PLoS One, 4, e4597.

LIU, Z., WANG, X., YU, Y., LI, X., WANG, T., JIANG, H., REN, Q., JIAO, Y., SAWA, A., MORAN, T., ROSS, C. A., MONTELL, C. & SMITH, W. W. 2008b. A Drosophila model for LRRK2-linked parkinsonism. Proc Natl Acad Sci U S A, 105, 2693-8.

LYNCH-DAY, M. A., MAO, K., WANG, K., ZHAO, M. & KLIONSKY, D. J. 2012. The role of autophagy in Parkinson's disease. Cold Spring Harb Perspect Med, 2, a009357.

MAAS, T., EIDENMULLER, J. & BRANDT, R. 2000. Interaction of tau with the neural membrane cortex is regulated by phosphorylation at sites that are modified in paired helical filaments. J Biol Chem, 275, 15733-40.

MACKEIGAN, J. P., CLEMENTS, C. M., LICH, J. D., POPE, R. M., HOD, Y. & TING, J. P. 2003. Proteomic profiling drug-induced apoptosis in non-small cell lung carcinoma: identification of RS/DJ-1 and RhoGDIalpha. Cancer Res, 63, 6928-34.

MAEHAMA, T. & DIXON, J. E. 1998. The tumor suppressor, PTEN/MMAC1, dephosphorylates the lipid second messenger, phosphatidylinositol 3,4,5-trisphosphate. J Biol Chem, 273, 13375-8.

MALGIERI, G. & ELIEZER, D. 2008. Structural effects of Parkinson's disease linked DJ-1 mutations. Protein Sci, 17, 855-68.

MANDELL, J. W. & BANKER, G. A. 1996. A spatial gradient of tau protein phosphorylation in nascent axons. J Neurosci, 16, 5727-40.

MANN, M., ONG, S. E., GRONBORG, M., STEEN, H., JENSEN, O. N. & PANDEY, A. 2002. Analysis of protein phosphorylation using mass spectrometry: deciphering the phosphoproteome. Trends Biotechnol, 20, 261-8.

MANNING, G., WHYTE, D. B., MARTINEZ, R., HUNTER, T. & SUDARSANAM, S. 2002. The protein kinase complement of the human genome. Science, 298, 1912-34.

MARCONDES, A. M., LI, X., GOOLEY, T. A., MILLESS, B. & DEEG, H. J. 2010. Identification of DJ-1/PARK-7 as a determinant of stroma-dependent and TNF-alpha-induced apoptosis in MDS using mass spectrometry and phosphopeptide analysis. Blood, 115, 1993-2002.

MARTIN, I., DAWSON, V. L. & DAWSON, T. M. 2011. Recent advances in the genetics of Parkinson's disease. Annu Rev Genomics Hum Genet, 12, 301-25.

MARTINAT, C., SHENDELMAN, S., JONASON, A., LEETE, T., BEAL, M. F., YANG, L., FLOSS, T. & ABELIOVICH, A. 2004. Sensitivity to oxidative stress in DJ-1-deficient dopamine neurons: an ES- derived cell model of primary Parkinsonism. PLoS Biol, 2, e327.

MARTINEZ-VICENTE, M., TALLOCZY, Z., KAUSHIK, S., MASSEY, A. C., MAZZULLI, J., MOSHAROV, E. V., HODARA, R., FREDENBURG, R., WU, D. C., FOLLENZI, A., DAUER, W., PRZEDBORSKI, S., ISCHIROPOULOS, H., LANSBURY, P. T., SULZER, D. & CUERVO, A. M. 2008. Dopamine-modified alpha-synuclein blocks chaperone-mediated autophagy. J Clin Invest, 118, 777-88.

MATTA, S., VAN KOLEN, K., DA CUNHA, R., VAN DEN BOGAART, G., MANDEMAKERS, W., MISKIEWICZ, K., DE BOCK, P. J., MORAIS, V. A., VILAIN, S., HADDAD, D., DELBROEK, L., SWERTS, J., CHAVEZ-GUTIERREZ, L., ESPOSITO, G., DANEELS, G., KARRAN, E., HOLT, M., GEVAERT, K., MOECHARS, D. W., DE STROOPER, B. & VERSTREKEN, P. 2012. LRRK2 controls an EndoA phosphorylation cycle in synaptic endocytosis. Neuron, 75, 1008-21.

MCKEITH, I. G., GALASKO, D., KOSAKA, K., PERRY, E. K., DICKSON, D. W., HANSEN, L. A., SALMON, D. P., LOWE, J., MIRRA, S. S., BYRNE, E. J., LENNOX, G., QUINN, N. P., EDWARDSON, J. A., INCE, P. G., BERGERON, C., BURNS, A., MILLER, B. L., LOVESTONE, S., COLLERTON, D., JANSEN, E. N., BALLARD, C., DE VOS, R. A., WILCOCK, G. K., JELLINGER, K. A. & PERRY, R. H. 1996. Consensus guidelines for the clinical and pathologic diagnosis of dementia with Lewy bodies (DLB): report of the consortium on DLB international workshop. Neurology, 47, 1113-24.

MILLER, D. W., AHMAD, R., HAGUE, S., BAPTISTA, M. J., CANET-AVILES, R., MCLENDON, C., CARTER, D. M., ZHU, P. P., STADLER, J., CHANDRAN, J., KLINEFELTER, G. R., BLACKSTONE, C. & COOKSON, M. R. 2003. L166P mutant DJ-1, causative for recessive Parkinson's disease, is degraded through the ubiquitin-proteasome system. J Biol Chem, 278, 36588-95.

MILLER-FLEMING, L., ANTAS, P., PAIS, T. F., SMALLEY, J. L., GIORGINI, F. & OUTEIRO, T. F. 2014. Yeast DJ-1 superfamily members are required for diauxic-shift reprogramming and cell survival in stationary phase. Proc Natl Acad Sci U S A, 111, 7012-7.

MINTON, A. P. 2005. Influence of macromolecular crowding upon the stability and state of association of proteins: predictions and observations. J Pharm Sci, 94, 1668-75.

MITSUGI, H., NIKI, T., TAKAHASHI-NIKI, K., TANIMURA, K., YOSHIZAWA-KUMAGAYE, K., TSUNEMI, M., IGUCHI-ARIGA, S. M. & ARIGA, H. 2013. Identification of the recognition sequence and target proteins for DJ-1 protease. FEBS Lett, 587, 2493-9.

MITSUMOTO, A. & NAKAGAWA, Y. 2001. DJ-1 is an indicator for endogenous reactive oxygen species elicited by endotoxin. Free Radic Res, 35, 885-93.

MIZOTE, T., TSUDA, M., SMITH, D. D., NAKAYAMA, H. & NAKAZAWA, T. 1999. Cloning and characterization of the thiD/J gene of Escherichia coli encoding a thiamin-synthesizing bifunctional enzyme, hydroxymethylpyrimidine kinase/phosphomethylpyrimidine kinase. Microbiology, 145 (Pt 2), 495-501.

MOORE, D. J., ZHANG, L., DAWSON, T. M. & DAWSON, V. L. 2003. A missense mutation (L166P) in DJ-1, linked to familial Parkinson's disease, confers reduced protein stability and impairs homo-oligomerization. J Neurochem, 87, 1558-67.

MOORHEAD, G. B., TRINKLE-MULCAHY, L. & ULKE-LEMEE, A. 2007. Emerging roles of nuclear protein phosphatases. Nat Rev Mol Cell Biol, 8, 234-44.

MORIKAWA, S., KURAUCHI, O., TANAKA, M., YONEDA, M., UCHIDA, K., ITAKURA, A., FURUGORI, K., MIZUTANI, S. & TOMODA, Y. 1997. Increased mitochondrial damage by lipid peroxidation in trophoblast cells of preeclamptic placentas. Biochem Mol Biol Int, 41, 767-75.

MULLETT, S. J., HAMILTON, R. L. & HINKLE, D. A. 2009. DJ-1 immunoreactivity in human brain astrocytes is dependent on infarct presence and infarct age. Neuropathology, 29, 125-31.

MUNTANE, G., DALFO, E., MARTINEZ, A. & FERRER, I. 2008. Phosphorylation of tau and alpha-synuclein in synaptic-enriched fractions of the frontal cortex in Alzheimer's disease, and in Parkinson's disease and related alpha-synucleinopathies. Neuroscience, 152, 913-23.

MYERS, M. P., PASS, I., BATTY, I. H., VAN DER KAAY, J., STOLAROV, J. P., HEMMINGS, B. A., WIGLER, M. H., DOWNES, C. P. & TONKS, N. K. 1998. The lipid phosphatase activity of PTEN is critical for its tumor supressor function. Proc Natl Acad Sci U S A, 95, 13513-8.

NAGAKUBO, D., TAIRA, T., KITAURA, H., IKEDA, M., TAMAI, K., IGUCHI-ARIGA, S. M. & ARIGA, H. 1997. DJ-1, a novel oncogene which transforms mouse NIH3T3 cells in cooperation with ras. Biochem Biophys Res Commun, 231, 509-13.

NARENDRA, D., TANAKA, A., SUEN, D. F. & YOULE, R. J. 2008. Parkin is recruited selectively to impaired mitochondria and promotes their autophagy. J Cell Biol, 183, 795-803.

NARENDRA, D., TANAKA, A., SUEN, D. F. & YOULE, R. J. 2009. Parkin-induced mitophagy in the pathogenesis of Parkinson disease. Autophagy, 5, 706-8.

NEUMANN, M., MULLER, V., GORNER, K., KRETZSCHMAR, H. A., HAASS, C. & KAHLE, P. J. 2004. Pathological properties of the Parkinson's disease-associated protein DJ-1 in alpha-synucleinopathies and tauopathies: relevance for multiple system atrophy and Pick's disease. Acta Neuropathol, 107, 489-96.

NEVE, R. L., HARRIS, P., KOSIK, K. S., KURNIT, D. M. & DONLON, T. A. 1986. Identification of cDNA clones for the human microtubule-associated protein tau and chromosomal localization of the genes for tau and microtubule-associated protein 2. Brain Res, 387, 271-80.

NGIM, C. H. & DEVATHASAN, G. 1989. Epidemiologic study on the association between body burden mercury level and idiopathic Parkinson's disease. Neuroepidemiology, 8, 128-41.

NIKI, T., TAKAHASHI-NIKI, K., TAIRA, T., IGUCHI-ARIGA, S. M. & ARIGA, H. 2003. DJBP: a novel DJ-1-binding protein, negatively regulates the androgen receptor by recruiting histone deacetylase complex, and DJ-1 antagonizes this inhibition by abrogation of this complex. Mol Cancer Res, 1, 247-61.

NISHITOH, H., MATSUZAWA, A., TOBIUME, K., SAEGUSA, K., TAKEDA, K., INOUE, K., HORI, S., KAKIZUKA, A. & ICHIJO, H. 2002. ASK1 is essential for endoplasmic reticulum stress-induced neuronal cell death triggered by expanded polyglutamine repeats. Genes Dev, 16, 1345-55.

NUYTEMANS, K., THEUNS, J., CRUTS, M. & VAN BROECKHOVEN, C. 2010. Genetic etiology of Parkinson disease associated with mutations in the SNCA, PARK2, PINK1, PARK7, and LRRK2 genes: a mutation update. Hum Mutat, 31, 763-80.

OKADA, M., MATSUMOTO, K., NIKI, T., TAIRA, T., IGUCHI-ARIGA, S. M. & ARIGA, H. 2002. DJ-1, a target protein for an endocrine disrupter, participates in the fertilization in mice. Biol Pharm Bull, 25, 853-6.

OLZMANN, J. A., BROWN, K., WILKINSON, K. D., REES, H. D., HUAI, Q., KE, H., LEVEY, A. I., LI, L. & CHIN, L. S. 2004. Familial Parkinson's disease-asso-

ciated L166P mutation disrupts DJ-1 protein folding and function. J Biol Chem, 279, 8506-15.

OOE, H., MAITA, C., MAITA, H., IGUCHI-ARIGA, S. M. & ARIGA, H. 2006. Specific cleavage of DJ-1 under an oxidative condition. Neurosci Lett, 406, 165-8.

OUTEIRO, T. F., PUTCHA, P., TETZLAFF, J. E., SPOELGEN, R., KOKER, M., CARVALHO, F., HYMAN, B. T. & MCLEAN, P. J. 2008. Formation of toxic oligomeric alpha-synuclein species in living cells. PLoS One, 3, e1867.

PAISAN-RUIZ, C., JAIN, S., EVANS, E. W., GILKS, W. P., SIMON, J., VAN DER BRUG, M., LOPEZ DE MUNAIN, A., APARICIO, S., GIL, A. M., KHAN, N., JOHNSON, J., MARTINEZ, J. R., NICHOLL, D., CARRERA, I. M., PENA, A. S., DE SILVA, R., LEES, A., MARTI-MASSO, J. F., PEREZ-TUR, J., WOOD, N. W. & SINGLETON, A. B. 2004. Cloning of the gene containing mutations that cause PARK8-linked Parkinson's disease. Neuron, 44, 595-600.

PARKER, W. D., JR., PARKS, J. K. & SWERDLOW, R. H. 2008. Complex I deficiency in Parkinson's disease frontal cortex. Brain Res, 1189, 215-8.

PATEL, D. A., PATEL, A. C., NOLAN, W. C., ZHANG, Y. & HOLTZMAN, M. J. 2012. High throughput screening for small molecule enhancers of the interferon signaling pathway to drive next-generation antiviral drug discovery. PLoS One, 7, e36594.

PETROV, D., MARGREITTER, C., GRANDITS, M., OOSTENBRINK, C. & ZAGROVIC, B. 2013. A systematic framework for molecular dynamics simulations of protein post-translational modifications. PLoS Comput Biol, 9, e1003154.

PHAM, F. H., SUGDEN, P. H. & CLERK, A. 2000. Regulation of protein kinase B and 4E-BP1 by oxidative stress in cardiac myocytes. Circ Res, 86, 1252-8.

PIGGEE, C. 2009. Phosphoproteomics: miles to go before it's routine. Anal Chem, 81, 2418-20.

PLUN-FAVREAU, H., KLUPSCH, K., MOISOI, N., GANDHI, S., KJAER, S., FRITH, D., HARVEY, K., DEAS, E., HARVEY, R. J., MCDONALD, N., WOOD, N. W., MARTINS, L. M. & DOWNWARD, J. 2007. The mitochondrial protease HtrA2 is regulated by Parkinson's disease-associated kinase PINK1. Nat Cell Biol, 9, 1243-52.

POLYMEROPOULOS, M. H., LAVEDAN, C., LEROY, E., IDE, S. E., DEHEJIA, A., DUTRA, A., PIKE, B., ROOT, H., RUBENSTEIN, J., BOYER, R., STENROOS, E. S., CHANDRASEKHARAPPA, S., ATHANASSIADOU, A., PAPAPETROPOULOS, T., JOHNSON, W. G., LAZZARINI, A. M., DUVOISIN, R. C., DI IORIO, G., GOLBE, L. I. & NUSSBAUM, R. L. 1997. Mutation in the alpha-synuclein gene identified in families with Parkinson's disease. Science, 276, 2045-7.

POOLE, A. C., THOMAS, R. E., ANDREWS, L. A., MCBRIDE, H. M., WHITWORTH, A. J. & PALLANCK, L. J. 2008. The PINK1/Parkin pathway regulates mitochondrial morphology. Proc Natl Acad Sci U S A, 105, 1638-43.

PREMKUMAR, A. & SIMANTOV, R. 2002. Mitochondrial voltage-dependent anion channel is involved in dopamine-induced apoptosis. J Neurochem, 82, 345-52.

PRIDGEON, J. W., OLZMANN, J. A., CHIN, L. S. & LI, L. 2007. PINK1 protects against oxidative stress by phosphorylating mitochondrial chaperone TRAP1. PLoS Biol, 5, e172.

PRITCHARD, S. M., DOLAN, P. J., VITKUS, A. & JOHNSON, G. V. 2011. The toxicity of tau in Alzheimer disease: turnover, targets and potential therapeutics. J Cell Mol Med, 15, 1621-35.

PUNO, M. R., PATEL, N. A., MOLLER, S. G., ROBINSON, C. V., MOODY, P. C. & ODELL, M. 2013. Structure of Cu(I)-bound DJ-1 reveals a biscysteinate metal binding site at the homodimer interface: insights into mutational inactivation of DJ-1 in Parkinsonism. J Am Chem Soc, 135, 15974-7.

PURSIHEIMO, J. P., RANTANEN, K., HEIKKINEN, P. T., JOHANSEN, T. & JAAKKOLA, P. M. 2009. Hypoxia-activated autophagy accelerates degradation of SQSTM1/p62. Oncogene, 28, 334-44.

PUTCHA, P., DANZER, K. M., KRANICH, L. R., SCOTT, A., SILINSKI, M., MABBETT, S., HICKS, C. D., VEAL, J. M., STEED, P. M., HYMAN, B. T. & MCLEAN, P. J. 2010. Brain-permeable small-molecule inhibitors of Hsp90 prevent alpha-synuclein oligomer formation and rescue alpha-synuclein-induced toxicity. J Pharmacol Exp Ther, 332, 849-57.

RAHMAN-ROBLICK, R., HELLMAN, U., BECKER, S., BADER, F. G., AUER, G., WIMAN, K. G. & ROBLICK, U. J. 2008. Proteomic identification of p53-dependent protein phosphorylation. Oncogene, 27, 4854-9.

REPICI, M., STRAATMAN, K. R., BALDUCCIO, N., ENGUITA, F. J., OUTEIRO, T. F. & GIORGINI, F. 2013. Parkinson's disease-associated mutations in DJ-1 modulate its dimerization in living cells. J Mol Med (Berl), 91, 599-611.

REYNOLDS, C. H., GARWOOD, C. J., WRAY, S., PRICE, C., KELLIE, S., PERERA, T., ZVELEBIL, M., YANG, A., SHEPPARD, P. W., VARNDELL, I. M., HANGER, D. P. & ANDERTON, B. H. 2008. Phosphorylation regulates tau interactions with Src homology 3 domains of phosphatidylinositol 3-kinase, phospholipase Cgamma1, Grb2, and Src family kinases. J Biol Chem, 283, 18177-86.

RIGBOLT, K. T., PROKHOROVA, T. A., AKIMOV, V., HENNINGSEN, J., JOHANSEN, P. T., KRATCHMAROVA, I., KASSEM, M., MANN, M., OLSEN, J. V. & BLAGOEV, B. 2011. System-wide temporal characterization of the pro-

teome and phosphoproteome of human embryonic stem cell differentiation. Sci Signal, 4, rs3.

RIZZU, P., HINKLE, D. A., ZHUKAREVA, V., BONIFATI, V., SEVERIJNEN, L. A., MARTINEZ, D., RAVID, R., KAMPHORST, W., EBERWINE, J. H., LEE, V. M., TROJANOWSKI, J. Q. & HEUTINK, P. 2004. DJ-1 colocalizes with tau inclusions: a link between parkinsonism and dementia. Ann Neurol, 55, 113-8.

ROBERT, G., PUISSANT, A., DUFIES, M., MARCHETTI, S., JACQUEL, A., CLUZEAU, T., COLOSETTI, P., BELHACENE, N., KAHLE, P., DA COSTA, C. A., LUCIANO, F., CHECLER, F. & AUBERGER, P. 2012. The caspase 6 derived N-terminal fragment of DJ-1 promotes apoptosis via increased ROS production. Cell Death Differ, 19, 1769-78.

RUSH, J., MORITZ, A., LEE, K. A., GUO, A., GOSS, V. L., SPEK, E. J., ZHANG, H., ZHA, X. M., POLAKIEWICZ, R. D. & COMB, M. J. 2005. Immunoaffinity profiling of tyrosine phosphorylation in cancer cells. Nat Biotechnol, 23, 94-101.

SAHA, S., GUILLILY, M. D., FERREE, A., LANCETA, J., CHAN, D., GHOSH, J., HSU, C. H., SEGAL, L., RAGHAVAN, K., MATSUMOTO, K., HISAMOTO, N., KUWAHARA, T., IWATSUBO, T., MOORE, L., GOLDSTEIN, L., COOKSON, M. & WOLOZIN, B. 2009. LRRK2 modulates vulnerability to mitochondrial dysfunction in Caenorhabditis elegans. J Neurosci, 29, 9210-8.

SAITO, Y. 2014. Oxidized DJ-1 as a possible biomarker of Parkinson's disease. J Clin Biochem Nutr, 54, 138-44.

SAITOH, M., NISHITOH, H., FUJII, M., TAKEDA, K., TOBIUME, K., SAWADA, Y., KAWABATA, M., MIYAZONO, K. & ICHIJO, H. 1998. Mammalian thioredoxin is a direct inhibitor of apoptosis signal-regulating kinase (ASK) 1. EMBO J, 17, 2596-606.

SAJJAD, M. U., GREEN, E. W., MILLER-FLEMING, L., HANDS, S., HERRERA, F., CAMPESAN, S., KHOSHNAN, A., OUTEIRO, T. F., GIORGINI, F. & WYTTENBACH, A. 2014. DJ-1 modulates aggregation and pathogenesis in models of Huntington's disease. Hum Mol Genet, 23, 755-66.

SATAKE, W., NAKABAYASHI, Y., MIZUTA, I., HIROTA, Y., ITO, C., KUBO, M., KAWAGUCHI, T., TSUNODA, T., WATANABE, M., TAKEDA, A., TOMIYAMA, H., NAKASHIMA, K., HASEGAWA, K., OBATA, F., YOSHIKAWA, T., KAWAKAMI, H., SAKODA, S., YAMAMOTO, M., HATTORI, N., MURATA, M., NAKAMURA, Y. & TODA, T. 2009. Genome-wide association study identifies common variants at four loci as genetic risk factors for Parkinson's disease. Nat Genet, 41, 1303-7.

SCARFFE, L. A., STEVENS, D. A., DAWSON, V. L. & DAWSON, T. M. 2014. Parkin and PINK1: much more than mitophagy. Trends Neurosci, 37, 315-24.

SCHAFER, K. N., CISEK, K., HUSEBY, C. J., CHANG, E. & KURET, J. 2013. Structural determinants of Tau aggregation inhibitor potency. J Biol Chem, 288, 32599-611.

SCHAPIRA, A. H. 2004. Disease modification in Parkinson's disease. Lancet Neurol, 3, 362-8.

SCHAPIRA, A. H., COOPER, J. M., DEXTER, D., CLARK, J. B., JENNER, P. & MARSDEN, C. D. 1990. Mitochondrial complex I deficiency in Parkinson's disease. J Neurochem, 54, 823-7.

SCHAPIRA, A. H. & JENNER, P. 2011. Etiology and pathogenesis of Parkinson's disease. Mov Disord, 26, 1049-55.

SCHLATTERER, S. D., TREMBLAY, M. A., ACKER, C. M. & DAVIES, P. 2011. Neuronal c-Abl overexpression leads to neuronal loss and neuroinflammation in the mouse forebrain. J Alzheimers Dis, 25, 119-33.

SCHMIDT, C., PENG, B., LI, Z., SCLABAS, G. M., FUJIOKA, S., NIU, J., SCHMIDT-SUPPRIAN, M., EVANS, D. B., ABBRUZZESE, J. L. & CHIAO, P. J. 2003. Mechanisms of proinflammatory cytokine-induced biphasic NF-kappaB activation. Mol Cell, 12, 1287-300.

SELLEY, M. L. 1998. (E)-4-hydroxy-2-nonenal may be involved in the pathogenesis of Parkinson's disease. Free Radic Biol Med, 25, 169-74.

SERGEANT, N., DELACOURTE, A. & BUEE, L. 2005. Tau protein as a differential biomarker of tauopathies. Biochim Biophys Acta, 1739, 179-97.

SHAHANI, N. & BRANDT, R. 2002. Functions and malfunctions of the tau proteins. Cell Mol Life Sci, 59, 1668-80.

SHAHANI, N., SUBRAMANIAM, S., WOLF, T., TACKENBERG, C. & BRANDT, R. 2006. Tau aggregation and progressive neuronal degeneration in the absence of changes in spine density and morphology after targeted expression of Alzheimer's disease-relevant tau constructs in organotypic hippocampal slices. J Neurosci, 26, 6103-14.

SHENDELMAN, S., JONASON, A., MARTINAT, C., LEETE, T. & ABELIOVICH, A. 2004. DJ-1 is a redox-dependent molecular chaperone that inhibits alpha-synuclein aggregate formation. PLoS Biol, 2, e362.

SHIBASAKI, Y., BAILLIE, D. A., ST CLAIR, D. & BROOKES, A. J. 1995. High-resolution mapping of SNCA encoding alpha-synuclein, the non-A beta component of Alzheimer's disease amyloid precursor, to human chromosome 4q21.3-->q22 by fluorescence in situ hybridization. Cytogenet Cell Genet, 71, 54-5.

SHIN, C. J., WONG, S., DAVIS, M. J. & RAGAN, M. A. 2009. Protein-protein interaction as a predictor of subcellular location. BMC Syst Biol, 3, 28.

SHIN, N., JEONG, H., KWON, J., HEO, H. Y., KWON, J. J., YUN, H. J., KIM, C. H., HAN, B. S., TONG, Y., SHEN, J., HATANO, T., HATTORI, N., KIM, K. S., CHANG, S. & SEOL, W. 2008. LRRK2 regulates synaptic vesicle endocytosis. Exp Cell Res, 314, 2055-65.

SHINBO, Y., NIKI, T., TAIRA, T., OOE, H., TAKAHASHI-NIKI, K., MAITA, C., SEINO, C., IGUCHI-ARIGA, S. M. & ARIGA, H. 2006. Proper SUMO-1 conjugation is essential to DJ-1 to exert its full activities. Cell Death Differ, 13, 96-108.

SHINBO, Y., TAIRA, T., NIKI, T., IGUCHI-ARIGA, S. M. & ARIGA, H. 2005. DJ-1 restores p53 transcription activity inhibited by Topors/p53BP3. Int J Oncol, 26, 641-8.

SIMON-SANCHEZ, J., SCHULTE, C., BRAS, J. M., SHARMA, M., GIBBS, J. R., BERG, D., PAISAN-RUIZ, C., LICHTNER, P., SCHOLZ, S. W., HERNANDEZ, D. G., KRUGER, R., FEDEROFF, M., KLEIN, C., GOATE, A., PERLMUTTER, J., BONIN, M., NALLS, M. A., ILLIG, T., GIEGER, C., HOULDEN, H., STEFFENS, M., OKUN, M. S., RACETTE, B. A., COOKSON, M. R., FOOTE, K. D., FERNANDEZ, H. H., TRAYNOR, B. J., SCHREIBER, S., AREPALLI, S., ZONOZI, R., GWINN, K., VAN DER BRUG, M., LOPEZ, G., CHANOCK, S. J., SCHATZKIN, A., PARK, Y., HOLLENBECK, A., GAO, J., HUANG, X., WOOD, N. W., LORENZ, D., DEUSCHL, G., CHEN, H., RIESS, O., HARDY, J. A., SINGLETON, A. B. & GASSER, T. 2009. Genome-wide association study reveals genetic risk underlying Parkinson's disease. Nat Genet, 41, 1308-12.

SINGLETON, A. B., FARRER, M., JOHNSON, J., SINGLETON, A., HAGUE, S., KACHERGUS, J., HULIHAN, M., PEURALINNA, T., DUTRA, A., NUSSBAUM, R., LINCOLN, S., CRAWLEY, A., HANSON, M., MARAGANORE, D., ADLER, C., COOKSON, M. R., MUENTER, M., BAPTISTA, M., MILLER, D., BLANCATO, J., HARDY, J. & GWINN-HARDY, K. 2003. alpha-Synuclein locus triplication causes Parkinson's disease. Science, 302, 841.

SKIBINSKI, G., NAKAMURA, K., COOKSON, M. R. & FINKBEINER, S. 2014. Mutant LRRK2 toxicity in neurons depends on LRRK2 levels and synuclein but not kinase activity or inclusion bodies. J Neurosci, 34, 418-33.

SMITH, W. W., PEI, Z., JIANG, H., MOORE, D. J., LIANG, Y., WEST, A. B., DAWSON, V. L., DAWSON, T. M. & ROSS, C. A. 2005. Leucine-rich repeat kinase 2 (LRRK2) interacts with parkin, and mutant LRRK2 induces neuronal degeneration. Proc Natl Acad Sci U S A, 102, 18676-81.

SPILLANTINI, M. G., SCHMIDT, M. L., LEE, V. M., TROJANOWSKI, J. Q., JAKES, R. & GOEDERT, M. 1997. Alpha-synuclein in Lewy bodies. Nature, 388, 839-40.

STAMBOLIC, V., SUZUKI, A., DE LA POMPA, J. L., BROTHERS, G. M., MIRTSOS, C., SASAKI, T., RULAND, J., PENNINGER, J. M., SIDEROVSKI, D. P. & MAK, T. W. 1998. Negative regulation of PKB/Akt-dependent cell survival by the tumor suppressor PTEN. Cell, 95, 29-39.

STAMLER, J. S., SIMON, D. I., OSBORNE, J. A., MULLINS, M. E., JARAKI, O., MICHEL, T., SINGEL, D. J. & LOSCALZO, J. 1992. S-nitrosylation of proteins with nitric oxide: synthesis and characterization of biologically active compounds. Proc Natl Acad Sci U S A, 89, 444-8.

STOKOE, D., STEPHENS, L. R., COPELAND, T., GAFFNEY, P. R., REESE, C. B., PAINTER, G. F., HOLMES, A. B., MCCORMICK, F. & HAWKINS, P. T. 1997. Dual role of phosphatidylinositol-3,4,5-trisphosphate in the activation of protein kinase B. Science, 277, 567-70.

SULTAN, A., NESSLANY, F., VIOLET, M., BEGARD, S., LOYENS, A., TALAHARI, S., MANSUROGLU, Z., MARZIN, D., SERGEANT, N., HUMEZ, S., COLIN, M., BONNEFOY, E., BUEE, L. & GALAS, M. C. 2011. Nuclear tau, a key player in neuronal DNA protection. J Biol Chem, 286, 4566-75.

SUN, H., LESCHE, R., LI, D. M., LILIENTAL, J., ZHANG, H., GAO, J., GAVRILOVA, N., MUELLER, B., LIU, X. & WU, H. 1999. PTEN modulates cell cycle progression and cell survival by regulating phosphatidylinositol 3,4,5,-trisphosphate and Akt/protein kinase B signaling pathway. Proc Natl Acad Sci U S A, 96, 6199-204.

SUN, X., MAJUMDER, P., SHIOYA, H., WU, F., KUMAR, S., WEICHSELBAUM, R., KHARBANDA, S. & KUFE, D. 2000. Activation of the cytoplasmic c-Abl tyrosine kinase by reactive oxygen species. J Biol Chem, 275, 17237-40.

TAIRA, T., SAITO, Y., NIKI, T., IGUCHI-ARIGA, S. M., TAKAHASHI, K. & ARIGA, H. 2004. DJ-1 has a role in antioxidative stress to prevent cell death. EMBO Rep, 5, 213-8.

TAIRA, T., TAKAHASHI, K., KITAGAWA, R., IGUCHI-ARIGA, S. M. & ARIGA, H. 2001. Molecular cloning of human and mouse DJ-1 genes and identification of Sp1-dependent activation of the human DJ-1 promoter. Gene, 263, 285-92.

TAKAHASHI, K., TAIRA, T., NIKI, T., SEINO, C., IGUCHI-ARIGA, S. M. & ARIGA, H. 2001. DJ-1 positively regulates the androgen receptor by impairing the binding of PIASx alpha to the receptor. J Biol Chem, 276, 37556-63.

TAO, X. & TONG, L. 2003. Crystal structure of human DJ-1, a protein associated with early onset Parkinson's disease. J Biol Chem, 278, 31372-9.

TAYMANS, J. M. & COOKSON, M. R. 2010. Mechanisms in dominant parkinsonism: The toxic triangle of LRRK2, alpha-synuclein, and tau. Bioessays, 32, 227-35.

THOMAS, K. J., MCCOY, M. K., BLACKINTON, J., BEILINA, A., VAN DER BRUG, M., SANDEBRING, A., MILLER, D., MARIC, D., CEDAZO-MINGUEZ, A. & COOKSON, M. R. 2011. DJ-1 acts in parallel to the PINK1/parkin pathway to control mitochondrial function and autophagy. Hum Mol Genet, 20, 40-50.

TOBIN, J. E., LATOURELLE, J. C., LEW, M. F., KLEIN, C., SUCHOWERSKY, O., SHILL, H. A., GOLBE, L. I., MARK, M. H., GROWDON, J. H., WOOTEN, G. F., RACETTE, B. A., PERLMUTTER, J. S., WATTS, R., GUTTMAN, M., BAKER, K. B., GOLDWURM, S., PEZZOLI, G., SINGER, C., SAINT-HILAIRE, M. H., HENDRICKS, A. E., WILLIAMSON, S., NAGLE, M. W., WILK, J. B., MASSOOD, T., LARAMIE, J. M., DESTEFANO, A. L., LITVAN, I., NICHOLSON, G., CORBETT, A., ISAACSON, S., BURN, D. J., CHINNERY, P. F., PRAMSTALLER, P. P., SHERMAN, S., AL-HINTI, J., DRASBY, E., NANCE, M., MOLLER, A. T., OSTERGAARD, K., ROXBURGH, R., SNOW, B., SLEVIN, J. T., CAMBI, F., GUSELLA, J. F. & MYERS, R. H. 2008. Haplotypes and gene expression implicate the MAPT region for Parkinson disease: the GenePD Study. Neurology, 71, 28-34.

TOBIUME, K., MATSUZAWA, A., TAKAHASHI, T., NISHITOH, H., MORITA, K., TAKEDA, K., MINOWA, O., MIYAZONO, K., NODA, T. & ICHIJO, H. 2001. ASK1 is required for sustained activations of JNK/p38 MAP kinases and apoptosis. EMBO Rep, 2, 222-8.

TOKUDA, T., QURESHI, M. M., ARDAH, M. T., VARGHESE, S., SHEHAB, S. A., KASAI, T., ISHIGAMI, N., TAMAOKA, A., NAKAGAWA, M. & EL-AGNAF, O. M. 2010. Detection of elevated levels of alpha-synuclein oligomers in CSF from patients with Parkinson disease. Neurology, 75, 1766-72.

TREMPE, J. F. & FON, E. A. 2013. Structure and Function of Parkin, PINK1, and DJ-1, the Three Musketeers of Neuroprotection. Front Neurol, 4, 38.

TRINCZEK, B., EBNETH, A., MANDELKOW, E. M. & MANDELKOW, E. 1999. Tau regulates the attachment/detachment but not the speed of motors in microtubule-dependent transport of single vesicles and organelles. J Cell Sci, 112 (Pt 14), 2355-67.

UVERSKY, V. N. 2003. A protein-chameleon: conformational plasticity of alpha-synuclein, a disordered protein involved in neurodegenerative disorders. J Biomol Struct Dyn, 21, 211-34.

VALENTE, E. M., ABOU-SLEIMAN, P. M., CAPUTO, V., MUQIT, M. M., HARVEY, K., GISPERT, S., ALI, Z., DEL TURCO, D., BENTIVOGLIO, A. R., HEALY, D. G., ALBANESE, A., NUSSBAUM, R., GONZALEZ-MALDONADO, R., DELLER, T., SALVI, S., CORTELLI, P., GILKS, W. P., LATCHMAN, D. S., HARVEY, R. J., DALLAPICCOLA, B., AUBURGER, G. & WOOD, N. W. 2004. Hereditary early-onset Parkinson's disease caused by mutations in PINK1. Science, 304, 1158-60.

VAN DUIJN, C. M., DEKKER, M. C., BONIFATI, V., GALJAARD, R. J., HOUWING-DUISTERMAAT, J. J., SNIJDERS, P. J., TESTERS, L., BREEDVELD, G. J., HORSTINK, M., SANDKUIJL, L. A., VAN SWIETEN, J. C., OOSTRA, B. A. & HEUTINK, P. 2001. Park7, a novel locus for autosomal recessive early-onset parkinsonism, on chromosome 1p36. Am J Hum Genet, 69, 629-34.

VAN LAAR, V. S. & BERMAN, S. B. 2009. Mitochondrial dynamics in Parkinson's disease. Exp Neurol, 218, 247-56.

VAN LAAR, V. S., MISHIZEN, A. J., CASCIO, M. & HASTINGS, T. G. 2009. Proteomic identification of dopamine-conjugated proteins from isolated rat brain mitochondria and SH-SY5Y cells. Neurobiol Dis, 34, 487-500.

VAN ROSSUM, B., FISCHLE, W. & SELENKO, P. 2012. Asymmetrically modified nucleosomes expand the histone code. Nat Struct Mol Biol, 19, 1064-6.

VASSEUR, S., AFZAL, S., TARDIVEL-LACOMBE, J., PARK, D. S., IOVANNA, J. L. & MAK, T. W. 2009. DJ-1/PARK7 is an important mediator of hypoxia-induced cellular responses. Proc Natl Acad Sci U S A, 106, 1111-6.

VASSEUR, S., AFZAL, S., TOMASINI, R., GUILLAUMOND, F., TARDIVEL-LACOMBE, J., MAK, T. W. & IOVANNA, J. L. 2012. Consequences of DJ-1 upregulation following p53 loss and cell transformation. Oncogene, 31, 664-70.

VED, R., SAHA, S., WESTLUND, B., PERIER, C., BURNAM, L., SLUDER, A., HOENER, M., RODRIGUES, C. M., ALFONSO, A., STEER, C., LIU, L., PRZEDBORSKI, S. & WOLOZIN, B. 2005. Similar patterns of mitochondrial vulnerability and rescue induced by genetic modification of alpha-synuclein, parkin, and DJ-1 in Caenorhabditis elegans. J Biol Chem, 280, 42655-68.

VENDA, L. L., CRAGG, S. J., BUCHMAN, V. L. & WADE-MARTINS, R. 2010. alpha-Synuclein and dopamine at the crossroads of Parkinson's disease. Trends Neurosci, 33, 559-68.

VENDEROVA, K. & PARK, D. S. 2012. Programmed cell death in Parkinson's disease. Cold Spring Harb Perspect Med, 2.

VIDI, P. A., CHEMEL, B. R., HU, C. D. & WATTS, V. J. 2008. Ligand-dependent oligomerization of dopamine D(2) and adenosine A(2A) receptors in living neuronal cells. Mol Pharmacol, 74, 544-51.

VINGTDEUX, V., SERGEANT, N. & BUEE, L. 2012. Potential contribution of exosomes to the prion-like propagation of lesions in Alzheimer's disease. Front Physiol, 3, 229.

VON BERGEN, M., BARGHORN, S., BIERNAT, J., MANDELKOW, E. M. & MANDELKOW, E. 2005. Tau aggregation is driven by a transition from random coil to beta sheet structure. Biochim Biophys Acta, 1739, 158-66.

WAAK, J., WEBER, S. S., WALDENMAIER, A., GORNER, K., ALUNNI-FABBRONI, M., SCHELL, H., VOGT-WEISENHORN, D., PHAM, T. T., REUMERS, V., BAEKELANDT, V., WURST, W. & KAHLE, P. J. 2009. Regulation of astrocyte inflammatory responses by the Parkinson's disease-associated gene DJ-1. FASEB J, 23, 2478-89.

WALDEN, H. & MARTINEZ-TORRES, R. J. 2012. Regulation of Parkin E3 ubiquitin ligase activity. Cell Mol Life Sci, 69, 3053-67.

WALSH, C. T., GARNEAU-TSODIKOVA, S. & GATTO, G. J., JR. 2005. Protein post-translational modifications: the chemistry of proteome diversifications. Angew Chem Int Ed Engl, 44, 7342-72.

WALSH, D. M., LOMAKIN, A., BENEDEK, G. B., CONDRON, M. M. & TEPLOW, D. B. 1997. Amyloid beta-protein fibrillogenesis. Detection of a protofibrillar intermediate. J Biol Chem, 272, 22364-72.

WANG, H. L., CHOU, A. H., YEH, T. H., LI, A. H., CHEN, Y. L., KUO, Y. L., TSAI, S. R. & YU, S. T. 2007. PINK1 mutants associated with recessive Parkinson's disease are defective in inhibiting mitochondrial release of cytochrome c. Neurobiol Dis, 28, 216-26.

WANG, X. & SCHWARZ, T. L. 2009. The mechanism of Ca2+ -dependent regulation of kinesin-mediated mitochondrial motility. Cell, 136, 163-74.

WANG, Y., LIU, W., HE, X. & ZHOU, F. 2013. Parkinson's disease-associated DJ-1 mutations increase abnormal phosphorylation of tau protein through Akt/GSK-3beta pathways. J Mol Neurosci, 51, 911-8.

WANG, Z., LIU, J., CHEN, S., WANG, Y., CAO, L., ZHANG, Y., KANG, W., LI, H., GUI, Y., CHEN, S. & DING, J. 2011. DJ-1 modulates the expression of Cu/Zn-superoxide dismutase-1 through the Erk1/2-Elk1 pathway in neuroprotection. Ann Neurol, 70, 591-9.

WEIHOFEN, A., THOMAS, K. J., OSTASZEWSKI, B. L., COOKSON, M. R. & SELKOE, D. J. 2009. Pink1 forms a multiprotein complex with Miro and Milton, linking Pink1 function to mitochondrial trafficking. Biochemistry, 48, 2045-52.

WILSON, M. A. 2011. The role of cysteine oxidation in DJ-1 function and dysfunction. Antioxid Redox Signal, 15, 111-22.

WILSON, M. A., COLLINS, J. L., HOD, Y., RINGE, D. & PETSKO, G. A. 2003. The 1.1-A resolution crystal structure of DJ-1, the protein mutated in autosomal recessive early onset Parkinson's disease. Proc Natl Acad Sci U S A, 100, 9256-61.

WINKLHOFER, K. F. & HAASS, C. 2010. Mitochondrial dysfunction in Parkinson's disease. Biochim Biophys Acta, 1802, 29-44.

XU, J., ZHONG, N., WANG, H., ELIAS, J. E., KIM, C. Y., WOLDMAN, I., PIFL, C., GYGI, S. P., GEULA, C. & YANKNER, B. A. 2005. The Parkinson's disease-associated DJ-1 protein is a transcriptional co-activator that protects against neuronal apoptosis. Hum Mol Genet, 14, 1231-41.

XU, X. M., LIN, H., MAPLE, J., BJORKBLOM, B., ALVES, G., LARSEN, J. P. & MOLLER, S. G. 2010. The Arabidopsis DJ-1a protein confers stress protection through cytosolic SOD activation. J Cell Sci, 123, 1644-51.

YAMAGUCHI, S., YAMANE, T., TAKAHASHI-NIKI, K., KATO, I., NIKI, T., GOLDBERG, M. S., SHEN, J., ISHIMOTO, K., DOI, T., IGUCHI-ARIGA, S. M. & ARIGA, H. 2012. Transcriptional activation of low-density lipoprotein receptor gene by DJ-1 and effect of DJ-1 on cholesterol homeostasis. PLoS One, 7, e38144.

YAMASHITA, S., MORI, A., KIMURA, E., MITA, S., MAEDA, Y., HIRANO, T. & UCHINO, M. 2010. DJ-1 forms complexes with mutant SOD1 and ameliorates its toxicity. J Neurochem, 113, 860-70.

YANCOPOULOU, D. & SPILLANTINI, M. G. 2003. Tau protein in familial and sporadic diseases. Neuromolecular Med, 4, 37-48.

YANG, F., MOSS, L. G. & PHILLIPS, G. N., JR. 1996. The molecular structure of green fluorescent protein. Nat Biotechnol, 14, 1246-51.

YANG, Y., OUYANG, Y., YANG, L., BEAL, M. F., MCQUIBBAN, A., VOGEL, H. & LU, B. 2008. Pink1 regulates mitochondrial dynamics through interaction with the fission/fusion machinery. Proc Natl Acad Sci U S A, 105, 7070-5.

YAO, C., EL KHOURY, R., WANG, W., BYRD, T. A., PEHEK, E. A., THACKER, C., ZHU, X., SMITH, M. A., WILSON-DELFOSSE, A. L. & CHEN, S. G. 2010. LRRK2-mediated neurodegeneration and dysfunction of dopaminergic neurons in a Caenorhabditis elegans model of Parkinson's disease. Neurobiol Dis, 40, 73-81.

YAO, D., GU, Z., NAKAMURA, T., SHI, Z. Q., MA, Y., GASTON, B., PALMER, L. A., ROCKENSTEIN, E. M., ZHANG, Z., MASLIAH, E., UEHARA, T. & LIPTON, S. A. 2004. Nitrosative stress linked to sporadic Parkinson's disease: S-nitrosylation of parkin regulates its E3 ubiquitin ligase activity. Proc Natl Acad Sci U S A, 101, 10810-4.

YORITAKA, A., HATTORI, N., UCHIDA, K., TANAKA, M., STADTMAN, E. R. & MIZUNO, Y. 1996. Immunohistochemical detection of 4-hydroxynonenal protein adducts in Parkinson disease. Proc Natl Acad Sci U S A, 93, 2696-701.

YOSHIDA, K., YAMAGUCHI, T., NATSUME, T., KUFE, D. & MIKI, Y. 2005. JNK phosphorylation of 14-3-3 proteins regulates nuclear targeting of c-Abl in the apoptotic response to DNA damage. Nat Cell Biol, 7, 278-85.

YOSHINO, H., HATTORI, N., URABE, T., UCHIDA, K., TANAKA, M. & MIZUNO, Y. 1997. Postischemic accumulation of lipid peroxidation products in the rat brain: immunohistochemical detection of 4-hydroxy-2-nonenal modified proteins. Brain Res, 767, 81-6.

YU, Y. & LUTZ, S. 2011. Circular permutation: a different way to engineer enzyme structure and function. Trends Biotechnol, 29, 18-25.

ZHANG, L., SHIMOJI, M., THOMAS, B., MOORE, D. J., YU, S. W., MARUPUDI, N. I., TORP, R., TORGNER, I. A., OTTERSEN, O. P., DAWSON, T. M. & DAWSON, V. L. 2005. Mitochondrial localization of the Parkinson's disease related protein DJ-1: implications for pathogenesis. Hum Mol Genet, 14, 2063-73.

ZHANG, S., MA, C. & CHALFIE, M. 2004. Combinatorial marking of cells and organelles with reconstituted fluorescent proteins. Cell, 119, 137-44.

ZHONG, N., KIM, C. Y., RIZZU, P., GEULA, C., PORTER, D. R., POTHOS, E. N., SQUITIERI, F., HEUTINK, P. & XU, J. 2006. DJ-1 transcriptionally up-regulates the human tyrosine hydroxylase by inhibiting the sumoylation of pyrimidine tract-binding protein-associated splicing factor. J Biol Chem, 281, 20940-8.

ZHOU, C., HUANG, Y., SHAO, Y., MAY, J., PROU, D., PERIER, C., DAUER, W., SCHON, E. A. & PRZEDBORSKI, S. 2008. The kinase domain of mitochondrial PINK1 faces the cytoplasm. Proc Natl Acad Sci U S A, 105, 12022-7.

ZHOU, H., TIAN, R., YE, M., XU, S., FENG, S., PAN, C., JIANG, X., LI, X. & ZOU, H. 2007. Highly specific enrichment of phosphopeptides by zirconium dioxide nanoparticles for phosphoproteome analysis. Electrophoresis, 28, 2201-15.

ZHOU, W. & FREED, C. R. 2005. DJ-1 up-regulates glutathione synthesis during oxidative stress and inhibits A53T alpha-synuclein toxicity. J Biol Chem, 280, 43150-8.

ZHOU, W., ZHU, M., WILSON, M. A., PETSKO, G. A. & FINK, A. L. 2006. The oxidation state of DJ-1 regulates its chaperone activity toward alpha-synuclein. J Mol Biol, 356, 1036-48.

ZHU, J. & CHU, C. T. 2010. Mitochondrial dysfunction in Parkinson's disease. J Alzheimers Dis, 20 Suppl 2, S325-34.

ZIVIANI, E., TAO, R. N. & WHITWORTH, A. J. 2010. Drosophila parkin requires PINK1 for mitochondrial translocation and ubiquitinates mitofusin. Proc Natl Acad Sci U S A, 107, 5018-23.

ZONDLER, L., MILLER-FLEMING, L., REPICI, M., GONCALVES, S., TENREIRO, S., ROSADO-RAMOS, R., BETZER, C., STRAATMAN, K. R., JENSEN, P. H., GIORGINI, F. & OUTEIRO, T. F. 2014. DJ-1 interactions with alpha-synuclein attenuate aggregation and cellular toxicity in models of Parkinson's disease. Cell Death Dis, 5, e1350.

APPENDICES

Appendix 1: A) Kinase inhibitor library used in this study

Item Name	Plate location	Molecular Weight	Cas Number	Concentration (dissolved in DMSO)	Target	Catalog Number	Brief Description
BMS-599626	a2-L1200-01	567.0144232	8173837-23-1	10mM	EGFR | HER2	S1056	BMS-599626 (AC480) is a highly selective pan-HER Kinase inhibitor with IC50 of 20 and 30 nM for the inhibition of HER1and HER2, respectively.
Erlotinib Hydrochloride	a3-L1200-01	429.89666	183319-69-9	10mM	EGFR	S1023	Erlotinib Hydrochloride also known as Tarceva, CP-358774, OSI-774, NSC-718781 is a HCL salt with IC50 of 2 nM for HER1/ EGFR TK.
Gefitinib(Iressa)	a4-L1200-01	446.9023632	184475-35-2	10mM	EGFR | Akt	S1025	Gefitinib also known as ZD-1839 & Iressa is a novel potent EGFR tyrosine kinase & Akt phosphorylations inhibitor with IC50 of 37, 26 and 57 nM.
Neratinib	a5-L1200-01	557.04266	698387-09-6	10mM	HER2	S2150	Neratinib is an orally available, irreversible tyrosine kinase inhibitor with IC50 of 59 nM and 92 nM for HER2 and EGFR, respectively.
PD153035 hydrochloride	a6-L1200-01	396.6662	183322-45-4	10mM	EGFR	S1079	PD153035 is an inhibitor of EGFR, competitive with ATP. EGF Receptor: IC50 = 25 pM (Ki = 6 pM).
Pelitinib	a7-L1200-01	467.9231232	257933-82-7	10mM	EGFR	S1392	Pelitinib is a 3-cyanoquinoline pan-ErbB tyrosine kinase inhibitor with potential antineoplastic activity.
Vandetanib	a8-L1200-01	475.3539632	443913-73-3	10mM	VEGFR | EGFR | Src	S1046	Vandetanib (Zactima) is a VEGFR and EGFR antagonist and a tyrosine kinase inhibitor with IC50 of 60, 90, 40 nM for HUVEC proliferation, PC-9 cells and tyrosine kinase activity, respectively.
WZ3146	a9-L1200-01	464.9473	1214265-56-1	10mM	EGFR	S1170	WZ3146 is an irreversiblely inhibitor against EGFR T790M.
WZ4002	a10-L1200-01	494.97328	1213269-23-8	10mM	EGFR	S1173	WZ4002 is an EGFR T790M inhibitor(IC50<20nM).
WZ8040	a11-L1200-01	481.0129	1214265-57-2	10mM	EGFR	S1179	WZ8040 is an irreversiblely EGFR T790M inhibitor (IC50<10nM).
AV-951(Tivozanib)	b1-L1200-01	454.86306	475108-18-0	10mM	VEGFR | PDGFR	S1207	Tivozanib also known as AV-951 is an orally bioavailable potent VEGFR-1, 2 and 3, c-Kit and PDGFR inhibitor with IC50 of 0.21, 0.16, 0.24, 1.63 and 1.72 nM, respectively.
Axitinib	b2-L1200-01	386.46952	319460-85-0	10mM	VEGFR	S1005	Axitinib is a receptor kinase inhibitor with IC50 of 0.1 nmol (VEGFR-1), 0.2 nmol (VEGFR-2), 0.1–0.3 nmol (VEGFR-3), 1.6 nmol (PDGFR-β) and 1.7 nmol (c-KIT).
BIBF1120(Vargatef)	b3-L1200-01	539.62482	928326-83-4	10mM	FGFR | VEGFR | PDGFR	S1010	BIBF1120 (Vargatef) is a potent VEGF receptor (VEGFR), PDGFR and FGFR kinase inhibitor to VEGFR1, VEGFR2,VEGFR3 with IC50 of 34, 13 and 13 nM, respectively.
BMS 794833	b4-L1200-01	468.8400064	1174046-72-0	10mM	VEGFR | c-Met | Flt	S2201	BMS-794833 is a potent ATPcompetitive Met/VEGFR-2 kinase inhibitor and it also inhibits Ron (Met family),Axl and Flt-3 with IC50 values <3 nM.
Cediranib(AZD2171)	b6-L1200-01	450.5052832	288383-20-0	10mM	VEGFR	S1017	Cediranib (AZD2171) inhibited VEGF-stimulated proliferation and KDR phosphorylation with IC50 of 0.4 and 0.5 nM, respectively.
CYC116	b8-L1200-01	368.456	693228-63-6	10mM	Aurora | VEGFR	S1171	CYC116 is an orally bioavailable, small molecule Aurora kinase and VEGFR2 inhibitor.

Appendix 1A: Continued.

Imatinib(STI571)	b10-L1200-01	493.60274	152459-95-5	10mM	VEGFR	PDGFR	S2475	Imatinib(STI571) is a number of tyrosine kinase enzymes specific inhibitor.
Imatinib Mesylate	b11-L1200-01	589.7084	220127-57-1	10mM	c-Kit	PDGFR	S1026	Imatinib Mesylate is a multitargeted c-kit, PDGF-R and c-ABL inhibitor with IC50 of 3.9 and 2.9 μM for the inhibition of T-cell proliferation stimulated by DCs and PHA, respectively.
Ki8751	c1-L1200-01	469.4126296	228559-41-9	10mM	c-Kit	VEGFR	PDGFR	S1363	Ki8751 is a potent, selective VEGFR-2 tyrosine kinase inhibitor with IC50 of 0.9 nM, 40, 67, 170 nM for VEGF-2, c-Kit, PDGFRα and FGFR-2, respectively.
KRN 633	c2-L1200-01	416.85814	286370-15-8	10mM	VEGFR	S1557	KRN 633 is a cell-permeable, reversible, ATP-competitive VEGFR kinase inhibitor with IC50 of 170 nM, 160 nM, and 125 nM for VEGFR-1, VEGFR-2, VEGFR-3, respectively.
Masitinib(AB1010)	c3-L1200-01	498.6424	790299-79-5	10mM	c-Kit	PDGFR	FGFR	S1064	Masitinib also known as Masivet, AB1010 is a tyrosine kinase, c-Kit, PDGFR, FGFR3, the FAK pathway inhibitor with IC50 of 150 ± 80, 200 ± 40 nM.
MGCD-265	c4-L1200-01	517.5977032	875337-44-3	10mM	c-Met	VEGFR	Tie-2	S1361	MGCD-265 is a multi-targeted kinase inhibitor, which targets the c-MET, VEGFR1, VEGFR2, VEGFR3, Tie-2 and Ron receptor tyrosine kinases.
Motesanib Diphosphate	c5-L1200-01	569.441282	857876-30-3	10mM	VEGFR	PDGFR	Src	S1032	Motesanib is a multiple inhibitor of VEGFR1/2/3(IC50: 2 ηM /3 ηM /6 ηM), PDGFR (84ηM), kit (8ηM) & Ret (59ηM) receptors.
MP-470 (Amuvatinib)	c6-L1200-01	447.50954	850879-09-3	10mM	c-Kit	PDGFR	c-Met	S1244	MP470 is a multi-targeted tyrosine kinase inhibitor with potent activity against mutant c-Met, c-Kit, PDGFRalpha, Flt3, and c-Ret and with an IC50 of median 5 μM.
OSI-930	c7-L1200-01	443.4415496	728033-96-3	10mM	c-Kit	VEGFR	S1220	OSI-930 is an inhibitor of the receptor tyrosine kinases c-Kit (IC50:9.5nM) and VEGFR-2 (IC50:10.1nM).
Pazopanib Hydrochloride	c8-L1200-01	473.97896	635702-64-6	10mM	VEGFR	S1035	Pazopanib is a VEGFR inhibitor, IC50 of 10, 30, and 47 nM for VEGFR-1, -2, and -3.
Sorafenib Tosylate	c9-L1200-01	637.0265696	475207-59-1	10mM	VEGFR	PDGFR	RAF	M	S1040	Sorafenib Tosylate is a novel, small molecular inhibitor of several tyrosine protein kinases (VEGFR and PDGFR) and RAF/MEK/ERK cascade inhibitor with an IC50 of 6, 22, 38 nM for Raf-1, wt BRAF and V599E mutant BRAF.
Sunitinib Malate	c10-L1200-01	532.5612232	341031-54-7	10mM	FLT3	PDGFR	VEGFR	S1042	Sunitinib Malate (Sutent) is a multitargeted FLT3, PDGFRs, VEGFRs, and Kit kinase inhibitor with Ki of 0.009 and 0.008 μM for Flk-1 and PDGFR.
TSU-68	c11-L1200-01	310.34712	252916-29-3	10mM	VEGFR	PDGFR	FGFR	S1470	TSU-68 (SU6668)is a novel multiple receptor tyrosine kinase inhibitor with IC50 of 2.1 μM, 8 nM and 1.2 μM for VEGF-R1, PDGF-Rβ and FGF-R1, respectively.
Vatalanib	d1-L1200-01	419.73478	212141-51-0	10mM	VEGFR	c-Kit	VEGFR	S1101	Vatalanib (PTK787/ZK 222584) is a novel VEGFR and c-Kit tyrosine kinases and angiogenesis inhibitor with IC50 of 0.037, 0.077, 0.27 and 0.73 μM for KDR, Flt-1, Flk and c-Kit, respectively.
XL880(GSK1363089)	d2-L1200-01	632.6537664	849217-64-7	10mM	c-Met	VEGFR	S1111	Foretinib(GSK1363089, XL880) is a novel MET and VEGFR2/KDR kinases inhibitor with an IC50 of 0.4 and 0.8 nM for MET and KDR, respectively.
PHA-739358(Danusertib)	d3-L1200-01	474.5548	827318-97-8	10mM	Aurora	Bcr-Abl	S1107	PHA-739358(Danusertib) is a pyrrolo-pyrazole and small molecule Aurora kinases and Bcr-Abl kinase inhibitor with IC50 of 13, 79, and 61 nM for Aurora A, B, and C, respectively.
AT9283	d4-L1200-01	381.43162	896466-04-9	10mM	Aurora	JAK	Bcr-Abl	S1134	AT9283 is a small molecule a multi-targeted c-ABL, JAK2, Aurora A and B inhibitor with of 4, 1.2, 1.1 and approximate 3 nM for Bcr-Abl(T3151), Jak2 and Jak3, aurora A and B, respectively.

Appendix 1A: Continued.

AZD0530(Saracatinib)	d5-L1200-01	542.02648	379231-04-6	10mM	Src	Abl	S1006	Saracatinib (AZD0530) is a highly selective, orally available, dual-specific Src/Abl kinase inhibitor with IC50 of 2.7 and 30 nM for c-Src and Abl kinase, respectively.
Bosutinib(SKI-606)	d6-L1200-01	530.44616	380843-75-4	10mM	Src		S1014	Bosutinib (SKI-606) is a Src family kinase inhibitor. It inhibited migration of breast cancer cell lines with IC50 values of 0.1 to 0.3 umol/L.
Dasatinib	d7-L1200-01	488.00554	302962-49-8	10mM	SRC	Abl	S1021	Dasatinib also known as BMS-354825, Sprycel, BMS354825 is ATP-competitive, dual SRC/ABL inhibitor. BMS-354825 inhibits all members of the Src family, including c-Src, Lck, Fyn, and Yes (IC50 < 1.1nmol/L).
Nilotinib	d8-L1200-01	529.5157896	641571-10-0	10mM	Bcr-Abl		S1033	Nilotinib (AMN-107) is inhibitor of BCR-ABL with IC50 < 30nM.
Quercetin(Sophoretin)	d9-L1200-01	302.2357	117-39-5	10mM	PI3K	PKC	S2391	Quercetin is a PI3K and PKC inhibitor with IC50 of 3.8 μM and 15μg/ml.
NVP-ADW742	d10-L1200-01	453.57864	475488-23-4	10mM	IGF-1R		S1088	NVP-ADW742 is an IGF-1R inhibitor with an IC50 of 0.1 to 0.2 μM.
AC-220	d11-L1200-01	560.66718	950769-58-1	10mM	FLT-3		S1526	AC220 is a uniquely potent and selective FLT3 inhibitor with IC50 of 0.56 ± 0.3 nM and >10 mM for MC4-11 and A375, respectively.
AP24534	e1-L1200-01	532.5594896	943319-70-8	10mM	VEGFR	FGFR	PDGFR	S1490	AP24534 is a novel potent, orally available small molecule multitargeted kinase inhibitor with IC50 of 0.37, 2, 1.5, 2.2, 1.1, 1and 0.24 nM for native pan-BCR-ABL, mutated form, VEGFR2, FGFR1, PDGFRα, mutant FLT3 phosphorylation and LYN.
Tandutinib (MLN518)	e2-L1200-01	562.70298	387867-13-2	10mM	FLT-3	PDGFR	KIT	S1043	Tandutinib (MLN518) is a FLT3 inhibitor. In cell-based assays tandutinib inhibited FLT3 ,PDGFR, and KIT with IC50 values of 95-122 ng/mL.
KW 2449	e3-L1200-01	332.399	1000669-72-6	10mM	FLT-3	ABL	Aurora	S2158	KW-2449 is a multi-kinase inhibitor of FLT3(IC50 at 6.6pM), ABL(IC50 at 14pM), ABL-T315I and Aurora kinase.
CI-1033(Canertinib)	e4-L1200-01	485.9384032	267243-28-7	10mM	HER2	EGFR	S1019	CI-1033 (Canertinib) is an orally bioavailable irreversible Pan-erbB tyrosine kinase inhibitor, targeting EGFR with IC50 of 0.8, 19 and 7 nM for EGFR, HER-2 and ErbB-4, respectively.
CP-724714	e5-L1200-01	469.53498	537705-08-1	10mM	HER2		S1167	HER-2 tyrosine kinase inhibitor, IC50 of 15 ng/ml
BAY 73-4506(Regorafenib)	e6-L1200-01	482.8154128	755037-03-7	10mM	c-KIT	VEGFR	B-Raf	S1178	BAY 73-4506(Regorafenib) is a multikinase inhibitor with IC50 of 17, 40 and 69 nM c-KIT, VEGFR2, B-Raf.
JNJ-38877605	e7-L1200-01	377.3502264	943540-75-8	10mM	c-Met		S1114	JNJ-38877605 is a c-MET inhibitor with an IC50 of 4 nM.
PF-04217903	e8-L1200-01	372.38334	956905-27-4	10mM	c-Met		S1094	PF-04217903 is an orally bioavailabe, small-molecule MET tyrosine kinase inhibitor with an IC50 from 3.1 nM to142 nM.
PF-2341066	e9-L1200-01	450.3366832	877399-52-5	10mM	c-Met	ALK	S1068	Inhibitor of the c-Met kinase and the NPM-ALK. PF-2341066 inhibited cell proliferation in ALK-positive ALCL cells (IC50s=30 nM).
SGX-523	e11-L1200-01	359.40772	1022150-57-7	10mM	c-Met		S1112	SGX-523 is an exquisitely selective, ATP-competitive MET receptor tyrosine kinase inhibitor with an IC50 of 4 nM for the inhibition of HGFR.

Appendix 1A: Continued.

SU11274(PKI-SU11274)	f1-L1200-01	568.0869	658084-23-2	10mM	c-Met	S1080	SU11274 is a c-Met inhibitor (IC50 at 0.012μM).
NVP-TAE684	f2-L1200-01	614.2017	761439-42-3	10mM	ALK	S1108	ALK inhibitor with an IC50 between 2 and 10 nM.
SB 525334	f3-L1200-01	343.42494	356559-20-1	10mM	ALK	TGF-β	S1476	SB525334 is a selective inhibitor of transforming growth factor-β receptor I (ALK5, TGF-βRI) (IC50 = 14.3 nM).
R406	f4-L1200-01	628.6286632	841290-81-1	10mM	Syk	S2194	R406 is an orally available spleen tyrosine kinase inhibitor with an IC50 of 41 nM.
R406(free base)	f5-L1200-01	470.4536232	841290-80-0	10mM	Syk	S1533	R406(free base) is an orally available spleen tyrosine kinase inhibitor with a Ki of 30 nM.
XL184	f6-L1200-01	501.5056632	849217-68-1	10mM	c-Met	FLT-3	Tie2	S1119	XL184 (Cabozantinib, BMS-907351) is a potent multitargeted VEGFR2, Met, FLT3, Tie2, Kit and Ret inhibitor with IC50 of 0.035, 1.8, 14.4, 14.3 and 4.6 nM for VEGFR2, Met, FLT3, Tie2 and Kit, respectively.
BI 2536	f7-L1200-01	521.65436	755038-02-9	10mM	PLK	S1109	BI 2536 is a small molecule Plk1 inhibitor with an IC50 of 0.83 nM.
GSK461364	f8-L1200-01	543.6037296	929095-18-1	10mM	PLK	S2193	GSK 461364 is a potent small molecule Polo-like kinase 1 (PLK1) inhibitor with a Ki of 2.2 nM.
HMN-214	f9-L1200-01	424.4696	173529-46-9	10mM	PLK	S1485	HMN-214(a prodrug of HMN-176) is a potent PLK1 inhibitor (an average cell IC50 of 118nM).
ON-01910	f10-L1200-01	473.47193	1225497-78-8	10mM	PLK	S1362	ON-01910 is a non-ATP-competitive small molecule Plk1inhibitor with an IC50 of 9 nM.
AT7519	f11-L1200-01	382.24448	844442-38-2	10mM	CDK	S1524	AT7519 is a kinase inhibitor with IC50 of 0.19, 0.044, 0.51, 0.067, 0.66 and 0.018 μM for CDK1/cyclinB, CDK2/CyclinA, CDK2/Cyclin E, CDk4/CyclinD1, CDK6/Cyclin D3, CDk5/p35.
Flavopiridol(Alvocidib)	g1-L1200-01	401.8402	146426-40-6	10mM	CDK	S1230	A pan-cdk inhibitor. Flavopiridol is a potent inhibitor of CDKs 1, 2 and 4 in cell-free assays (IC50 in the region of 100 nM) and tumour cell growth in vitro (typical IC50 in the region of 100 nM). Flavopiridol inhibited rhabdoid cell growth (IC50 of 200nmol/L).
BS-181 hydrochloride	g2-L1200-01	416.99062	N/A	10mM	CDK	S1572	BS-181 is a selective cyclin-dependent kinase inhibitor with an IC50 of 21 nM for the inhibition of CDK-activating kinase.
PD0332991	g3-L1200-01	447.53276	571190-30-2	10mM	CDK	S1116	PD 0332991 is a CDK inhibitor with IC50 of 0.011 μM for Cdk4 and IC50 of 0.016 μM for Cdk6.
PHA-793887	g4-L1200-01	361.48174	718630-59-2	10mM	CDK	S1487	PHA-793887 is a novel pan-cdk inhibitor, including cdk1, cdk2, cdk4, cdk5, cdk7, and cdk9 with IC50 in the 5 to 140 nM range.
Roscovitine(CYC202)	g5-L1200-01	354.44934	186692-46-6	10mM	CDK	S1153	Roscovitine also known as CYC202 & Seliciclib. Roscovitine with purity >99% & solubility DMSO is available.
SNS-032(BMS-387032)	g6-L1200-01	380.52806	345627-80-7	10mM	CDK	S1145	SNS-032(BMS-387032) is a potent and selective cyclin-dependent kinases (CDK) 9, 7 and 2 inhibitor with IC50 of 4, 62 and 38 nM for CDK9, CDK2/cyclin A and CDK7/Cyclin H.

Appendix 1A: Continued.

AZD7762	g7-L1200-01	362.4217632	860352-01-8	10mM	CHK	S1532	AZD7762 is a novel checkpoint kinase inhibitor with an IC50 of 5 and <10 nM for CHK1 and CHK2, respectively.
Aurora A Inhibitor I	g8-L1200-01	588.0749432	1158838-45-9	10mM	Aurora	S1451	Aurora A Inhibitor I is a selective Aurora A inhibitor (Aurora A: IC50 at 0.0034 μM; Aurora B: IC50 at 3.4 μM), (B / A ratio=1000).
AZD1152-HQPA(Barasertib)	g9-L1200-01	507.5599032	722544-51-6	10mM	Aurora	S1147	AZD1152-HQPA is a highly potent and selective inhibitor of Aurora B (Ki, 0.36 nM)
CCT129202	g10-L1200-01	497.0156	942947-93-5	10mM	Aurora	S1519	CCT129202 is a Aurora kinase inhibitor with IC50 of 0.042 ± 0.022, 0.198 ± 0.05, and 0.227 ± 0.064 μmol/L for Aurora A, Aurora B, and Aurora C, respectively.
ENMD-2076	g11-L1200-01	525.55694	934353-76-1	10mM	Aurora I Flt-3 I Src I	S1181	ENMD-2076 (ENMD-981693, ENMD2076) is a antiangiogenic and Aurora kinase inhibitor with IC50 of 3, 13, 350, 23, 40, 93 and 120 nM for Flt-3, AurA, AurB, Src, KDR/VEGFR2 and FGFR1.
Hesperadin	h1-L1200-01	516.65438	422513-13-1	10mM	Aurora	S1529	Hesperadin is a human Aurora B inhibitor with an IC50 of 40 nM for the prevention of the phosphorylation of substrate.
MLN8237	h2-L1200-01	518.9235032	1028486-01-2	10mM	Aurora	S1133	MLN8237 (MLN-8237) is a selective Aurora kinase A inhibitor with a median IC50 of 61 nM.
PHA-680632	h4-L1200-01	501.6232	398493-79-3	10mM	Aurora	S1454	PHA-680632 is the first representative of a new class of Aurora inhibitors (Aurora A/B/C IC50 at 27,135 and 120 nM, respectively).
SNS-314 Mesylate	h5-L1200-01	527.03996	1057249-41-8	10mM	Aurora	S1154	Inhibitor of Aurora kinases A(IC50=9.0nM),B(IC50=31nM),and C(IC50=3.4nM)
VX-680	h6-L1200-01	464.58642	639089-54-6	10mM	Aurora	S1048	VX-680 (MK-0457) is an inhibitor of Aurora-A,-B,-C kinases with apparent inhibition constant values of 0.6,18,4.6 nM respectively. Order VX-680 (MK-0457) from supplier Selleck for research use only.
ZM-447439	h7-L1200-01	513.58754	331771-20-1	10mM	Aurora	S1103	ZM-447439 is a poten, selective ATP-competitive Aurora B kinase inhibitor with an IC50 of 50 nM, 1 μM and 250 nM for Aurora B, A and C, respectively.
AS703026	h8-L1200-01	431.2007732	1236699-92-5	10mM	MEK	S1475	AS703026 is a novel, selective, orally bioavailable MEK1/2 inhibitor (cell IC50 ranging from 0.005 to 2 μM).
AZD6244(Selumetinib)	h9-L1200-01	457.6814032	606143-52-6	10mM	MEK	S1008	AZD6244 (Selumetinib) is MEK 1/2 inhibitor with GI50 values ranging from 14 to 50 nm.
AZD8330	h10-L1200-01	461.2267532	869357-68-6	10mM	MEK	S2134	AZD8330 (RRY-424704，ARRY-704) is an orally active, selective MEK inhibitor with an IC50 of 7 nM.
BIX 02188	h11-L1200-01	426.51024	1094614-84-2	10mM	MEK	S1530	BIX02188 is a MEK5-selective inhibitor with an IC50 of 0.8 ± 1.0 μM.
BIX 02189	a1-L1200-02	440.53682	1094614-85-3	10mM	MEK	S1531	BIX 02189 is a selective MEK5/ERK5 inhibitor with an IC50 of 59 nM.
BMS 777607	a2-L1200-02	512.8925664	1196681-44-3	10mM	c-Met	S1561	BMS 777607 is a Small-Molecule Met Kinase Inhibitor with an IC50 of < 0.1 μM.

Appendix 1A: Continued.

CI-1040 (PD184352)	a3-L1200-02	478.6595364	212631-79-3	10mM	MEK	S1020	CI-1040 is a MEK 1/2 inhibitor with a Ki of 300nM
PD318088	a4-L1200-02	561.0890996	391210-00-7	10mM	MEK	S1568	PD318088 is a non-ATP competitive allosteric MEK1/2 inhibitor.
PD0325901	a5-L1200-02	482.1930396	391210-10-9	10mM	MEK	S1036	PD0325901 is MEK inhibitor and non-competitive with ATP, Kiapp of 1 nM against activated MEK1 and MEK2.
PD98059	a6-L1200-02	267.27932	167869-21-8	10mM	MEK	S1177	PD 98059 is an inhibitor of MEK1 and MEK2 with IC50 values of 4 μM and 50 μM.
U0126-EtOH	a7-L1200-02	426.55828	1173097-76-1	10mM	MEK	S1102	Inhibitor of both MEK1 and MEK2 with an IC50 of 72 nM and 58 nM respectively.
LY2228820	a8-L1200-02	612.7369832	862507-23-1	10mM	p38 MAPK	S1494	LY2228820 is a novel and potent p38MAPK inhibitor (the IC50 for p38αMAPK and p38βMAPK were 7 nM and 3 nM, respectively).
BIRB 796	a9-L1200-02	527.65718	285983-48-4	10mM	p38 MAPK	S1574	BIRB796 Doramapimod a small molecule of p38 MAPK inhibitor with Kd of 0.1 nM is available at Selleck.
SB 202190	a10-L1200-02	331.3430632	152121-30-7	10mM	p38 MAPK	S1077	P38 MAP(mitogen activated protein) Kinase inhibitor.
SB 203580	a11-L1200-02	377.4346432	152121-47-6	10mM	p38 MAPK	S1076	SB 203580 is a potent inhibitor of LPS-induced cytokine synthesis in the human monocyte cell line THP-1 (IC50 = 50-100 nM).
Vinorelbine(Navelbine)	b1-L1200-02	778.93226	71486-22-1	10mM	p38 MAPK	S1527	Vinorelbine is the first 5′NOR semi-synthetic vinca alkaloid and an anti-mitotic chemotherapy drug. (IC50=0.8 M)
VX-702	b2-L1200-02	404.3177928	479543-46-9	10mM	p38 MAPK	S6005	VX-702 is a P38 MAPK inhibitor, IL-6, IL-1β and TNFα (IC50 = 59, 122 and 99 ng/ml, respectively)
VX-745	b3-L1200-02	436.2620664	209410-46-8	10mM	p38 MAPK	S1458	VX-745 is a lead anti-inflammatory candidate, p38 MAPK inhibitor (IC50=10 nM) for the treatment of Rheumatoid arthritis (RA).
GDC-0879	b4-L1200-02	334.37182	905281-76-7	10mM	B-Raf	S1104	GDC-0879 is an B-Raf inhibitor(EC50 = 0.75 μM).
PLX-4720	b6-L1200-02	413.8261664	918505-84-7	10mM	B-Raf	S1152	B-raf inhibitor with IC50 of 160 nM.
RAF265	b7-L1200-02	518.4138592	927880-90-8	10mM	RAF & VEGFR	S2161	RAF265(CHIR-265) is an oral, highly selective RAF and VEGFR kinase inhibitor with IC50 of of 5 to 10 μM.
SP600125	b8-L1200-02	220.22612	129-56-6	10mM	JNK	S1460	SP600125 is a JNK inhibitor with IC50=40 nM for JNK-1 and JNK-2 and 90 nM for JNK-3.
AS-605240	b10-L1200-02	257.27	648450-29-7	10mM	PI3K	S1410	AS-605240 is a novel, potent, and selective PI3Kγ inhibitor with IC50 of 8 nM.

Appendix 1A: Continued.

GDC-0941	b11-L1200-02	513.63558	957054-30-7	10mM	PI3K	S1065	Inhibitor of Class I PI3 Kinase,p110a IC50=0.003uM,U87MG IC50=0.95μM.
IC-87114 (PIK-293)	c1-L1200-02	397.43256	371242-69-2	10mM	PI3K	S1268	IC-87114 was the first isoform-selective PI3K inhibitor : p110δ(IC50 = 0.13 μM) vs. p110α(IC50 = 200 μM), p110β(IC50 = 16 μM) and p110γ(IC50 = 61 μM).
LY294002	c2-L1200-02	307.34318	154447-36-6	10mM	PI3K | casein kinase II	S1105	PI3k inhibitor (cell IC50 about 10 μM) and a casein kinase II inhibitor.
PIK-293	c3-L1200-02	397.43256	900185-01-5	10mM	PI3K	S2207	PIK-293 is a PI3-K inhibitor.PIK-293 inhibit the p110α, p110β, p110δ, and p110γ with IC50 of 100uM,25uM,0.24uM,and 10uM.
PIK-90	c4-L1200-02	351.35928	677338-12-4	10mM	PI3K	S1187	PI3K inhibitor,IC50=11 , 350, 18, and 58 for p110 α, β, γ and δ isoforms.
PIK-93	c5-L1200-02	389.87754	593960-11-3	10mM	PI3K	S1489	PIK-93 is a PI4KIIIβinhibitor (IC50 at 19 nM).
TG100-115	c6-L1200-02	346.34276	677297-51-7	10mM	PI3K	S1352	TG100–115 is a PI3K γ and -δ inhibitor (IC50 = 83 and 235 nM, respectively)
TGX-221	c7-L1200-02	364.44086	663619-89-4	10mM	PI3K	S1169	TGX-221 is a low-nanomolar range PI3Kβ inhibitor (IC50=10nM), shows about 1000-fold higher selectivity over PI3Kα, and is cell permeable.
XL147	c8-L1200-02	448.52074	956958-53-5	10mM	PI3K	S1118	XL147 is a selective inhibitor of Class I PI3K isoforms.
XL765	c9-L1200-02	599.65686	1123889-87-1	10mM	PI3K	S1523	XL765(SAR245409) is a mixed mTOR/PI3k inhibitor with IC50 of 157, 39, 113, 9 and 43 nM for mTOR, p110α, β, γ and δ, respectively.
ZSTK474	c10-L1200-02	417.4125464	475110-96-4	10mM	PI3K	S1072	ZSTK474 is an inhibitor of PI3K γ(IC50 at 6 nM).
AZD8055	c11-L1200-02	465.54474	1009298-09-2	10mM	mTOR	S1555	AZD8055 is a potent, selective, and orally bioavailable ATP-competitive mTOR kinase inhibitor with an IC50 of 0.8 nM.
Deforolimus(MK-8669)	d1-L1200-02	990.206121	572924-54-0	10mM	mTOR	S1022	Deforolimus (Ridaforolimus) is a small-molecule inhibitor of mTOR.
Everolimus(RAD001)	d2-L1200-02	958.22442	159351-69-6	10mM	mTOR	S1120	Everolimus (RAD001) also known as SDZ-RAD, Certican, Zortress, Afinitorm is TOR inhibitor available at Selleck with IC50 of 0.63 nM.
KU-0063794	d3-L1200-02	465.54474	938440-64-3	10mM	mTOR	S1226	mTOR inhibitor, IC50 ~10 nM for mTORC1 and mTORC2, respectively.
Rapamycin(Sirolimus)	d4-L1200-02	914.17186	53123-88-9	10mM	mTOR	S1039	Rapamycin also known as Sirolimus & Rapamune is a mTOR inhibitor. Rapamycin Sirolimus inhibits cell motility by suppression of mTOR-mediated pathways.
Temsirolimus	d5-L1200-02	1030.28708	162635-04-3	10mM	mTOR	S1044	Temsirolimus (Torisel) is a mTOR inhibitor.

Appendix 1A: Continued.

WYE-354	d6-L1200-02	495.53096	1062169-56-5	10mM	mTOR	S1266	WYE-354 is a mTOR inhibitor with an IC50 of 5 nM.
PIK-75 Hydrochloride	d8-L1200-02	488.7434	372196-77-5	10mM	PI3K	S1205	PIK-75 Hydrochloride is a hydrochloride salt form of PIK-75, which is a preferential p110α/γ forms of PI3K inhibitor with IC50 of 6, 1300, 76, 510 nM for p110α, p110β, p110γ, p110δ, respectively.
CHIR-99021	d9-L1200-02	465.33792	252917-06-9	10mM	GSK-3	S1263	CHIR-99021 (CT99021) is a GSK-3 inhibitor, IC50= 7 nM.
Indirubin	d10-L1200-02	262.2628	479-41-4	10mM	GSK-3	S2386	Indirubin is a potent cyclin-dependent kinases and GSK-3β inhibitor with IC50 of about 75 nM and 0.19 μM.
SB 216763	d11-L1200-02	371.21678	280744-09-4	10mM	GSK-3	S1075	SB 216763 inhibited human GSK-3α with IC50s of 34 nM.
KU-55933	e1-L1200-02	395.49458	587871-26-9	10mM	ATM	S1092	ATM inhibitor with an IC50 of 13 nM and a Ki of 2.2 nM.
KU-60019	e2-L1200-02	547.66512	925701-49-1	10mM	ATM	S1570	KU-60019 is a specific improved ATM kinase inhibitor.
MK-2206	e3-L1200-02	480.38902	1032350-13-2	10mM	Akt	S1078	MK2206 an Akt inhibitor with IC50 at 8 nm, 2 mM, 65 mM for Akt1, Akt2 and Akt3, respectively is available on Selleck.
AT7867	e5-L1200-02	337.8459	857531-00-1	10mM	Akt | S6 kinase	S1558	AT7867 is a potent and oral AKT and p70 S6 kinase inhibitor with an IC50 of 17 nM.
AZD1480	e7-L1200-02	348.7659632	935666-88-9	10mM	JAK	S2162	AZD1480 is a novel potent small JAK2 inhibitor with an IC50 of 0.26 nM.
LY2784544	e9-L1200-02	469.9423032	1229236-86-5	10mM	JAK	S2179	LY2784544 is a small molecule selective mutant JAK2 kinase inhibitor with an IC50 of 68 nM.
Enzastaurin	e11-L1200-02	515.60496	170364-57-5	10mM	PKC	S1055	Enzastaurin (LY317615) is a potent PKC beta inhibitor with an IC50 of 6 nM.
SB 431542	f3-L1200-02	384.38744	301836-41-9	10mM	ALK	S1067	SB-431542 is an inhibitor of activin receptor-like kinase (ALK)5 (the TGF-βtype I receptor) (IC50 = 94 nM).
ABT-869(Linifanib)	f4-L1200-02	375.3989232	796967-16-3	10mM	RTK | VEGFR | PDGFR	S1003	Linifanib (ABT-869) is a structurally novel, potent RTK and VEGF and PDGF receptor families inhibitor to human endothelial cells, PDGFR-β, KDR, and CSF-1R, with IC50 of 0.2, 2, 4, and 7 nM, respectively.
AEE788	f5-L1200-02	440.58318	497839-62-0	10mM	EGFR | HER1/2 | VEGFR |	S1486	AEE788 is a novel multitargeted human epidermal receptor (HER) 1/2 and vascular endothelial growth factor receptor (VEGFR) 1/2 receptor family tyrosine kinases inhibitor with IC50 of 2, 6, 77, 59 nM for EGFR, ErbB2, KDR, and Flt-1.
BIBW2992(Tovok)	f6-L1200-02	485.9384032	439081-18-2	10mM	EGFR | HER2	S1011	Inhibitor of VEGFR, PDGFR and FGFR. all three VEGFR subtypes (IC50=13–34nmol/L) , PDGFRa and PDGFRh (IC50=59and65nmol/L) , and FGFRtypes 1, 2, and 3 (IC50=69, 37, and 108 nmol/L,respectively).
Lapatinib Ditosylate	f7-L1200-02	925.4607832	388082-77-7	10mM	EGFR | HER2	S1028	EGFR and HER2 autophosphorylation inhibitor, against purified EGFR and HER2 of 10.2 and 9.8 nM, respectively.

Appendix 1A: Continued.

JNJ-7706621	f8-L1200-02	394.3559864	443797-96-4	10mM	Aurora / CDK	S1249	JNJ-7706621 is a dual cyclin-dependent kinases and aurora kinases inhibitor with IC50 of 9 and 11 nM for CDK1/Cyclin B and aurora-A, respectively.
BEZ235	f10-L1200-02	469.53652	915019-65-7	10mM	PI3K / mTOR	S1009	BEZ235 (NVP-BEZ235) is a dual ATP-competitive phosphatidylinositol 3-kinase (PI3K) and mammalian target of rapamycin (mTOR) inhibitor with an IC50 of 4, 5, 7 and 75 nM for p110α, p110γ, p110δ and p110β, respectively.
GSK1059615	f11-L1200-02	333.36384	958852-01-1	10mM	PI3K / mTOR	S1360	GSK1059615 is a pan-PI3K reversible inhibitor,IC50:PI3Kα(0.4 nM), β (0.6 nM),γ (5 nM),δ (2 nM) and mTOR(12 nM).
PI-103	g1-L1200-02	348.35534	371935-74-9	10mM	PI3K / mTOR	S1038	MEK inhibitor and non-competitive with ATP, Kiapp of 1 nM against activated MEK1 and MEK2.
AG-490	g2-L1200-02	294.30466	133550-30-8	10mM	EGFR / JAK	S1143	AG 490 is a potent epidermal growth factor receptor kinase autophosphorylation inhibitor with an IC50 of 100 nM and 56.8 μM for EGFR and JAK, respectively.
CP-690550(Tofacitinib)	g3-L1200-02	312.3696	540737-29-9	10mM	JAK	S5001	Tofacitinib (CP-690550) is a novel, small molecule potent and selective JAK-3 kinase inhibitor with an IC50 of 1 nM for inhibition of the JAK-3 activities.
Crenolanib (CP-868569)	g4-L1200-02	443.54076	670220-88-9	10mM	PDGFR	S2730	Crenolanib (CP-868569) is a highly selective and potent PDGFR-α inhibitor with IC50 of 0.9 and 1.8 nM against PDGFRα and PDGFRβ, respectively.
GSK1838705A	g5-L1200-02	532.5693632	1116235-97-2	10mM	IGF-1R	S2703	GSK1838705A is a potent small-molecule IGF-IR, the insulin receptor and anaplastic lymphoma kinase (ALK) inhibitor with IC50 of 2.0, 1.6 and 0.5 nM, respectively.
KX2-391	g6-L1200-02	431.52676	897016-82-9	10mM	SRC	S2700	KX2-391 is a synthetic, orally bioavailable small molecule and non-ATP competitive Src tyrosine kinase signaling inhibitor with an IC50 of average 72 nM.
NVP-BSK805	g7-L1200-02	563.4695064	1092499-93-8	10mM	JAK	S2686	NVP-BSK805 is a potent and selective quinoxaline JAK2 inhibitor with IC50 of 0.48, 0.56 and 0.58 nM for JAK2 JH1, FL JAK V617F and FL JAK2 wt, respectively.
PCI-32765	g8-L1200-02	440.49706	936563-96-1	10mM	SRC	S2680	PCI-32765 is a high potent irreversible BTK inhibitor with an IC50 of 0.46 nM for the purified Btk.
PF-562271	g9-L1200-02	507.4888096	717907-75-0	10mM	FAK	S2672	PF-562271 is a potent ATP-competitive FAK and proline-rich tyrosine kinase (Pyk2) inhibitor with potential antineoplastic and antiangiogenic activities.
DCC-2036	g10-L1200-02	553.5868232	1020172-07-9	10mM	Src-bcr-Abl	S2634	DCC-2036 is an ABL switch control inhibitor with IC50 of 0.8 and 2 nM for u-ABL1native and p-ABL1native, respectively.
LDN193189	g11-L1200-02	406.48238	1062368-24-4	10mM	BMP	S2618	LDN193189 is a highly potent small molecule BMP inhibitor with IC50 of 5 and 30 nM for ALK2 and ALK3, respectively.
AZD8931	a1-L1200-03	473.9277032	848942-61-0	10mM	EGFRl, HER2	S2192	AZD8931 is a novel potent reversible small molecule epidermal growth factor receptor, ERBB2 (HER2) and ERBB3 inhibitor with an IC50 of 4, 3, 4 nM, respectively.
Raf265 derivative	a2-L1200-03	504.3872792	N/A	10mM	Syk	S2200	Raf265 derivative is a derivative of Raf265 that is an oral, highly selective RAF and VEGFR kinase inhibitor with IC50 of of 5 to 10 μM.
NVP-BHG712	a3-L1200-03	503.4785096	940310-85-0	10mM	VEGFR, SRCl, c-Abll, B-	S2202	NVP-BHG712 is a small molecule specific EphB4, VEGFR2, c-raf, c-src and c-Abl kinase inhibitor with ED50 of 25 nM, 4.2, 0.4, 1.3 and 1.7μM, respectively.

Appendix 1A: Continued.

OSI-420	a4-L1200-03	415.87008	183320-51-6	10mM	EGFR	S2205	OSI-420 (Desmethyl Erlotinib,CP-473420) is an active metabolite of erlotinib which is an orally active EGFR tyrosin kinase inhibitor with IC50 of 2 and 20 nM for the inhibition of human EGFR and EGFR autophosphorylation in tumor cells.
R935788	a5-L1200-03	624.4231642	1025687-58-4	10mM	Syk	S2206	R935788 (Fostamatinib disodium) is a selective Syk inhibitor with an IC50 of 41 nM.
AZ 960	a6-L1200-03	354.3566464	905586-69-8	10mM	JAK, Aurora Kinase	S2214	AZ 960 is a novel small molecule JAK2 kinase inhibitor with an IC50 and Ki of 3 mM and 0.45 nM in vitro, respectively.
Mubritinib	a7-L1200-03	468.4709296	366017-09-6	10mM	EGFR, CDK	S2216	Mubritinib(TAK 165) is a potent EGFR and p34cdc2 inhibitor with IC50 of 6 nM and 0.2 μM, respectively.
PP242	a8-L1200-03	308.33784	1092351-67-1	10mM	mTOR	S2218	PP242 is a novel potent and selective mTOR inhibitor with an IC50 of 8 nM.
Cyt387	a9-L1200-03	414.45978	1056634-68-4	10mM	JAK	S2219	Cyt387 is an ATP-competitive small molecule JAK1/JAK2 inhibitor with IC50 of 11 and 18 nM for JAK1 and JAK2, respectively.
Apatinib	a10-L1200-03	493.57798	811803-05-1	10mM	EGFR	S2221	Apatinib (YN968D1) is a small-molecule selective multitargeted tyrosine kinase inhibitor with an IC50 of 2.43 nM for the inhibition of VEGFR2.
CAL-101	a11-L1200-03	415.4230232	870281-82-6	10mM	PI3K	S2226	CAL-101 is a potent PI3K p110δ inhibitor with an IC50 of 65 nM.
PIK-294	b1-L1200-03	489.52792	900185-02-6	10mM	PI3K	S2227	PIK-294 is a highly selective p110 inhibitor with an IC50 of 3 nM.
VX-765	b2-L1200-03	508.99502	273404-37-8	10mM	Caspase	S2228	VX-765 is a novel and irreversible IL-converting enzyme/caspase-1 inhibitor with an IC50 of 0.8 nM
Telatinib	b3-L1200-03	409.82574	332012-40-5	10mM	VEGFR|,PDGFR|,c-Kit	S2231	Telatinib (BAY 57-9352) is an orally available, potent multitargeted VEGFR-2, VEGFR-3, PDGFR-β and c-Kit tyrosine kinases inhibitor with an IC50 of 19 nM for the inhibition of VEGFR-2 autophosphorylation.
BI6727	b4-L1200-03	618.8126	755038-65-4	10mM	PLK	S2235	BI 6727 is a highly potent Polo-like kinase inhibitor with an IC50 of 0 .87 nM.
WP1130	b5-L1200-03	384.26972	856243-80-6	10mM	DUB	S2243	WP1130 is a novel selective small molecular deubiquitinase (DUB) inhibitor and a Bcr/Abl destruction pathway activator with an IC50 of 1.8 μM for K562 cells.
BKM-120	b6-L1200-03	410.3935496	1202777-78-3	10mM	PI3K	S2247	BKM120 (NVP-BKM120) is a bioavailable specific oral pan-class I phosphatidylinositol 3-kinase (PI3K) kinase inhibitor.
CX-4945	b7-L1200-03	349.77048	1009820-21-6	10mM	PKC	S2248	CX-4945 (CX 4945) is a potent and selective ATP-competitive small molecule protein kinase CK2 inhibitor with a Ki and an IC50 of 0.38 and 1 nM for recombinant human CK2α, respectively.
Phenformin hydrochloride	b8-L1200-03	241.72054	834-28-6	10mM	NULL	S2542	Phenformin hydrochloride is a hydrochloride salt of phenformin that is an anti-diabetic drug from the biguanide class.
TAK-733	b9-L1200-03	504.2266764	1035555-63-5	10mM	MEK	S2617	TAK-733 is highly potent and selective novel MEK allosteric site inhibitor with an IC50 of 3.2 nM.

Appendix 1A: Continued.

AZD5438	b10-L1200-03	371.45664	602306-29-6	10mM	CDK	S2621	AZD5438 is a potent cyclin-dependent kinase (cdk) 1, 2 and 9 inhibitor with IC50 of 16, 6 and 20 nM, respectively.
PP121	b11-L1200-03	319.36378	1092788-83-4	10mM	DNA-PK, mTOR, PDGF	S2622	PP121 is a multitargeted dual receptor tyrosine kinases inhibitor with IC50 of 0.052, 1.4, 0.15, 1.1, 0.06, 0.01and 0.002 μM for p110α, p110β, p110δ, p110γ, DNA-PK, mTOR and PDGFR, respectively.
OSI027	c1-L1200-03	406.43778	936890-98-1	10mM	mTOR	S2624	OSI027 is a potent mammalian target of rapamycin (mTOR) kinase inhibitor.
LY2603618	c2-L1200-03	436.30298	911222-45-2	10mM	CHK	S2626	LY2603618 (IC-83) is a highly selective Chk 1 inhibitor with potential antitumor activity.
PKI587	c3-L1200-03	615.72584	1197160-78-3	10mM	mTOR, PI3K	S2628	PKI-587 is a highly potent dual PI3K/mTOR kinase inhibitor with IC50 of 0.4 nM and <0.1 μM for PI3K-α and mTOR, respectively.
CCT128930	c4-L1200-03	341.8379	885499-61-6	10mM	Akt	S2635	CCT128930 is a novel potent ATP-competitive, AKT inhibitor with an IC50 of 6 nM.
A66	c5-L1200-03	393.52682	1166227-08-2	10mM	PI3K	S2636	A66 is a highly specific and selective p110α inhibitor with IC50 of 32,30 and 43 nM for p110α, p110α/E545K, p110α/H1047R, respectively.
NU7441	c6-L1200-03	413.48826	503468-95-9	10mM	ATM / DNA-PK / mTOR / P	S2638	NU7441 is a potent and selective DNA-dependent protein kinase (DNA-PK) inhibitor with IC50 of 0.01, 1.7 and 5 μM for DNA-PK, mTOR and PI 3-K, respectively.
GSK2126458	c7-L1200-03	505.4959864	1086062-66-9	10mM	PI3K	S2658	GSK2126458 is a highly potent PI3K and mTOR inhibitor with an app Ki of 19 pM for PI3K.
WYE-125132	c8-L1200-03	519.59542	1144068-46-1	10mM	mTOR	S2661	WYE-125132 is a highly potent, ATP-competitive and specific mTOR kinase inhibitor with an IC50 of 0.19 nM.
WYE-687	c9-L1200-03	528.60548	1062161-90-3	10mM	mTOR	S2668	WYE-687 is a potent ATP-competitive mTOR inhibitor with an IC50 of 7 nM.
A-674563	c10-L1200-03	358.43628	552325-73-2	10mM	Akt	S2670	A-674563 is a potent selective protein kinase B/Akt inhibitor with an IC50 of 14 nM.
AS252424	c11-L1200-03	305.2810232	900515-16-4	10mM	PI3K	S2671	AS-252424 is a potent and selective PI3k γ inhibitor with IC50 of 33 and 935 nM for PI3Kγ and PI3Kα, respectively.
GSK1120212	d1-L1200-03	615.3947932	871700-17-3	10mM	MEK	S2673	GSK1120212 (JTP-74057) is a reversible, selective, allosteric MEK1/MEK2 kinase activity inhibitor with IC50 of 0.7 and 0.9 nM for MEK1 and MEK2.
Flavopiridol hydrochlori	d2-L1200-03	438.30114	131740-9-5	10mM	CDK	S2679	Flavopiridol hydrochloride is a pan-cdk inhibitor.
AS604850	d3-L1200-03	285.2235064	648449-76-7	10mM	PI3K	S2681	AS-604850 is a selective, ATP-competitive PI3Kγ inhibitor with IC50 of 0.25, >20, >20, and 4.5 μM for the human recombinant γ, δ, β, and α isoforms, respectively.
WAY-600	d4-L1200-03	494.5908	1062159-35-6	10mM	mTOR	S2689	WAY-600 is a potent ATP-competitive mTOR inhibitor with an IC50 of 9 nM.

Appendix 1A: Continued.

TG101209	d5-L1200-03	509.6668	936091-14-4	10mM	FLT-3 / JAK	S2692	TG101209 is a potent and small molecule JAK2-selective kinase inhibitor with IC50 of 6, 25, 17 and 169 nM for JAK2, FLT3, RET and JAK3, respectively.
GDC-0980	d6-L1200-03	498.6011	1032754-93-0	10mM	mTOR / PI3K	S2696	GDC-0980 (RG7422) is a selective, dual PI3 Kinase and mTOR Kinase inhibitor with IC50 of 5, 27, 7, and 14 nM for PI3Kα, β, δ, and γ, respectively.
A-769662	d7-L1200-03	360.38588	844499-71-4	10mM	AMPK	S2697	A-769662 is a potent, reversible AMP-activated protein kinase (AMPK) activator with an EC50 of 0.8 μM.
TAK-901	d8-L1200-03	504.64368	934541-31-8	10mM	Aurora	S2718	TAK-901 is a small-molecule inhibitor of the serine-threonine kinase Aurora B with potential antineoplastic activity.
AMG 900	d9-L1200-03	503.57764	945595-80-2	10mM	Aurora	S2719	AMG 900 is a novel potent and highly selective Pan-aurora kinase inhibitor with an IC50 of median 3.5 nM.
ZM 336372	d10-L1200-03	389.44702	208260-29-1	10mM	B-Raf	S2720	Zm 336372 is a potent, selective c-Raf inhibitor with an IC50 of 70 nM for inhibition of human c-Raf in vitro.
PH-797804	e1-L1200-03	477.2986664	586379-66-0	10mM	p38 MAPK	S2726	PH-797804 is a highly selective, potent, and ATP-competitive p38 MAP kinase inhibitor with an IC50 of 2.3 nM.
PF-04691502	e2-L1200-03	425.48	1013101-36-4	10mM	mTOR / PI3K	S2743	PF-04691502 is a potent and selective dual PI3K/mTOR inhibitor to phosphorylation of AKT T308 and AKT S473 with IC50 of 7.5 and 3.8 nM, respectively.

Appendix 1: B) Layout of kinase inhibitors in library plates.

Plate layout:L1200-01

	1	2	3	4	5	6	7	8	9	10	11	12
a	Empty	BMS-599626	Erlotinib Hydrochloride	Gefitinib(Iressa)	Neratinib	PD153035 hydrochloride	Pelitinib	Vandetanib	WZ3146	WZ4002	WZ8040	Empty
b	AV-951(Tivozanib)	Axitinib	BIBF1120(Vargatef)	BMS 794833	Empty	Cediranib(AZD2171)	Empty	CYC116	Empty	Imatinib(STI571)	Imatinib Mesylate	Empty
c	Ki8751	KRN 633	Masitinib(AB1010)	MGCD-265	Motesanib Diphosphate	MP-470 (Amuvatinib)	OSI-930	Pazopanib Hydrochloride	Sorafenib Tosylate	Sunitinib Malate	TSU-68	Empty
d	Vatalanib	XL880(GSK1363089)	PHA-739358(Danusertib)	AT9283	AZD0530(Saracatinib)	Bosutinib(SKI-606)	Dasatinib	Nilotinib	Quercetin(Sophoretin)	NVP-ADW742	AC-220	Empty
e	AP24534	Tandutinib (MLN518)	KW 2449	CI-1033(Canertinib)	CP-724714	BAY 73-4506(Regorafenib)	JNJ-38877605	PF-04217903	PF-2341066	Empty	SGX-523	Empty
f	SU11274(PKI-SU11274)	NVP-TAE684	SB 525334	R406	R406(free base)	XL184	BI 2536	GSK461364	HMN-214	ON-01910	AT7519	Empty
g	Flavopiridol(Alvocidib)	BS-181 hydrochloride	PD0332991	PHA-793887	Roscovitine(CYC202)	SNS-032(BMS-387032)	AZD7762	Aurora A Inhibitor I	AZD1152-HQPA(Barasertib)	CCT129202	ENMD-2076	Empty
h	Hesperadin	MLN8237	Empty	PHA-680632	SNS-314 Mesylate	VX-680	ZM-447439	AS703026	AZD6244(Selumetinib)	AZD8330	BIX 02188	Empty

Plate layout:L1200-02

	1	2	3	4	5	6	7	8	9	10	11	12
a	BIX 02189	BMS 777607	CI-1040 (PD184352)	PD318088	PD0325901	PD98059	U0126-EtOH	LY2228820	BIRB 796	SB 202190	SB 203580	Empty
b	Vinorelbine(Navelbine)	VX-702	VX-745	GDC-0879	Empty	PLX-4720	RAF265	SP600125	Empty	AS-605240	GDC-0941	Empty
c	IC-87114	LY294002	PIK-293	PIK-90	PIK-93	TG100-115	TGX-221	XL147	XL765	ZSTK474	AZD8055	Empty
d	Deforolimus(MK-8669)	Everolimus(RAD001)	KU-0063794	Rapamycin(Sirolimus)	Temsirolimus	WYE-354	Empty	PIK-75 Hydrochloride	CHIR-99021	Indirubin	SB 216763	Empty
e	KU-55933	KU-60019	MK-2206	Empty	AT7867	Empty	AZD1480	Empty	LY2784544	Empty	Enzastaurin	Empty
f	Empty	Empty	SB 431542	ABT-869(Linifanib)	AEE788	BIBW2992(Tovok)	Lapatinib Ditosylate	JNJ-7706621	Empty	BEZ235	GSK1059615	Empty
g	PI-103	AG-490	CP-690550(Tofacitinib)	Crenolanib (CP-868569)	GSK1838705A	KX2-391	NVP-BSK805	PCI-32765	PF-562271	DCC-2036	LDN193189	Empty

Plate layout:L1200-03

	1	2	3	4	5	6	7	8	9	10	11	12
a	AZD8931	Raf265 derivative	NVP-BHG712	OSI-420	R935788 (Fostamatinib)	AZ 960	Mubritinib (TAK 165)	PP242	Cyt387	Apatinib	CAL-101	Empty
b	PIK-294	VX-765	Telatinib (BAY 57-9352)	BI6727 (Volasertib)	WP1130	BKM120 (NVP-BKM120)	CX-4945	Phenformin hydrochloride	TAK-733	AZD5438	PP-121	Empty
c	OSI-027	LY2603618 (IC-83)	PKI-587	CCT128930	A66	NU7441	GSK2126458	WYE-125132	WYE-687	A-674563	AS-252424	Empty
d	GSK1120212 (JTP-74057)	Flavopiridol hydrochloride	AS-604850	WAY-600	TG101209	GDC-0980 (RG7422)	A-769662	TAK-901	AMG900	ZM336372	Empty	Empty
e	PH-797804	PF-04691502	Empty	Empty	Empty	Empty	Empty	Empty	Empty	Empty	Empty	Empty

Appendix 2: Phosphatase inhibitor library used in this study.

Structure	SMILES	IUPAC	Name	Molecular weight	Plate Location	Plate description	CAS	Catalog number	Concentration	Compound description	Solvent	Plate part number
	[H][C@]12CC[C@]([H])(O1)[C@](C)(C(O)=O)[C@]2(C)C(O)=O	(1R,2S,3R,4S)-2,3-dimethyl-7-oxabicyclo[2.2.1]heptane-2,3-dicarboxylic acid	Cantharidic acid	214.2	B-01	Phosphatase Inhibitor Library	28874-45-5	PR-106	10mM	PP1 and PP2A	DMSO	2834
	[H][C@]12CC[C@]([H])(O1)[C@]1(C)C(=O)OC(=O)[C@]21C	(1R,2S,6R,7S)-2,6-dimethyl-4,10-dioxatricyclo[5.2.1.0^{2,6}]decane-3,5-dione	Cantharidin	196.2	B-02	Phosphatase Inhibitor Library	56-25-7	PR-105	10mM	PP1 and PP2A	DMSO	2834
	[H][C@]12CC[C@]([H])(O1)C(C2C(O)=O)C(O)=O	(1R,4S)-7-oxabicyclo[2.2.1]heptane-2,3-dicarboxylic acid	Endothall	186.2	B-03	Phosphatase Inhibitor Library	145-73-3	PR-107	10mM	PP2A	DMSO	2834
	OP(O)(=O)CC1=CC=CC=C1	benzylphosphonic acid	Benzylphosphonic acid	172.1	B-04	Phosphatase Inhibitor Library	6881-57-8	EI-244	10mM	Tyrosine phosphatases	DMSO	2834
	OC(=O)C(O)=O.BrC1=CC=C(C=C1)[C@H]1CN2CCSC2=N1	(6S)-6-(4-bromophenyl)-2H,3H,5H,6H-imidazo[2,1-b][1,3]thiazole; oxalic acid	L-p-Bromotetramisole oxalate	373.2	B-05	Phosphatase Inhibitor Library	62284-79-1	T-100	10mM	Tyrosine phosphatases	DMSO	2834
	CCCCCCCCCCCCCCCC(=O)C1=C(O)C(CO)OC1=O	3-hexadecanoyl-4-hydroxy-5-(hydroxymethyl)-2,5-dihydrofuran-2-one	RK-682	368.5	B-06	Phosphatase Inhibitor Library	154639-24-4	PR-112	10mM	Tyrosine phosphatases	DMSO	2834
	OC(C1=CC(=CC=C1OC1=CC=C(Br)C=C1)[N+]([O-])=O)P(O)=O	{[2-(4-bromophenoxy)-5-nitrophenyl](hydroxy)methyl}phosphinic acid	RWJ-60475	388.1	B-07	Phosphatase Inhibitor Library	204130-08-5	PR-109	10mM	CD45 tyrosine phosphatase	DMSO	2834
	CC(=O)OCOC(C1=CC(=CC=C1OC1=CC=C(Br)C=C1)[N+]([O-])=O)P(=O)(OCOC(C)=O)OCOC(C)=O	({[(acetyloxy)methoxy]({[(acetyloxy)methoxy][2-(4-bromophenoxy)-5-nitrophenyl]methyl})phosphoryl}oxy)methyl acetate	RWJ-60475 (AM)3	620.3	B-08	Phosphatase Inhibitor Library	1069116-45-5	PR-110	10mM	CD45 tyrosine phosphatase (cell permeable)	DMSO	2834
	ClC1CN2C[C@@H](N=C2S1)C1=CC=CC=C1	(6S)-6-phenyl-2H,3H,5H,6H-imidazo[2,1-b][1,3]thiazole hydrochloride	Levamisole HCl	240.8	B-09	Phosphatase Inhibitor Library	16595-80-5	AC-1102	10mM	Mammalian alkaline phosphatase	DMSO	2834
	ClC1CN2CC(N=C2S1)C1=CC=CC=C1	6-phenyl-2H,3H,5H,6H-imidazo[2,1-b][1,3]thiazole hydrochloride	Tetramisole HCl	240.8	B-10	Phosphatase Inhibitor Library	5086-74-8	AC-1104	10mM	Mammalian alkaline phosphatase	DMSO	2834
	CC1(C)C(C=C(Cl)Cl)C1C(=O)OC(C#N)C1=CC=CC(OC2=CC=CC=C2)=C1	(3-phenoxyphenyl)(cyano)methyl 3-(2,2-dichloroethenyl)-2,2-dimethylcyclopropane-1-carboxylate	Cypermethrin	416.3	B-11	Phosphatase Inhibitor Library	52315-07-8	PR-100	10mM	Calcineurin (PP2B)	DMSO	2834
	CC1(C)[C@@H](C=C(Br)Br)[C@H]1C(=O)O[C@H](C#N)C1=CC(OC2=CC=CC=C2)=CC=C1	(S)-(3-phenoxyphenyl)(cyano)methyl (1R,3R)-3-(2,2-dibromoethenyl)-2,2-dimethylcyclopropane-1-carboxylate	Deltamethrin	505.2	B-12	Phosphatase Inhibitor Library	52918-63-5	PR-101	10mM	Calcineurin (PP2B)	DMSO	2834

Appendix 2: Continued.

	CC(C)C(C(=O)OC(C#N)C1=CC=CC(OC2=CC=CC=C2)=C1)C1=CC=C(Cl)C=C1	(3-phenoxyphenyl)(cyano)methyl 2-(4-chlorophenyl)-3-methylbutanoate	Fenvalerate	419.9	C-01	Phosphatase Inhibitor Library	51630-58-1	PR-102	10mM	Calcineurin (PP2B)	DMSO	2834
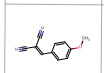	COC1=CC=C(C=C(C#N)C#N)C=C1	2-[(4-methoxyphenyl)methylidene]propanedinitrile	Tyrphostin 8	184.2	C-02	Phosphatase Inhibitor Library	2826-26-8	PR-113	10mM	Calcineurin (PP2B)	DMSO	2834
	CC(C)C[C@H](NC(=O)[C@H](CCC(O)=O)NC(=O)CNC(=O)C1=CC=C(C=C1)\C=C\C(O)=O)C(N)=O	(4S)-4-{[(1S)-1-carbamoyl-3-methylbutyl]carbamoyl}-4-[2-({4-[(1E)-2-carboxyeth-1-en-1-yl]phenyl}formamido)acetamido]butanoic acid	CinnGel	490.5	C-03	Phosphatase Inhibitor Library	172796-68-8	PR-114	10mM	PTP1B	DMSO	2834
	OCCSC1=C(SCCO)C(=O)C2=C(C=CC=C2)C1=O	2,3-bis[(2-hydroxyethyl)sulfanyl]-1,4-dihydronaphthalene-1,4-dione	NSC-95397	310.4	C-04	Phosphatase Inhibitor Library	93718-83-3	EI-309	10mM	Cdc25	DMSO	2834
	COC1=C(O)C(CN(C)CCC2=CC=C(C=C2)[N+]([O-])=O)=CC(=C1)N(C)C	4-(dimethylamino)-2-methoxy-6-({methyl[2-(4-nitrophenyl)ethyl]amino}methyl)phenol	BN-82002	359.4	C-05	Phosphatase Inhibitor Library	396073-89-5	PR-124	10mM		DMSO	2834
	CC(C)=CC[C@@H](O)C1=CC(=O)C2=C(O)C=CC(O)=C2C1=O	5,8-dihydroxy-2-[(1R)-1-hydroxy-4-methylpent-3-en-1-yl]-1,4-dihydronaphthalene-1,4-dione	Shikonin	288.3	C-06	Phosphatase Inhibitor Library	517-89-5	CT-115	10mM		DMSO	2834
	ClC1=C(NCCN2CCOCC2)C(=O)C2=C(C=CC=N2)C1=O	6-chloro-7-{[2-(morpholin-4-yl)ethyl]amino}-5,8-dihydroquinoline-5,8-dione	NSC-663284	321.8	C-07	Phosphatase Inhibitor Library	383907-43-5	PR-116	10mM	CDC25	DMSO	2834
	CC[C@@H]1NC(=O)[C@H]([C@H](O)[C@H](C)C\C=C\C)N(C)C(=O)[C@H](C(C)C)N(C)C(=O)[C@H](CC(C)C)N(C)C(=O)[C@H](CC(C)C)N(C)C(=O)[C@@H](C)NC(=O)[C@H](C)NC(=O)[C@H](CC(C)C)N(C)C(=O)[C@@H](NC(=O)[C@H](CC(C)C)N(C)C(=O)CN(C)C1=O)C(C)C	(3S,6S,9S,12R,15S,18S,21S,24S,30S,33S)-30-ethyl-33-[(1R,2R,4E)-1-hydroxy-2-methylhex-4-en-1-yl]-1,4,7,10,12,15,19,25,28-nonamethyl-6,9,18,24-tetrakis(2-methylpropyl)-3,21-bis(propan-2-yl)-1,4,7,10,13,16,19,22,25,28,31-undecaazacyclotritriacontan-2,5,8,11,14,17,20,23,26,29,32-undecone	Cyclosporin A	1202.6	C-08	Phosphatase Inhibitor Library	59865-13-3	A-105	10mM	Calcineurin (PP2B)	DMSO	2834
	NC(=N)C1=CC=C(OCCCCCCOC2=CC=C(C=C2)C(N)=N)C=C1	4-{[5-(4-carbamimidoylphenoxy)pentyl]oxy}benzene-1-carboximidamide	Pentamidine	340.4	C-09	Phosphatase Inhibitor Library	100-33-4	PR-118	10mM	PRL1	DMSO	2834
	CC1(C)C(=O)N=C2C1=C(O)C(=O)C1=C2C=CC=C1	4-hydroxy-3,3-dimethyl-2H,3H,5H-benzo[g]indole-2,5-dione	BVT-948	241.2	C-10	Phosphatase Inhibitor Library	39674-97-0	PR-125	10mM	Tyrosine phosphatases	DMSO	2834
	BrC1=CC=C(OCC2=C(Br)C=CC=C2)C(\C=C2/SC(=S)NC2=O)=C1	(5Z)-5-({5-bromo-2-[(2-bromophenyl)methoxy]phenyl}methylidene)-2-sulfanylidene-1,3-thiazolidin-4-one	B4-Rhodanine	485.2	C-11	Phosphatase Inhibitor Library	893449-38-2	PR-126	10mM	PRL3	DMSO	2834
	Cl.Cl.CCCCC(CC)CNC(=N)NC(=N)NCCCCCCNC(=N)NC(=N)NCC(CC)CCCC	N-(2-ethylhexyl)-1-3-(6-{N-[3-(2-ethylhexyl)carbamimidamidomethanimidoyl]amino}hexyl)carbamimidamidomethanimidamide dihydrochloride	Alexidine·2HCl	581.7	C-12	Phosphatase Inhibitor Library	1715-30-6	AC-1562	10mM	PTPMT1	DMSO	2834

Appendix 2: Continued.

	O=C1C(=O)C2=CC=CC=C2C2=CC=CC=C12	9,10-dihydrophenanthrene-9,10-dione	9,10-Phenanthrenequinone	208.2	D-01	Phosphatase Inhibitor Library	84-11-7	AC-1402	10mM	CD45 tyrosine phosphatase	DMSO	2834
	OC(=O)C1=CC=C(C=C1)N1C(=S)S\C(=C/C2=CC=CC=C2)C1=O	4-[(5Z)-4-oxo-5-(phenylmethylidene)-2-sulfanylidene-1,3-thiazolidin-3-yl]benzoic acid	BML-260	341.4	D-02	Phosphatase Inhibitor Library	862827-45-0	PR-119	10mM	JSP-1	DMSO	2834
	[Cl-].C[N+]1=CC2=C(C=CC3=C2OCO3)C2=C1C1=C(C=C2)C=C2OCOC2=C1	24-methyl-5,7,18,20-tetraoxa-24-azahexacyclo[11.11.0.0^{2},^{10}.0^{4},^{8}.0^{14},^{22}.0^{17},^{21}]tetracosa-1(13),2(10),3,8,11,14(22),15,17(21),23-nonaen-24-ium chloride	Sanguinarine chloride	367.8	D-03	Phosphatase Inhibitor Library	5578-73-4	AC-1563	10mM	PP2C	DMSO	2834
	OC(=O)C(F)(F)F.CN1CCC2=C(C1)SC(NC(=O)C(O)=O)=C2C(O)=O	2-(carboxyformamido)-6-methyl-4H,5H,6H,7H-thieno[2,3-c]pyridine-3-carboxylic acid; trifluoroacetic acid	BML-267	398.3	D-04	Phosphatase Inhibitor Library		PR-121	10mM	PTP1B	DMSO	2834
	CCOC(=O)C(=O)NC1=C(C(=O)OCC)C2=C(CN(C)CC2)S1	ethyl 2-(2-ethoxy-2-oxoacetamido)-6-methyl-4H,5H,6H,7H-thieno[2,3-c]pyridine-3-carboxylate	BML-267 Ester	340.4	D-05	Phosphatase Inhibitor Library	474843-73-7	PR-129	10mM	PTP1B (cell permeable)	DMSO	2834
	OC(=O)C(=O)NC1=CC=CC=C1C(O)=O	2-(carboxyformamido)benzoic acid	OBA	209.2	D-06	Phosphatase Inhibitor Library	5651-01-4	PR-122	10mM	Tyrosine phosphatases	DMSO	2834
	CCOCC(=O)C(=O)NC1=CC=CC=C1C(O)=O	2-(3-ethoxy-2-oxopropanamido)benzoic acid	OBA Ester	251.2	D-07	Phosphatase Inhibitor Library		PR-130	10mM	Tyrosine phosphatases (cell permeable)	DMSO	2834
	CC(C)C1=C(O)C(O)=C(C=O)C2=C1C=C(C)C(=C2O)C1=C(O)C2=C(C=C1C)C(C(C)C)=C(O)C(O)=C2C=O	7-[8-formyl-1,6,7-trihydroxy-3-methyl-5-(propan-2-yl)naphthalen-2-yl]-2,3,8-trihydroxy-6-methyl-4-(propan-2-yl)naphthalene-1-carbaldehyde	Gossypol	518.6	D-08	Phosphatase Inhibitor Library	303-45-7	EI-130	10mM	Calcineurin (PP2B)	DMSO	2834
	[Na+].NCCCC(O)(P(O)(O)=O)P(O)([O-])=O	sodium hydrogen (4-amino-1-hydroxy-1-phosphonobutyl)phosphonate	Alendronate	271.1	D-09	Phosphatase Inhibitor Library	121268-17-5	PR-123	10mM	Tyrosine phosphatases	DMSO	2834

Appendix 3: Primary screen using 194 kinase inhibitor library and 33 phosphatase inhibitor library. The HEK 293T stable clone expressing DJ-1 BiFC constructs was transiently transfected with the plasmid encoding RFP. 24 hours post-transfection cells were treated with kinase inhibitors (5 μM) or phosphatase inhibitors (1 and 5 μM) for 4 hours, with a single biological replicate for each compound. DJ-1 BiFC signal was analysed and quantified using the Cell^R Scan^R screening station. Graphs show the ratio intensity (green/red) per well.

A) Primary screen using kinase inhibitors plate L1200-1. Order of compounds in the experiment plate listed in Table A3A.

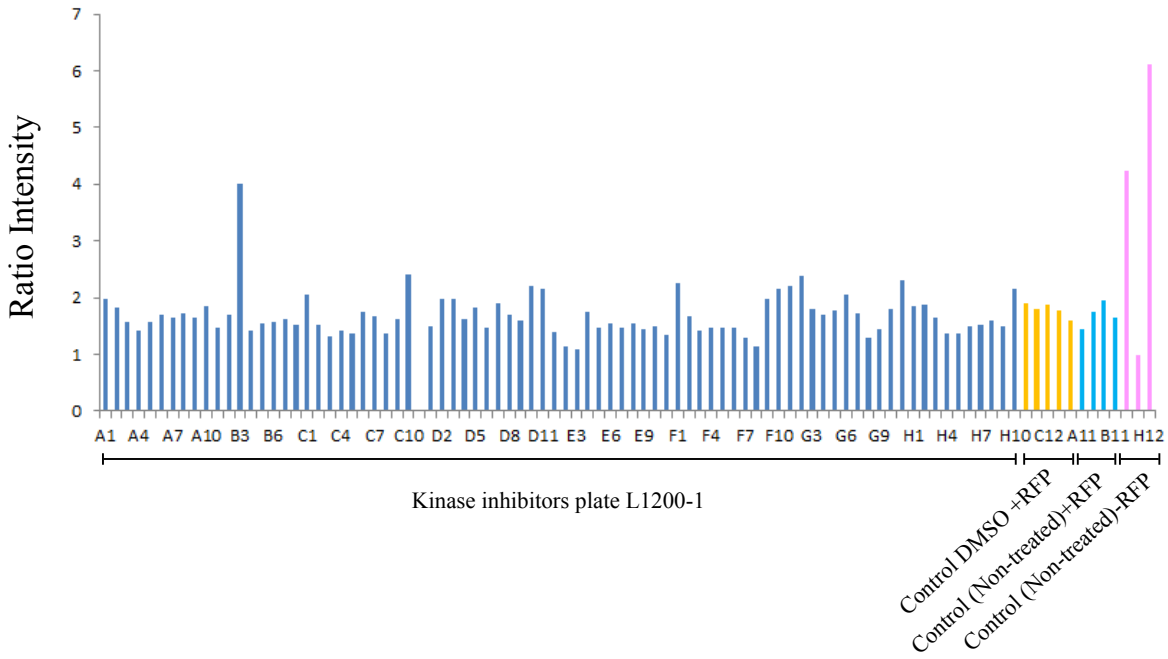

Table A3A: Plate layout of primary screen using kinase inhibitors plate L1200-1.

A	BMS-599626	Erlotinib hydrochloride	Gefitinib	Neratinib	PD153035 hydrochloride	Pelitinib	Vandetanib	WZ3146	WZ4002	WZ8040	+Control	DMSO Control
B	AV-951	Axitinib	BIBF1120	BMS-794833	Cediranib	CYC116	Imatinib	Imatinib Mesylate	+Control	+Control	+Control	DMSO Control
C	Ki8751	KRN 633	Masitinib	MGCD 265	Motesanib Diphosphate	MP-470	OSI-930	Pazopanib hydrochloride	Sorafenib Tosylate	Sunitinib Malate	TSU-68	DMSO Control
D	Vatalanib	XL880	PHA 739358	AT9283	AZD0530	Bosutinib	Dasatinib	Nilotinib	Quercentin	NVP-ADW742	AC 220	DMSO Control
E	AP24534	Tandutinib	KW2449	CI 1033	CP 724714	BAY 73-4506	JNJ-38877 605	PF-04217903	PF-2341066	ϕ	SGX-523	-Control
F	SU11274	NVP-TAE684	SB 525334	R406	R406 (free base)	XL184	BI 2536	GSK461364	HMN-214	ON 01910	AT7519	-Control
G	Flavopiridol	BS-181 hydrochloride	PD 0332991	PHA-793887	Roscovitine	SNS-032	AZD7762	Aurora A inhibitor 1	AZD1152-HQPA	CCT 120202	ENMD 2076	-Control
H	Hesperadin	MLN8237	PHA-680632	SNS-314 Mesylate	VX-680	ZM-447439	AS703026	AZD6244	AZD8330	BIX 02188	-Control	-Control

+Control: Cell transfected with RFP but not-treated with DMSO
-Control: Not-transfected cell

B) Primary screen using kinase inhibitors plate L1200-2. Order of compounds in the experiment plate shown in Table A3B.

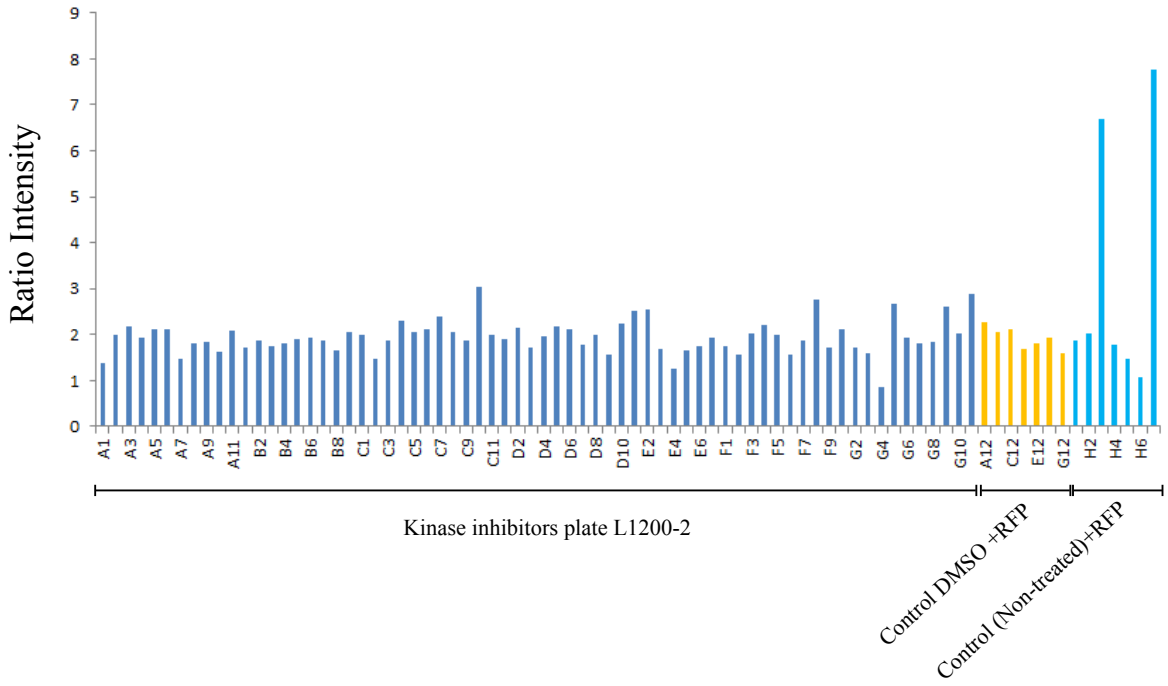

Table A3B: Plate layout of primary screen using kinase inhibitors plate L1200-2.

A	BIX 02189	BMS777607	CI-1040	PD318088	PD0325901	PD98059	U0126-EtOH	LY2228820	BIRB 796	SB 202190	SB203580	DMSO Control
B	Vinorelbine	VX-702	VX-745	GDC-0879	PLX-4720	RAF265	SP600125	AS-605240	GDC-0941	ϕ	ϕ	DMSO Control
C	IC-87114	LY294002	PIK-294	PIK90	PIK93	TG100-115	TGX-221	XL147	XL765	ZSTK474	AZD8055	DMSO Control
D	Deforolimus	Everolimus	MK-2206	Rapamycin	Temsirolimus	WYE-354	PIK-75 hydrochloride	CHIR-99021	Indirubin	SB 216763	ϕ	DMSO Control
E	KU-55933	KU-60019	KU-0063794	AT7867	AZD1480	LY2784544	Enzastaurin	ϕ	ϕ	ϕ	ϕ	DMSO Control
F	SB 431542	ABT-869	AEE788	BIBW29992	Lapatinib Ditosylate	JNJ-7706621	BEZ235	GSK1059615	ON-01910	ϕ	ϕ	DMSO Control
G	PI-103	AG-490	CP-690550	Crenolanib	GSK 1838705A	KX2-391	NVP-BSK805	PCI-32765	PF-562271	DCC-2036	LDN 193189	DMSO Control
H	+Control	+Control	+Control	+Control	+Control	+Control	ϕ	ϕ	ϕ	ϕ	ϕ	ϕ

+Control: Cell transfected with RFP but not-treated with DMSO

C) Primary screen using kinase inhibitors plate L1200-3. Order of compounds in the experiment plate listed in Table A3C.

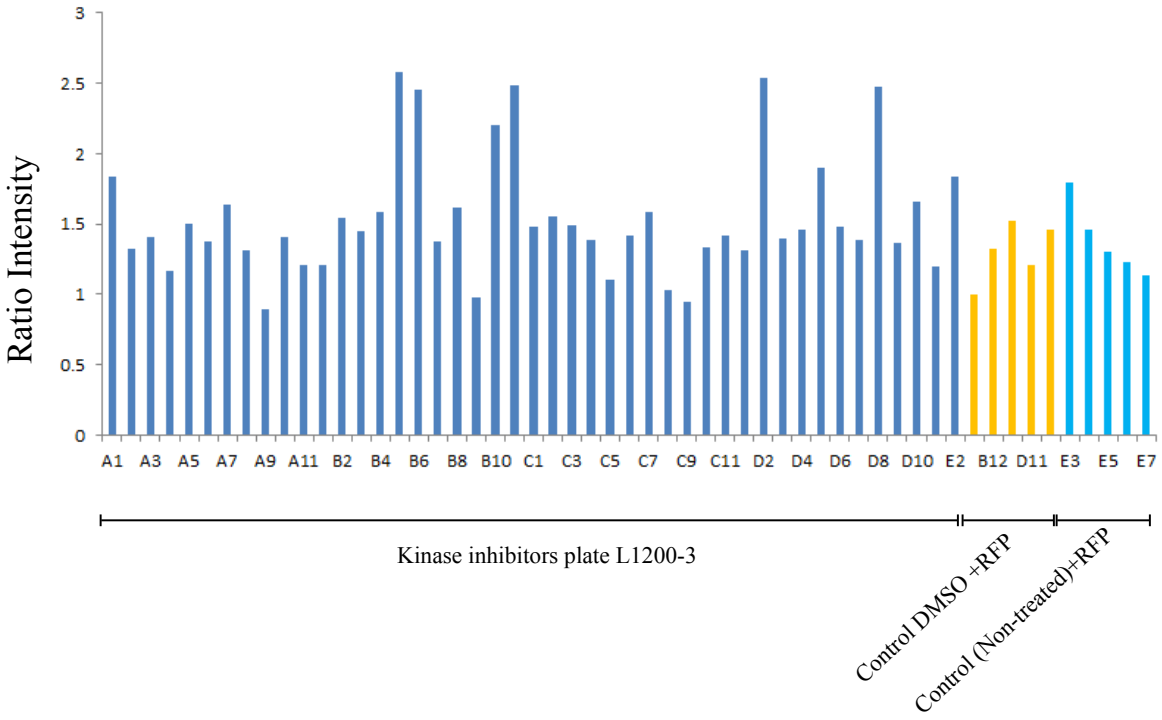

Table A3C: Plate layout of primary screen using kinase inhibitors plate L1200-3.

A	AZD8931	Raf265 derivative	NVP-BHG712	OSI-420	R935788	AZ960	Mubritinib	PP242	Cyt387	Apatinib	CAL-101	DMSO Control
B	PIK-294	VX-765	Telatinib	BI6727	WP1130	BKM-120	CX-4945	Phenformin hydrochloride	TAK-733	AZD5438	PP121	DMSO Control
C	OSI027	LY2603618	PK1587	CCT 128930	A66	NU7441	GSK2126458	WYE-125132	WYE-687	A-674563	AS252424	DMSO Control
D	GSK 1120212	Flavopiridol hydrochlori	AS604850	WAY-600	TG101209	GDC-0980	A-769662	TAK-901	AMG 900	ZM 336372	DMSO Control	DMSO Control
E	PH-797804	PF-04691502	+Control	+Control	+Control	+Control						
F												
G												
H												

+Control: Cell transfected with RFP but not-treated with DMSO

D) Primary screen using phosphatase inhibitors at 1µM and 5 µM concentrations. Order of compounds in the experiment plate listed in Table A3D.

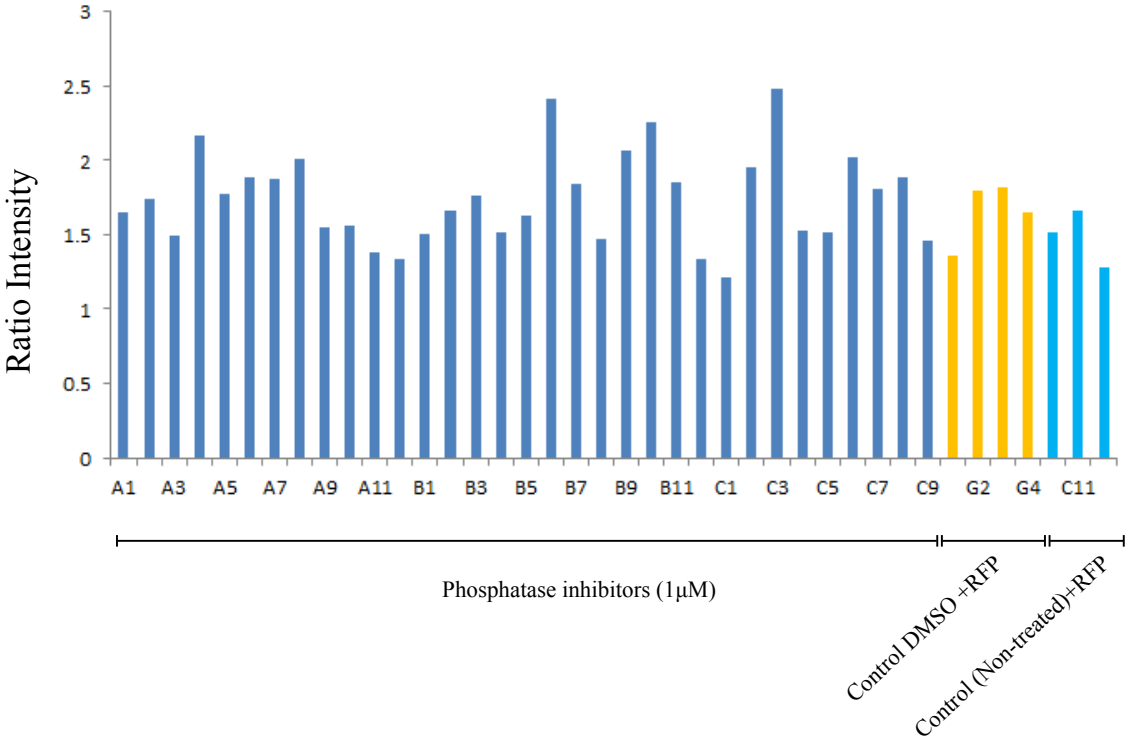

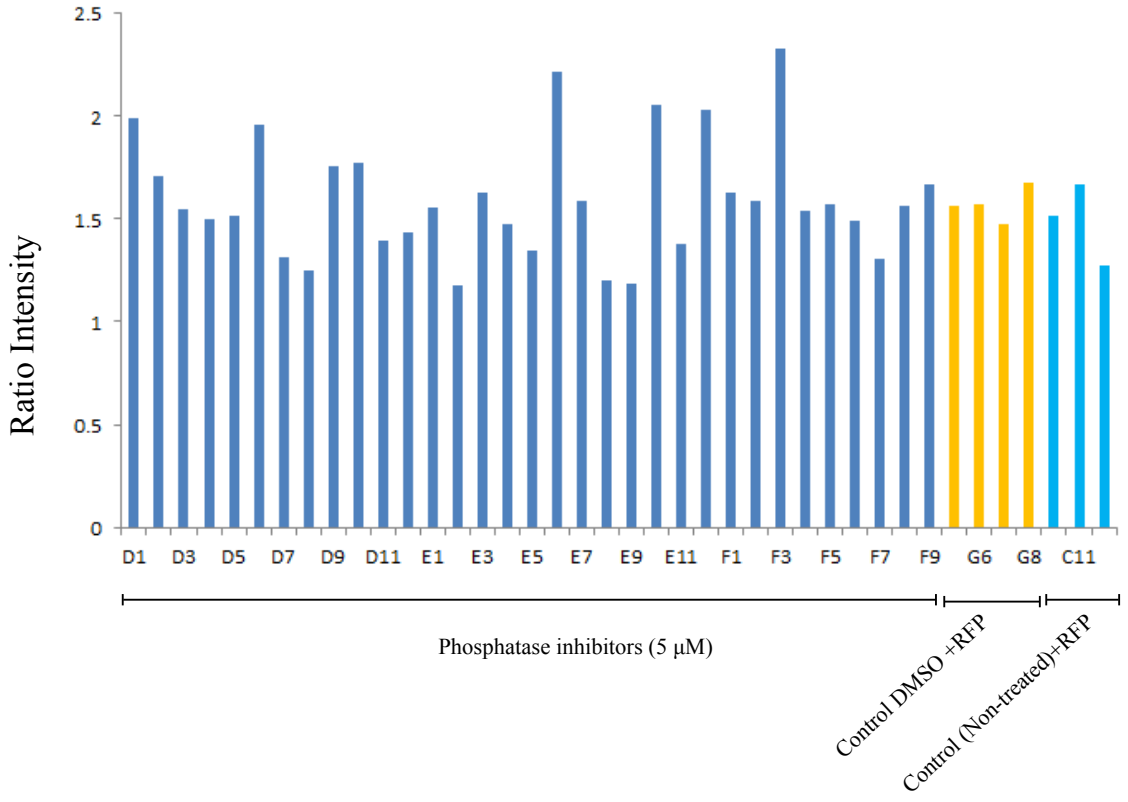

Table A3D: Plate layout of primary screen using Phosphatase inhibitor library. A1-C12 show phosphatase inhibitors at 1 μM and D1-F9 show phosphatase inhibitors at 5 μM.

A	Cantharidic acid	Cantharidin	Endothall	Benzylphosphonic acid	(6S)-6-(4-bromcL-p-Bromotetramisole oxalate	RK-682	RWJ-60475	RWJ-60475 (AM)3	Levamisole HCl	Tetramisole HCl	Cypermethrin	Deltamethrin
B	Fenvalerate	Tyrphostin 8	CinnGel	NSC-95397	BN-82002	Shikonin	NSC-663284	Cyclosporin A	Pentamidine	BVT-948	B4-Rhodanine	Alexidine 2HCl
C	9,10-phenanthrenequinone	BML-260	Sanguinarin Chloride	BML-267	BML-267 Ester	OBA	OBA Ester	Gossypol	Alendronate	+Control	+Control	+Control
D	Cantharidic acid	Cantharidin	Endothall	Benzylphosphonic acid	(6S)-6-(4-bromcL-p-Bromotetramisole oxalate	RK-682	RWJ-60475	RWJ-60475 (AM)3	Levamisole HCl	Tetramisole HCl	Cypermethrin	Deltamethrin
E	Fenvalerate	Tyrphostin 8	CinnGel	NSC-95397	BN-82002	Shikonin	NSC-663284	Cyclosporin A	Pentamidine	BVT-948	B4-Rhodanine	Alexidine 2HCl
F	9,10-phenanthrenequinone	BML-260	Sanguinarin Chloride	BML-267	BML-267 Ester	OBA	OBA Ester	Gossypol	Alendronate			
G	DMSO Control	DMSO Control	DMSO Control	DMSO Control	DMSO Control	DMSO Control	DMSO Control	DMSO Control				
H												

Appendix 4: Sample of images taken during primary screen. A) cells after treatment with kinase inhibitor, AV-951 (plate L1200-1). **B)** cells treated with kinase inhibitor, CI-1040 (plate L1200-2). **C)** cells treated with kinase inhibitor B16727 (plate L1200-3). **D and E):** images taken during primary screen using phosphatase inhibitors at 1 and 5 μM respectively. **F)** cells treated with DMSO as control in our screen experiments. Scale bar = 100 μm.

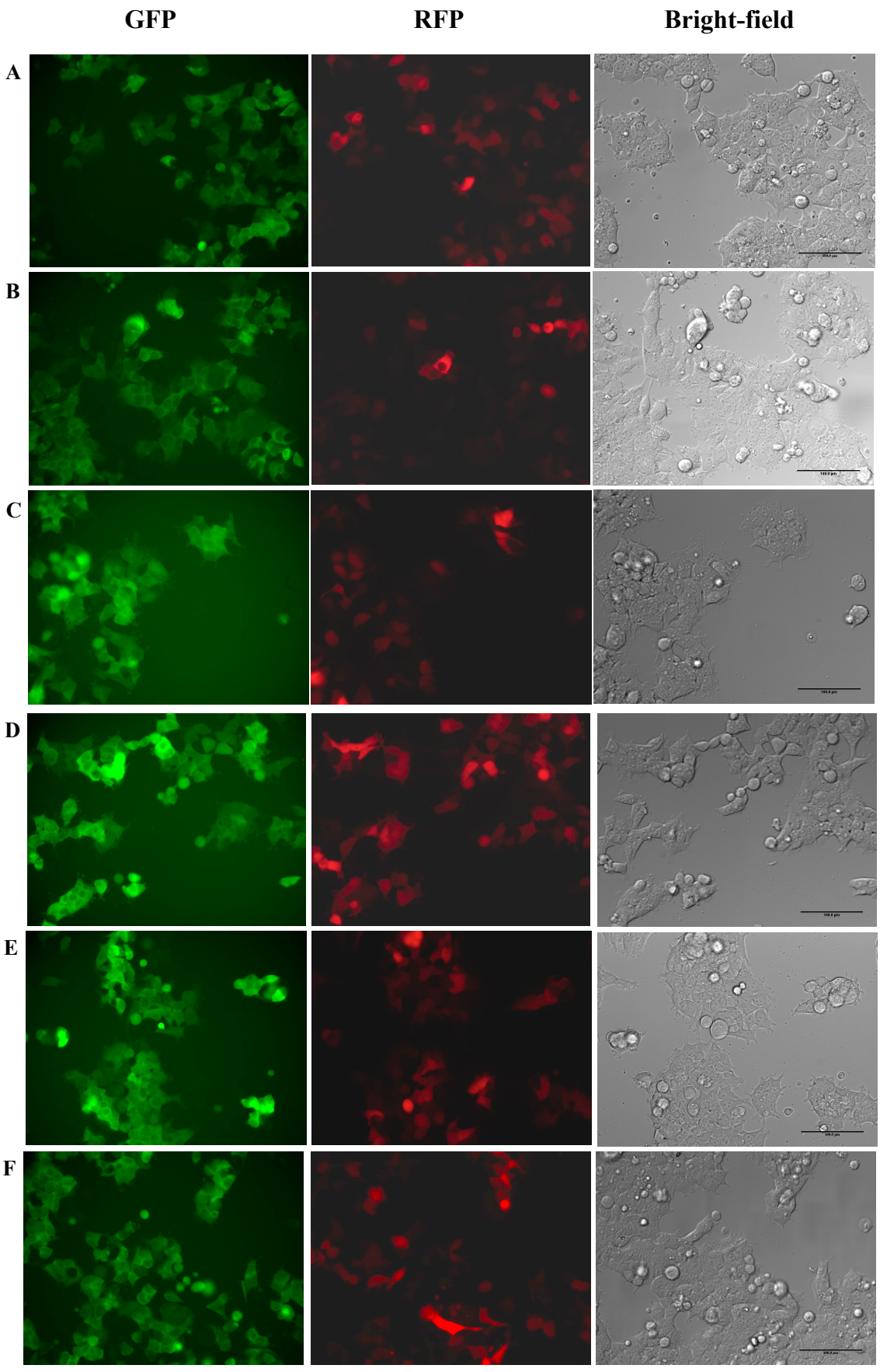
GFP
RFP
Bright-field
A
B
C
D
E
F

Appendix 5: Secondary screen for validating candidates identified in the primary screen. Compounds able to modulate DJ-1 dimerisation in the primary screen (42 out of 194 kinase inhibitors and 13 out of 33 phosphatase inhibitors), were re-tested in quadruplicate. Graphs display the average ratio intensity (green/red) per well.

A) Cells treated with kinase inhibitors at 5 µM concentration in quadruplicate.

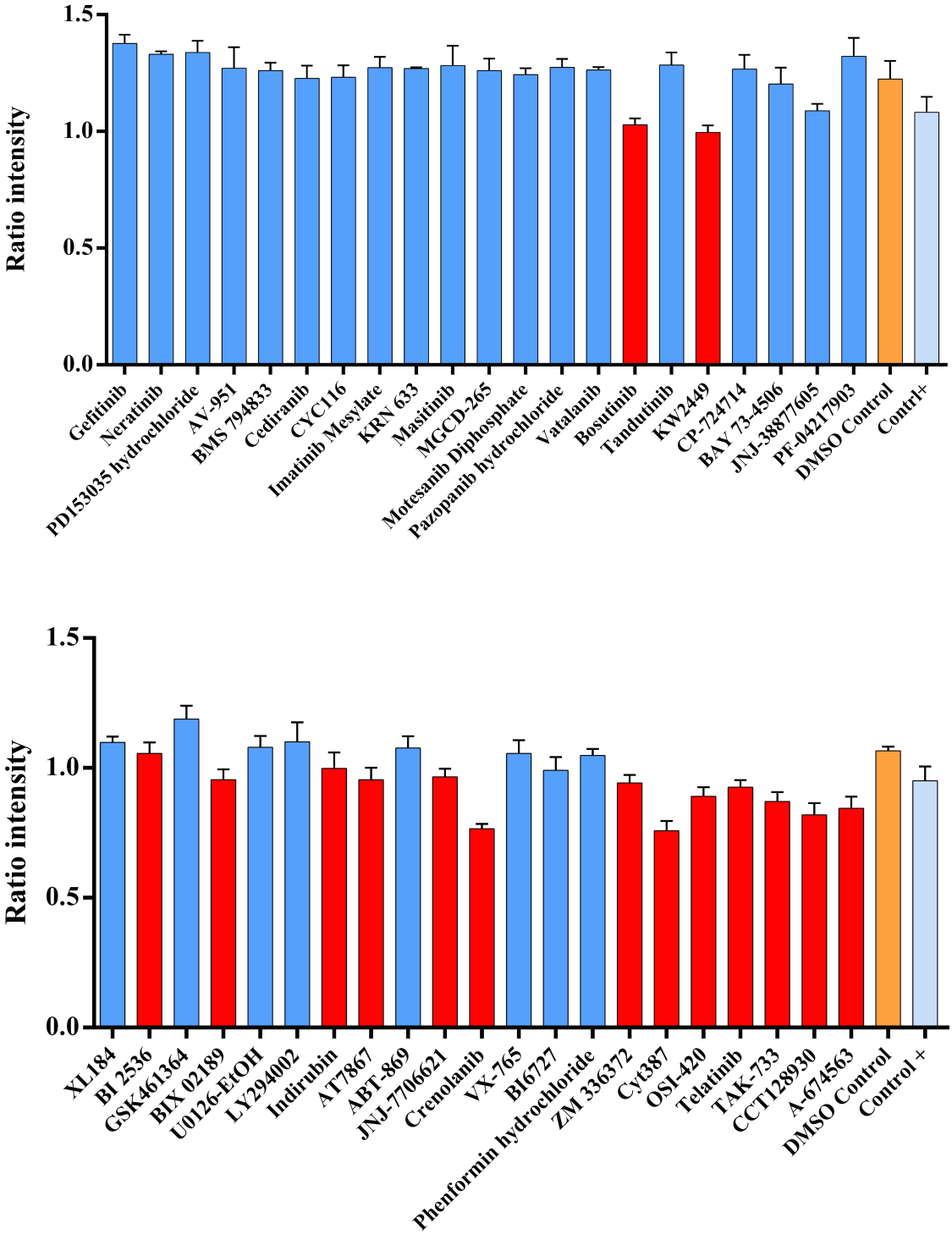

B) Cells treated with phosphatase inhibitors at 1 and 5 µM concentrations in quadruplicate.

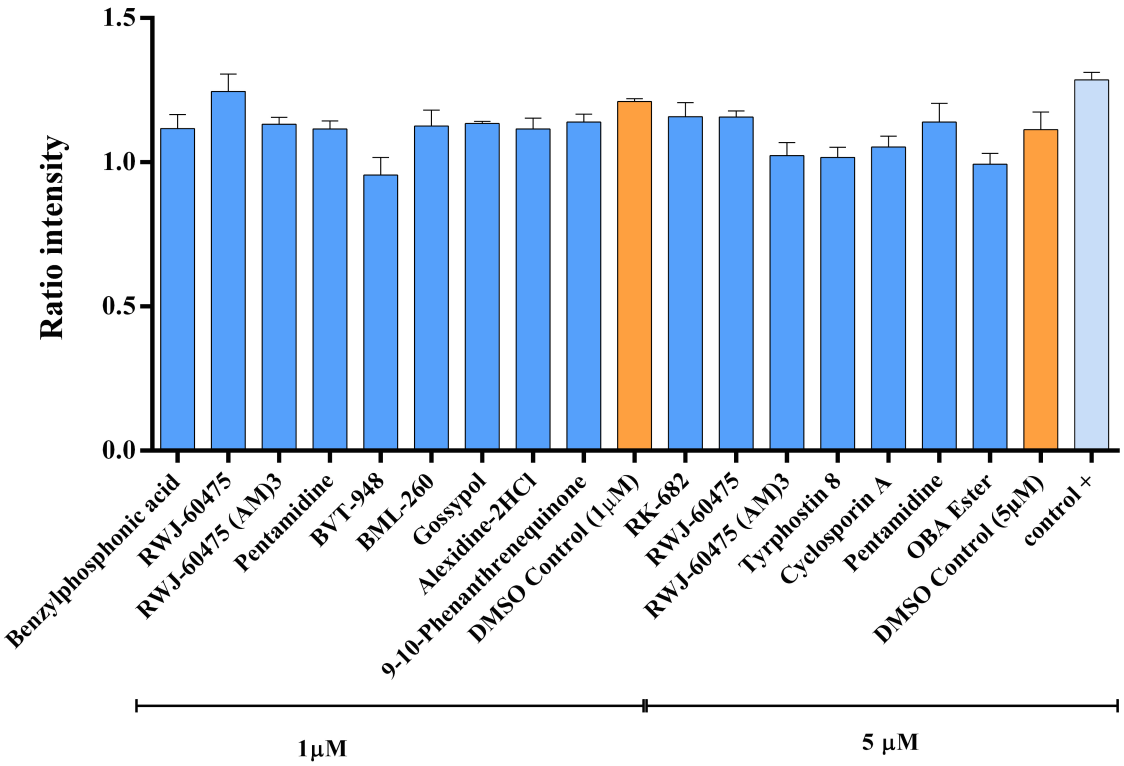

C) Sample of images taken during secondary screen.